A Study of the Growth and Hydrogen Production of *Cyanothece* sp. ATCC 51142

Pongsathorn Dechatiwongse

Imperial College London

Department of Chemical Engineering

Supervised by Professor Klaus Hellgardt and Professor Geoffrey C. Maitland

Submitted for the Degree of Doctor of Philosophy

July 2015

Abstract

Hydrogen (H_2) has long been promoted as an ideal fuel, as it permits a completely clean combustion and has great potential to provide clean power needed for transport and electricity generation. The unicellular, nitrogen-fixing cyanobacterium *Cyanothece* sp. ATCC 51142 is a promising strain with a remarkable capability of producing large quantities of H_2. Under anaerobic condition, the cyanobacterium carries out the biological fixation of atmospheric nitrogen (N_2) into ammonia (NH_3), concurrently producing H_2 as by-product. The aim of this thesis was to improve our understanding of the growth and H_2 production of *Cyanothece* sp. ATCC 51142 in order to develop a continuous and practical cyanobacterial H_2 production process.

In order to achieve effective H_2 production, it is prerequisite to grow dense and healthy *Cyanothece* 51142 cultures. Favourable cyanobacterial growth conditions included a continuous illumination at 207 - 320 μmol m^{-2} s^{-1}, temperature of 35 °C and nitrogen-replete (addition of nitrate salts) condition. The critical temperature, which induces photoinhibition upon the cyanobacterium, was found at 40 °C. In the case of H_2 production, favourable conditions included a continuous illumination at low light intensities of 46 – 92 μmol m^{-2} s^{-1}, temperature of 30 °C, nitrogen-fixing (sole presence of atmospheric N_2) and photoheterotrophic (sole presence of organic glycerol substrate) growth condition.

In order to effectively handle incompatible requirements between the cyanobacterial growth and its sequential H_2 production, a novel two-stage chemostat photobioreactor (PBR) system was designed and developed, with an aim to improve H_2 production yield as well as extend its production duration. The system has been operated non-stop for consecutive 31 days without any losses in its performance and subsequently demonstrated a remarkable improvement in H_2 production, with more than 6.4 times higher yield than that of a single-stage batch system. With the continuous mode of operation, a continuous collection of produced biomass from the PBR is also permitted (more than 7.3 times improvement in biomass yield than that of a single-stage batch system). At an industrial scale, this biomass could undergo further downstream processing to generate a multi-streamline of high valued by-products such as e.g. vitamins, pharmaceuticals and human nutrition, which can subsequently contribute to a significant improvement in an economic viability of biohydrogen process.

Author Declaration

I declare that the contents of this thesis are my own work except where otherwise acknowledged.

The work was carried out between October 2011 and July 2015 at Department of Chemical Engineering, Imperial College London under the supervision of Professor Klaus Hellgardt and Professor Geoffrey C Maitland.

This thesis is part of the Solar Hydrogen Project, managed by the Energy Futures Lab at Imperial College London, and was funded by the UK Engineering and Physical Sciences Research Council (EPSRC) project reference EP/F00270X/1.

Pongsathorn Dechatiwongse
July 2015

Acknowledgements

I would like to start by thanking my supervisors Professor Klaus Hellgardt and Professor Geoffrey C Maitland for their invaluable supports and advices over three and a half years of my PhD study. It has been my great pleasure to work with them and my time spent with them had been the most fulfilling. This thesis would not have been possible without their constant encouragement and moral support.

My PhD journey may not be as successful without the assistance and help from Dr. Bojan Tamburic, who has taught me fundamental laboratory skills and shared his extensive knowledge of biochemical engineering with me at the beginning of this project. I would also like to acknowledge Suna Srisamai, for teaching me an analytical technique of nuclear magnetic resonance as well as for being a great senior. I am thankful to the help of Dongda Zhang, my indispensable colleague and great friend from the University of Cambridge, who provided me many valuable advices in dynamic modelling of microalgal growth and H_2 production kinetics.

I would also like to convey my gratitude to Professor Peter J Nixon for allowing me to use his biochemistry laboratory and equipment throughout my PhD study. In addition, thank you to everybody else who contributed to this thesis, including: my Chemical Engineering departmental staffs – Dr. Fessehaye Zemichael, Richard Wallington, Gavin Barnes, Keith Walker, Ben Kistnah, Chin Lang, Patricia Carry, Andrew Macey, Sarah Payne, Jessica Baldock, Nam Ly and Susi Underwood, my PhD colleagues – Dr. Chin Kin Ong, Hussein Haji Taha, Chonlathep Usaku, Bhavish Patel, Arash Izadpanah and Xu Zhao, my MSc students – Fei Zhe, Geoffrey Morrier and Martta Nieminen - and lastly my undergraduate students - Sarita Lee, Pasit Chulajata, Kee Aik Chua and Nikzad Falahati.

My PhD study was funded by Ministry of Science and Technology of Thailand, the Royal Thai Government Scholarship, whom I am highly appreciated. I am also deeply grateful to the Office of Educational Affairs, the Royal Thai Embassy, London for taking a good care of me, since I firstly arrived the UK in July 2006.

I would like to dedicate this thesis to my parents, my grandparents, and my brother, for their unconditional love and support.

Pongsathorn Dechatiwongse

List of Publications

Peer-reviewed journal articles

Zhang, D., **P. Dechatiwongse**, E. A. del Rio-Chanona, G. C. Maitland, K. Hellgardt and V. S. Vassiliadis (2015). "Dynamic modelling of high biomass density cultivation and biohydrogen production in different scales of flat-plate photobioreactors." Biotechnology & Bioengineering (in press)

Del Rio-Chanona, E.A., **P. Dechatiwongse**, D. Zhang, G. C. Maitland; K. Hellgardt, H. Arellano-Garcia and V. S. Vassiliadis (2015)" Optimal operation strategy for biohydrogen production." Industrial & Engineering Chemistry Research **54**(24): 6334–6343.

Dechatiwongse, P., G. C. Maitland and K. Hellgardt (2015). "Demonstration of a two-stage aerobic / anaerobic chemostat for the enhanced production of hydrogen and biomass from unicellular nitrogen-fixing cyanobacterium." Algal Research **10**(0): 189 – 201.

Zhang, D., **P. Dechatiwongse**, E. A. del Rio-Chanona, G. C. Maitland, K. Hellgardt and V. S. Vassiliadis (2015). "Modelling of light and temperature influences on cyanobacterial growth and biohydrogen production." Algal Research **9**(0): 263-274.

Zhang, D., **P. Dechatiwongse**, E. A. Del-Rio-Chanona, K. Hellgardt, G. C. Maitland and V. S. Vassiliadis (2015). "Analysis of the cyanobacterial hydrogen photoproduction process via model identification and process simulation." Chemical Engineering Science **128**(0): 130-146.

Zhang, D., **P. Dechatiwongse** and K. Hellgardt (2015). "Modelling light transmission, cyanobacterial growth kinetics and fluid dynamics in a laboratory scale multiphase photo-bioreactor for biological hydrogen production." Algal Research **8**(0): 99-107.

Dechatiwongse, P., S. Srisamai, G. Maitland and K. Hellgardt (2014). "Effects of light and temperature on the photoautotrophic growth and photoinhibition of nitrogen-fixing cyanobacterium *Cyanothece* sp. ATCC 51142." Algal Research **5**(0): 103-111.

Tamburic, B., **P. Dechatiwongse**, F. W. Zemichael, G. C. Maitland and K. Hellgardt (2013). "Process and reactor design for biophotolytic hydrogen production." Physical Chemistry Chemical Physics **15**(26): 10783-10794.

Patel, B., B. Tamburic, F. W. Zemichael, **P. Dechatiwongse** and K. Hellgardt (2012). "Algal biofuels: a credible prospective?" ISRN Renewable Energy 2012: 631574-Article ID 631574.

Book chapter

Patel, B., **P. Dechatiwongse** and K. Hellgardt (2014). "Enzyme-catalysed processes in a potential algal biorefinery", Chapter 29, in Industrial Biocatalysis (Grunwald P. ed.), Pan Stanford Publishing Pte. Ltd., Singapore, 2014.

Forthcoming publications

Dechatiwongse, P., D. Zhang, V. Vassiliadis, G. Maitland and K. Hellgardt (in preparation). "Comprehensive review of bioreactor: biochemical reaction, light transfer, fluid dynamics and scale-up." Algal Research (provisional).

Dechatiwongse, P., D. Zhang, A. Del-Rio-Chanona, V. Vassiliadis, G. Maitland and K. Hellgardt (in preparation). "Effects of light intensity and temperature on biohydrogen production of nitrogen-fixing cyanobacterium *Cyanothece* sp. ATCC 51142." Algal Research (provisional).

Zhao, X., D. Zhang, **P. Dechatiwongse**, Q. Liao, R. Chen, K. Hellgardt and X. Zhu (in preparation). "Dynamic simulation of cyanobacterial growth in a tubular photobioreactor." Bioresource Technology (provisional).

Table of Contents

List of Figures

List of Tables

Nomenclature

A	Pre-exponential factor of synthetic process
ATCC	American Type Culture Collection
Ar	Argon gas
ADP	Adenosine diphosphate
ATP	Adenosine triphosphate
AU	Absorbance units
(aq)	Aqueous solution
a_c	Sum of a spectral-averaged absorption coefficient on a dry biomass concentration, X, and a volume-averaged reflection coefficient on bubble volume fraction
B	Pre-exponential factor of denaturation process
C	Speed of light and
[C(t)]	Quantity of nutrient consumed at any specific time
$[C_{total}]$	Total quantity of nutrient consumed
$[C_{final}]$	Final quantity of nutrient available in the system
$[CO_2^*]$	Theoretically saturated CO_2 concentration
$[CO_2]$	Dissolved CO_2 concentration
C. reinhardtii	Green alga *Chlamydomonas reinhardtii*
$CaCl_2\ 2H_2O$	Calcium chloride dihydrate
CBB	Calvin-Benson-Bassham
CCS	Carbon capture and sequestration
Chl	Chlorophyll molecule
$(CH_2O)_n$	Starch

$C_6H_{12}O_6$	Glucose
CH_3COOH	Acetic acid
$CH_3CH_2CH_2COOH$	Butyric acid
$C_3H_8O_3$	Glycerol
$C_{24}H_{42}O_{21}$	Glycogen
CO_2	Carbon dioxide
CoA	Coenzyme A
Cyanothece 51142	Unicellular, nitrogen-fixing, cyanobacterium, *Cyanothece* sp. ATCC 51142
Cyt b_6/f	Cytochrome complex involved in electron transport
D	Dilution rate
DD	Continuous dark
D_c	Critical dilution rate
DCMU	3-(3, 4-dichlorophenyl)-1, 1-dimethylurea
E_a	Activation energy of synthetic process
E_b	Activation energy of denaturation process
E_v	Phonic energy
e^-	Electron
F	Feed rate
FCV	Fuel cell vehicle
Fd	Ferredoxin
Fe	Iron
$FeCl_3$ $6H_2O$	Iron(III) chloride hexahydrate
FNR	Ferredoxin oxidoreductase enzyme
GM	Genetic modification / genetically modified

G3P	Glyceraldehyde 3-phosphate
H	Planck's constant
H^+	Proton
H_{CO_2}	Henry's constant for CO_2
H_{O_2}	Henry's constant for O_2
H_2	Molecular hydrogen
H_2O	Water
H_2O_2	Hydrogen peroxide
HCl	Hydrochloric acid
He	Helium gas
HVPs	High-value products
$h(I)_G$	Light intensity function for growth process
$h(I)_H$	Light intensity function for H_2 production process
$h(T)_G$	Temperature function for growth process
$h(T)_H$	Temperature function for H_2 production process
I	Average light intensity
I_{in}	Incident light intensity
I_l	Local light intensity
I_{out}	Transmitted light intensity
IC	Ion chromatography
ICL	Imperial College London
IR	Infra-red light
$k_L{}^i a$	Volumetric gas–liquid mass transfer coefficient for component "i"
k_s	Photosaturation coefficient in Aiba model
k_i	Photoinhibition coefficient in Aiba model

KCl	Potassium chloride
K_2HPO_4	Potassium phosphate dibasic
L	Light path length along bioreactor
LCA	Life cycle analysis
LD	Alternating light / dark cycles
LED	Light-emitting diode
LHC	Light-harvesting complex
LL	Continuous light
M	Molecular weight
$MgCl_2$	Magnesium chloride
$MgSO_4$	Magnesium sulphate
MIMS	Membrane-inlet mass spectrometry
Mn	Manganese
Mo	Molybdenum
MS	Mass spectrometer / mass spectrometry
Mw_C	Molecular weight of carbon
Mw_{CO_2}	Molecular weight of CO_2
N_2	Molecular nitrogen
N_A	Avogadro's number
$NaNO_3$	Sodium nitrate
NaOH	Sodium hydroxide
NaCl	Sodium chloride
Na_2EDTA	Ethylenediamine tetraacetate
ND	NADPH-dehydrogenase enzyme
NH_3	Ammonia

NH_4^{+1}	Ammonium cation
NO_3^{-1}	Nitrate anion
NAD^+	Oxidised nicotinamide adenine dinucleotide
NADH	Reduced nicotinamide adenine dinucleotide
$NADP^+$	Oxidised nicotinamide adenine dinucleotide phosphate
NADPH	Reduced nicotinamide adenine dinucleotide phosphate
Ni	Nickel
N-deprivation	Nitrogen-deprivation
$[O_2^*]$	Theoretically saturated O_2 concentration
$[O_2]$	Dissolved O_2 concentration
O_2	Oxygen molecule
OD	Optical density
P	Pressure
P_{max}	Maximum biomass productivity
PAR	Photosynthetically active radiation
PBR	Photobioreactor
PBS	Phycobilisome
PC	Plastocyanin
PDC	Pyruvate decarboxylase enzyme
PDMS	Polydimethylsiloxane polymer membrane
PEM	Proton exchange membrane fuel cell
Perspex	Polymethyl methacrylate
PFA	Perfluoroalkoxy plastic tubing
Photoautotrophic	Growth using CO_2 as the only carbon source
Photoheterotrophic	Growth using organic substrate as the only carbon source

Photomixotrophic	Growth using both CO_2 and organic substrate
P_i	Inorganic phosphate ion
P_{CO_2}	Partial pressure of CO_2
P_{O_2}	Partial pressure of O_2
pCO_2	Dissolved CO_2 concentration
pO_2	Dissolved O_2 concentration
PO_4^{-3}	Phosphate ion
PQ	Plastoquinone pool
Fe-solution	Iron solution
PSI	Photosystem I protein complex
PSII	Photosystem II protein complex
PV	Photovoltaic
r_{max}	Maximum specific growth rate
R	Universal gas constant
R_s	Total substrate consumption rate
R_{CO_2}	Total CO_2 consumption rate
R_{H_2}	H_2 production rate
R_{max,H_2}	Maximum H_2 production rate
rpm	Rotations per minute
RuBisCO	Ribulose-bisphosphate carboxylase enzyme
S	Substrate concentration
S_0	Initial substrate concentration
SO_4^{-2}	Sulphate ion
SHEC efficiency	Solar-to-H_2 energy conversion efficiency
T	Temperature

TAPS	N-tris(hydroxymethyl)methyl-3-aminopropanesulfonic acid
TAPSO	3-[N-tris(hydroxymethyl)methylamino]-2-hydroxypropanesulfonic acid
t	Time
t_0	Time of inflection in logistic growth model
TAGs	Triglycerides
TCA	Tricarboxylic acid
UV	Ultra-violet light
V	Working volume of bioreactor
X	Dry biomass concentration
X(t)	Dry biomass concentration at any time specific time
$X_{C1}(t)$	Dry content of elemental carbon within the biomass
X_{max}	Maximum biomass concentration
WT	Wild type
$Y_{H/X}$	H_2 yield coefficient
μ_d	Specific decay rate
μ_{max}	Maximum specific growth rate
$\mu_{max,s}$	Maximum specific growth rate at saturating light intensity
μ (t)	Specific growth rate at any specific time
$\frac{d[CO_2]}{dt}$	Rate of change of CO_2
$\frac{d[O_2]}{dt}$	Rate of change of O_2
λ	Wavelength of the photon
ρ	Density

1. General Introduction

Energy is one of key drivers for an economic growth of every nation. Due to a rapid rise in global population, demands on energy have been projected to be more than doubled over the coming decades (IEA 2011). More than 80% of energy we use today comes from the combustion of fossil fuels (US EPA 2010), which at the same time generates significant quantity of carbon dioxide. The accumulation of this particular gas in the atmosphere has raised environmental concerns around the world, as it intensifies the global warming effect that could pose a serious threat to our humanity (Stern 2006).

Cyanobacteria, also known as blue-green algae, are a diverse group of photosynthetic microorganisms, which have an ability to directly derive their energy from sunlight. They are regarded as an important contributor to an oxygenation of the global atmosphere - the process which biologically induces appearance of oxygen and subsequently stimulates an evolution of plants and animals on the Earth (Buick 1992). The habitats of cyanobacteria are widespread in fresh water, sea water and terrestrial ecosystems. Therefore, they are readily available, affordable and flexible. Because of their high nutritional content, the first human use of cyanobacteria started in food industry (Spolaore, Joannis-Cassan *et al.,* 2006). Cyanobacteria are also capable of producing various types of fuels, including biohydrogen, biodiesel, bioethanol and biomethane (Parmar, Singh *et al.,* 2011). In particular, hydrogen has a great potential to be an alternative and sustainable fuel option of the future, because it can enable a completely clean combustion, which produces only heat energy and pure water. Among all fuels, hydrogen has the highest energy density per unit mass and can be efficiently converted into electricity using a proton exchange membrane fuel cell (Barbir 2005). As more than 95% of our today hydrogen is still produced from fossil fuels (US DoE 2008), a more renewable

and cleaner production route is required for a long-term sustainability of our societies. Cyanobacteria produce hydrogen via the biological process of nitrogen fixation, which involves the reduction of ambient nitrogen into ammonia by the nitrogenase enzymes (Dutta, De *et al.,* 2005).

Although cyanobacterial hydrogen has been extensively considered as an ideal energy carrier, there are several challenges to be resolved include: the low photochemical efficiency of the biohydrogen production process (Masukawa, Kitashima *et al.,* 2012), the short duration of cyanobacterial hydrogen production (Dechatiwongse, Maitland *et al.,* 2015) and the high cost of commercial photobioreactors (Ugwu, Aoyagi *et al.,* 2008). As a result, the crucial remaining question that has to be answered is whether cyanobacterial hydrogen production can be operated sustainably and economically. Addressing some of these challenges is the aim of this thesis.

In order to develop a commercial cyanobacterial hydrogen production platform, more works need to be conducted in order to improve our understanding of the underlying biological mechanism of cyanobacteria. Advanced engineering approaches, including genetic modification of cyanobacterial cells and determination of their optimum operating conditions, will also play a key role to enhance hydrogen production. Effective, affordable, scalable photobioreactors need to be designed in order to commercially facilitate this process at an industrial scale. Experimental techniques that extend hydrogen production over long time periods, at large scales, under ambient conditions, also need to be developed.

2. Microalgae and Hydrogen for Sustainable Energy

2.1. Introduction

This chapter will provide an introduction to the global energy challenge and the motivation for producing sustainable, renewable and clean energy. The availability and affordability of solar power will be discussed. The benefits, the limitations and the historical development of traditional biofuels will also be included in the discussion. An argument will be made for the utilisation of microalgae as biological factories for biofuel production. The development of H_2 as the sustainable fuel of the future and a brief account of the different biohydrogen production processes will be provided.

2.2. The Global Energy Challenge

Today, our global economy and energy supply rely extensively on non-renewable fossil fuels. World population has been projected to increase from 6.6 billion in 2008 to 9.2 billion by 2050 (Stephens, Ross *et al.,* 2010) and therefore the global energy requirement is expected to be more than doubled in order to accommodate that increase (WEC 2007). Although concerns over depleting fossil fuel reserves may become less serious in some countries such as the United States and Canada, after their increased exploration of newer unconventional reserves such as shale oil, the UK is importing ever-increasing amounts of oil from the Middle East and natural gas from Russia, due to diminishing fossil fuel reserves in the North Sea. This increasing dependence on imported fuels makes the UK more vulnerable to supply disruptions and price fluctuations (DBERR 2007). In order to improve the national energy

security, there is a strong necessity for the UK (as well as other oil-importing countries) to develop local energy resources, which also have to be affordable, renewable and sustainable on an urgent timescale.

Globally increasing fossil fuels utilisation is a substantial driver for enhancing the world economy, but it also causes an ever fast escalating level of greenhouse gases, which in turn raises the perils of global warming. Unless addressed effectively, this environmental phenomenon could have major impact for natures as well as humanity (IPCC 2007). Carbon dioxide (CO_2) is one of greenhouse gases and therefore can raise the global temperature by emitting its absorbed infrared radiation onto the Earth's surface. Two thirds of world CO_2 emissions are associated with the way we presently produce and use energy, a sector that is still dominated by the combustion of fossil fuels (EPA 2010). Anthropogenic CO_2 is released into the atmosphere at the rate of around 34 gigatonnes of CO_2 per annum (Gt CO_2 yr^{-1}) (IPCC 2007), whereas natural processes could remove only about 12 Gt CO_2 yr^{-1} (Bilanovic, Andargatchew *et al.,* 2009). This imbalance subsequently results in significant quantities of CO_2 trapped in our biosphere. At present, the concentration of atmospheric CO_2 is approximately 390 parts per million (ppm), which is significantly higher than the pre-industrial (historic) level of 280 ppm, and can potentially intensify the greenhouse effect. In order to mitigate these environmental issues, substantial effort is being put in at the international level to search for alternative forms of energy that could replace fossil fuels as well as being renewable and non-polluted to the environment. The Kyoto Protocol of 1997 set a target of 5.2 % reduction in global greenhouse gas emissions from 1990 values (Wang, Li *et al.,* 2008). In order to be in line with the international agreement, the UK government has committed to make a significant reduction of CO_2 emissions by at least 80% below emissions in 1990, by the year 2050 (DBERR 2007). To move towards reaching this target,

near-term actions could be made by improving energy efficiency as well as decarbonising existing power generation technologies, but a major overhaul of a whole energy sector will eventually be necessary. It is highly certain that this overhaul will involve the complete replacement of fossil fuels with alternative low-carbon fuels such as H_2 fuel, especially in the transport sector (Weiss, Heywood *et al.,* 2000). According to the Stern review on climate change, it would be more economically prudent to perform a strong, early action (through devotion of a small percentage of global GDP now) to tackle climate change rather than to pay for the costs of inaction in the future (Stern 2006).

2.3. Solar Energy and Biofuels

With aims to accommodate huge global energy demand, while mitigating the climate change, it would require a renewable, locally available and low-carbon energy resource. Among all of renewable energy sources, solar energy, coming from the Sun, is by far the most abundant and largest source of energy available to humanity. Earth receives solar energy at the rate of approximately 120,000 TW (1 TW = 10^{12} W) (Blankenship, Tiede *et al.,* 2011), which is 8,000 times greater than the current total global energy consumption of 15 TW (Hoffert, Caldeira *et al.,* 2002). If the yearly averaged solar energy falling upon the Earth's surface of 170 W m^{-2} could be captured with 10% efficient energy converters, it would require only 0.17 % of the total global lands in order to meet the world energy requirement (Stephens, Ross *et al.,* 2010). The utilisation of solar power consists of three steps: capture, conversion and storage - and can be classified into three categories based on its primary energy produced: solar electricity, solar thermal and solar fuel. Solar electricity is the direct conversion from solar into electrical energy, the process that involves the excitation of electrons and holes in a photovoltaic (PV) cell, usually constructed from a semiconductor

such as silicon. Today, the power conversion efficiency of commercial PV cell module is typically 18 ± 2 % (Green, Emery *et al.,* 2010), but its electricity produced is 5 - 10 times more expensive than that produced from fossil fuels, and thereby being unable to compete as a primary energy source (US DoE 2010). Alternatively, thermal energy can also be generated from solar energy using solar concentrators, where sunlight collected over a large area is focused, using mirrors, onto a heat absorber such as water or molten salts. While PV power can be produced in small distributed generation facilities located at the point of end-use, such as local residence, solar thermal power generally requires large, expensive, central facilities and has to be built in places, which have the high amount of solar radiation such as dessert (DBERR 2007). A third option is to use the natural process of photosynthesis to capture solar energy and store it as chemical energy in a wide range of feedstocks such as starch, sugars and lipids within biomass of crops, plants and microalgae (Stephens, Ross *et al.,* 2010). The biomass can later be processed into various types of transport biofuels, depending on organic compound within the biomass, such as bioethanol, biodiesel, biomethane or biohydrogen (Demirbas 2007, Stephens, Ross *et al.,* 2010). Although the Sun generates huge solar power for the Earth, the major problem to be resolved is the low energy storing capability of our existing technologies. Even the use of high-efficient PV panels installed in the Sun Belt region, the collected power density can only be achieved as low as 20 W m^{-2} (US DoE 2010), which in turn results in two major disadvantages: high production costs per unit of power generated and requirements for large surface area. Nevertheless, the former issue can be addressed by biofuels generated from traditional energy crops, at the expense of the latter.

Over last decade, there has been a massive investment in the development of liquid biofuel alternatives to petroleum-based fuels, such as bioethanol and biodiesel, with the US, Brazil and the European Union as major leading nations (Evans 2007). Of all biofuels, bioethanol,

derived from corn and sugarcane, have been the primary recipients of biofuel grants and subsidies. However, these first generation biofuels not only failed to deliver on CO_2 mitigation targets, but also contributed to a host of environmental and socio-economic problems. As the human population continues to rise rapidly, there are greater demands for energy, food, water and arable land. The low power density of first generation biofuels, produced from food crops, results in requirements for large land area that are impractical condition for most European countries. For example, in order to replace petroleum-derived transport fuel by biodiesel, derived from palm oil, it would require to cover an area of 111 million hectares, which is around 61 % of all agricultural cropping land in the United States, with oil palm field (Chisti 2008). According to the World Health Organisation, more than 3.7 billion people, which accounts for 56 % of the global population, are currently malnourished, the cultivation of agricultural crops for biofuels production has led to a heated 'food versus fuel' debate and partially responsible for the world food price crisis in 2008 (Pimentel, Marklein *et al.,* 2009). In some developing tropical countries such as Brazil and Indonesia, deforestation for sugarcane plantations not only damages local biodiversity, but it also diminishes a crucial CO_2 sink (IPCC 2007). Growing energy crops also demands large amounts of water, which would be better used by African nations, where their water reserves are limited, to feed their respective populations (Pimentel, Marklein *et al.,* 2009). In addition, first generation biofuels require ammonium-based fertilisers produced in the fossil fuel intensive Haber-Bosch process during plantation of energy crops. By taking into account carbon footprint of fertiliser, harvesting, processing and land-use, recent life cycle analyses (LCAs) have shown that some first generation biofuels actually increase CO_2 emissions, instead of reducing them (Searchinger, Hamburg *et al.,* 2009).

In order to address several drawbacks listed in the previous paragraph, second generation biofuels, derived from biomass of non-food plants, is being developed (Gomez, Steele-King *et al.,* 2008). The most important of these includes lignocellulosic processes, which convert cellulose-based products from plants such as *Sorghum*, *Miscanthus* and switchgrass (*Panicum virgatum*) into liquid fuels (Stephens, Ross *et al.,* 2010). However, at present, the production of such fuels is still non-commercial, as they remain limited by the same low power density as their predecessors as well as inefficient manufacturing processes (Naik, Goud *et al.,* 2010). In addition to biofuels, electricity generated from renewable energy sources such as wind, solar photovoltaic or nuclear could be used to produce H_2 fuel, via electrolytic water splitting (more detail will be discussed in section 2.5). Produced H_2 can be directly used to power fuel cell vehicles (FCVs) or to generate alternative liquid fuels such as methanol (Taylor 2008). Even today efficiencies of electrolysis systems are higher than those of natural photosynthetic processes; they would be many times more expensive, due to high material costs (Peharz, Dimroth *et al.,* 2007). As the consequence, it is more economically practical to use the renewable electricity as direct power source rather than for production of H_2 fuel. Recent efforts also evolve in the area of artificial photosynthesis, a chemical process that aims to replicate the natural process of photosynthesis, directly splitting water into O_2 and H_2 fuel (Lewis and Nocera 2006, Hammarström, Winkler *et al.,* 2011). Despite its fascinating concept, this approach is still under development. Main challenges include the difficulty in replications of very complex biological photosynthesis, which involves a number of proteins and enzymes, corrosive destruction of materials over time and requirements for efficient, affordable gas separation system, as $H_2 – O_2$ gas mixture is potentially explosive.

Since most crude oil ultimately came from microalgae – green algae and cyanobacteria, which were buried deep under the ground over millions of years ago, therefore it become

certainly plausible that future transport fuels could be obtained from the same source (Schenk, Thomas-Hall *et al.,* 2008). Microalgae are simple photosynthetic microorganisms, which can do photosynthesis at much better efficiencies than terrestrial plants (Blankenship, Tiede *et al.,* 2011), while not competing with agricultural crops for arable land and water resources. As a result, they have a great potential to serve as a viable biofuel source (Posten and Schaub 2009). Full detail of microalgal biofuel production will be explained in section 2.4.

2.4. Microalgae as Biofuel Production Factories

Microalgae are unicellular plants and, like in terrestrial plants, are capable of capturing solar energy and subsequently converting it into chemical energy that can be later released to power organisms' activities. This biochemical reaction is well-known as photosynthesis and fundamentally supports all biofuel synthetic processes (Beer, Boyd *et al.,* 2009). Photosynthesis involves the fixation of CO_2 into intracellular carbon storage products such as carbohydrates and lipids, which can be subsequently used to form biomass. The CO_2 requirement for microalgae is stoichiometrically about 1.7 kg CO_2 per kg dry biomass (Posten and Schaub 2009). Therefore, it becomes a potentially attractive option to use microalgal cultures to capture the CO_2 emitted by fossil fuel combustion in power stations and subsequently produce biomass.

At present, microalgae are at the forefront of research efforts aimed at developing technologies for renewable biofuels production (Dismukes, Carrieri *et al.,* 2008, Schenk, Thomas-Hall *et al.,* 2008). There is a number of different biofuels, which can be extracted from microalgae. The most common approach is to process the microalgal lipid fraction into

biodiesel or jet fuel. The residual biomass of microalgae could then be further used to produce biogas via processes of anaerobic digestion or fermentation (Mussgnug, Klassen *et al.,* 2010). Some species of microalgae can also release a new generation of biofuels such as hydrogen and isoprene as gaseous products during their growth, thereby providing an ease of product collection making them much easier to harvest (Hejazi and Wijffels 2004, Melis 2012).

In comparison with plants, microalgae can achieve higher energy efficiencies of photosynthesis. Numerically, annual averaged efficiencies of 3 % are reported for microalgae, whereas those of crops typically do not exceed 1 % (Blankenship, Tiede *et al.,* 2011). Because of their high photosynthetic efficiency, microalgae can grow extremely fast. Fully grown microalgal cultures can usually be achieved within 10 - 14 days, while it takes orders of months for plants to reach their mature stage. Since microalgae do not need to grow roots, leaves or flowers, therefore they require much smaller geographical footprint and less water for cultivation (Dismukes, Carrieri *et al.,* 2008). Many species of microalgae can grow in diverse extreme conditions such as brackish water, industrial wastewater ponds as well as sea water (Posten and Schaub 2009), making the scalability of microalgal biofuel production facilities become possible without affecting food crops or endangering forested ecosystems (Sheehan, Dunahay *et al.,* 1998). Since a large proportion of their biomass is usable as fuel, microalgae can produce more biofuel than any other plants on an area basis. On average, 30 % of microalgal biomass is composed of lipids (as high as 80 % was previously reported for some genetically engineered species); in comparison with only 5 % of the biomass as lipids in the case of oil palm (Chisti 2008). It was previously estimated that, in order to produce enough quantities of biodiesel for meeting 50% of transport fuel needed in the United States, 24 % of the total cropland would be required for oil palm plantation, while, for microalgal

cultivation, only 1 – 3 % of the total area would be sufficient (Chisti 2007). With their superior features over terrestrial plants, microalgal biomass is often classified as the third generation biofuel (Posten and Schaub 2009).

Although microalgal biofuel system could be the solution to the great energy challenge of humanity, to date none of such systems have achieved economic viability (Stephens, Ross *et al.,* 2010). The major barriers for microalgae-based fuel commercialisation include: requirements for photobioreactors that are affordable for large-scale deployment, selection and / or development of more productive microalgal species and requirements for more energy-efficient and cost-effective downstream processing of biomass (Hannon, Gimpel *et al.,* 2010). A recent economic case study also indicates the potential opportunity of improving the financial state of microalgal biofuel production by introducing co-production of high-value products (HVPs) from microalgal biomass (Stephens, Ross *et al.,* 2010). This multiproduct paradigm, extensively known as the microalgal biorefinery concept, enables the maximum utilisation of microalgal materials as well as operational processes to subsequently generate multiple streams of revenue (Subhadra 2010, Patel, Tamburic *et al.,* 2012). Figure 2.1 shows how different parts of the microalgal cell that could be used in the biorefinery. In contrast with microalgae-based biofuel, cultivation of microalgae for HVP extraction is already a mature and very profitable industry (Spolaore, Joannis-Cassan *et al.,* 2006). Biomass of some microalgae such as green alga *Chlorella* and cyanobacterium (blue-green alga) *Arthrospira platensis* (also known as *Spirulina*), usually contains high level of protein and is typically used to produce valuable commodities such as vitamins, dyes, pharmaceuticals, insecticides and various precursor chemicals. The success of microalgal HVPs means that some of the infrastructure required for starting up microalgal biofuels already exists.

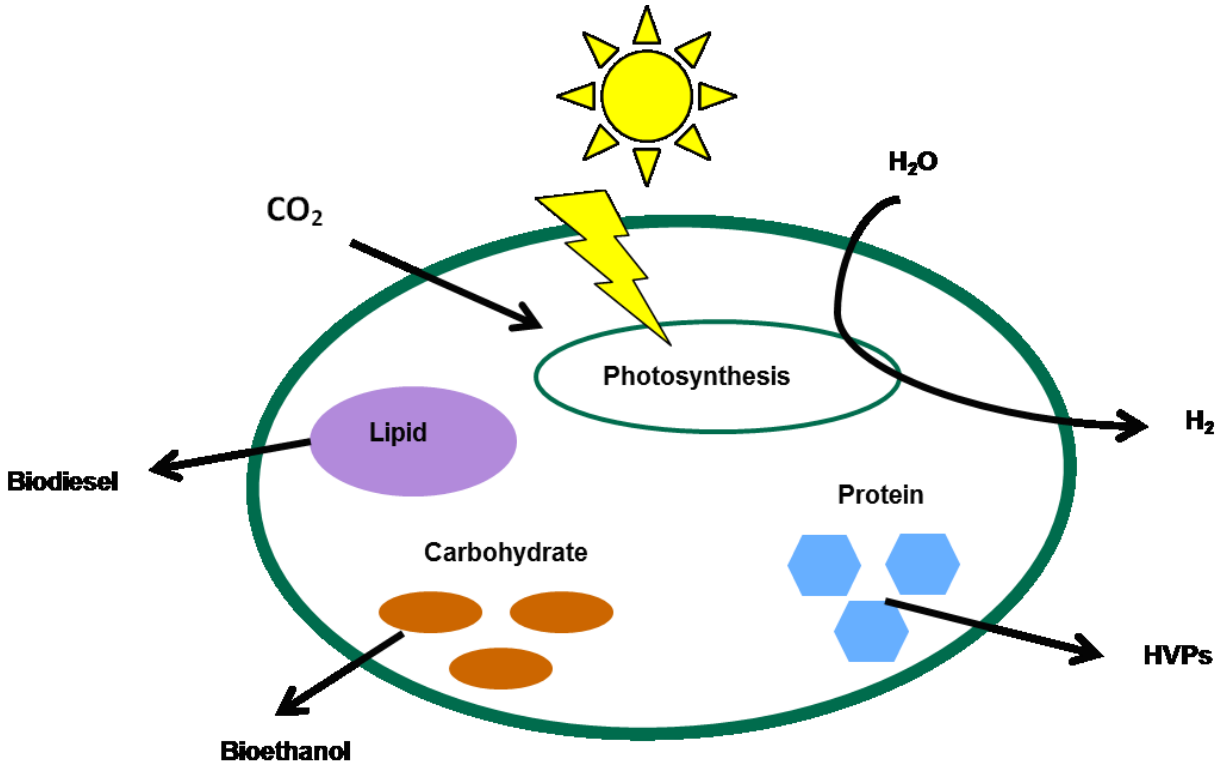

Figure 2.1: Schematic diagram of microalgal biorefinery.

Adapted from (Beer, Boyd et al. 2009)

2.5. Hydrogen as a Sustainable Fuel

Over the last decade, interest in molecular hydrogen (H_2) as a fuel and energy carrier has internationally grown as a response to increasing concerns over environmental and energy security issues (Ricci, Bellaby *et al.,* 2008). Following, a significant number of H_2 research and demonstration projects have been developed, with the parallel development of "hydrogen economy", which represents a system that promotes H_2 as a mean of delivering energy in order to solve some of negative effects of a fossil fuel-based economy (US DoE 2008). Nevertheless, H_2 fuel is still at a relatively early stage of development and has been limited to some applications in the space sector. Currently, the largest demand of H_2, over 53 million metric tons per year (Mt yr^{-1}), is commercially primarily for petroleum refinery, the manufacture of ammonia-based fertilisers and petrochemicals and glass purification (US DoE 2008). The market value of global H_2 production was estimated to be $ 82.6 billion, with an annual growth rate of 5.6 %.

Even hydrogen is the most abundant element in the universe; it does not naturally exist in its elemental form on Earth. Pure hydrogen can only be produced from hydrogen-containing compounds, such as fossil fuels and biomass. Hydrogen gas is a diatomic molecule; under standard temperature and pressure, it exists as a colourless, odourless and tasteless gas, which is lighter than air (Hemmes, A. *et al.,* 1986). Only a trace quantity of H_2 is present in atmospheric air. On combustion, H_2 produces only heat energy and water and hence it is considered to be the cleanest and carbon-neutral fuel (Momirlan and Veziroğlu 1999). In addition, with its high energy per unit mass of 143 kJ g^{-1}, which is approximately 3 times higher than that of petrol (46 kJ g^{-1}) (Hemmes, Driessen *et al.,* 1986), H_2 is regarded as an

ideal fuel for transportation uses. However, due to a very low energy per unit volume of H_2 (US DoE 2008), this raises some significant storage challenges.

H_2 can be efficiently converted into electricity, at low temperatures, using proton exchange membrane (PEM) fuel cells (Levin, Pitt *et al.,* 2004), with conversion efficiencies of 50%, compared with a 20% efficiency of petrol in an internal combustion engine (Barbir 2005). However, due to the use of expensive platinum catalyst, PEM fuel cells are consequently uneconomical at present, although there has been significant research and progress in this area recently (US DoE 2005). Fuel cell vehicles (FCVs), which are fuelled with hydrogen, emit only water, with no gaseous pollutants such as CO_2, nitrous oxide or sulphur oxide, they are hence considered zero emission vehicles at the point of use. At present, compressed gaseous H_2 fuel of FCVs is stored in a fuel tank pressurised to 350 - 700 bar (US DoE 2008). This is not an ideal solution, because the fuel tank is still much larger and heavier than what is ultimately desired for light-duty vehicles (US DOE 2008). Alternative options for H_2 storage are under development and include cryogenic liquid and material storage in metal hydrides, carbon-based structures, high surface area sorbents or other chemical hydrogen storages (US DoE 2008). In addition to technological challenges, H_2 would also need to be accepted by the general public, who often associate hydrogen with fire and explosions, particularly with the Hindenburg airship disaster and with the hydrogen bomb (Ricci, Bellaby *et al.,* 2008). This issue could be resolved by a carefully-planned policy of public consultation and education, which will help convincing members of the public to accept H_2 as a fuel, as well as to potentially be prepared to pay more for a sustainable H_2 economy.

In order to be economically competitive with petroleum, whose current price is at approximately $ 2 - 3 per gallon (March 2015), the US Department of Energy (US DOE) has

set a target price of $ 2.6 per kg H_2 for renewable H_2 technologies (Amos 2004), assuming no taxation of the H_2 fuel (Bartels, Pate *et al.,* 2010). Today, most H_2 is industrially produced through thermochemical steam reforming of methane at high temperatures (700 – 1000 ^oC) (Momirlan and Veziroğlu 1999). Methane reforming is regarded as the most cost-effective process, with the current cost of produced H_2 in the order of $3 per kg H_2 (Bartels, Pate *et al.,* 2010). However, its major disadvantage is significant CO_2 emissions (Christopher and Dimitrios 2012), which therefore negates the primary benefit of using H_2 as a fuel. To be genuinely clean, it is important that H_2 itself is also produced by an equally environmentally benign, as well as economical, process. The production of H_2 generally fall into three categories – thermal, electrolytic, and photolytic processes (US DoE 2008).

Decarbonisation of H_2 production could be achieved via the gasification of coal coupled to carbon capture and sequestration (CCS) technologies, which are being developed to separate CO_2 at the point of production and store it in deep underground geologic formations. Alternatively, biomass could also be used as feedstock to produce H_2 via gasification, with the near-zero emission of greenhouse gases, as biomass resources often consume CO_2 as part of their natural growth processes. Clean H_2 production could also be carried out using electrolytic processes, which directly use electricity, derived from nuclear or renewable sources such as solar or wind, to split water into H_2 and O_2. The cost of H_2 produced from the gasification of coal and biomass would cost approximately $ 1 and $ 1 - 3 per kg H_2 respectively (Bartels, Pate *et al.,* 2010). However, the requirement of CCS for decarbonising the coal gasification would certainly raise its price of H_2 production. The disadvantages of using biomass from traditional energy crops have already been discussed in section 2.3. For electrolytic processes, the price of H_2 production was estimated to be $ 7 per kg H_2 for nuclear power and $ 6 - 22 per kg H_2 for renewable sources, where wind power and solar PV

are the most and the least economical sources, respectively (US DoE 2009, James, Baum *et al.,* 2009). The high H_2 production cost of electrolysis is due to an initial requirement for the generation of electricity, followed by the subsequent process of water splitting, which is at its best efficiency of 14% (Topic, Brecl *et al.,* 2006). In addition, it would be more practical to directly use the generated electricity, in the first place, rather than use it to produce H_2.

As discussed previously in section 2.4, microalgae – green algae and cyanobacteria, are superior to terrestrial plants, due to their faster growth rates as well as capability to attain higher biomass and biofuel yields, without competing for arable lands (Wijffels and Barbosa 2010). These outstanding features potentially offer more economical biofuel, including biohydrogen, production from microalgae (Benemann 1999). In addition, some microalgal strains are also capable of releasing H_2 directly from the cell culture, without the need for energy-intensive drying, processing and gasification processes (Das and Veziroğlu 2001). There are three main routes of direct biohydrogen production from microalgae: dark fermentation, photofermentation and biophotolysis.

2.6. Biohydrogen Production

Biological H_2 production processes can be classified into two groups, depending on whether the process is light-dependent or not. Dark fermentation is a light-independent process. The light-dependent processes can be further classified into either a photosynthetic or a fermentation process. The detailed description of each process can be found from sections 2.6.1 to 2.6.3. Advantages and disadvantages between different processes are also summarised in Table 2.1.

2.6.1. Dark Fermentation

Dark fermentation is by far considered as the most practical biological H_2 production process (Levin, Pitt *et al.,* 2004, Brentner, Peccia *et al.,* 2010), due to its high volumetric H_2 productivity, an ease of process operation and inexpensive feedstock, usually organic acids collected from various sources of wastewater. This process is carried out most efficiently by strict anaerobes such as *Clostridium* and facultative anaerobic bacteria such as *Escherichia coli* (Hallenbeck and Benemann 2002, Mathews and Wang 2009). During the operation, these bacteria are cultivated using carbohydrate-rich organic substrates such as glucose, sucrose under dark environment. These substrates are degraded by an oxidative reaction to provide building blocks and metabolic energy for bacterial growth. The oxidation also generates electrons, which, in an oxic environment, would reduce O_2 to water. In anaerobic conditions, other compounds such as protons need to act as electron acceptor and are subsequently reduced to form H_2.

In the case of glucose fermentation, glucose is initially converted into pyruvate by the glycolytic pathways. The oxidation of pyruvates then produces acetyl-coenzyme A (acetyl CoA), which can later be converted to acetyl phosphate and results in the generation of the energy carrier adenosine triphosphate (ATP) as well as the excretion of acetic and butyric acids (Nath, Kumar *et al.,* 2005). Pyruvate oxidation also requires the reduction of the electron carrier ferredoxin (Fd). Reduced Fd is re-oxidised by the hydrogenase enzymes to produce H_2.

Dark fermentation redox pathways:

$$\text{Pyruvate} + \text{CoA} + 2\text{Fd}_{\text{oxidised}} \rightarrow \text{Acetyl-CoA} + 2\text{Fd}_{\text{reduced}} + \text{CO}_2$$

$2H^+ + 2Fd_{reduced} \rightarrow H_2 + 2Fd_{oxidised}$

Glucose dark fermentation reaction:

$C_6H_{12}O_6$ (glucose) + $2H_2O \rightarrow 2CH_3COOH$ (acetic acid) + $4H_2 + 2CO_2$

$C_6H_{12}O_6$ (glucose) $\rightarrow CH_3CH_2CH_2COOH$ (butyric acid) + $2H_2 + 2CO_2$

Theoretically, the maximum H_2 yield of dark fermentation is 4 mol H_2 mol^{-1} of glucose if all of the glucose is completely metabolised to only H_2 and acetate (Hallenbeck and Benemann 2002). In actual practice, dark fermentation normally leads to the formation of the number of side products, such as acetic, propionic, butyric acids and ethanol (Hallenbeck and Ghosh 2009) and subsequently results in approximately 2 – 3 mol H_2 mol^{-1} of glucose (Sen, Manish *et al.,* 2008). In term of volumetric productivity, dark fermentative H_2 production rate is within a range of 1,000 - 1,500 ml of H_2 per litre of culture per hour (ml H_2 L^{-1} hr^{-1}) (Hallenbeck, Abo-Hashesh *et al.,* 2012). Due to co-formation of various fermentative products, the concentration of produced H_2 is between 40 – 60 % volume H_2 $volume^{-1}$ effluent gas (Sen, Manish *et al.,* 2008). This high impurity of fermentative effluent gas cannot be fed directly to fuel cell applications and an additional purification step is required.

2.6.2. Photofermentation

Photofermentation is a light-dependent photoheterotrophic process carried out by purple non-sulphur photosynthetic bacteria, using carbon substrates, typically organic acids and alcohols, together with the solar energy captured by their photosystem to produce H_2. Similar to dark fermentation, organic acids are initially oxidise to produce ATP and electrons, at which the latter are used to reduce Fd (Das and Veziroğlu 2001). But in this case, reduced Fd is re-

oxidised by the nitrogenase enzymes, which catalyse the N_2-fixation reaction. During nitrogen-fixing reaction, electrons reduce dinitrogen (N_2) into ammonia (NH_3), at the same time producing H_2 as by-product (Akkerman, Janssen *et al.,* 2002). With a pure N_2 atmosphere, the ratio of an electron allocation for the N_2 reduction and H_2 formation would be at 3 : 1 (Tamagnini, Axelsson *et al.,* 2002). However, in the absence of N_2, bacteria are capable of diverting all of the fermentative electrons towards H_2 production, enhancing the stoichiometric H_2 yield by a factor of 4 (Yeager, Milliken *et al.,* 2011).

Photofermentation reaction: $2CH_3COOH$ (acetic acid) + $4H_2O \rightarrow 4CO_2 + 8H_2$

N_2-fixation:

In the presence of N_2: $N_2 + 8H^+ + 8e^- + 16ATP \rightarrow 2NH_3$ (ammonia) + H_2 + 16ADP + $16P_i$

In the absence of N_2: $8H^+ + 8e^- + 16ATP \rightarrow 4H_2 + 16ADP + 16P_i$

As N_2-fixation is an irreversible process, it permits an unidirectional conversion of substrates into products. In addition, photosynthetic bacteria are also useful in converting organic wastes to H_2 and CO_2 (Hallenbeck and Ghosh 2009), with a very high purity of 96% volume H_2 volume^{-1} effluent gas (Tao, He *et al.,* 2008). However, the process suffers from low light conversion efficiencies and a high energy demand by the nitrogenase enzymes (16 moles of ATP is required per mole of N_2 fixed). In term of productivity, H_2 production rates of 12 - 83 ml H_2 L^{-1} hr^{-1} have been previously reported (Hallenbeck, Abo-Hashesh *et al.,* 2012).

2.6.3. Biophotolysis

Biophotolysis is a completely sustainable H_2 production process, as H_2 is produced from the world's two most plentiful resources – sunlight and water. Once it has been used up as a fuel, H_2 also returns to water. Biophotolytic H_2 production process can be classified into two types – direct and indirect. For direct biophotolysis, the photosystem II (PSII) protein complex within the chlorophyll (Chl) of green algae and cyanobacteria captures sunlight and utilises this energy to dissociate water into its constituents – protons (H^+), electrons (e^-) and oxygen (O_2). The photosynthetic electrons are transported by Fd and other intermediates to the hydrogenase enzyme, which catalyses the recombination reaction of proton-electron to eventually produce H_2 (Esper, Badura *et al.,* 2006). However, as hydrogenase is rapidly inactivated by photosynthetically evolved O_2, the direct biophotolytic H_2 production is only possible when the cultures are incubated under some special conditions such as sulphur-deprivation of green alga *Chlamydomonas reinhardtii* (*C. reinhardtii*) culture (Melis, Zhang *et al.,* 2000, Kosourov, Tsygankov *et al.,* 2002). Fundamentally, sulphur is a key component of the *C. reinhardtii*'s photosynthetic mechanism, since it is required to repair the D_1 protein, a major component of the PSII reaction centre (Ghirardi, Dubini *et al*., 2009). As a result, sulphur-limitation leads to the significant reduction in the rate of photosynthesis and its concurrent O_2 evolution, while having minimal effect on the cellular respiration rate (Melis, Zhang *et al.,* 2000). Due to the greater rate of respiration than photosynthesis of the cells, after about 24 to 30 hr of sulphur deprivation, the *C. reinhardtii* culture would become anaerobic in the light and subsequently start to produce H_2.

Direct biophotolysis reactions:

Water-splitting process: $2H_2O \rightarrow O_2 + 4H^+ + 4e^-$

Proton-electron recombination: $2H^+ + 2e^- \rightarrow H_2$

In the case of indirect biophotolysis, electrons from water are used in the carbon fixation of the Calvin cycle and subsequently stored in some form of endogenous reserve carbohydrates, which are later used to produce H_2. The process, which re-converts carbohydrates into electrons, is known as cellular respiration. The indirect biophotolytic H_2 production is usually found in many nitrogen-fixing cyanobacteria (blue-green algae), in which photosynthetic O_2 evolution and its incompatible H_2 production reactions are temporarily or physically separated from each other (Hansel and Lindblad 1998).

Indirect biophotolysis reactions:

Oxygenic photosynthesis: $6CO_2 + 6H_2O \rightarrow C_6H_{12}O_6 + 6O_2$

Aerobic cellular respiration: $C_6H_{12}O_6 + 6O_2 \rightarrow 6CO_2 + 6H_2O + \text{Energy}$

As nitrogenase enzymes are also sensitive to O_2, heterocystous cyanobacteria such as *Anabaena* sp. PCC 7120, contain a specialised biological structure called a heterocyst, a differentiated low-O_2 compartment within the cell, which allows its N_2-fixation to be spatially separated from photosynthetic process (Yeager, Milliken *et al.,* 2011). For non-heterocystous cyanobacteria, such as *Cyanothece* sp. ATCC 51142, even it does not possess the heterocyst; it is still capable of temporally separating photosynthesis and N_2-fixation by carrying out these two incompatible metabolisms during different time period of a day – light and dark periods respectively (Bandyopadhyay, Stoeckel *et al.,* 2010).

Table 2.1: Different biological H_2 production processes and their advantages and disadvantages

Process	Dark fermentation	Photofermentation	Biophotolysis
Organisms	Strict anaerobes and facultative anaerobes	Purple non-sulphur photosynthetic bacteria	Green algae and cyanobacteria
Substrate	Organic acids	Organic acids	Water
Light dependence	No	Yes	Yes
H_2 productivity (ml H_2 L^{-1} hr^{-1})	1,000 – 1,500	12 - 83	2.5 - 13
Purity of H_2 (% vol H_2 vol^{-1} effluent gas)	40 - 60	90 - 96	Almost 100
Advantages	Simple operation High H_2 productivity Capable of using various types of wasted substrates	High purity of H_2 Nearly complete conversion Capable of using various types of wasted substrates	Very abundant, inexpensive substrate
Disadvantages	Many side products Low purity of H_2	Low-light conversion efficiencies Low H_2 production rate	Incompatibility between photosynthetically evolved O_2 and H_2-evolving catalyst Extremely low H_2 production rate

2.7. Summary

Today power, driving the world, is dominantly provided by fossil fuels, which at the same time intensively pollute our ecosystem with greenhouse gases. Increasing environmental concerns has led to an increase in global interest and investment in sustainable energy sector. Solar energy, coming from the Sun, is by far the only renewable energy resource that is large enough to meet energy demand of humanity. Since the electricity generation by PV systems remains prohibitively expensive, there are large market and business opportunities for solar biofuels, traditionally produced from biomass of food crops e.g. corn and sugarcane.

Due to low power density of traditional energy crops, there are significant requirements for arable land and agricultural resources (such as water and fertiliser), which has led to the food versus fuel and food versus forest issues. Photosynthetic microalgae - green algae and cyanobacteria – possess a number of superior features over terrestrial plants, and could replace crops for biofuel production. Microalgae do photosynthesis at high efficiencies; they grow fast and a large percentage of their biomass is usable as fuel. Commercial cultivation of microalgae for various HVPs (e.g. vitamins, pharmaceuticals and human nutrition) is already a reality, while microalgal biofuels are under research development. Biofuels can be extracted from microalgal biomass (e.g. biodiesel and bioethanol) as well as released as gaseous products (e.g. hydrogen and isoprene) during microalgal growth. A concept of microalgal biorefinery represents a promising approach to significantly improve an economic viability of microalgal biofuel productions, as it enables multiple products manufacturing with the added advantage of utilising all microalgal components and generating several revenue streamlines. H_2 is the cleanest and most efficient available fuel, making it suitable as an alternative and sustainable energy carrier of the future. However, the utilisation of H_2 as fuel remains in an

early stage of development and is limited to space applications. A hydrogen economy would require development of more-efficient PEM fuel cell and H_2 storage technologies as well as sustainable and economical H_2 production. The direct biohydrogen production can be carried out in three biological processes: dark fermentation, photofermentation and biophotolysis.

3. Biohydrogen Production by *Cyanothece* sp. ATCC 51142

3.1. Selection of Studied Species: Introduction to *Cyanothece* sp. ATCC 51142

Cyanothece sp. ATCC 51142 (*Cyanothece* 51142) is a marine, unicellular, non-heterocystous, nitrogen-fixing cyanobacterium (blue-green alga), which was isolated from the intertidal sands of the Texas Gulf coast (temperature varies within a range of 20 – 35 ^{o}C) (Reddy, Haskell *et al.,* 1993). Individual cells of *Cyanothece* 51142 are spherical and have approximately 4 to 5 μm in diameter. Its cell division proceeds by binary fission. An oxygenic photosynthesis of *Cyanothece* 51142 is virtually identical to higher plants and green algae, except for the difference in accessory pigments. The cyanobacterium captures the solar energy using two essential light-harvesting units - chlorophyll a and phycobilins (Tucker and Sherman 2000). Chlorophyll a is housed inside the thylakoid membranes, whereas phycobilins, usually organised into hemispherical phycobilisomes, which are attached to the outside of the thylakoid membranes. *Cyanothece* 51142 belongs to the genus of *Cyanothece*, which was separated from the *Synechococcus* spp. genus (Reddy, Haskell *et al.,* 1993).

As the laboratory wild type (WT) *Cyanothece* 51142 strain has an ability to aerobically produce H_2, albeit the highest rate was observed under anaerobic conditions (Bandyopadhyay, Stoeckel *et al.,* 2010), it is used as a model organism for bioenergy research and studies on how a unicellular organism balances multiple, often incompatible, photosynthetic and N_2-fixation processes within the same cell (Sherman, Min *et al.,* 2010). Like many oxygenic cyanobacteria, *Cyanothece* 51142 possesses both hydrogenase and nitrogenase enzymes, which are directly involved with its

biological H_2 formation reaction (Hansel and Lindblad 1998). However, the catalytic activity of nitrogenase is reported to be predominant for the H_2 formation by this particular strain (Min and Sherman 2010). In addition to standard photoautotrophic conditions, *Cyanothece* 51142 has advantageous growth flexibility and is able to grow under various conditions - photo/chemoheterotrophic and mixotrophic conditions (Schneegurt 1994, Schneegurt, Sherman *et al.,* 1997, Feng, Bandyopadhyay *et al.,* 2010). In term of its biochemistry studies, the genome of *Cyanothece* 51142 has been successfully sequenced (Welsh, Liberton *et al.,* 2008) and subsequently reveals many interesting features at both the transcriptional (ColonLopez, Sherman *et al.,* 1997, Meunier, ColonLopez *et al.,* 1998) and proteomic (Aryal, Callister *et al.,* 2013) levels. Nevertheless, studies on its metabolome and transcriptome are still in progress.

This chapter will explore the biochemistry of *Cyanothece* 51142 biohydrogen production, covering both the biophotolytic and fermentative routes. The parameters that affect the growth and H_2 production of *Cyanothece* 51142 will be documented and analysed. This will include the rationale behind choosing the particular *Cyanothece* 51142 strain that was used in this thesis. The photobioreactor (PBR) design challenges and geometries will be reviewed. Finally, the issues surrounding the process design, scale-up, costs and efficiencies of biohydrogen production by *Cyanothece* 51142 will be discussed.

3.2. Biochemistry of Biohydrogen Production

Cyanothece 51142 is capable of producing H_2 via either an indirect biophotolysis or photofermentation. Under the standard photoautotrophic growth condition, the cyanobacterium carries its biophotolytic H_2 production using electrons and energy from its endogenous reserve carbohydrates, which are photosynthetically synthesised. When *Cyanothece* 51142 culture is

supplied with an organic carbon, typically glycerol, the cyanobacterium undergoes photoheterotrophic growth condition and ferments the substrate to produce H_2.

3.2.1. Biophotolytic H_2 Production

Non-heterocystous cyanobacteria such as *Cyanothece* 51142 are photoautotrophic microorganisms, which employ a cyclic metabolic switch strategy to protect their O_2-sensitive nitrogenase from photosynthetically produced O_2 (Hansel and Lindblad 1998), as shown in Figure 3.1. During day time, the cyanobacterium captures solar energy and converts it into some stable forms of biosynthesised intracellular carbohydrates via photosynthesis. Upon an arrival of dark period, photosynthetic activity is temporarily deactivated, whereas cellular respiration becomes active (ColonLopez, Sherman *et al.,* 1997). The high rate of *Cyanothece* 51142 respiration subsequently causes of the total depletion of O_2 level within the cells and thereby inducing an anoxic environment, which is necessary for an activation of nitrogenase enzymes (Bandyopadhyay, Stoeckel *et al.,* 2010). Chemical energy and electrons, required to power the N_2-fixation reaction, are also derived back from an oxidation of intracellular carbohydrates via cellular respiration. In this section, the biochemistry of indirect biophotolytic of *Cyanothece* 51142 strain will be explained in sequential stages, starting with how solar energy is photosynthetically captured, stored and eventually converted into chemical energy in the form of H_2 energy carrier.

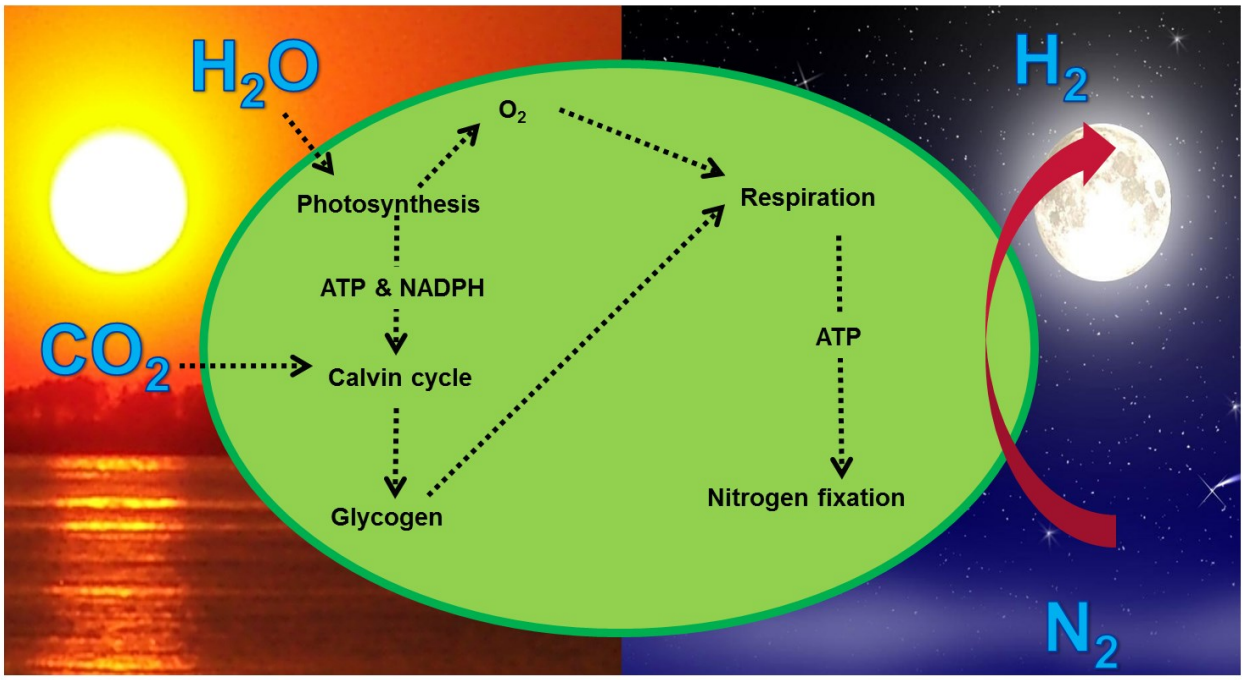

Figure 3.1: Schematic diagram of biophotolytic H_2 production of *Cyanothece* 51142. Adapted from (Welsh, Liberton et al. 2008).

3.2.1.1. Oxygenic Photosynthesis

Photosynthesis is a radical energy storage system naturally possessed by oxygenic photoautotrophs – plants, green algae and cyanobacteria (Blankenship 2008). The process consists of two sub-processes, taking place in sequence: 1) light-dependent reaction and 2) light-independent reaction (dark reaction). The photosynthetic light reaction of *Cyanothece* 51142 begins with the absorption of light by two essential light-harvesting antenna systems - chlorophyll (Chl) a and phycobilins. Pigmented Chl a biomolecules are grouped together to form light-harvesting complex (LHC) proteins. LHC proteins arrange themselves into light-harvesting antennae, which are bound into two multi-membrane protein complexes: photosystem I (PSI) and PSII. In contrast, phycobilins are only present in cyanobacteria, at which they are organised together in large multi-protein complexes,

called phycobilisomes (PBSs) (Shevela, Pishchalnikov *et al.,* 2013). The light-harvesting photosystems and most of the photosynthetic electron transport chain involved in the photosynthesis process are located within the thylakoid membrane: an internal membrane system that separates the cytoplasm of cyanobacterial cells from their lumen (Peschek 1999).

3.2.1.2. Photosynthetic Electron Transport

Photosynthetic electron transport is the light-driven biological process, essentially facilitating the production of the energy-rich compounds – adenosine triphosphate (ATP) and reduced nicotinamide adenine dinucleotide phosphate (NADPH), from electrons, which are derived from water photolysis. The energy stored in both ATP and NADPH is later used for biosynthesis of intracellular carbohydrates via the reactions of CO_2 fixation. The pattern of cyanobacterial electron transport chain is similar to those of plants and green algae (Peschek 1999) and commonly represented by the Z-scheme arrangement (Figure 3.2). Upon the light absorption, the building block of pigmented Chl a and PBSs antenna systems transfer the energy of absorbed light to the reaction centre pigments of PSII and PSI, where the electrons within the reaction centres are excited into the higher energy level. This deficiency of electrons in photosystem II can be fulfilled by electrons extracted from water. In order to re-gain their stabilisation, excited electrons from photosystem II move through the electron transport chain (PQ – cyt b_6/f – PC, PQ: plastoquinone pool, cyt b_6/f: cytochrome b_6/f complex and PC: plastocyanin) in the thylakoid membrane to the lower-energy electron acceptor in photosystem I, at the same time inducing a proton electrochemical potential gradient across the membrane, which subsequently drives ATP synthase for the production of ATP. Upon their arrival to photosystem I, electrons are re-excited by solar energy and eventually trapped by ferredoxin (Fd). The Fd carries electrons to the enzyme ferredoxin

oxidoreductase (FNR), which then reduces an oxidised nicotinamide adenine dinucleotide phosphate ($NADP^+$) to NADPH (Melis and Happe 2004, Ghirardi, Dubini *et al.,* 2009).

In addition, cyanobacteria are also capable of deriving additional ATP through cyclic electron transport mechanism (shown as blue line on Figure 3.2). During this process, the produced NADPH donates electrons back into PQ via the NADPH-dehydrogenase enzyme (ND) (Melis and Happe 2004). The flow of these electrons to Fd via the thylakoid membrane then creates an additional proton gradient (Iwai, Takizawa et al. 2010). Generally, the cyclic electron transport pathway is employed, when microalgae are placed under an extracellular stress conditions such as nutrient deprivaiton or photoinhibition (Melis 2007). This process may be repaeted until sufficient amount of ATP has been generated to overcome the stress.

Light reaction of photosynthesis: $2H_2O + 2NADP^+ + 3ADP + 3P_i \rightarrow O_2 + 2NADPH + 3ATP$

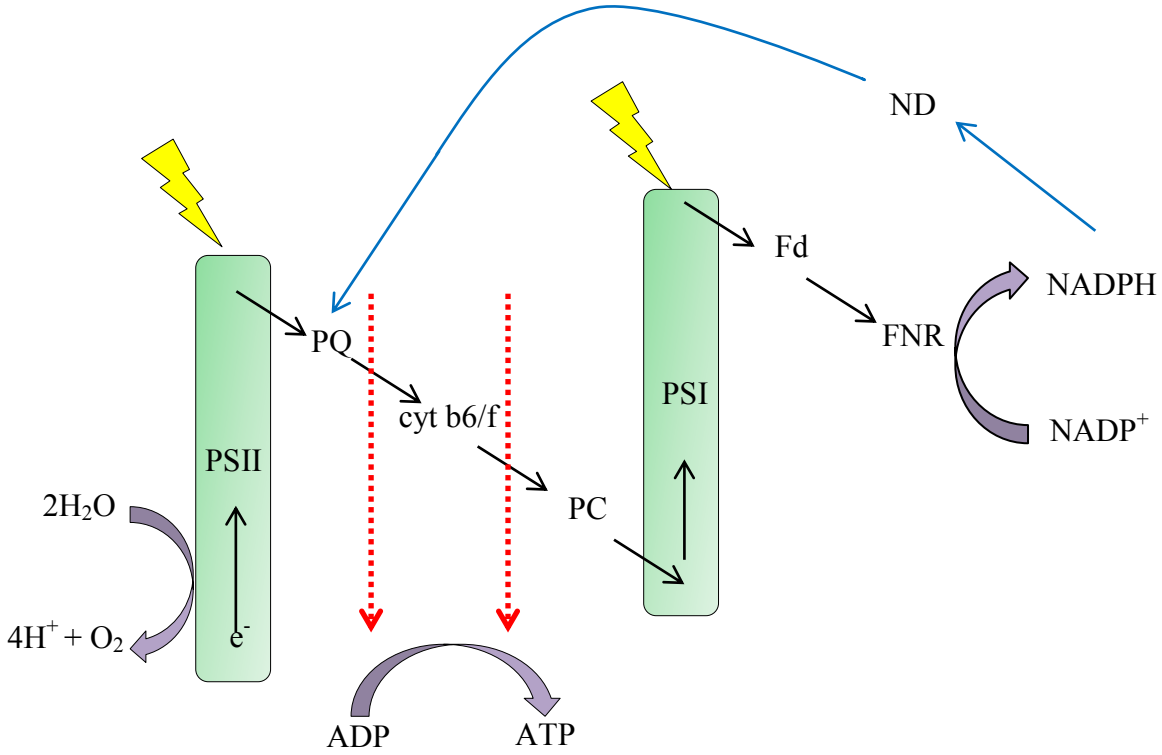

Figure 3.2: Schematic diagram of photosynthetic electron transport pathway in *Cyanothece* 51142. Black arrows show the direction and the movement of noncyclic electron transfer pathway. Blue arrows show the direction and the movement of cyclic electron transfer pathway. Red arrows show the proton flow through the thylakoid membrane. Adapted from (Blankenship 2008, Ghirardi, Dubini *et al*., 2009).

3.2.1.3. CO_2 Fixation

As shown in Figure 3.3, the secondary light-independent stage of photosynthesis is essentially the multi-stage cyclic reduction of atmospheric CO_2 into reserve carbohydrates with the utilisation of both ATP and NADPH energy carriers, being synthesised during the primary light-dependent stage. This metabolism is extensively known as the Calvin-Benson-Bassham (CBB) cycle, which is catalysed by the ribulose-bisphosphate carboxylase enzyme (RubisCO) (Boyle and Morgan 2009).

The primary product of the Calvin cycle is glyceraldehyde 3-phosphate (G3P), which is then grouped together to form glucose, monosaccharide sugars, which in turn pack together as insoluble polysaccharides such as starch (simply denoted as $(CH_2O)_n$). For *Cyanothece* 51142 cells, the carbohydrate reserve is the second highest content of the cyanobacterial chemical composition and accounted for approximately 25 – 34 % of its dry biomass weight (the highest chemical reserve is protein ~ 52 – 60 %) (Schneegurt, Arieli *et al.,* 1995). The intracellular carbohydrate of *Cyanothece* 51142 strain is stored in large interthylakoidal granules and chemically identified as glycogen ($C_{24}H_{42}O_{21}$) (Reddy, Haskell *et al.,* 1993, Schneegurt 1994, Schneegurt, Sherman *et al.,* 1997). The size of the *Cyanothece* 51142 glycogen granule is estimated to be up to 36 nm and its structure appears to be composed of multiple glycogen chains.

Dark reaction of photosynthesis: $CO_2 + 2NADPH + 2H^+ + 3ATP \rightarrow (CH_2O)_n$ (starch) $+ O_2 + 2NADP^+ + 3ADP + 3P_i$

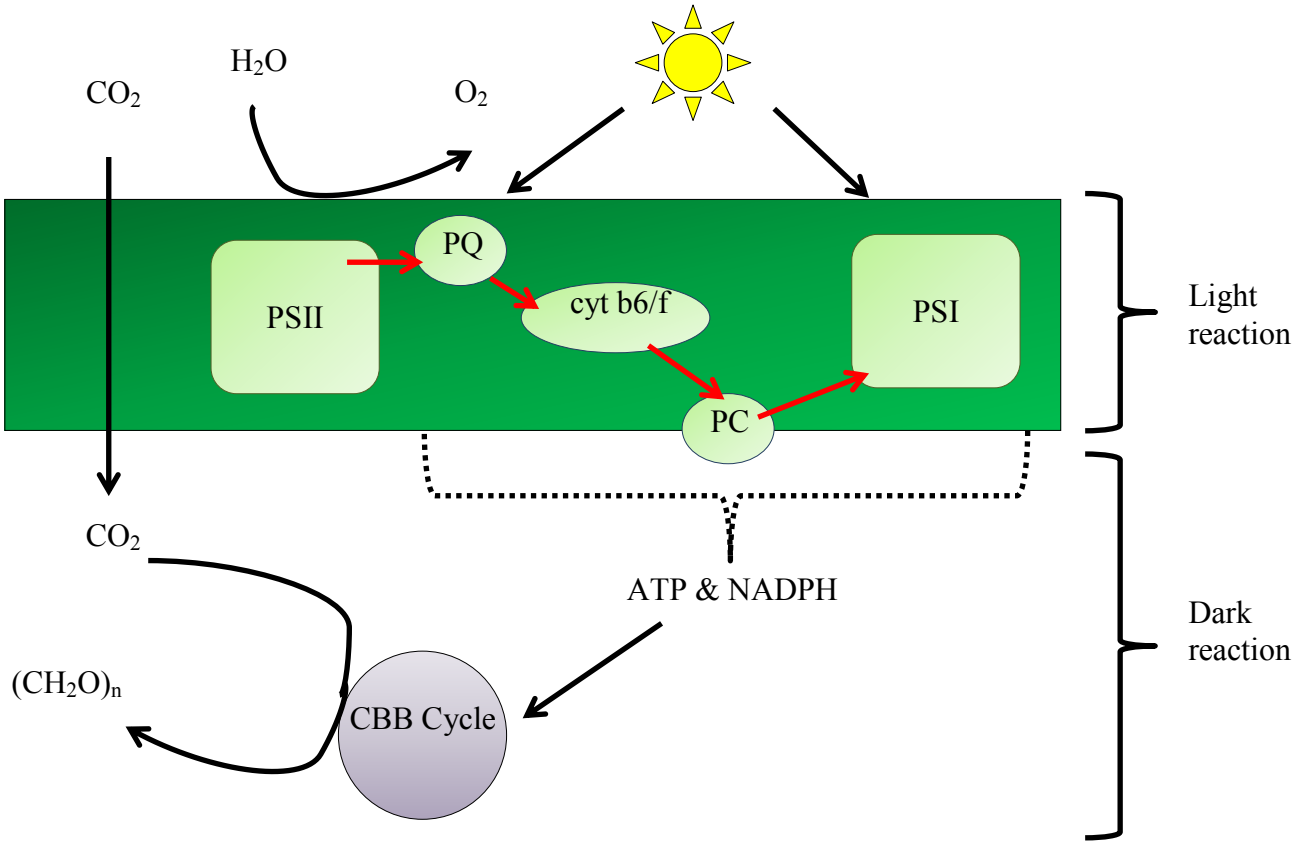

Figure 3.3: Schematic diagram, simply summarizing oxygenic photosynthesis process. Light energy captured by cell's harvesting pigments is utilised to split water. Electron transport chain inside the membrane, represented by red arrow, induces the synthesis of ATP and NADPH during light reaction. In subsequent dark reaction, both ATP and NADPH are then used to fix CO_2 into organic carbon compounds, $(CH_2O)_n$. Adapted from (Lange, Rujan et al. 2000, Withers and Keasling 2007, Allakhverdiev, Kreslavski et al. 2009, Kirchman 2012)

3.2.1.4. Aerobic Respiration

During dark periods, *Cyanothece* 51142 carries out an aerobic cellular respiration, which is basically an inverse process of photosynthesis, since it involves a set of metabolic reactions converting carbohydrate reserve back into chemical energy, as shown in Figure 3.4. This energy is then utilised to fuel basic physiological functions of microorganisms, including growth, motivity and cell maintenance as well as several energy-dependent biochemical reactions such as H_2 evolution (Melis, Zhang *et al.,* 2000). The respiration begins with a catabolic process of glycolysis,

at which large molecules of intracellular carbohydrate compound undergo an oxidative breakdown, using O_2 evolved from the photosynthetic water splitting process as the oxidising agent, into smaller ones, so called pyruvates. Pyruvate is an important intermediate for many biochemical reactions. It serves as the primary compound for production of amino acid alanine, which can be further used for the biosynthesis and repair of proteins (Grossman, Catalanotti *et al.,* 2011). Under anaerobic conditions, it can also be converted via fermentation into lactate or ethanol (Welsh, Liberton *et al.,* 2008). After glycolysis, produced pyruvates go through an oxidative decarboxylation process, at which they are oxidised to acetyl-CoA and CO_2 by the pyruvate dehydrogenase complex (PDC) enzyme. The former intermediate then moves into the tricarboxylic acid (TCA) cycle, at which it is fully oxidised by O_2 to produce CO_2 and reduced nicotinamide adenine dinucleotide (NADH). The NADH generated from the TCA cycle is then fed into the electron transport, where it is used to produce further ATP. In addition, fatty acids, used for the biosynthesis of triacylglycerides (TAGs) and other lipids, are also originated from acetyl-CoA (Chisti 2007).

Overall aerobic respiration: $C_6H_{12}O_6$ (glucose) + $6O_2 \rightarrow 6CO_2 + 6H_2O$ + Energy

Glycolysis: Glucose + $2NAD^+ + 2P_i + 2ADP \rightarrow 2$Pyruvate + 2NADH + $2ATP + 2H^+$

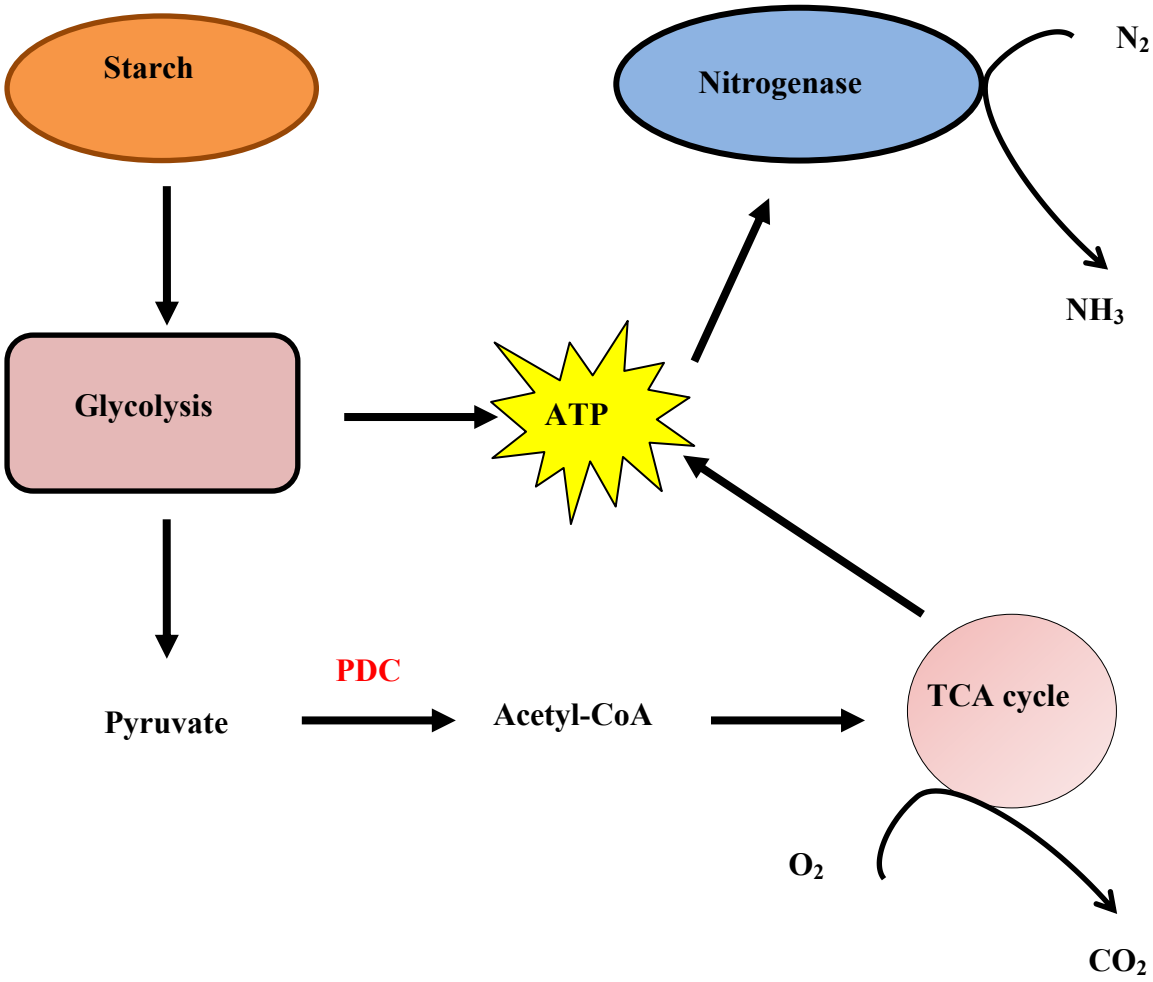

Figure 3.4: Schematic diagram of aerobic respiration of *Cyanothece* 51142

3.2.1.5. H_2 production by *Cyanothece* 51142

Two major types of biological enzymes are reported to be involved in the H_2 formation reaction by nitrogen-fixing cyanobacteria: 1) nitrogenase and 2) hydrogenase enzymes (Hansel and Lindblad 1998). As mentioned previously in section 2.6, the former catalyses the production of H_2 concomitantly with the reduction of N_2 into NH_3, whereas the latter catalyse the proton-electron recombination reaction to form H_2.

N_2-fixation: $N_2 + 8H^+ + 8e^- + 16ATP \rightarrow 2NH_3$ (ammonia) $+ H_2 + 16ADP + 16P_i$

Proton-electron recombination: $4H^+ + 4e^- \rightarrow 2H_2$

Nitrogenases consist of three different classes, depending on their metallic active sites (Seefeldt, Yang *et al.,* 2013). The most widely distributed and best-studied class is molybdenum-iron (Mo-Fe) nitrogenases, while the other forms contain vanadium and Fe in place of Mo. In the case of hydrogenase enzymes, they can be further classified into two types: 1) bidirectional hydrogenase and 2) uptake hydrogenase (Tsygankov 2007), both of which also consist of three classes: Fe-Fe, Fe-Ni and metal-free (Vignais, Billoud *et al.,* 2001). Nevertheless, in all bacterial classes, the majority of hydrogenases are Fe-Ni types (Przybyla, Robbins *et al.,* 1992, Cammack 1999). These two hydrogenase enzymes can be clearly distinguished by their physiological roles. Specifically, the uptake hydrogenase catalytically supports the consumption of H_2 produced by nitrogenase, which has been suggested as the cellular mechanism of recycling electrons lost to nitrogenase-mediated H_2 evolution for other cellular functions (Tamagnini, Axelsson *et al.,* 2002). In the case of bidirectional hydrogenase, it has an ability to either evolve H_2 or oxidise it by the direct interaction with the redox partner NADH and / or NADPH as the electron donor in the presence of H_2 and vice versa (Tsygankov 2007, Carrieri, Wawrousek *et al.,* 2011). However, its role is still unclear, but believed

to serve as an additional electron sink for reduced Fd under anaerobic condition (Redding, Cournac *et al.,* 1999).

Reversible reaction catalysed by bidirectional hydrogenase: $2H^+ + 2e^- \Leftrightarrow H_2$

Irreversible reaction catalysed by uptake hydrogenase: $H_2 \rightarrow 2H^+ + 2e^-$

Although *Cyanothece* 51142 possesses Mo-Fe nitrogenase and both bidirectional and uptake hydrogenase enzymes (Welsh, Liberton *et al.,* 2008), the majority of its H_2 photoproduction is due to the catalytic activity of nitrogenase (Min and Sherman 2010). This is due to a substantial difference in enzymatic activities between nitrogenase and bidirectional hydrogenase. Numerically, the activity of the latter is always approximately only 1 % of the former (Sherman, Min *et al.,* 2010). Both nitrogenase and uptake hydrogenase genes are strictly expressed during dark environment and usually transcribed to the similar levels (Toepel, Welsh *et al.,* 2008, Toepel, McDermott *et al.,* 2009), thereby leading to the negligible rate of H_2 production, as the gas produced by nitrogenase is consumed by the synthesised hydrogenase. However, once the *Cyanothece* 51142 cultures have been adapted to the standard light / dark cycles and then transferred to the continuous illumination, they are capable of suppressing uptake hydrogenase genes (Aryal, Callister *et al.,* 2013), while maintaining a high transcript level of the nitrogenase genes (Toepel, McDermott *et al.,* 2009).

3.2.2. Photofermentation

The *Cyanothece* 51142 cells are capable of photoheterotrophically producing H_2 via photofermentation, when the cultures are supplied with an organic glycerol. As a result, this cyanobacterium has a potential to offer a biological conversion of wasted glycerol, which is generally generated as by-product from biodiesel production, into useful H_2 fuel. However, as wasted glycerol may contain numerous kinds of impurities such as methanol, salts and heavy metal, further purification and pre-treatment of this organic carbon compound are thus prerequisite (Chatzifragkou and Papanikolaou 2012). In this particular process, energy and reducing powers, used for the N_2-fixation reaction, are directly derived from sunlight and the organic substrate, without the need of carbon photosynthate (Das and Veziroğlu 2001). In presence of glycerol, there are a number of significant changes in the cyanobacterial metabolic pathway, comparing to when the cyanobacterium is grown under the standard photoautotrophic growth condition (Aryal, Callister *et al.,* 2013). As shown in Figure 3.5, glycerol reduces the expression of key enzymes, catalysing the photosynthetic carbon fixation, while inducing higher level of cellular respiration. The reduction in photosynthesis-related enzymes indicates that *Cyanothece* 51142 prefers to utilise an exogenous carbon source over photosynthetically fixed carbon for cellular metabolism. As the rate of O_2 consumption via respiration increases, but the photosynthetic O_2 evolution is no longer possible, this results in an eventual depletion of O_2 within the cells, together with higher level of glycogen breakdown (Aryal, Callister *et al.,* 2013). With the greater amount of energy generated from broken glycogen, the expression of nitrogenase genes is facilitated even under light conditions. Therefore, it becomes possible to enable a remarkable rate of H_2 production by the glycerol-supplemented *Cyanothece* 51142 cultures under continuous light condition, at which the dark-induced expression of uptake hydrogenase is inhibited (Toepel, Welsh *et al.,* 2008, Min and Sherman 2010). The biochemical conversion of glycerol into energy is also similar to that of

intracellular carbohydrate: the process consists of three sequential sub-stages - glycolysis, oxidative decarboxylation and TCA cycle. Higher levels of key enzymes of both glycolysis and TCA cycle are also induced by the addition of glycerol (Aryal, Stockel *et al.,* 2011, Aryal, Stöckel *et al.,* 2011, Stöckel, Jacobs *et al.,* 2011).

Overall aerobic respiration: $C_3H_8O_3$ (glycerol) + $5O_2 \rightarrow 3CO_2 + 4H_2O$ + Energy

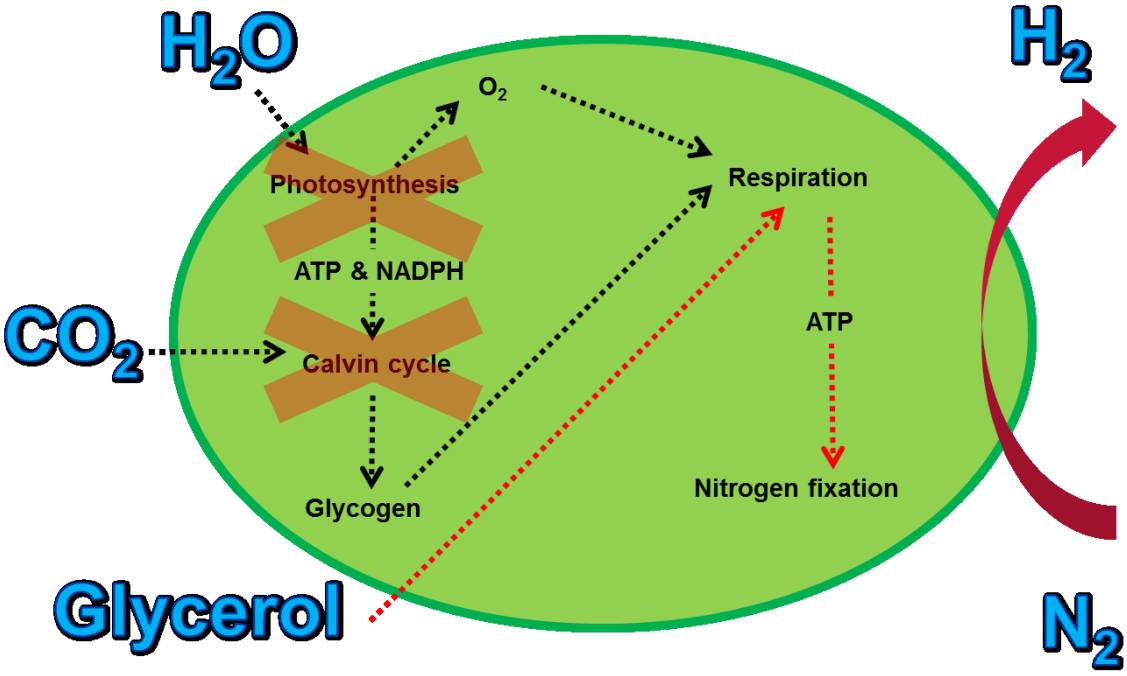

Figure 3.5: Schematic diagram of photofermentation of *Cyanothece* 51142. Glycerol inhibits photosynthetic CO_2 fixation, while promoting respiration. With higher level of respiration, the greater amount of chemical energy is generated and subsequently used to power N_2-fixation.

3.3. Parameters Affecting *Cyanothece* 51142 Growth

Like most microorganisms, the growth of a *Cyanothece* 51142 culture is characterised by five distinct phases: lag (adaptation), exponential, linear, stationary and cell death (Tomaselli 2004) and can normally be described by the standard logistic (sigmoid) population growth model (Molina Grima, Fernández *et al.,* 1999, Lemesle and Mailleret 2008). After adapting themselves into the new environment, cells proceed into the exponential phase, during which they reproduce at the maximum specific growth rate (μ_{max}). The rate is maintained as long as both light and nutrients are sufficient. However, in reality, as the cell density increases, the cells closer to the light source start to shade those behind them (Degrenne, Pruvost *et al.,* 2011). This naturally shading effect not only places a saturation limit on the total cell density of a given culture, but also could result in localised cell death and culture fouling (Carvalho, Meireles *et al.,* 2006). Under light-limited growth condition, the specific growth rate is reduced to a constant value, which is lower than μ_{max}. The maximum cell density is observed during the stationary growth phase, which is typically initiated by the depletion of nutrient (Sinetova, Červený *et al.,* 2012). During the stationary phase, the specific growth rate of the culture becomes equal to zero and cells generally start to utilise their intracellular accumulated metabolites in order to sustain their physiological activities (Clark 2006). As soon as these metabolites are used up, the growth phase is eventually transformed into the death phase, where the rate of cell death is greater than the rate of cell reproduction, μ (t) <0. The parameters that affect the specific growth rate of *Cyanothece* 51142 cultures include illumination, nutrients, temperature, pH and fluid dynamics (Dutta 2005, Sinetova, Červený *et al.,* 2012, Dechatiwongse, Srisamai *et al.,* 2014)

3.3.1. Illumination

Light is the most important parameters, affecting the growth of microalgae, as it provides the fundamental energy to drive a variety of physiological activities and metabolic processes. Undoubtedly, microalgal growth is impossible without illumination (Kosourov, Tsygankov *et al.,* 2002). The growth of microalgal cultures is influenced by various aspects of illumination: light intensity, photosaturation, photoinhibition, light path (light penetration), light mixing (light diffusion), wavelength, and light regime (light-dark cycle or continuous light).

Light intensity is a measure of the incident photon flux density falling upon the microalgal culture. In general, the photosynthetic activity and the growth rate of microorganism increases with an increasing light intensity. The photosaturation of microalgal cultures occurs when the photosynthetic activity reaches its maximum value, and this specific intensity is also known as the "light-saturated intensity". By raising light intensity above the photosaturation limit, the excess energy, beyond cellular light-absorption capacity, will be lost in forms of heat (Li, Wakao *et al.,* 2009) and subsequently reduces the photosynthetic efficiency of the microalgal cells (Melis 2009). Even further increase in the intensity can eventually lead to photoinhibition, at which the light-induced breakdown of the protein D_1, located at the reaction centre of PSII, occurs and results in the reduced activity of photosynthetic mechanism (Andersson and Styring 1991). Under the photoinhibitive phenomenon, the microbial growth is reported to be much reduced (Kim, Chang *et al.,* 1992, Baroli and Melis 1996, Martínez, Morán *et al.,* 2012).

Within one microalgal culture, it consists of millions individual cells of microalgae. When the culture is still young and diluted, it can be virtually assumed that every cell receives approximately the same light intensity. However, this is not the case for highly dense culture, at which the light

path - the distance that light can penetrate through culture - becomes a function of the cell density of that culture (Janssen, Janssen *et al.,* 2000). This is because the cells near the light exposed surface shade the cells behind them. In this scenario, appropriate mixing , which is determined by the fluid dynamics of that reactor (Grima, Fernandez *et al.,* 1999), has to be assured, as it defines whether cells are distributed homogenously to have access to the same average illumination.

Across spectrum of solar radiation, there is a specific wavelength range from 400 to 700 nm, which can be photosynthetically utilised by microorganisms, and known as the photosynthetically active radiation (PAR). For *Cyanothece* 51142, absorption maxima of its two light-harvesting units - phycocyanin and chlorophyll a – are located at 620 and 680 nm, respectively (Reddy, Haskell *et al.,* 1993). Although most authors tend to use cool-white light, whose wavelength range is specifically from 400 to 700 nm, Wang and co-workers showed that *Spirulina platensis*, a kind of cyanobacteria known for its high contents of proteins and can be consumed by humans and other animals, is able to grow fastest under the red-light incubation (Wang, Fu *et al.,* 2007). Meanwhile, its lowest growth rate was observed under the use of blue light, whose wavelength range is not overlapped by the absorption bands of phycocyanin. As a consequence, this understanding could lead to the design of solar filters, which only allow the selective wavelength of solar spectrum to pass through and subsequently provides positively influence upon the microalgal growth.

Up to now, some studies have been carried out to optimise the condition of light intensity for *Cyanothece* 51142 growth (Sinetova, Červený *et al.,* 2012, Dechatiwongse, Srisamai *et al.,* 2014). A recent study by Dechatiwonsge and colleagues shows that increasing light intensity of cool-white fluorescent up to 320 μE m^{-2} s^{-1} results in an enhanced maximum specific growth rate of *Cyanothece* 51142 (Dechatiwongse, Srisamai *et al.,* 2014). Under this intensity range, *Cyanothece* 51142 growth is also predominantly influenced by photosaturation rather than photoinhibition. In

general, the photosaturation of microorganisms starts to occur at light intensities of approximately 300 – 400 μE m^{-2} s^{-1}, while the effect of photoinhibition has been observed for light intensities above 500 – 800 μE m^{-2} s^{-1} (Janssen 2002). However, by using different photobioreactors (PBRs) for the microalgal cultivation, it becomes common that the different experiments do not result in the same optimal light intensity. This is because each PBR has its own particular light mixing pattern as well as the surface-to-volume ratio, at which the latter character is influenced by the geometry of the PBR (Janssen, Janssen *et al.,* 2000). Specifically, a high surface-to-volume ratio implies that cultures have an increased exposure to an unattenuated light intensity available at the surface of the reactor and are therefore more likely to obtain better photosynthetic efficiencies. In contrast, a low surface-to-volume ratio allows more cells to be cultivated within the same surface area, resulting in better biofuel yield, provided that there is appropriate level of light mixing to ensure that all cells have access to sufficient illumination (Carvalho, Meireles *et al.,* 2006). Therefore, there is a trade-off between the capital cost of required surface area of the PBR and the energy cost due to the reactor mixing (Amos 2004).

Cyanothece 51142 cells are very flexible to adapt themselves with changes in the light regime, as they are able to sustain their metabolic balancing act under an outdoor condition of a diurnal light-dark cycle as well as continuous illumination (Schneegurt 1994, ColonLopez, Sherman *et al.,* 1997). During day time, the cyanobacterial cells carry out photosynthesis to fix CO_2 into intracellular glycogen. During the dark or subjective dark, the photosynthetic light-harvesting mechanism is temporally suspended and the cyanobacteria focus instead on generating chemical energy, required for their survival and N_2-fixing reaction, from their glycogen reserve. A number of studies have been conducted to investigate the effect of light regime on *Cyanothec*e 51142 growth (ColonLopez, Sherman *et al.,* 1997, Toepel, Welsh *et al.,* 2008, Alagesan, Gaudana *et al.,* 2013).

3.3.2. Nutrients

The *Cyanothece* 51142 cells must be suspended in any forms of aqueous solution so that they can carry out the photosynthetic water-splitting process. The aqueous solution should contain sources of essential macro-nutrients - carbon, nitrogen, sulphur and phosphorus, as well as a number of trace metals. Among four macro-nutrients, carbon and nitrogen, in particular, are the most two important elements, as their contents are accounted for 40 and 9 % of *Cyanothece* 51142 dry biomass respectively (Schneegurt, Arieli *et al.,* 1995). Generally, cyanobacteria do not need large amounts of phosphorus, as their biomass contains less than 1% of this macro-nutrient (Markou and Georgakakis 2011).

The cyanobacterium *Cyanothece* 51142 is a very versatile microorganism, as it can grow in various growth conditions – standard photoautotrophic, photo/chemoheterotrophic and mixotrophic conditions (Schneegurt, Sherman *et al.,* 1994, Schneegurt, Sherman *et al.,* 1997, Feng, Bandyopadhyay *et al.,* 2010). Under standard photoautotrophic growth condition, the cells routinely carry out photosynthetic CO_2 fixation. The autotrophic growth rate of *Cyanothece* 51142 cultures is between 0.012 – 0.024 hr^{-1} (Feng, Bandyopadhyay *et al.,* 2010, Alagesan, Gaudana *et al.,* 2013). However, when organic acids are provided to the cultures, they can adapt themselves into heterotrophic as well as mixotrophic growth conditions (Feng, Bandyopadhyay *et al.,* 2010). Among various types of organic carbon compounds, the optimal growth enhancement was observed when the culture was supplemented with glycerol, whereas some compounds such as citrate, fructose and methanol have an inhibitive effect on the cyanobacterial growth and eventually kill the culture (Schneegurt, Sherman *et al.,* 1997). In presence of glycerol, *Cyanothece* 51142 specific growth rates (0.026 - 0.043 hr^{-1}) were much greater than those of the photoautotrophic controls by approximately two fold (Alagesan, Gaudana *et al.,* 2013). In addition to growth rate, glycerol also

promotes the stationary-phase cell densities by a factor of two (Schneegurt, Sherman *et al.,* 1997). The optimal glycerol concentration for the growth was reported to be 30 mM, whereas the critical concentration, which causes the growth inhibition, was found to be 75 mM (Alagesan, Gaudana *et al.,* 2013).

Being part of diazotrophic (N_2-fixing) cyanobacteria, *Cyanothece* 51142 has an ability to derive its essential nitrogen source from ambient N_2 in air - 78 % volume N_2 volume air^{-1}, through biological N_2-fixation process (Reddy, Haskell *et al.,* 1993). Under N_2-fixing condition, the autotrophic specific growth rate of the cyanobacterial cultures is 0.012 hr^{-1} (Feng, Bandyopadhyay *et al.,* 2010). In addition to N_2, *Cyanothece* 51142 is also able to utilise fixed forms of nitrogen source e.g. nitrate (NO_3^{-1}) and ammonium (NH_4^{+1}) salts. In general, cyanobacteria prefer to utilise nitrogen in the order of NH_4^{+1}, NO_3^{-1} and N_2, respectively (Markou and Georgakakis 2011). Specifically, in presence of ammonium, cyanobacteria do not consume other nitrogen sources until the completion of the compound. However, high concentration of ammonium salts - 17 mM - was found to fully inhibit the *Cyanothece* 51142 growth (Feng, Bandyopadhyay *et al.,* 2010), due to their deleterious effect on the photosystems of cyanobacteria (Dai, Deblois *et al.,* 2008, Drath, Kloft *et al.,* 2008). As a result, nitrate salts are commonly used as additional nitrogen source for *Cyanothece* 51142 cultures. Nitrogen-replete condition is commonly referred to the growth condition, at which cyanobacterial cultures are supplied with nitrate. Under nitrogen-replete condition, *Cyanothece* 51142 possesses the autotrophic specific growth rate of 0.024 hr^{-1} (Feng, Bandyopadhyay *et al.,* 2010), which is approximately 2 times higher than that observed under N_2-fixing condition. Differently, as cyanobacterial H_2 production is catalysed by nitrogenase enzymes, which are suppressed by nitrate salts (Dutta, De *et al.,* 2005), it is very important to deprive nitrate out of the *Cyanothece* 51142 cultures in order to promote N_2-fixing condition.

3.3.3. Temperature

There is a close connection between temperature, light and photoinhibition (Markou and Georgakakis 2011). Specifically, if light intensity is maintained below its critical value, the degree of microbial susceptibility to photoinhibition is predominantly influenced by temperature (Powles 1984). Temperature is an important physical factor, which has long been known to have a strong influence on the photosynthetic activity of plants and microalgae. Similar to light intensity, an increase in temperature generally enhances microbial photosynthesis and subsequent growth rates up to a critical temperature, above which these activities start to decline (Konopka and Brock 1978, Lester, Adams *et al.,* 1988, Torzillo and Vonshak 1994, Inoue, Taira *et al.,* 2001). Under low temperature (below 20 $^{\circ}$C), the recovery of damaged D_1 protein, located at the reaction centre of PSII, has been shown to be suppressed, which leads to the reduction of cellular photosynthetic activities. However, these activities can be recovered and subsequently return to their original functionality by exposing cells to a higher temperature (Gombos 1994, Kanervo, Tasaka *et al.,* 1997). Conversely, under extreme heat stress, the detachment of the Mn-stabilising extrinsic 33 kDa protein from the PS II core complex has been reported as the potential cause of high temperature-induced inactivation of the photosynthetic capability (Yamane, Kashino *et al.,* 1998). In open raceways, where the control of temperature is impossible without using external heating or cooling devices, a marked decrease in biomass productivity was previously observed as the consequence of photoinhibition (Richmond, Lichtenberg *et al.,* 1990, Vonshak and Guy 1992). For *Cyanothece* 51142 strain, the cyanobacterium is able to grow effectively at temperatures in the range of 25 – 37 $^{\circ}$C, beyond which an exponential decline in its biomass productivity was observed (Dechatiwongse, Srisamai *et al.,* 2014). The optimal biomass productivity of 0.1 g L^{-1} hr^{-1} was observed at 35 $^{\circ}$C, whereas 40 $^{\circ}$C was seen to rapidly inhibit the cyanobacterial growth.

3.3.4. pH and Fluid Dynamics

pH is a measure of the acidity or basicity of an aqueous solution. Any solutions with a pH less than 7 are said to be acidic and solutions with a pH greater than 7 are basic or alkaline. Generally, the optimal growth of cyanobacteria is facilitated by alkaline growth mediums, whose pH are between 7.7 – 9.4 (Wicks and Thiel 1990). A significant decrease in *Cyanothece* 51142 growth rate was previously observed when the pH is brought below pH of 4 – 5 (Dechatiwongse, Maitland *et al.,* 2015). Min and Sherman stated that the optimal pH for the *Cyanothece* 51142 H_2 production is in the region of 7.4 (Min and Sherman 2010).

In term of fluid dynamics, it is very important that the microalgal culture is properly and continuously mixed in order to prevent individual cells from agglomerating in clusters or drifting to the bottom of the photobioreactor, where they would have insufficient access to light and nutrients (Morweiser, Kruse *et al.,* 2010). The understanding of the fluid dynamics within a particular reactor geometry is a prerequisite to establishing good light mixing within the microalgal culture (Zhang, 2011). Beside light transfer, a good mixing is also required to enhance CO_2 mass transfer from the supplied gas stream into the liquid, which could then be utilised by cells. In addition to supporting photoautotrophic growth of microalgae, active CO_2 transport will also reduce the probability of dissolved O_2 accumulation, which otherwise would cause the growth inhibition (Chisti and Jauregui-Haza 2002). However, the mixing speed has to be carefully selected in order to avoid shear-related cell death during mixing (Barbosa, Hadiyanto *et al.,* 2004) and high associated energy costs. Numerically, the superficial gas velocity, which is defined as the volumetric gas flow rate per unit cross-sectional area of the bioreactor, above 0.03 m s^{-1} was discovered to result in significant cell death rate of two different microalgal strains – *Dunaliella tertiolecta* and *Dunaliella Salina*

(Barbosa, Hadiyanto *et al.,* 2004). Depending on the reactor design, mixing may be provided by a magnetic stirrer bar, a circulation pump or a gas-lift system (Hankamer, Lehr *et al.,* 2007).

3.4. Parameters Affecting Biohydrogen Production

The rate of H_2 production is closely dependent on the quantity of active cells within a *Cyanothece* 51142 culture. The higher cell densities increases the number of reaction centres of photosynthetic apparatus that have the potential to effectively produce H_2 under anaerobic conditions (Horner and Wolinsky 2002). Therefore, there are prerequisite requirements for obtaining fully grown and healthy *Cyanothece* 51142 cultures in order to greatly enhance the subsequent H_2 production. Similar to growth stage, the H_2 production is also influenced by environmental parameters, including illumination, nutrient and temperature (Dutta 2005, Min and Sherman 2010, Brauer, Stomp *et al.,* 2013). In addition, advanced engineering approaches such as different photobioreactor operation, H_2 induction techniques and genetic engineering, also play key roles in extending the duration of H_2 production, the produced yield as well as an overall photochemical efficiency of the process (Polle, Kanakagiri *et al.,* 2003, Fedorov, Kosourov *et al.,* 2005, Laurinavichene, Fedorov *et al.,* 2006, Melis 2009).

3.4.1. Illumination

Similar to their growth phase, microalgal cultures require the appropriate light intensity, light wavelength and light regime in order to effectively produce H_2 (Jo, Lee *et al.,* 2006, Park and Moon 2007). In general, the photo-dependence of nitrogenase-mediated H_2 production and N_2-fixation can be described in a similar manner to that of photosynthesis (Staal, Lintel-Hekkert *et al.,* 2001, Staal,

Hekkert *et al.,* 2002, Ariosa, Carrasco *et al.,* 2006, Melnicki, Pinchuk *et al.,* 2012), which was previously discussed in section 3.3.1. *Cyanothece* 51142 can start to produce H_2 even at relatively low irradiances of < 50 μmol m^{-2} s^{-1}, while maintaining an extremely low photosynthetic O_2 evolution (Melnicki, Pinchuk *et al.,* 2012). The saturation of cyanobacterial H_2 production occurs at 100 μmol m^{-2} s^{-1} (Ariosa, Carrasco *et al.,* 2006), while that of photosynthesis is approximately beyond 240 μmol m^{-2} s^{-1}, suggesting that N_2-fixing reaction is more efficient in term of light utilisation than photosynthetic CO_2 fixation (Osmond, Cooper *et al.,* 1985, Ariosa, Carrasco *et al.,* 2006). As light intensity increases further, the photo-induced reduction of nitrogenase activity begins at an extreme irradiance greater than 1400 μmol m^{-2} s^{-1} (Ariosa, Carrasco *et al.,* 2006). Under saturating irradiance of 100 μmol m^{-2} s^{-1}, the glycerol-supplemented *Cyanothece* 51142 culture was able to produce H_2 in the range of 410 - 470 μmol H_2 mg Chl^{-1} hr^{-1}, under argon incubation (Bandyopadhyay, Stoeckel *et al.,* 2010, Bandyopadhyay, Elvitigala *et al.,* 2013). Although nitrogenase enzymes possessed by *Cyanothece* 51142 are active regardless of illumination condition (Schneegurt 1994, ColonLopez, Sherman *et al.,* 1997), the H_2 production, in particular, is the light-dependent reaction (Bandyopadhyay, Stoeckel *et al.,* 2010). The resulting production rate of H_2 in the dark is reported to be more than 100-fold lower than that achieved under constant illumination. This reduction is reasonably resulted from the oxidation of nitrogenase-produced H_2, catalysed by uptake hydrogenases, as the hydrogenases are synthesised under dark condition (Toepel, Welsh *et al.,* 2008, Toepel, McDermott *et al.,* 2009). As a result, the provision of an artificial illumination during the dark cycle is necessary for outdoor H_2 production facility. Min and Sherman (Min and Sherman 2010) also measured the hydrogenase-catalysed H_2 production rate of *Cyanothece* 51142 under irradiances up to 200 μmol m^{-2} s^{-1}, but only found the maximum rate of < 10 μmol H_2 mg Chl^{-1} hr^{-1}, suggesting nitrogenase as dominant enzymes for the gas producing mechanism of this particular strain. In term of light wavelength, the beyond PAR

region of infrared illumination (750 – 950 nm) appears to have a positive effect on the H_2 production of microalgae (Uyar, Eroglu *et al.,* 2007).

3.4.2. Carbon and Nitrogen Sources

Under photoautotrophic condition, chemical energy, used to power N_2-fixation, is derived from intracellular carbohydrate reserves, which are synthesised from photosynthetically fixed CO_2. With provision of ambient CO_2 (0.03 % volume CO_2 volume air^{-1}), photoautotrophically grown *Cyanothece* 51142 was able to produce 133.21 ± 21.5 μmol H_2 mg Chl^{-1} hr^{-1}, under aerobic incubation conditions (Bandyopadhyay, Elvitigala *et al.,* 2013). When the culture was grown under 8% CO_2-enriched air, the aerobic H_2 production rate was approximately doubled to 230 μmol H_2 mg Chl^{-1} hr^{-1} (Bandyopadhyay, Stoeckel *et al.,* 2010). As the catabolism of intracellular glycogen reserves play a key role in H_2 evolution by *Cyanothece* 51142 (Melnicki, Pinchuk *et al.,* 2012), additional carbon sources, provided by concentrated CO_2, reasonably leads to the higher quantity of carbon reserve and then the subsequently enhanced production rate. Under photoheterotrophic condition, when 50 mM glycerol was supplemented to *Cyanothece* 51142 cultures, Bandyopadhyay and co-workers (Bandyopadhyay, Elvitigala *et al.,* 2013) reported the gas evolution rate of 250.48 ± 33.2 μmol H_2 mg Chl^{-1} hr^{-1}. This significant improvement may be resulted from enhanced level of glycerol-induced respiration (Aryal, Callister *et al.,* 2013), which in turn creating anoxic environment within cyanobacterial cells and subsequently inducing activation of nitrogenase enzymes.

In addition to evolved H_2, *Cyanothece* 51142 concurrently reduces atmospheric N_2 into NH_3, during N_2-fixation. The nitrogenase-generated ammonium was later assimilated into amino acids through the glutamine synthetase / glutamate synthase pathway (Postgate 1998). However, in presence of

exogenous nitrogen sources - either nitrate or ammonium salts, H_2 production by *Cyanothece* 51142 was completely vanished within 12 hours, regardless of the carbon substrate (Bandyopadhyay, Stoeckel *et al.,* 2010, Feng, Bandyopadhyay *et al.,* 2010). This observation is due to well-known inhibitive effect of these two nitrogen compounds upon activity of nitrogenase enzymes (Rawson 1985). As a result, expression of nitrogenases is strictly limited to nitrogen-fixing condition.

3.4.3. Temperature

The optimum temperature for H_2 production for most cyanobacteria is in the temperature range of 30 – 40 °C, which enhances the rate of cellular respiration (Dutta, De *et al.,* 2005). High level of respiration then effectively converts stored carbohydrate into chemical energy for powering N_2-fixation, at the same time significantly reducing intracellular O_2 levels – prerequisite condition for activation of nitrogenase enzymes (Bandyopadhyay, Stoeckel *et al.,* 2010). However, it is very important for the cultivating temperature not to be above the critical point in order to avoid the thermal-induced denaturation of photosynthetic light-harvesting pigments, which can subsequently lead to complete cessations in the cyanobacterial growth and gas generation. The critical temperature inhibiting the growth of *Cyanothece* 51142 was previously reported to start at 40 ^{o}C (Dechatiwongse, Srisamai *et al.,* 2014). The value of critical temperature is considerably diverse, varying from strains to strains (Dutta 2005). For the genus of *Cyanothece*, Brauer and co-workers recently reported that the cyanobacterium *Cyanothece* sp. Miami BG043511 expressed the highest nitrogenase activity and its subsequent specific growth rate at 30 ^{o}C (Brauer, Stomp *et al.,* 2013).

3.4.4. Biohydrogen Production Duration

After batch cultivation duration of 9 days, the H_2 production rate of mixotrophically grown *Cyanothece* 51142 cultures begins to decline (Feng, Bandyopadhyay *et al.,* 2010). These observations can be explained that, during stationary growth phase, cells eventually experience unfavourable conditions, caused by accumulation of toxic metabolites as well as starvation of essential growth substrates such as macro-nutrients and dissolved O_2 (Atsumi, Higashide *et al.,* 2009, Dechatiwongse, Maitland *et al.,* 2015), and are subsequently no longer able to sustain their physiological activities. This discontinuous production is one of major issues for biohydrogen process scale-up, because it results in an overall low productivity. Due to a closed nature of batch systems, at which replenishment of fresh medium or removal of toxic substances are not feasible, a number of modified bioreactor process have been proposed, with aims to overcome existing limitations. Oncel and Vardar-Sukan developed a semi-continuous process, at which old, starved *Chalmydomonas reinhardtii* (*C. reinhardtii*) culture was frequently replaced by fresh culture at an appropriated dilution ratio (Oncel and Vardar-Sukan 2009). They were able to significantly prolong H_2 production of the green alga from approximately a week up to 120 days, producing 1,100 ml H_2 L^{-1} at a maximum production rate of ~ 0.83 ml H_2 L^{-1} hr^{-1}. Tamburic and co-workers employed a fed-batch process, at which sulphur-starved *C. reinhardtii* culture was fed with a constant flow of required grown medium containing micromolar sulphate concentrations, and subsequently reported a maximum H_2 production rate close to 1 ml H_2 L^{-1} hr^{-1} over a short experimental period of 180 hours (Tamburic, Dechatiwongse *et al.,* 2013). Another possible mode of bioreactor operation is an open, continuous flow bioreactor system, at which old culture was constantly replaced by fresh culture at a carefully chosen flow rate, which would not completely flush out all cells within the system. In spite of being rarely employed, some studies demonstrated the potential feasibility of continuous systems (Lichtl, Bazin *et al.,* 1997, Fedorov, Kosourov *et al.,* 2005). In detail, a two-

stage continuous PBR system, developed by Fedorov and co-workers, was able to maintain H_2 production of sulphur-deprived *C. reinhardtii* culture for more than 4,000 hours (~5.5 months) at maximum rate of 0.58 ml H_2 L^{-1} hr^{-1} (Fedorov, Kosourov *et al.,* 2005). In the case of cyanobacteria, Lichtl and co-colleagues reported a continuous evolution of H_2 over 72 days, when the culture of N_2-fixing, heterocystous cyanobacterium *Nostoc flagelliforme* was cultivated in a single-stage continuous PBR (Lichtl, Bazin *et al.,* 1997). In addition to significantly extending the duration of the H_2 production, the continuous flow systems also allow the continuous collection of microalgal biomass of the growing cultures within the PBRs. The collected biomass may be used to produce high-value products or liquefied biofuels (Hejazi and Wijffels 2004) or dried and burnt to generate electricity (Putt 2007). It may also be possible to produce a higher yield of H_2 or biogas from residual biomass via an anaerobic digestion carried out by bacteria (Taylor 2008). These integrated biorefinery approaches would improve the overall value of the biohydrogen production and its commercial potential.

3.4.5. Induction of Biohydrogen Production

As nitrogenases, key enzymes catalysing N_2-fixation and H_2 production of *Cyanothece* 51142, are extremely sensitive to O_2 (Fay 1992), anaerobic conditions are strictly required within the cells for initiating H_2 production. Up to now, an induction of low-O_2 environment has been carried out in three major ways: direct O_2 removal, environmental stimulation and metabolic interfere.

Direct O_2 removal includes purging of inert gas (Greenbaum 1988) and addition of O_2 scavenger (Howarth and Codd 1985, Benemann 1997), both of which directly and immediately remove all of photosynthetic O_2, as it is being produced by cyanobacteria. Helium (He) and argon (Ar) are commonly used as purging gas, but the latter is practically preferred, due to its less expensive cost.

Under argon incubation, a maximum H_2 production rate of photoautotrophically grown *Cyanothece* 51142 culture was reported to be enhanced by a factor of 2.7, at the rate of 358.46 ± 40.3 μmol H_2 mg Chl^{-1} L^{-1} (Bandyopadhyay, Elvitigala *et al.,* 2013). Despite an effectiveness of purging, when it comes to the scale up of biohydrogen processes, such external interference is likely not to be a viable option, as it would lead to a more complex processing operation together with high associated costs of inert gas supply and gas pumping. Recently, Dechatiwongse and co-workers demonstrated glycerol as promising O_2 scavenger, particularly for *Cyanothece* 51142 (Dechatiwongse, Maitland *et al.,* 2015). Provision of glycerol increases cyanobacterial respiration rate and therefore its O_2 consumption, while inhibiting the O_2 production via photosynthesis (Aryal, Callister *et al.,* 2013). Consequently, this results in the net decrease of O_2 level and eventually turns the system into anaerobic conditions.

As photosynthetic O_2 evolution is a light-dependent process, microalgal H_2 production has historically been initiated by dark incubation (Gaffron 1939, Gaffron and Rubin 1942). The process of dark incubation starts when a fully grown microalgal culture is completely sealed and placed in dark environment. Under darkness, photosynthesis is rapidly shut down and any remaining O_2 is eventually used up by cellular respiration. As a result, anaerobic conditions are eventually established and activate an expression of hydrogenase and / or nitrogenase enzymes. Following this incubation period, the sealed culture is re-illuminated and H_2 production immediately commences. At the same time, photosynthesis is reactivated and starts to reproduce O_2. Initially, all of the photosynthetically evolved O_2 can be used up by O_2-hungry cells, but eventually, enough O_2 is accumulated within the system, subsequently inactivating the H_2-catalyesed enzymes and terminating H_2 production. Bandyopadhyay and co-workers showed that it is possible to obtain the maximum rate of 150 μmol H_2 mg Chl^{-1} L^{-1} from fully grown *Cyanothece* 51142 culture, which

was photoautotrophically grown under diurnal 12 hour light / 12 hour dark cycles, followed by a continuously illuminated incubation (Bandyopadhyay, Stoeckel *et al.,* 2010).

Another possibility of inducing anaerobic conditions is by interference with *Cyanothece* 51142 photosynthetic metabolism. This technique involves the inactivation of PSII, an essential light-harvesting unit of photosynthetic apparatus, using an inhibitor, most commonly 3-(3, 4-dichlorophenyl)-1, 1-dimethylurea (DCMU). The use of DCMU produces a similar effect to that of dark incubation, switching off photosynthetic O_2 evolution and eventually inducing anaerobic H_2 production. Min and Sherman measured the H_2 production of glycerol-supplemented *Cyanothece* 51142 culture and reported approximately 20% increment in the maximum rate, in presence of 10 mM DCMU (Min and Sherman 2010).

3.4.6. Immobilisation and Genetic Modification

Immobilisation of cells on solid substrate is effectively used to obtain high density of microalgal cells. Immobilised cells occupy less space and require a smaller volume of growth medium, and therefore the technique efficiently produces greater cell density than free cells in liquid suspension (Eroglu and Melis 2011). Increased cell density increases the number of reaction centres that have the potential to harness solar energy for anaerobic H_2 production (Horner and Wolinsky 2002). Kosourov and Seibert reported approximately five times increase in H_2 production rate from *C. reinhardtii* strain, immobilised on a thin (< 400 μm) alginate layer that was extracted from brown seaweed (Kosourov and Seibert 2009). This improvement was reasonably due to much higher cell densities of immobilised *C. reinhardtii* culture (~ 2,000 mg Chl L^{-1} of alginate matrix), which is around 100 times thicker than a typical *C. reinhardtii* culture. Laurinavichene and co-workers also employed a two-step H_2 production process by switching the immobilised cells between sulphur-

replete and sulphur-depleted conditions, producing a total H_2 yield of 380 ml over a period of 23 days, and the highest production rate of 1.87 ml hr^{-1} (Laurinavichene, Fedorov *et al.,* 2006). However, major drawbacks of immobilisation technique, including inhomogeneous environment and low mass diffusions, were previously reported, in comparison with freely suspended cells (Koku, Eroğlu *et al.,* 2003, Eroglu and Melis 2011). Alternatively, it is also possible to extract and immobilise individual hydrogenase enzymes onto gold electrodes (Krassen, Stripp *et al.,* 2009), but this process would be prohibitively expensive for any commercial applications.

Genetic modification (GM) involves the direct manipulation of an organism's genome, which subsequently results in modified physical or metabolic properties. Up to now, the GM techniques have shown promising consequences in improving photochemical efficiencies of microalgal H_2 production and can be categorised into three approaches: truncating the photosynthetic light-harvesting antennae size of microalgae, inactivation of uptake hydrogenase and elimination of alternative product synthesis. Truncated antennae sizes in the photosynthetic apparatus - reducing the number of pigmented molecules in order to make the cells less green (Melis 2009), would minimise excess absorption and wasteful dissipation of sunlight by individual cells as heat and fluorescence, under high-density culture conditions. Employing this approach, previous studies demonstrated an enhancement in the solar conversion efficiency up to 3-fold, compared to the wild-type strain (Polle, Kanakagiri *et al.,* 2003, Melis 2009). Most of N_2-fixing cyanobacteria also possess the uptake hydrogenase enzymes, which catalyse the oxidation of H_2 produced by nitrogenase enzymes. Therefore, it is possible to enhance the cyanobacterial H_2 production by deactivating the attendant uptake hydrogenase. For example, a genetically modified cyanobacterium *Anabaena* AMC 414, in which the large subunit of the uptake hydrogenase was inactivated, could produce H_2 at a maximum rate of 40 – 45 mmol H_2 g Chl^{-1} hr^{-1}, that was more than twice that of the parent wild-type strain, *Anabaena* PCC 7120 (Lindblad, Christensson *et al.,* 2002). The last

approach involves the modification of metabolic pathways, competing with H_2 evolution for electrons, which include the cyclic electron flow and the assimilation of CO_2 to produce organic acids such as ethanol and other fermentation products (Levin, Pitt *et al.,* 2004). As the consequence, it is possible to re-direct additional electrons to the nitrogenase or hydrogenase enzymes by knocking-down undesirable metabolic pathways and, hence improving H_2 production (Doebbe, Rupprecht *et al.,* 2007, Burgess, Tamburic *et al.,* 2011).

3.5. Photobioreactors

3.5.1. Design Principles

In order to facilitate the growth and subsequent H_2 production of microalgae, there is a requirement for efficient, economic and scaled-up photobioreactor (PBR) systems (Giannelli, Scoma *et al.,* 2009, Posten 2009, Morweiser, Kruse *et al.,* 2010). At an industrial scale, an easily constructed, inexpensive, simple design of open systems such as natural ponds, circular ponds with a rotating arm for stirring, and raceway ponds, have already been used for commercial production of microalgal biomass for human and animal consumption. Commercially grown microalgae include the green algae *Chlorella* (human nutrition) *Dunaliella salina* (β-carotene) and *Haematococcus pluvialis* (astaxanthin) and cyanobacterium *Arthrospira platensis* (human nutrition) (Borowitzka 1999, Spolaore, Joannis-Cassan *et al.,* 2006). However, such open pond systems are definitely not suitable for biohydrogen production process, due to their incapability to efficiently collect a highly mobile and diffusive gaseous molecule. The systems also possesses an inefficient control of temperature and fluid dynamics, poor mass transfer and gas exchange within the microalgal culture, as well as a strong possibility of contamination, predation and evaporative losses (Carvalho,

Meireles *et al.,* 2006). As the consequence, enclosed PBR systems generally offer the better biomass and H_2 productivity, as they enable more controllable cultivation conditions, with improved properties of heat and mass transfer. Nevertheless, the main drawbacks of enclosed PBR systems are their high capital and operating costs (Melis 2002).

A photobioreactor can be described as a complex, multiphase system, consisting of the gaseous nutrients (CO_2 and N_2) and product (H_2), the liquid growth medium, and the solid biomass of microalgae, as well as the superimposed light radiation field (Borowitzka 1999, Posten 2009). Fundamentally, the features of PBR should include: an ability to support optimum cultivating conditions of microalgae (previously discussed in sections 3.3 and 3.4), an ease of scalability and an economically acceptance (Borowitzka 1999). Specifically, the PBR should have a high surface-to-volume ratio, so that there is sufficient light available for every individual cell. The culture within the reactor has to be well-mixed in order to ensure a uniform temperature and high level of light transfer as well as gas exchange (Borowitzka 1999). The reactor should also be equipped with various measuring instruments for monitor of key process parameters of the microalgal culture such as cell density, pH, dissolved O_2, CO_2 and H_2 concentrations. For the economic consideration, additional factors to be included are: the cost of construction materials, land, labour, utilities, local climate and the type of final product and the potential income (Borowitzka 1999, Posten 2009).

From literature, there are four different types of PBR geometries, previously employed to facilitate microalgal H_2 production: the vertical-column reactor, the flat-plate reactor, the tubular reactor and the stirred-tank reactor (Borowitzka 1999, Pulz 2001, Akkerman, Janssen *et al.,* 2002, Melis 2002, Carvalho, Meireles *et al.,* 2006, Ugwu, Aoyagi *et al.,* 2008, Posten 2009, Dasgupta, Jose Gilbert *et al.,* 2010, Tamburic, Zemichael *et al.,* 2011). Detailed character of each geometry is described in section 3.6.2.

3.5.2. Photobioreactor Geometries

Vertical-column reactors have a simple design, composing of transparent tubes, which are regularly made of polyethylene or glass. Agitation is provided by means of an air-lift loop or a bubble column (Sánchez Mirón, García Camacho *et al.,* 2000, Xu, Dapeng *et al.,* 2002) to provide mixing, supply of CO_2 and / or N_2 gases and O_2 removal for the liquid culture. They are compact, low cost, easy to operate, and therefore frequently used especially in larger laboratory scale for indoor microalgal growth experiments (Sánchez Mirón, Cerón García *et al.,* 2002, Posten 2009). The main advantages of vertical-column reactors are the high mass transfer, good mixing with low shear stress on microalgal cultures, low energy consumption, and ease of sterilisation (Ugwu, Aoyagi *et al.,* 2008). However, the main drawback of this type of PBR is its relatively low surface-to-volume ratio, which may result in an insufficient access to light of individual microalgal cells. Other drawbacks include the need for sophisticated construction materials to keep the bioreactor H_2 leak-free and the decrease of illumination surface area upon scale-up (Uyar, Eroglu *et al.,* 2007).

Flat-plate reactors typically consist of a rectangular, transparent compartment with a depth of 1 - 5 cm (Akkerman, Janssen *et al.,* 2002). The height and width of the reactor up to a practical limit of 1 m have been studied. This type of photobioreactors provides operational flexibility as they may be run in batch, semi-continuous and continuous modes (Tamburic, Dechatiwongse *et al.,* 2013, Dechatiwongse, Maitland *et al.,* 2015). The main feature of flat-plate reactors is a high surface-to-volume ratio, which leads to the best photosynthetic efficiencies observed for any PBR (Tamburic, Zemichael *et al.,* 2011). Usually, these bioreactors are illuminated from one side of their surfaces by a vertical panel of an artificial light source, while under outdoor conditions; they tend to be tilted at an angle, which allows optimal exposure to solar irradiation (Akkerman, Janssen *et al.,* 2002). The light availability decreases exponentially, as it transfers from an illuminated surface through the reactor's body, with an effective depth of 0.8 mm for fully grown microalgal cultures. In order to

minimise these light gradients, an effective air-lift mixing is required in order to achieve high biomass productivity of microalgae (Janssen, Tramper *et al.,* 2003). Another advantage of these reactors is a sufficient mass transfer capacity, resulting in an effective CO_2 supply and low O_2 accumulation (Sierra, Acién *et al.,* 2008). However, drawbacks of flat-plate reactors include the challenge in scalability, which requires multiple compartments and support materials, the difficulty in controlling culture temperature, some degree of wall growth and possibility of hydrodynamic stress on microalgal cells (Ugwu, Aoyagi *et al.,* 2008).

Tubular reactors consist of long, transparent tubes, with diameters from 3 to 6 cm and lengths ranging from 10 to 100 m (Janssen, Tramper *et al.,* 2003, Posten 2009). The tubes can be laid out in the form of horizontal, vertical, conical and inclined arrangements (Pirt, Lee *et al.,* 1983, Lee and Low 1991, Watanabe and Saiki 1997). They can be made from a wide variety of materials ranging from glass capillaries to plastic bags (Janssen, de Bresser *et al.,* 2000, Kunjapur and Eldridge 2010). The mixing is generally provided by pumping liquid culture through these tubes by means of mechanical or air-lift pumps. Tubular reactors are characterised by large illumination surface area, with suitable diameter of no more than 10 cm, and therefore suitable for outdoor cultivations (Molina, Acién Fernández *et al.,* 2000, Ugwu, Aoyagi *et al.,* 2008). In addition, they can be easily scaled up by the connection between sections via manifolds (Borowitzka 1999). The main disadvantages of these reactors include gradients of temperature, pH, dissolved O_2 and CO_2 along the tubes, some degree of wall growth and the requirement for large land space (Ugwu, Aoyagi *et al.,* 2008).

Stirred-tank fermenter-type reactors have regularly been used to conduct laboratory-scale microalgal H_2 production experiments (Melis, Zhang *et al.,* 2000, Janssen, Tramper *et al.,* 2003, Berberoglu, Yin *et al.,* 2007). Their widespread use may be explained by an ease of constructions, as they can be simply built by modifying common laboratory glass flasks. However, these reactors

are characterised by a low surface area-to-volume ratio, resulting in a poor light penetration. Therefore, providing internal illumination to stirred-tank systems through the use of optical fibres has been demonstrated as a means of improving their photochemical efficiency (Borowitzka 1999). Nevertheless, this approach would be difficult to implement for large-scale reactors (Chen, Saratale *et al.,* 2008, Fouchard, Pruvost *et al.,* 2008). The mixing of culture is typically provided by means of a mechanical stirrer, which gives rise to a number of drawbacks of these reactors: high energy consumption at large operational volumes (Chisti and Jauregui-Haza 2002), high extensional stress on the microalgal cells (Rosello Sastre, Csögör *et al.,* 2007) as well as a possibility of back-mixing (Pulz 2001, Cornet and Dussap 2009).

3.5.3. Scale-up and Commercialisation

The scalability of the vertical-column, flat-plate and stirred tank PBRs may be carried out by repeating multiple PBR units or by increasing the size of the individual units. In the case of tubular PBR, it may be scaled up by connecting additional tubes via manifolds (Borowitzka 1999). To order to minimise operating cost, large-scale PBRs need to be positioned outdoors for the direct use of solar illumination. Scale-up requires the development of a continuous and fully automated H_2 production process, which can be achieved by switching cultures between the growth and H_2 production stages using cell immobilisation (Laurinavichene, Fedorov *et al.,* 2006) or prolonging microalgal lifetime using continuous flow PBR systems (Amos 2004, Dechatiwongse, Maitland *et al.,* 2015).

Although scaling-up reduces H_2 production costs due to economies of scale effect, it introduces new challenges relating to the control of fluid dynamics, system maintenance and the extraction of H_2 product (Cournac, Mus *et al.,* 2002). Microalgal cells cultivated in large-scale outdoor PBRs are

more likely to be subjected to diverse environmental conditions such as intensive solar irradiation, daily fluctuations of light and temperature and high shear stress. Therefore, there are requirements for the cells that are stable, robust and resistant to contamination and fouling (Wijffels and Barbosa 2010), the properties that may be induced upon natural strains by genetic engineering.

In order to determine the commercial potential of any large-scale PBR systems, the most important parameter to be considered is the cost per unit of H_2 produced (Wijffels and Barbosa 2010). Since no commercial H_2 production facility currently exists, the estimations for biohydrogen production cost are extremely difficult and uncertain. According to an early analysis conducted by the National Renewable Energy Laboratory, the cost of H_2 production was estimated at \$0.57 - 13.53 per kg of H_2 produced (kg^{-1} H_2), depending on designs of biohydrogen production systems (Amos 2004). A study conducted by Melis reports the cost of H_2 production to be \$1.37 $kg^{-1}H_2$ (Melis 2007), but its assumed photochemical efficiency is much higher and currently not achievable by any outdoor PBRs. A more realistic cost estimation comes from Norsker and co-workers, who reported the cost of microalgal biomass production at \$8 kg^{-1} biomass and \$11 kg^{-1} biomass in tubular and flat-plate reactors respectively (Norsker, Barbosa *et al.,* 2011); for H_2 production, the cost would be approximately doubled and hence is in the range of \$16 - 22 $kg^{-1}H_2$. One kilogram of H_2 is energetically equivalent to a gallon of gasoline, which is currently traded at around \$ 2 – 3 (March 2015), including all taxes and charges. This huge gap between prices of these two fuels emphasises the necessity to improve efficiencies of biological H_2 production by a least a factor of 7 - 8, if the product is to become commercially competitive. The currently achievable photochemical efficiencies of microalgal H_2 production are around 2 % (Rupprecht, Hankamer *et al.,* 2006), under optimal laboratory condition, and 0.1 % under full sunlight (Tsygankov, Fedorov *et al.,* 2002). Theoretically, the efficiency could be achieved up to 11 – 16 % (Kruse, Rupprecht *et al.,* 2005, Prince and Kheshgi 2005).

Table 3.1: Summary of the parameters that affect *Cyanothece* 51142 growth

Parameter	Description	Comments
Light intensity	46 - 320 μE m^{-2} s^{-1}	Increasing light intensity increases growth rate
Wavelength	400 - 700 nm PAR 750 - 950 nm near infrared	Cyanobacteria effectively absorb light at 620 and 680 nm
Photosaturation	300 - 400 μE m^{-2} s^{-1}	Increasing light intensity has little effect on growth rate
Photoinhibition	> 500 μE m^{-2} s^{-1}	Increasing light intensity inhibits growth rate
Nutrients	Cyanobacteria require usable source of carbon, nitrogen, sulphur, phosphorus and trace metals	
Carbon source	Photoautotrophic: CO_2 only C-source Photoheterotrophic: glycerol only C-source Photomixotrophic: CO_2 and glycerol	Photomixotrophic best growth
Nitrogen source	Nitrogen-replete: Nitrate as N-source Nitrogen-fixing: N_2 as only N-source	Nitrogen-replete best growth
Fluid dynamics	Magnetic stirrer bar Circulation pump Gas-lift system	Improve light mixing Reduce photo-limitation Eliminate O_2, temperature and pH gradients
Temperature	25 – 37 °C	35 °C optimum 40 °C inhibition

Parameter	Description	Comments
pH	7.7 – 9.4	7.4 optimum
Contamination	Foreign algae and bacteria Fungi Zooplankton	Use sterilised vessels, air filters and fungicides

Table 3.2: Summary of the parameters that affect *Cyanothece* 51142 H_2 production

Parameter	Description	Comments
Cell density	Fully grown: 14 - 20 mg Chl L^{-1}	May be increased by immobilisation and truncated antennae
Light intensity	46 - 320 μE m^{-2} s^{-1}	92 μE m^{-2} s^{-1} optimum
Enzyme	Nitrogenases: ~ 250 μmol H_2 mg Chl^{-1} L^{-1} Hydrogenases: < 10 μmol H_2 mg Chl^{-1} hr^{-1}	Nitrogenases are predominant enzymes
Carbon source	Photoautotrophic: ~ 130 μmol H_2 mg Chl^{-1} L^{-1} Photomixotrophic: ~ 250 μmol H_2 mg Chl^{-1} L^{-1}	Glycerol induces anaerobic condition and enhance H_2 production
Nitrogen source	Nitrogen-replete: Nitrate and ammonium Nitrogen-fixing: N_2	Nitrate inhibits H_2 production
Induction procedure	Ar purging and O_2 absorber Environmental stimulation: Dark incubation Metabolic interfere: DCMU	Glycerol is an effective and inexpensive O_2 absorber
H_2 production duration	Batch: 7 – 10 days Fed-batch: up to 15 days Semi-continuous: > 1 month Continuous: > 1 month	Continuous longest duration and optimum H_2 production
Genetic modification	Truncating antennae Eliminating uptake hydrogenase enzymes Knocking-down competing pathways	

Parameter	Description	Comments
Temperature	25 – 40 °C	30 °C optimum
pH	7.7 – 9.4	7.4 optimum

Table 3.3: Summary of photobioreactor (PBR) geometries

PBR geometry	Advantages	Disadvantages
Open ponds	Commercial large-scale demonstration Easy to clean up after cultivation Good for mass cultivation of microalgae	Little control of culture conditions Poor productivity Prone to contamination
Vertical-column	High mass transfer rates Good culture mixing Low shear stress Compact, low cost and easy to operate	Small illumination surface area Difficult to keep H_2 leak-free Require high degree of turbulence Decrease of illumination surface area upon scale-up
Flat-plate	Large surface-to-volume ratio Operational flexibility Suitable for outdoor use Low O_2 build-up	Difficulty temperature control Wall growth High shear stress Expensive to scale up
Tubular	Large illumination surface area Suitable for outdoor cultivation Easy to manufacture Easy to scale up	pH and O_2 gradients along the tubes Wall growth Difficult to keep H_2 leak-free
Stirred-tank	Common laboratory use Easy and inexpensive to construct	High degree of back-mixing Energy-intensive mixing High shear stress Poor light penetration Difficult to scale up

3.6. Summary

Cyanothece 51142 is a unicellular, diazotrophic, non-heterocystous cyanobacterium capable of producing a remarkable rate of H_2 under anaerobic conditions through biological N_2-fixation. Under standard photoautotrophic growth conditions, solar energy is initially captured by light-harvesting proteins in PSII and used to carry out the water-splitting process to produce O_2, protons and electrons. Photosynthetic electrons are then transported down an electron transport chain, within the thylakoid membrane, during which it drives the biochemical synthesis of the energy-rich compounds – ATP and NADPH. The two compounds are later used to run the Calvin Cycle, which involves the fixation of CO_2 into intracellular carbohydrate compound such as glycogen. Under anaerobic conditions, induced by strong respiration rate of *Cyanothece* 51142, the carbon compound is reconverted into chemical energy, which powers many physiological activities of cells, including H_2 production. Alternatively, electron reserves, required for H_2 production, can also be derived from organic carbon substrate such as glycerol, provided to promote photoheterotrophic growth of *Cyanothece* 51142.

N_2-fixaiton process of *Cyanothece* 51142, catalysed by nitrogenase enzymes, involves the reduction of atmospheric N_2 into ammonia, concurrently evolving H_2 as by-product. In addition to nitrogenases, the cyanobacterium can also produce H_2 via hydrogenase enzymes, which catalyse the recombination between electrons and protons, produced from photosynthetic water splitting, to form H_2. However, nitrogenases are predominant enzymes in cyanobacterial H_2 production processes. The nitrogenase enzymes are rapidly inactivated by O_2, yet the cyanobacterium constantly photosynthetically produces O_2 and thereby posing a major challenge for the induction of H_2 production. The solution is to remove the O_2 as it is being produced; includes purging the *Cyanothece* 51142 culture with an inert gas, using an oxygen scavenger, by subjecting the

cyanobacterial culture to a period of dark incubation or to a low light intensity or using photosynthetic inhibitor. However, the most effective method for inducing *Cyanothece* 51142 H_2 production is to use glycerol as O_2 scavenger, as the substrate significantly reduces the photosynthetic activity, while enhancing the rate of respiration. Once the rate of photosynthetic O_2 evolution becomes below that rate of cellular respiration, it results in a net consumption of O_2 and eventually creates anaerobic conditions, necessary for the onset of H_2 production, within cultures.

In order for *Cyanothece* 51142 to effectively grow, it requires sufficient access to illumination, water and essential nutrients, including usable sources of carbon, nitrogen, sulphur, phosphorus and trace metals. Temperature between 30 – 35 ^{o}C and neutral pH are generally suitable for facilitating cyanobacterial growth. The growth of cyanobacteria is characterised by five distinct phases, including lag, exponential, linear, stationary and death, and follows the logistic population growth model. The cultures continue to grow at a specific rate until illumination or nutrient become limited, the condition at which the cell density eventually reaches the final saturation value. The growth of *Cyanothece* 51142 cultures is strongly influenced by various aspects of illumination including: light intensity, light mixing, light regime, photosaturation, photoinhibition and wavelength. Careful control of fluid dynamics, through appropriated mixing, is required to ensure efficient nutrient consumption, gas exchange and light distribution within the culture. The photoheterotrophic state - an addition of glycerol, plays a role to provide additional carbon source for cyanobacteria and induce anaerobic conditions within *Cyanothece* 51142 cultures. Nitrate also effectively facilitates the nitrogen-replete growth of cyanobacteria, but severely inhibits their ability to produce H_2. Parameters that affect *Cyanothece* 51142 growth are summarised in Table 3.1.

To increase the H_2 production rate of *Cyanothece* 51142, it is a prerequisite to obtain the fully grown and healthy cyanobacterial culture, which indicates the maximum number of H_2-producing

cells. In addition to environmental parameters facilitating optimal growth, immobilisation of cells on solid substrate has also been effectively used to increase the density of microalgal culture and its subsequent H_2 production rate. Once anaerobic environment is induced, an enhanced H_2 production can also be achieved by employing optimal conditions, such as low light intensity, temperature of 30 ^oC and photoheterotrophic state, extending H_2 duration and redirecting additional electrons towards nitrogenase enzymes. The duration of H_2 production can be significantly extended from one week into several months by various designs of novel photobioreactor systems. Furthermore, genetic modification techniques, including truncating light-harvesting antennae of photosynthetic apparatus, eliminating the uptake hydrogenase enzymes and knocking down competing metabolic pathways has shown promising results in improving photochemical efficiencies of microalgae. Parameters affecting H_2 production of *Cyanothece* 51142 are summarised in Table 3.2.

In order to make cyanobacterial H_2 production a commercial reality, there are requirements for efficient, affordable and scalable PBR systems. In comparison with open ponds, enclosed PBRs can provide more controllable cultivation conditions, better heat and mass transfer, and efficient H_2 leak-free systems, albeit at higher capital and operating costs. Four different geometries of PBRs, including, the vertical-column reactor, the flat-plate reactor, the tubular reactor and the stirred-tank reactor, have been previously employed for biological H_2 production studies. The advantages and disadvantages of different PBR geometries have been summarised in Table 3.3. Scaling up requires the development of a continuous and fully-automated H_2 production process. Although scale-up reduces the cost of H_2 produced due to the effect of economies of scale, it also introduces new challenges relating to the control of fluid dynamics, process maintenance and H_2 extraction from the reactor.

At present, cyanobacterial H_2 photoproduction is too expensive to commercially compete with other renewable processes such as electrolysis, primarily due to its low photochemical efficiency. For future prospect, advanced engineering approaches such as genetic modification for improving the photochemical efficiency and a biorefinery concept, at which the exaction of high value products is pursued in parallel to biofuel production, will play a key role in improving the current economic viability of biohydrogen production facilities.

4. Aim and Objectives

4.1. Aim

The unicellular cyanobacterium *Cyanothece* 51142 has an ability to produce renewable H_2 fuel through the biological N_2-fixation process. The aim of this thesis is to improve our understanding of the growth and the H_2 production of *Cyanothece* 51142 in order to develop a continuous, practical and scaleable biophotolytic H_2 production process, as well as to evaluate the potential of this technology as a sustainable source of H_2. This aim will be achieved by addressing the following three objectives.

4.2. Objectives

Objective I: Evaluate *Cyanothece* 51142 growth kinetics (Chapter I)

In order to achieve an effective H_2 production, it is necessary to know how to primarily grow dense and healthy *Cyanothece* 51142 cultures. The first objective is to evaluate the effect of some growth parameters - light intensity, temperature and nitrogen as well as carbon sources on cyanobacterial growth. Key parameters of growth kinetics - the maximum specific growth rate and the final biomass concentration, and nutrient uptake kinetics - the maximum specific uptake rate and the total nutrient uptake, will be measured from growth experiments. Correlations between cyanobacterial growth rates and variations in the cultivation conditions will be determined using a mathematical growth model.

Objective II: Evaluate *Cyanothece* 51142 H_2 production kinetics (Chapter II)

H_2 production by *Cyanothece* 51142 is strictly initiated under anaerobic and N_2-fixing conditions. With the supplement of glycerol, the cellular respiration becomes enhanced and eventually consumes all dissolved O_2, thereby inducing an establishment of anaerobiosis within cyanobacterial cultures. The second objective is to facilitate cyanobacterial H_2 production using glycerol as anaerobic inducer and subsequently evaluate the effect of two key environmental parameters - light intensity and temperature - on H_2-producing capability of *Cyanothece* 51142. Key parameters of gas production kinetics, such as the maximum production rate and corresponding yield, will be obtained from *in situ* experimental measurements. Correlations between gas production and variations in environmental conditions will be determined using a mathematical H_2 production model.

Objective III: Extend H_2 production by two-stage chemostat PBR system (Chapter III)

Anaerobic *Cyanothece* 51142 cultures, cultivated in batch system, ultimately experience unfavourable growth conditions and die, thereby failing to sustain their H_2 production capability. The third and final objective is to extend H_2 production duration by using a two-stage chemostat PBR system. Under this reactor configuration, two incompatible biological processes - aerobic growth and anaerobic H_2 production - will be independently and effectively handled using two physically-separated PBRs. In order to sustain the cyanobacterial growth, nutrients will be continuously fed into the primary growth PBR. The dense and healthy culture will then be transferred into an anaerobic culture, cultivated in the secondary PBR, for H_2 production. Under

chemostat operation, a constant feed rate will be maintained throughout a whole system and subsequently optimised. H_2 production rates and yields obtained from the developed system will be compared to the results of batch biohydrogen production experiments carried out as part of this thesis, as well as to the values recorded in the literature.

5. Experimental Methods

5.1. Inventories

In this section all the equipment and materials used during this thesis are summarised and specified.

5.1.1. Cyanobacterial Strain

The liquid culture of wild-type *Cyanothece* 51142 was originally purchased from American Type Culture Collection (ATCC). Once arrived, the strain was cultivated on agar plates as well as stored in liquid nitrogen within Professor Peter Nixon's laboratory in the department of Life Sciences at Imperial College London (ICL). The *Cyanothece* 51142 strain was used in all of experiments, carried out as part of this thesis. The purity of the cyanobacterial culture was constantly monitored using two different techniques in parallel – i) microscopy and ii) bacterial growth assay. For the latter method, a small amount of liquid *Cyanothece* 51142 stock culture was added into Luria Bertani growth medium, which is generally suitable for facilitating the growth of any bacteria, under sterile conditions. The liquid mixture was then left being shaken in an oven overnight. On the following day, if some white particles are observed in the liquid mixture, the observation then indicates the contamination.

5.1.2. Photobioreactors

Two different photobioreactor (PBR) geometries were used in this thesis: tubular and flat-plate. The Sartorius tubular PBR was primarily used to investigate *Cyanothece* 51142 growth kinetics. The

ICL flat-plate PBRs were used to examine H_2 production experiments. Table 5.1 shows the full PBR inventory.

5.1.3. Equipment

A list of the important pieces of equipment (and their manufacturers) used during experiments of this thesis is given in Table 5.2. It includes PBR peripheries, such as the control & data logging systems (Sartorius control tower and flat-plate Compact RIO), agitation (ecoline peristaltic and diaphragm pumps), illumination (circular fluorescent and LED arrays). All measuring instruments, including the pH, pO_2 and OD probes, are listed. General laboratory equipment, such as the toolbox, centrifuges, rig construction equipment and sterilisation equipment are also taken into consideration. Finally, large analytical instruments, including the nuclear-magnetic resonance, the ion chromatography, the spectrophotometer and the mass spectrometer, are also catalogued.

5.1.4. Chemicals

The chemicals (and their suppliers) used during experiments of this thesis are listed in Table 5.3. The list includes chemicals used for cleaning PBRs (Trigene and hydrogen peroxide solutions), biowaste disposal (Virkon tablets) and general sterilisation (ethanol). Electrode calibration and maintenance chemicals, incorporating pH electrode standard buffer solutions and pO_2 probe electrolytes, are catalogued. The various types of gases used for calibration of pO_2 electrode, purging and as carrier gases for mass spectrometry are also provided. All of the chemicals used in cyanobacterial growth medium preparation are indexed. Finally the chemicals required for ion chromatography and nuclear magnetic resonance analyses are also listed.

Table 5.1: Photobioreactor inventory

Geometry	Name	Description	Units
Tubular	Sartorius Biostat PBR 2S	2 litre helix, 1 litre central vessel	1
Flat-plate	ICL flat-plate PBR	1 litre vertical compartment	2

Table 5.2: Equipment inventory - photobioreactor peripheries, measuring instruments, laboratory equipment and analytical instruments

Equipment (manufacturer)	Application
Solar Biofuels Consortium PBR	
Fluorescent array (Abalab)	Illumination
Mechanical shaker (Abalab)	Mixing
Sartorius Biostat PBR 2S	
Circular fluorescent array (Sartorius)	Illumination
Ecoline peristaltic pump (Ismatec)	Mixing
Control tower (Sartorius)	Control & data logging
Pt100 thermocouple (Sartorius)	Temperature measurement
Fundalux OD probe (Sartorius)	OD measurement

Equipment (manufacturer)	Application
Easyferm pH electrode (Hamilton)	pH measurement
Oxyferm pO_2 electrode (Hamilton)	pO_2 measurement
Reglo peristaltic pump (Ismatec)	Medium addition & culture removal
ICL flat-plate PBR	
LED array (LED Wholesalers)	Illumination
Diaphragm pumps (KNF Neuberger)	Mixing
Liquid pumps (KNF Neuberger)	Temperature control
Compact RIO (National Instruments)	Control & data logging
Syringe pump (Chemyx)	Glycerol feed
Reglo peristaltic pump (Ismatec)	Culture addition & removal
K-type thermocouple (RS Components)	Temperature measurement
Photodiode (RS Components)	OD measurement
SP10T pH electrode (Consort)	pH measurement
SZ10T pO_2 electrode (Consort)	pO_2 measurement
Vacuum Prisma MS (Pfeiffer)	H_2 measurement (MIMS)

Equipment (manufacturer)	Application
Glass burette (Sigma)	H_2 measurement (water displacement)
Miscellaneous	
Laptop computers (Toshiba; Acer; HP)	Data logging & control
Centrifuge (Beckman)	Dry biomass preparation
Light meter (StellarNet)	Illumination calibration
Mini-centrifuge (MSE)	Sample analysis
Mass flow controller (Porter)	Gas flow control
Pipetteman classic (Gilson)	Medium preparation; Titration
Balance (Mettler Toledo)	Medium preparation
Water deioniser (Elga)	Medium preparation
Glassware (VWR)	Medium preparation; Sterilisation
Autoclave (LTE Scientific)	Sterilisation
Laminar flow hood (Microflow)	Sterilisation
Toolbox (Draper)	Rig construction
Stainless steel fittings (Swagelok)	Rig construction
Spectrophotometer (Perkin-Elmer)	OD measurement

Equipment (manufacturer)	Application
Compact IC Plus (Metrohm)	Nitrate and sulphate concentration measurement
Nuclear magnetic resonance (Bruker)	Glycerol and fermentative products concentration measurement

Table 5.3: Chemical inventory - photobioreactor cleaning & maintenance chemicals, electrode calibration & maintenance chemicals, laboratory gases, medium preparation chemicals, analysis technique chemicals and general laboratory chemicals

Chemical (supplier)	Application
Cleaning	
Trigene (Medichem)	Cleaning, ICL flat-plate PBRs
H_2O_2 (Sigma-Aldrich)	Cleaning, Sartorius PBR
Virkon (Fisher Scientific)	Biowaste disposal
70% ethanol (Sigma-Aldrich)	Sterilisation
Calibration & maintenance	
pH buffer solutions (Hamilton)	pH electrode calibration
Oxylyte electrolyte (Hamilton)	pO_2 electrode maintenance
pO_2 electrolyte (Consort)	pO_2 electrode maintenance
Ar (BOC)	pO_2 electrode calibration MS carrier gas (MIMS)
Air (BOC)	pO_2 electrode calibration Diazotrophic growth experiments
10% CO_2 in air (BOC)	Autotrophic and diazotrophic growth experiments

Chemical (supplier)	Application
20% CO_2 in He (BOC)	Autotrophic growth experiments
H_2 (BOC)	MIMS calibration
Anion multi-element standards (Merck)	IC calibration
Acrylic polish (Xerapol)	ICL flat-plate PBR maintenance
Medium preparation	
Na_2EDTA (Sigma-Aldrich)	ASP2
P1 metals (ICL)	ASP2
Iron solution (ICL)	ASP2
KCl (Sigma-Aldrich)	ASP2
$CaCl_2$ $2H_2O$ (Sigma-Aldrich)	ASP2
K_2HPO_4 (Sigma-Aldrich)	ASP2
NaCl (Sigma-Aldrich)	ASP2
Buffer solution (ICL)	ASP2
$MgSO_4$ (Sigma-Aldrich)	ASP2
Deionised water (ICL)	ASP2
$FeCl_3$ $6H_2O$ (Sigma-Aldrich)	Iron solution

Chemical (supplier)	Application
HCl (Sigma-Aldrich)	Iron solution; pH titration
NaOH (Sigma-Aldrich)	pH titration
TAPS (Sigma-Aldrich)	Buffer solution
TAPSO (Sigma-Aldrich)	Buffer solution
H_3BO_3 (Sigma-Aldrich)	P1 metal
$MnCl_2$ $4H_2O$ (Sigma-Aldrich)	P1 metal
$ZnSO_4$ $7H_2O$ (Sigma-Aldrich)	P1 metal
$CuSO_4$ $5H_2O$ (Sigma-Aldrich)	P1 metal
$CoCl_2$ $6H_2O$ (Sigma-Aldrich)	P1 metal
Na_2MoO_4 $2H_2O$ (Sigma-Aldrich)	P1 metal
Glycerol (Sigma-Aldrich)	Photoheterotrophic experiment; glycerol-feed
$NaNO_3$ (Sigma-Aldrich)	Nitrogen-replete experiment
Ion chromatography (IC) analysis	
Sodium carbonate (Merck)	IC liquid phase
Sodium bicarbonate (Merck)	IC liquid phase
Sulphuric acid (Merck)	IC liquid phase; HPLC liquid phase

Chemical (supplier)	Application
Nuclear magnetic resonance (NMR) analysis	
KHP	NMR reference
D_2O	NMR sample preparation

5.2. Unit Conversion

In this thesis, a number of different units and conversion factors have been used to quantify some key variables. This section summarises the measures used and how they are inter-related.

5.2.1. Light Intensity

Light intensity is one of the most important parameters that affect *Cyanothece* 51142 growth and H_2 production. There are two commonly used units for the measurement of light intensity in the field of microalgal research - photosynthetically active radiation (PAR) units and SI units (W m^{-2}) (Molina Grima, Fernández *et al.,* 1999). The former is a unit commonly used in biology to measure the solar irradiance in the wavelength range of 400 – 700 nm, the specific region of the solar spectrum which can be photosynthetically harvested by microalgae. It is given in units of microEinstein per square metre per second (µmol m^{-2} s^{-1}). Principally, one Einstein is the energy carried by one mole of photons. It is possible to calculate the amount of energy carried by a single photon using Equation 5.1.

$$E_v = \frac{h \cdot C}{\lambda} \qquad \text{Equation 5.1}$$

In this equation, E_v is the photonic energy, h is the Planck's constant, c is the speed of light and λ is the wavelength of the photon. Given a mean PAR wavelength of 550 nm, the photon would have an energy of 3.6×10^{-19} J. The energy of one mole of such photons, known as one Einstein, is calculated by multiplying the energy of a single photon by Avogadro's number, N_A, as shown in Equation 5.2.

$$E = E_v \cdot N_A = 216{,}000\ J \qquad \text{Equation 5.2}$$

Therefore, the power carried by one microEinstein of photons per second (1 μmol m^{-2} s^{-1}) is 0.216 J s^{-1}, and the corresponding surface irradiance is thus 0.216 W m^{-2}.

$$1\ \mu mol\ m^{-2}\ s^{-1} = 0.216\ W\ m^{-2} \qquad \text{Equation 5.3}$$

However, Equation 5.3 is only true if all the photons have a wavelength of exactly 550 nm. Since this is normally not the case, an approximate SI value is obtained by dividing the PAR value by 5.

5.2.2. Cyanobacterial Growth

During experiments of this thesis, the growth of *Cyanothece* 51142 was monitored by measuring the chlorophyll (Chl) concentration and the optical density (OD) of the cyanobacterial culture. The main advantage of using Chl content as a measure of growth is that it is strongly related to the health of the microalgal culture (Markov, Eivazova *et al.,* 2006). Any sign of contamination or malnutrition can quickly be detected and immediate actions can be taken to prevent further fouling of the culture (Siaut, Cuine *et al.,* 2011). However, it is not possible to carry out *in situ* Chl measurements, as manual samplings are required. On the other hand, OD measurements can be performed continuously and *in situ*, using OD probes that were readily available on the market (Akkerman, Janssen *et al.,* 2002). For Sartorius tubular PBR (section 5.3.1), the OD probe consists of a light emitting diode (LED) and a photodetector, located a short distance apart. Light scattering caused by cyanobacterial cells reduces the photocurrent in the probe and generates an OD measurement in terms of absorbance units (AU). The more scattering, the higher the generated OD.

In the case of Imperial College London flat-plate PBR (section 5.3.2), the light-measuring probe is a photodiode that measures the light coming through; hence, the more scattering, the lower the produced electrical signal (mV). It should be noted here that as the light-measuring probes for both PBRs are different, they subsequently yield different units of measurements and trends of correlations (Figures 5.1.A and B). Still, the main disadvantage of OD measurements is that they do not discriminate between healthy cells, dead cells, contaminants or impurities and hence may not fully represent the cell density of the microalgal culture (Melis and Melnicki 2006). As a result, both Chl and OD were simultaneously measured during the conduction of all experiments and finally related through mathematical correlations (Figures 5.1.A and B), which then allows the direct conversion from obtained OD output into Chl concentration. Using this approach, it became possible to online monitor the Chl concentration of the cyanobacterial cultures, thereby overcoming the drawback possessed by individual OD and Chl measurements.

Figure 5.1: Linear correlation between Chl concentration and optical density output of following PBRs.

A) Sartorius tubular

B) ICL Flat-plate

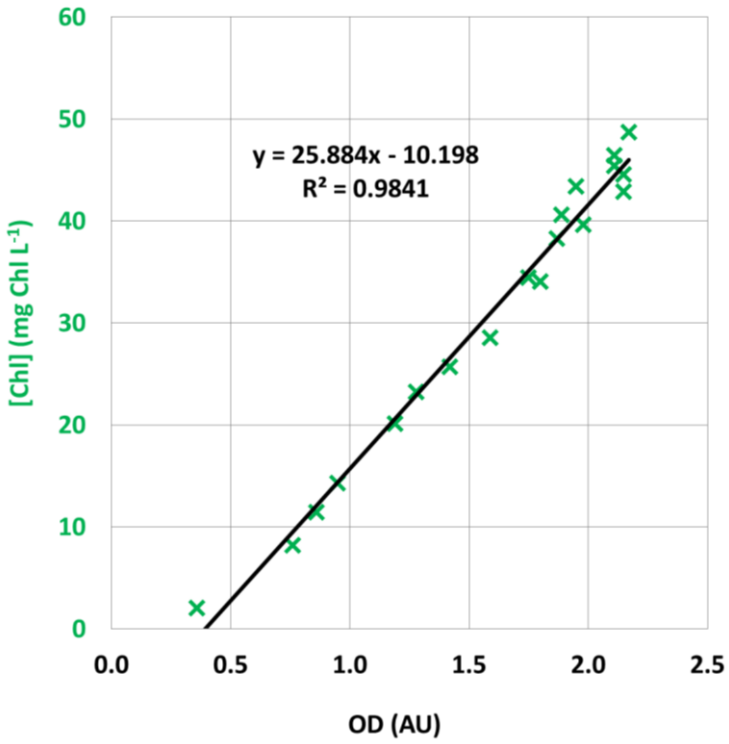

Figure 5.1.A: Chl concentration versus optical density output correlation of Sartorius tubular PBR, whose OD probe contains an LED that operates in the 870 - 910 nm wavelength range.

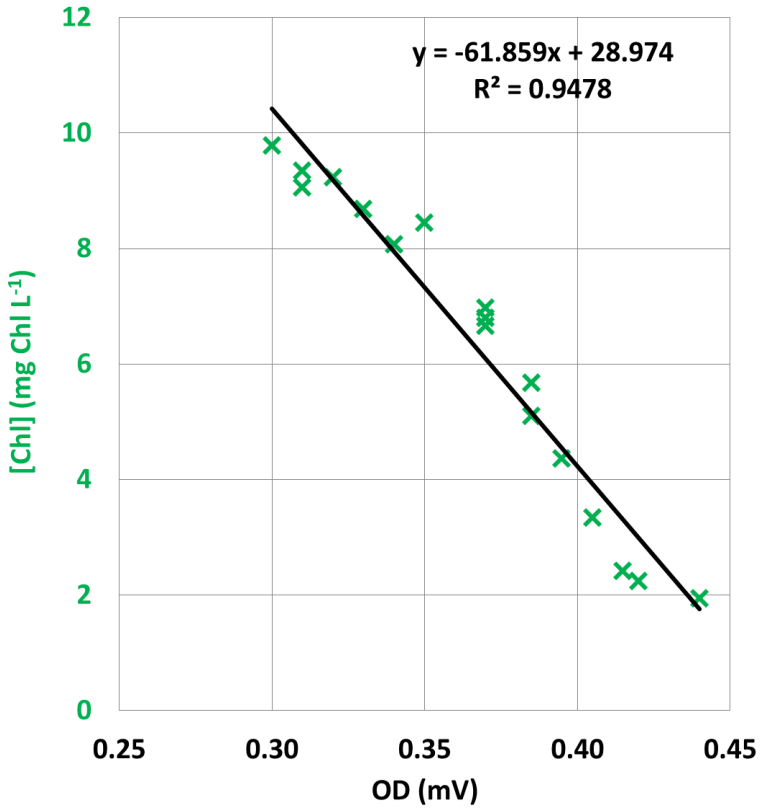

Figure 5.1.B: Chl concentration versus optical density output correlation of ICL flat-plate PBR, whose photodiode operates with an absorption bandwidth of 650 – 700 nm.

Specifically, Chl measurements were performed using a Lambda 40 UV / Vis Spectrometer from Perkin-Elmer Instruments running UV WinLab software. At any specific value of OD measurements, a small sample of culture (5 - 10 ml) was removed from PBRs under sterile conditions. Samples were then analysed in a 1.5 ml cuvette and the instrument was autozeroed with the light absorbed measurement from a cuvette filled with ASP2 medium. The total chlorophyll (Chl) concentration of cells was determined using Equation 5.4, previously proposed by Min and Sherman (Min and Sherman 2010).

$$[\text{Chl}]\ (\text{mg Chl L}^{-1}) = 14.97(A_{678} - A_{750}) - 0.615(A_{620} - A_{750}) \qquad \text{Equation 5.4}$$

In this equation, A_n is an absorbance spectrophotometrically determined at the specific wavelengths of 620, 678 and 750 nm, respectively. The obtained Chl concentration was then converted into the dry biomass concentration (X) using the previously determined linear regression correlation, Equation 5.5, which was based on a set of individual 32 gravimetrically determined data points, R^2 = 0.9617 (Dechatiwongse, Srisamai *et al.,* 2014).

$$X\ (\text{g L}^{-1}) = 0.0764 \cdot [\text{Chl}](\text{mg Chl L}^{-1}) + 0.0084 \qquad \text{Equation 5.5}$$

Using Equation 5.5, it becomes possible to convert individual data point of the measured Chl concentration into its corresponding dry biomass concentration and subsequently yield two new correlations (Figures 5.2.A and B), which enable a quick calculation of the biomass content from measured OD value without the need to continuously implement gravimetric method. The relationships are given in Equation 5.6 and 5.7 and will be utilised throughout the analysis of all growth experiments.

$$X\ (g\ L^{-1}) = 1.9755 \cdot OD\ (AU) - 0.7707 \qquad \text{Equation 5.6}$$

$$X\ (g\ L^{-1}) = -4.726 \cdot OD\ (mV) + 2.222 \qquad \text{Equation 5.7}$$

Figure 5.2: Linear correlation between biomass concentration and optical density output of following PBRs.

A) Sartorius tubular

B) ICL Flat-plate

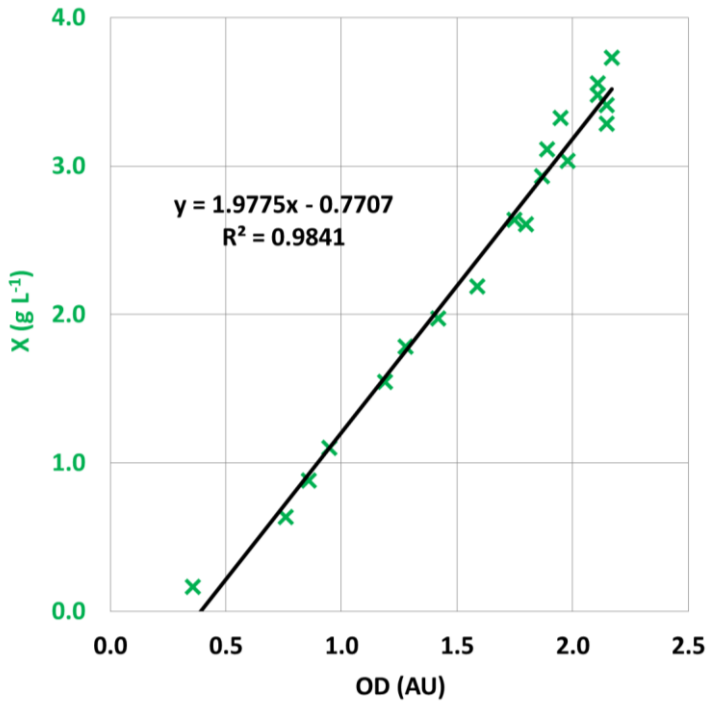

Figure 5.2.A: Biomass concentration versus optical density output correlation of Sartorius tubular PBR

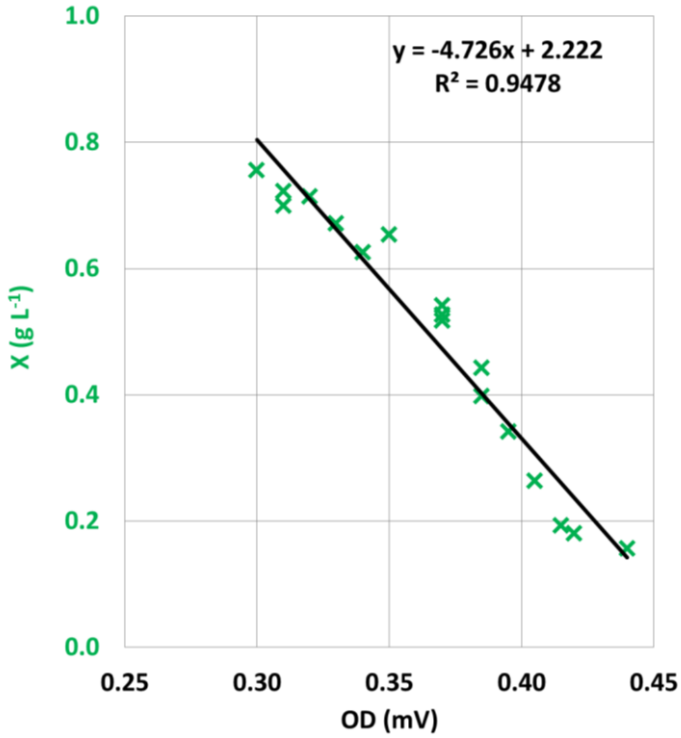

Figure 5.2.B: Biomass concentration versus optical density output correlation of ICL flat-plate PBR

5.2.3. Biohydrogen Production

Units of biohydrogen production, used during this thesis, can be expressed in terms of a production rate (ml H_2 L^{-1} hr^{-1}), a production yield (ml H_2 L^{-1}), or a solar-to-H_2 energy conversion (SHEC) efficiency (%). Both production rate and yield are similar in the way that they only consider the quantity of gas produced, whereas the efficiency also takes into account the solar energy input as well as the PBR dimension.

Even the measured H_2 production is usually expressed in volumetric basis (ml H_2 L^{-1}); it is possible to calculate the corresponding yields in mass (mg H_2 L^{-1}) and molar (mmol H_2 L^{-1}) basis, using

Equations 5.8 – 5.10. It should be noted here that H_2 production rates follow the same unit conversions as H_2 production yields.

$$\rho = \frac{P \cdot M}{R \cdot T} \qquad \text{Equation 5.8}$$

From Equation 5.8 - perfect gas law, ρ is the density of H_2 under given condition (g m^{-3}), P is the pressure (Pa), M is the molecular weight of H_2 = 2 g mol^{-1}, R is the universal gas constant = 8.314 J mol^{-1} K^{-1} and T is an absolute temperature (K). Given that operating temperature and pressure are maintained at 35 ^{o}C = 308 K and 1 bar = 10^5 Pa, the density can be estimated as 78.1 g m^{-3} or 0.078 mg ml^{-1}.

Once the density is calculated, the mass and molar H_2 yields can be estimated using Equations 5.9 and 5.10 respectively.

$$H_2 \text{ yield } (\text{mg L}^{-1}) = \text{Density } (\text{mg ml}^{-1}) \cdot H_2 \text{ yield } (\text{ml L}^{-1}) \qquad \text{Equation 5.9}$$

$$H_2 \text{ yield } (\text{mmol L}^{-1}) = \frac{H_2 \text{ yield } (\text{mg L}^{-1})}{H_2 \text{molecular mass } (\text{g mol}^{-1})} \qquad \text{Equation 5.10}$$

In the case of SHEC efficiency, it is defined as ratio of an equivalent energy output, generated from H_2 production, over an energy input from the supplied light source. Numerically, its expression is given as Equation 5.11 (Giannelli, Scoma *et al.,* 2009).

$$\text{SHEC efficiency (\%)} = \frac{\text{H}_2 \text{ yield} \cdot \text{H}_{2,\text{energy content}}}{\text{Light intensity} \cdot \text{Duration of illumination} \cdot \text{Irradiated area}} \cdot 100$$

Equation 5.11

In Equation 5.11, considering per litre of PBR volume, the H_2 yield (ml) is experimentally measured. The H_2 energy content is assumed to be the upper combustion value for H_2 = 12.94 J ml^{-1}. The input energy depends on an incident light intensity (W m^{-2}), the duration of illumination (s) and the active surface area of ICL flat-plate PBR - 0.048 m^2 (Tamburic, Zemichael *et al.,* 2011).

5.2.4. Concentration

For concentration of any compounds, the SI unit is a mole per decimetre cubed (mol dm^{-3}), which is the equivalent of a mole per litre (mol L^{-1}), or a millimolarity (mM). Measurements of small concentrations of the aqueous ions of nitrate (NO_3^{-1}), sulphate (SO_4^{-2}), phosphate (PO_4^{-3}) and glycerol were necessary to achieve the objectives of this thesis. These ions were incorporated into the cyanobacterial growth medium by dissolving a small mass of the appropriate salt, for example sodium nitrate ($NaNO_3$) in the case of NO_3^{-1}. It is therefore useful to express their concentrations in terms of the mass quantity - milligrams of dissolved ion per litre of growth medium (mg L^{-1}), which is also equivalent to parts per million (ppm). In the case of NO_3^{-1}, with a molar mass of 62 g mol^{-1}, this unit conversion is given in Equation 5.12.

$$1 \text{ mM } (NO_3^{-1}) = 1 \text{ mmol } L^{-1} (NO_3^{-1}) = 62 \text{ mg } L^{-1} (NO_3^{-1}) \qquad \text{Equation 5.12}$$

The remaining dissolved ion concentration conversions are shown in Table 5.4, together with all the other relevant unit conversions. Another important concentration measurement was that of dissolved oxygen content (pO_2), which indicates whether the *Cyanothece* 51142 culture is aerobic or anaerobic. Dissolved oxygen is normally measured as a percentage of O_2 saturation (%): 0% for an anaerobic culture, 21% for an aerated culture and 100% for an O_2-saturated culture. Under temperature and pressure of 35 °C and 1 bar respectively, the concentration of O_2-saturated seawater is ~ 180.1 µmol O_2 L^{-1} (Ramsing and Gundersen Unisense) ~ 5.8 mg O_2 L^{-1}. This relationship has been expressed in Equation 5.13.

$$1\ \text{mg}\ L^{-1}\ (O_2) = 17.2\ \%\ O_2\ \text{saturation} \qquad \text{Equation 5.13}$$

Table 5.4: Important unit conversions

Variable	Unit 1	Unit 2
Light intensity	1 µmol m^{-2} s^{-1}	0.2 $W \cdot m^{-2}$
OD (Sartorius)	1 AU	1.21 g L^{-1}
OD (ICL flat-plate)	0.1 mV	1.75 g L^{-1}
NO_3^{-1} concentration	1 mM	62 mg L^{-1}
SO_4^{-2} concentration	1 mM	96 mg L^{-1}
PO_4^{-3} concentration	1 mM	95 mg L^{-1}

Variable	Unit 1	Unit 2
Glycerol concentration	1 mM	92 mg L^{-1}
pO_2 concentration	1 mg L^{-1}	17.2 %

5.3. Photobioreactors

5.3.1. Tubular PBR

The Sartorius Biostat PBR 2S is a tubular flow reactor, purchased from Sartorius Stedim Biotech GmbH, Göttingen, Germany. The PBR consists of two major compartments, a 1-litre central vessel, surrounded by a 2-litre helix and has a maximum working volume of 2.9 litres. The central vessel houses all sampling and aerating equipment, measuring probes and temperature control systems and enables *in situ* measurements of temperature, pH, pO_2 and OD within the *Cyanothece* 51142 culture (Figure 5.3.A). The temperature of the aqueous culture is measured by a Pt100 Type 25-3 thermocouple and is controlled by means of a heated water jacket that encompasses the central vessel of the PBR. pH and pO_2 are measured by probes from Hamilton – Easyferm : Plus K8 160 pH electrode and OxyfermFDA 160 oxygen tension probe, respectively. The growth of the cyanobacterium is real-time monitored by the Sartorius Fundalux II OD probe, containing an LED that operates in the 870 - 910 nm wavelength range. In the case of the helix module, it has been designed to provide optimum illumination efficiency per surface area. Cultures within the helix are exposed to a circular array of cool white fluorescent lights, which is located between the central vessel and the helix (Figure 5.3.B). The circulation of cells up and around the helix, through the central vessel, and back into the helix is efficiently executed using an Ismatec peristaltic pump at a recirculation rate of 2,200 ml min^{-1}.

The major advantage of the Sartorius PBR is that all cultivating variables, such as the light intensity, temperature and pH, can be precisely controlled using the touch-screen Micro DCU-System display on the control tower (Figure 5.3.A). Every measurements collected can be data-

logged using specialised software. The tower and software were also supplied by Sartorius Stedim Biotech GmbH. Nevertheless, limitations of this tubular PBR, including the complexity of the reactor design with large numbers of joints on the fluid flow line, along with the nature of its peristaltic pump, make it very difficult to minimise diffusive H_2 losses from the reactor. As a result, during experiments of this thesis, the Sartorius PBR was primarily used to study the cyanobacterial growth kinetics under different conditions of environmental parameters (e.g. light intensity and temperature). It is also possible to run the Sartorius PBR in an open system using CO_2 as an exogenous carbon source to enable the autotrophic or mixotrophic growth conditions.

As the light intensity of the accompanying fluorescent light array, incorporated with the Sartorius PBR, is given as a percentage (%) of the maximum light output, a light meter, purchased from StellarNet, was used to determine a linear relationship between the Sartorius percentage units and PAR units, as shown in Figure 5.4 and Equation 5.14.

$$\text{PAR unit } (\mu\text{mol m}^{-2}\text{ s}^{-1}) = 4.41 \cdot \text{Sartorius units } (\%) - 65.1 \qquad \text{Equation 5.14}$$

Figure 5.3: Schematic diagram of Sartorius tubular PBR (Dechatiwongse, Srisamai *et al.,* 2014)

A) Side view

B) Top view

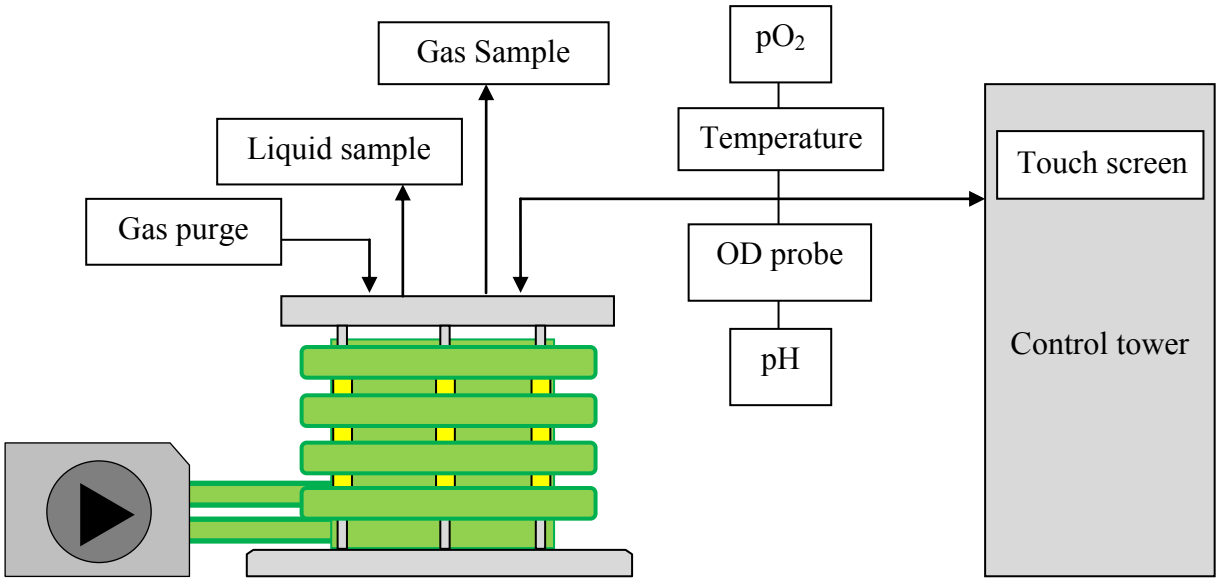

Figure 5.3.A: A schematic diagram showing the 3-L tubular PBR with its control tower, peristaltic pump and measuring and sampling instruments.

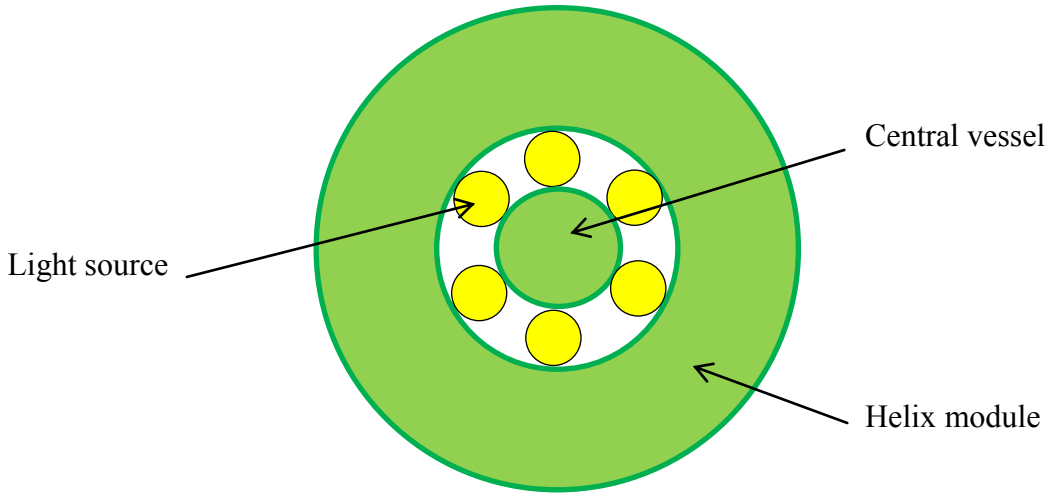

Figure 5.3.B: An outer green ring represents the 2-L helix module, whereas an inner green circle represents the 1-L central vessel. This figure does not show the top cover, which hosts all probes and sampling locations.

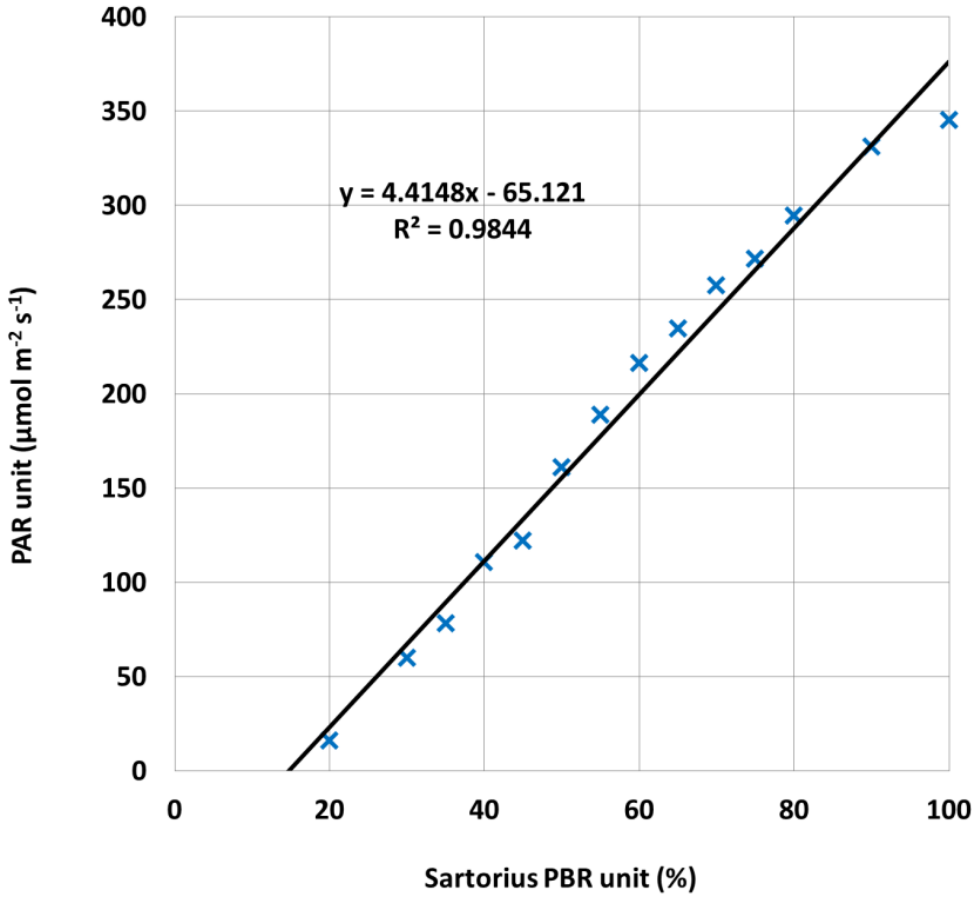

Figure 5.4: Light intensity calibration of Sartorius PBR

5.3.2. Flat-plate PBR

The ICL flat-plate PBR is a 1-litre dual compartment reactor, which was designed and developed by *Reaction Engineering and Catalytic Technology* (*REaCT*) research group, Department of Chemical Engineering, Imperial College London for a specific purpose of measuring and optimising photobiological H_2 production (Tamburic, Zemichael *et al.,* 2011), see Figures 5.5. The primary compartment is specifically used for cultivation of the *Cyanothece* 51142 strain as well as to host all of probe sensors for *in situ* measurements of pH, pO_2, temperature and OD within liquid cultures. The temperature of the culture is measured by a K-type thermocouple supplied by Omega. Two probes from Consort BVBA – the SP01T pH electrode and the SZ10T galvanic pO_2 electrode are used for *in situ* measurement of pH and dissolved O_2 concentration, respectively. The cyanobacterial growth is monitored using a photodiode operating with an absorption bandwidth of 650 – 700 nm. All measurements, datalogging and operational control were carried out using the National Instruments Compact RIO controller. Beside *in situ* measurements, it is also possible to manually collect gas sampling, from the headspace of the reactor, for mass spectrometry analysis. A syringe-based dosing pump can be employed to deliver sterile glycerol solution into the primary compartment for glycerol re-addition experiments. The use of the secondary compartment is for hot water recirculation, which then control the temperature of the primary compartment via heat transfer between these two compartments. The recirculation of hot water was executed using KNF Liquid pumps at the constant rate of 680 ml min^{-1}. Due to heat losses along the hot water pipeline, it thus becomes useful to determine a linear correlation between the cultural temperature and the water temperature of the water bath, as shown in Figure 5.6 and Equation 5.15.

$$\text{Cultural temperature } (^{o}\text{C}) = 0.67 \cdot \text{Water temperature } (^{o}\text{C}) + 6.87 \quad \text{Equation 5.15}$$

An illumination, facilitating the growth and H_2 production of cyanobacterial cultures, is provided by a panel of cool-white LED array, with a maximum operating intensity of 320 μmol m^{-2} s^{-1}. Similar to Sartorius PBR, as the light intensity of the LED array is also given as a percentage (%) of the maximum light output, the light meter was again used to determine a linear relationship between the ICL percentage units and PAR units, as shown in Figure 5.7and Equation 5.16. Agitation of the culture is achieved by means of a recirculating gas-lift flow powered by a KNF diaphragm pump.

$$\text{PAR unit } (\mu\text{molm}^{-2}\ \text{s}^{-1}) = 3.25 \cdot \text{ICL units } (\%) - 3.76 \qquad \text{Equation 5.16}$$

The main advantage of the ICL flat-plate PBR is its ability to enable rapid and accurate measurements of the key parameters in the biohydrogen production process under well-controlled conditions. Essentially, the technique of membrane-inlet mass spectrometry (MIMS) was developed and incorporated into the primary compartment to measure H_2 production *in situ* (Figure 5.5). In addition, the carefully considered reactor design, including the selection of Perspex (polymethyl methacrylate) for the construction of reactor's body, perfluoroalkoxy plastic (PFA) tubing for the set-up of air recirculation system together with the use of hydrogen-impermeable O-rings and stainless steel fittings, also minimise diffusive H_2 losses from the reactor.

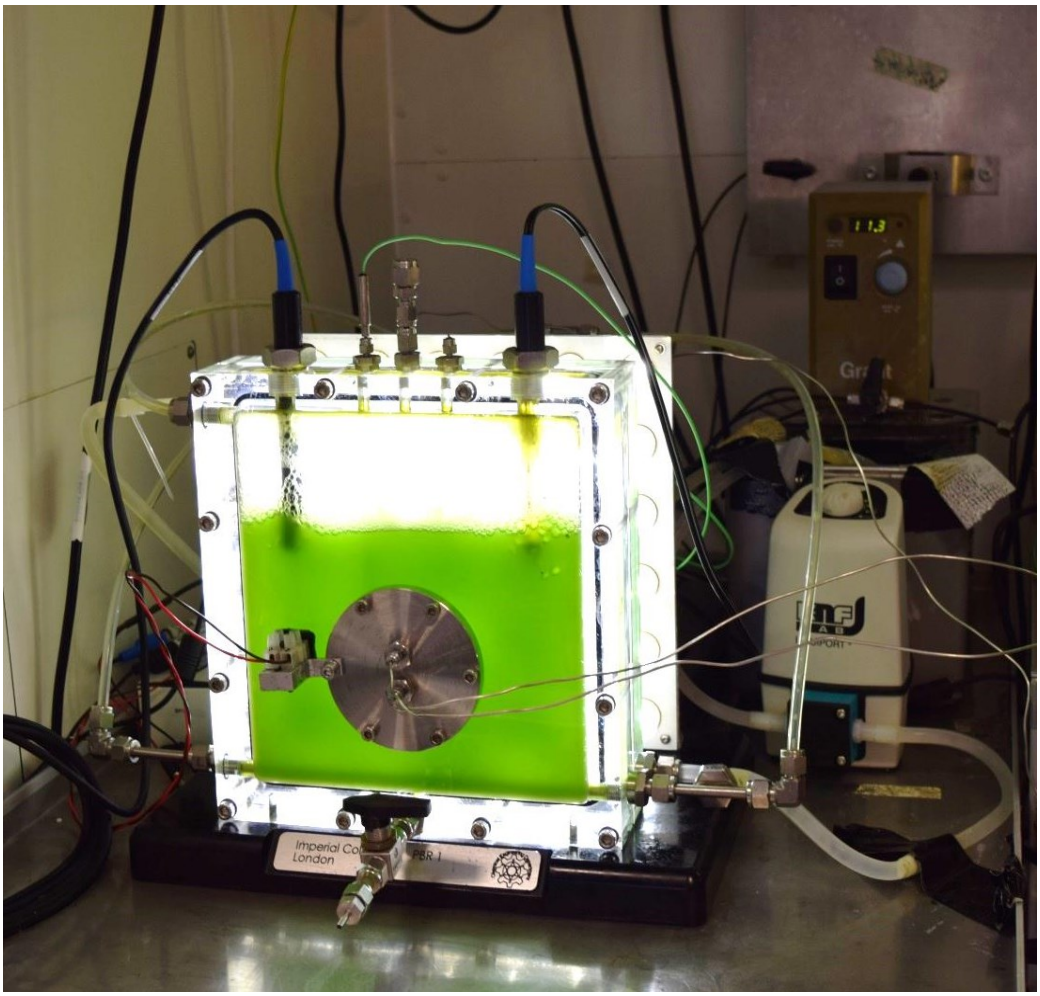

Figure 5.5: Experimental set-up of the ICL flat-plate PBR at Department of Chemical Engineering, Imperial College London

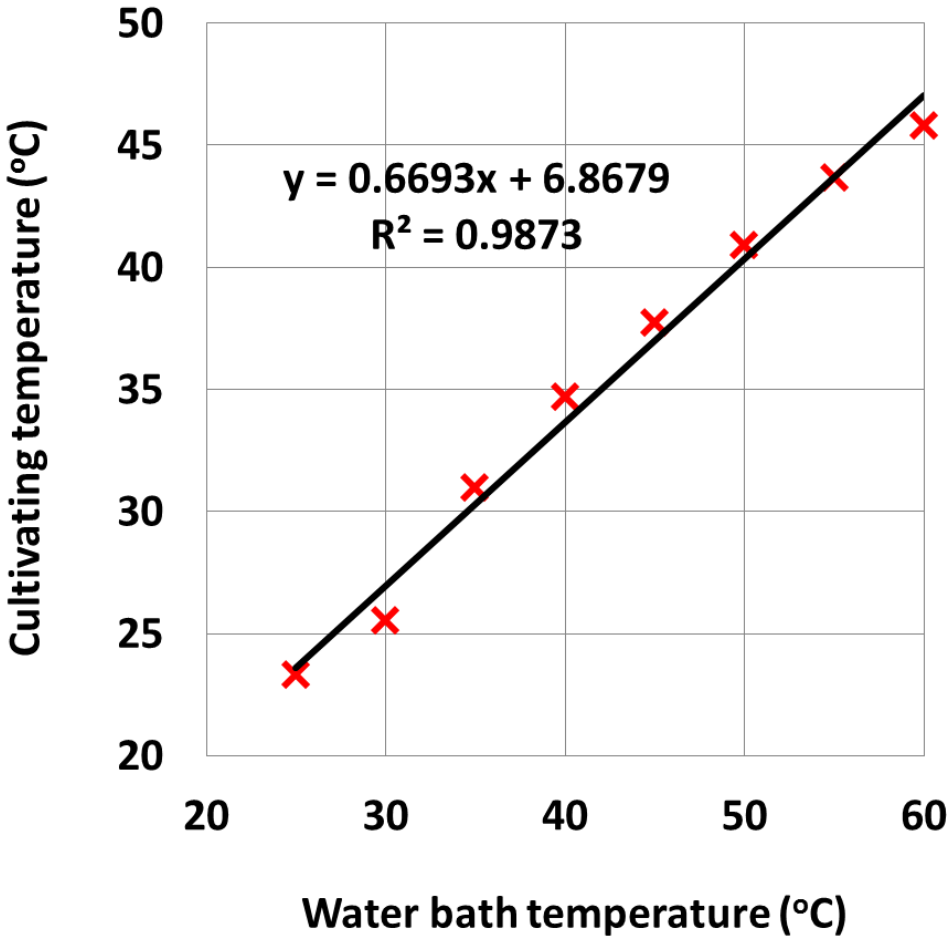

Figure 5.6: Temperature calibration of ICL flat-plate PBR

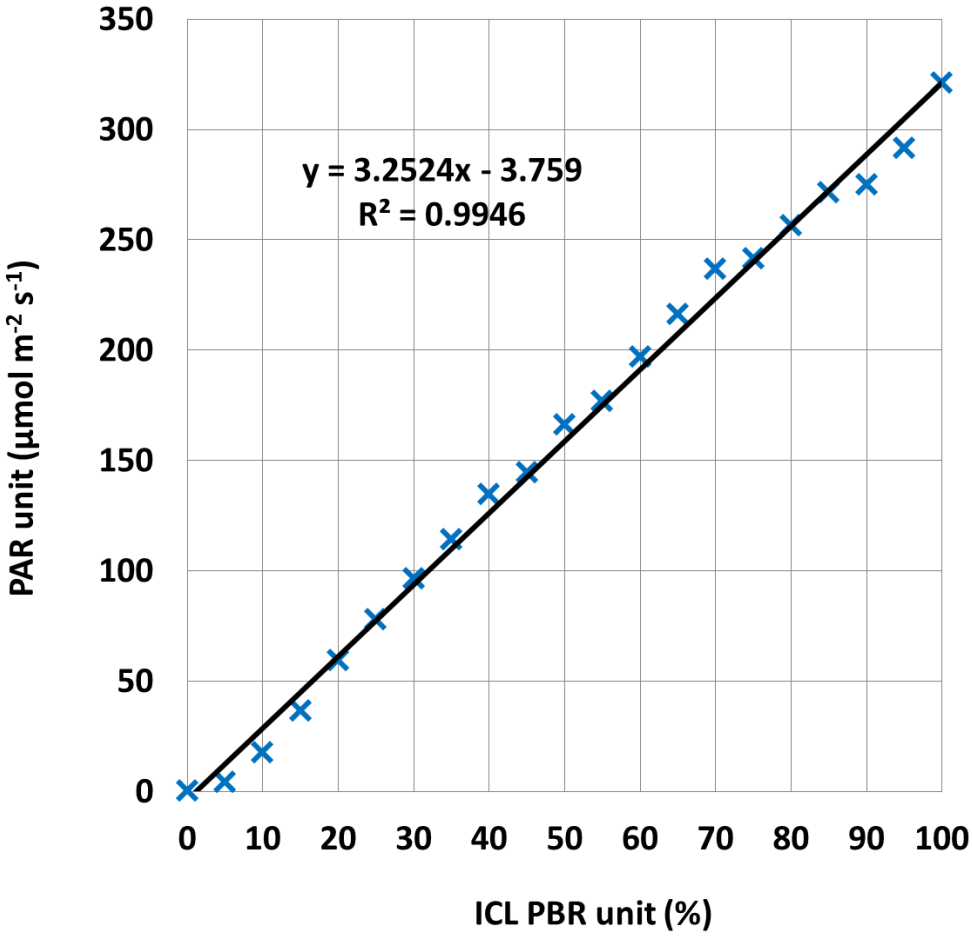

Figure 5.7: Light intensity calibration of ICL flat-plate PBR

5.4. Instrumentation

5.4.1. Measuring Instruments and Probes

The temperature of the aqueous culture within the Sartorius tubular PBR was measured by a Pt100 Type 25-3 thermocouple and maintained by means of a water bath in the double-layered central vessel. pH was measured by Easyferm : Plus K8 160 pH electrode (Hamilton). Dissolved oxygen concentration (pO_2) was measured by Oxyferm FDA 160 oxygen tension probe (Hamilton) by means of a Clark electrode suspended in oxylyte electrolyte. The OD of the cyanobacterial culture was monitored by the Sartorius Fundalux II OD probe, containing an LED that operates in the 870-910 nm wavelength range. This OD was correlated with the biomass content using Equation 5.6.

The temperature of the culture in the ICL flat-plate PBRs was measured with a K-type thermocouple supplied by Omega. Two probes from Consort BVBA – the SP01T pH electrode and the SZ10T galvanic pO_2 electrode were used for *in situ* measurement of pH and pO_2, respectively. The OD of the cyanobacterial culture was monitored using a photodiode operating with an absorption bandwidth of 650 – 700 nm. This OD was correlated with the biomass content using Equation 5.7. All measurements were recorded using a National Instruments datalogging and control system based around a National Instrument Compact RIO processor and running Lab View software (Tamburic, Zemichael *et al.,* 2011).

5.4.2. Calibration

In practise, all calibrations were repeated prior to the start of every experiment to ensure consistency of results and protect against systematic errors. The pO_2 probe proved to be particularly unstable and prone to blockage by cyanobacterial cells; as a precaution, the pO_2 electrolyte was always replaced, whereas the electrode membrane was frequently checked and replaced if necessary.

For ICL flat-plate PBRs, the pH probes were calibrated using three standard buffer solutions with known pH values of 4, 7 and 10. The relationship between pH value and its corresponding signal (mV) is strongly linear (Figures 5.8.A and B) and can be expressed as Equation 5.17. During calibration process, the probe-buffer contact was maintained over a brief period of time to ensure the stable pH signal.

$$\mathrm{pH\ (pH)} = -19.1 \cdot \mathrm{pH\ (mV)} + 7 \qquad \text{Equation 5.17}$$

To calibrate the pO_2 probes, the PBR was initially filled with the ASP2 growth medium, which was then flushed with gas containing known O_2 concentrations i.e. 0% oxygen in Ar-saturated water and 21% in air-saturated water. A linear correlation between pO_2 value and its corresponding signal (mV) is illustrated in Figures 5.9.A and B) and can be numerically expressed as Equation 5.18. The photodiode was calibrated using spectrophotometric measurements, as mentioned in section 5.2.2.

$$\mathrm{pO_2\ (\%)} = 398 \cdot \mathrm{pO_2\ (mV)} + 14 \qquad \text{Equation 5.18}$$

In the case of Sartorius PBR, the same procedures for pH and pO_2 calibrations were employed. However, there was no need of showing their calibrating equations here, as both pH and pO_2 signals were automatically converted into their corresponding concentrations by the Sartorius control tower. The OD probe reading was auto-zeroed in the ASP2 growth medium.

Figure 5.8: pH calibration of ICL flat-plate PBR

A) pH signal measurement at three known buffer solution

B) pH calibration

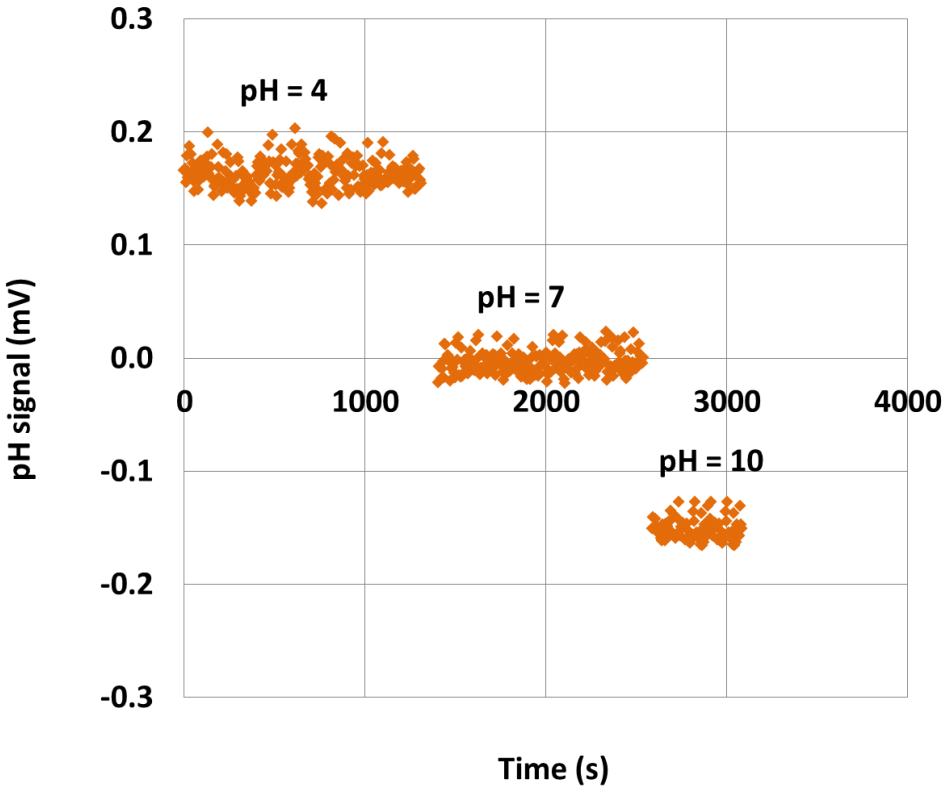

Figure 5.8.A: pH signal measurement at three known buffer solution – pH values of 4, 7 and 10.

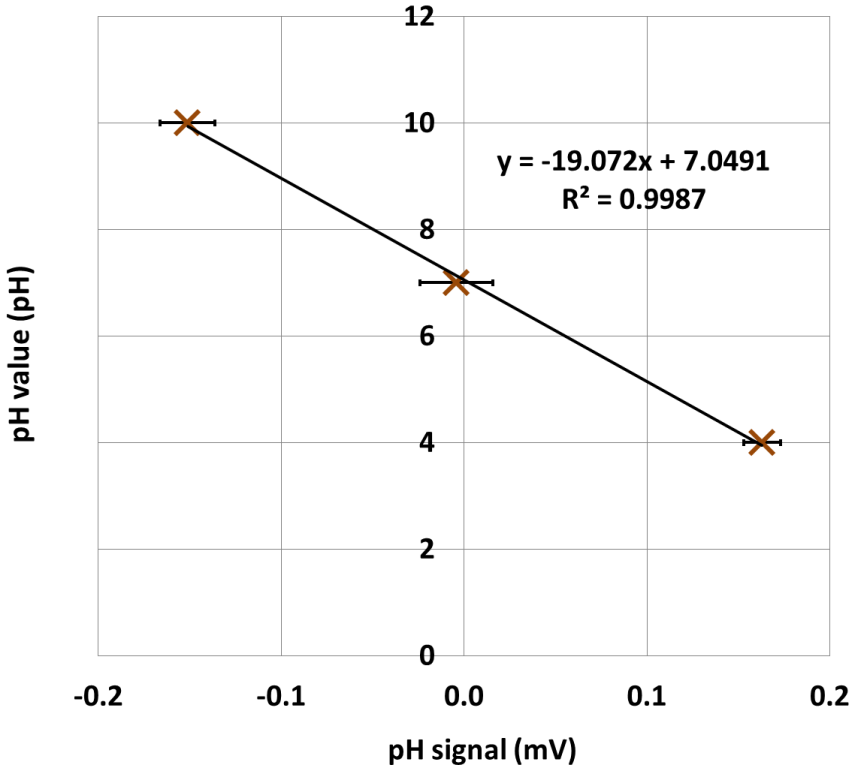

Figure 5.8.B: A linear correlation between pH value and probe signal

Figure 5.9: pO_2 calibration of ICL flat-plate PBR

A) pO_2 signal measurement at two known O_2 concentration

B) pO_2 calibration

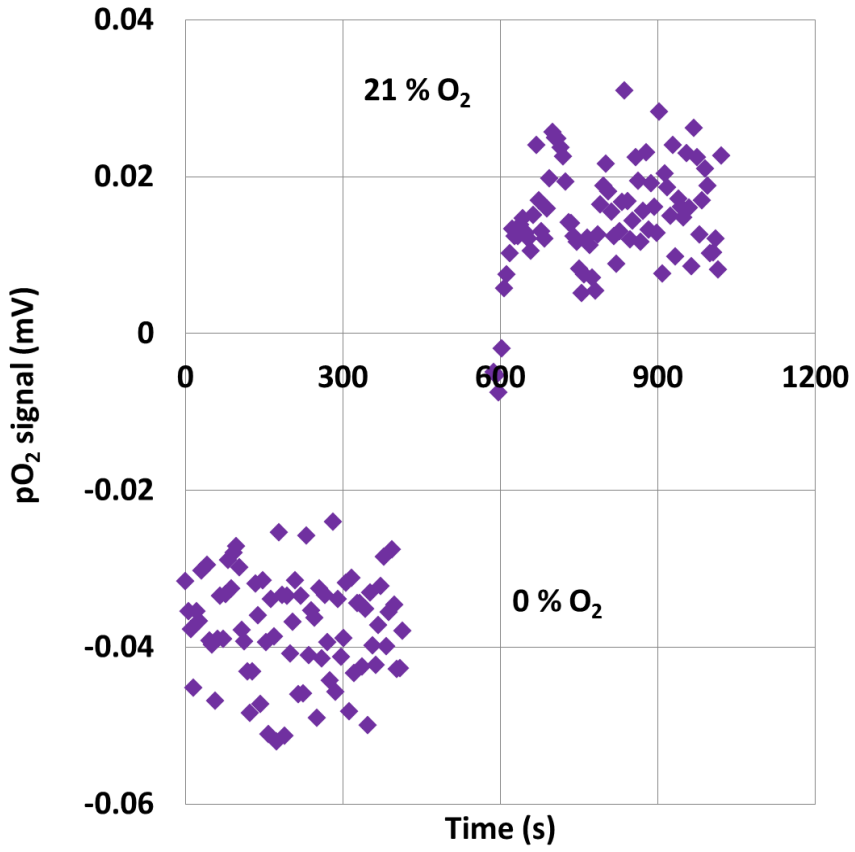

Figure 5.9.A: pO_2 signal measurement at two known O_2 solution – 0% and 21% O_2 saturation

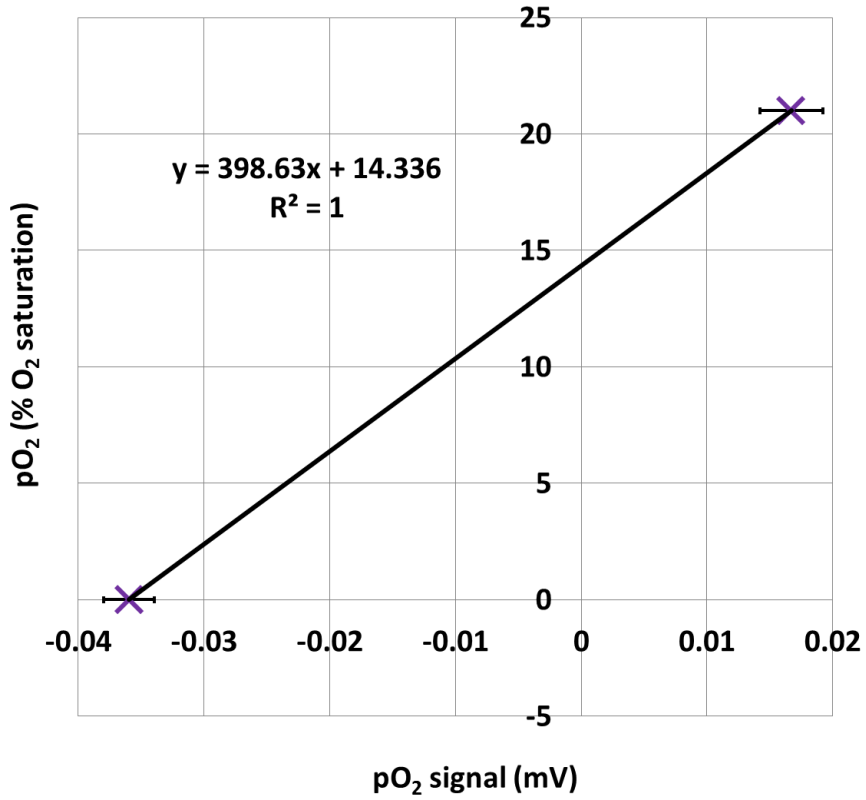

Figure 5.9.B: A linear correlation between pO_2 value and probe signal

5.5. Cleaning and Maintenance

It is very important to ensure that all PBRs are carefully cleaned and constantly maintained in order to avoid damage and contamination. After draining cultures out of flat-plate PBRs, reactors were manually disassembled and their individual interior parts were cleaned with common kitchen bleach. After that, reactors were re-assembled and fully filled with 50 % volume of Trigene in deionised water in order to remove all contaminants. The use of Trigene for PBR sterilisation proved to be a very effective, as this chemical is particularly a powerful bleach that is used to sterilise medical equipment and to clean blood stains, faeces and other high-level contaminants. Prior to experiments, Trigene was drained out and flat-plate PBRs were eventually rinsed with deionised water until there was no longer foam being produced.

The Sartorius PBR proved particularly difficult to clean because there is no direct access to the interior of the tubular helix module. It is impractical to use Trigene since it is difficult to rinse out of the helix and it would therefore be likely to affect subsequent experiments. Instead, cleaning was carried out with dilute hydrogen peroxide (H_2O_2), a strong oxidising agent that is frequently used as a disinfectant and an antiseptic. H_2O_2 was used to rinse out and decontaminate the inside of the PBR. It offers the added benefit of dissociating into water and O_2 upon the addition of hot water, hence leaving no harmful chemicals in the PBR at the end of the cleaning procedure. After the use of H_2O_2, the reactor was rinsed 2 - 3 times with warm water to remove all traces of H_2O_2 and any remaining cyanobacterial cell clusters. The sensitive measuring probes (OD, temperature, pH and pO_2) were not directly exposed to H_2O_2 but cleaned separately and re-inserted into the reactor before the start of experiments.

These cleaning protocols for both PBRs proved to be effective throughout the conduction of this thesis, as minimal level of contamination was detected within the liquid cyanobacterial culture being extracted from the cultivation system. Means to detect contamination have already been mentioned in section 5.1.1.

The cleaning procedures generally produce a large volume of cyanobacterial biowaste that must be disposed of. In a large-scale industrial process, it becomes a viable option to dry these cyanobacterial wet cultures so that the biomass can be later processed for fuel applications (electricity generation or biodiesel production) or used as human/animal nutritional supplementary (Morweiser, Kruse *et al.,* 2010, Stephens, Ross *et al.,* 2010). However, it is neither beneficial nor practical to do this with small laboratory-scale cyanobacterial volumes. As a result, wild type *Cyanothece* 51142 cells were therefore left for at least 24 hours in a biowaste container, containing Virkon tablets, at which point all cells were dead and could be disposed of safely down the sink.

5.6. Medium Preparation

5.6.1. ASP2

Cyanothece 51142 strain is a marine cyanobacterium, which is known to grow well in artificial seawater (ASP2) growth medium (Reddy, Haskell *et al.,* 1993). The ASP2 medium was prepared according to the classic recipe devised by Provasoli and colleagues (Provasoli, McLaughlin *et al.,* 1957). Stock solutions of ASP2 salts, iron solution, buffer solution, and P1 metal solution were prepared first. Preparations of ASP2 salts were simply done by dissolving disodium ethylenediamine tetraacetate (Na_2EDTA), potassium chloride (KCl), calcium chloride dihydrate ($CaCl_2$ $2H_2O$) and potassium phosphate dibasic (K_2HPO_4) in deionised water (Table 5.5.A). Iron solution was prepared from iron(III) chloride hexahydrate ($FeCl_3$ $6H_2O$) and hydrochloric acid (HCL) dissolved in deionised water (Table 5.5.B). Buffer solution is a buffer solution prepared from TAPS ($C_7H_{17}NO_6S$) and TAPSO ($C_7H_{17}NO_7S$) salts dissolved in deionised water (Table 5.5.C). P1 metal solution includes traces of boron, manganese, zinc, copper, cobalt and molybdenum; this solution was prepared by dissolving required quantity of each compound in deionised water (Table 5.5.D). The ASP2 recipe, shown in Table 5.5.E, includes ASP2 salts, iron solution, buffer solution, P1 metal solution, sodium chloride (NaCl) and magnesium sulphate ($MgSO_4$). The addition of NaCl and $MgSO_4$ is to increase the salinity of ASP2 medium in order to match that of actual seawater.

Once prepared, ASP2 growth medium was finally brought to the pH appropriate for cyanobacterial growth (typically pH 7.7) (Min and Sherman 2010) by titration with hydrochloric acid (HCl) and sodium hydroxide (NaOH), using a standard pH sensor as the indicator. A magnetic stirrer bar was

inserted into the glass flask containing the growth medium to enable a homogenous mixing of the system during this titration process. After titration, the flask was sterilised in an autoclave at 120 °C to kill any contaminating microorganisms. Stock solutions of ASP2 salts, iron solution, buffer solution and P1 metal solution were prepared in 100 - 1,000 ml batches and stored in a refrigerator at 5 °C. On the other hand, the ASP2 medium was prepared, titrated and autoclaved shortly before an experiment to minimise the risk of bacterial or fungal contamination.

Table 5.5.A: ASP2 salts recipe

Salt	Mass
Na_2EDTA	3 g
KCl	60 g
$CaCl_2\ 2H_2O$	37 g
K_2HPO_4	5 g

Dissolve in 1 litre of deionised water

Table 5.5.B: Iron solution recipe

Salt	Mass
$FeCl_3\ 6H_2O$	1.95 g
10 M HCl	5 ml

Dissolve in 500 ml of deionised water

Table 5.5.C: Buffer solution recipe

Salt	Mass
TAPS ($C_7H_{17}NO_6S$)	100.0 g
TAPSO ($C_7H_{17}NO_7S$)	100.0 g

Dissolve in 1 litre of deionised water, titrate to pH 7.7

Table 5.5.D: P1 metals recipe

Salt	Quantity
H_3BO_3	17.15 ml
$MnCl_2$ $4H_2O$	2.16 g
$ZnSO_4$ $7H_2O$	0.334 g
$CuSO_4$ $5H_2O$ (0.02 g ml^{-1})	0.075 ml
$CoCl_2$ $6H_2O$ (0.02 g ml^{-1})	0.3 ml
Na_2MoO_4 $2H_2O$ (0.022 g ml^{-1})	1.0 ml

Dissolve in 500 ml of deionised water

Table 5.5.E: ASP2 medium recipe

Component	Quantity
ASP2 salts	10 ml
P1 metals	1 ml
Iron solution	1 ml
Buffer solution	10 ml
NaCl	18 g
$MgSO_4$	2.44 g

Dilute to 1 litre with deionised water, titrate to pH 7.4

5.6.2. ASP2+N

Although *Cyanothece* 51142 has an ability to fix ambient nitrogen (N_2) and subsequently utilise the compound as its nitrogen source, its growth can be greatly enhanced in presence of fixed nitrogen sources – nitrate (NO_3^{-1}) or ammonium (NH_4^{+1}) (Markou and Georgakakis 2011). Between these two compounds, nitrate proves to be more effective at facilitating the *Cyanothece* 51142 growth without causing any deleterious effect, whereas an ammonium-induced growth inhibitory was reported (Feng, Bandyopadhyay *et al.,* 2010). Therefore, whenever in need of nitrogen-replete condition, sodium nitrate ($NaNO_3$) was added into the ASP2 growth medium, which was then renamed as the "ASP2+N" growth medium. The recipe of ASP2+N growth medium (Table 5.6) is

almost identical to that of ASP2 growth medium, with one additional step: $NaNO_3$ is supplemented into the growth medium at the concentration of 1.5 g L^{-1}, as recommended in literature (Reddy, Haskell *et al.,* 1993).

Table 5.6: ASP2+N medium recipe

Component	Quantity
ASP2 salts	10 ml
P1 metals	1 ml
Iron solution	1 ml
Buffer solution	10 ml
NaCl	18 g
$MgSO_4$	2.44 g
$NaNO_3$	1.5 g

Dilute to 1 litre with deionised water, titrate to pH 7.4

5.6.3. ASP2+C

H_2 production by *Cyanothece* 51142 is initiated when nitrate and oxygen are deprived from the culture, as the absence of both parameters fully activates the activity of nitrogenase enzymes (Dutta, De *et al.,* 2005). Under autotrophic growth conditions, *Cyanothece* 51142 photosynthesises, using

water and solar energy to fix CO_2 and subsequently produce sugar and oxygen. The cells also undergo respiration using up O_2 and stored carbon to provide the energy needed for their reproduction. Because of its circadian-regulated metabolic shift behaviour, *Cyanothece* 51142 performs photosynthesis and respiration in light / dark cycles (Bandyopadhyay, Stoeckel *et al.,* 2010), thereby causing periodically alternating environment between aerobic and anaerobic. In order to impose a continuous anaerobic condition upon cyanobacterial cultures, CO_2, as an original sole carbon source, was replaced by glycerol ($C_3H_8O_3$) (Dechatiwongse, Maitland *et al.,* 2015), thereby changing the growth condition from autotrophic to heterotrophic. Glycerol addition results in metabolic changes within *Cyanothece* 51142. Specifically, it inhibits photosynthetic activity, while promoting respiration rate (Aryal, Callister *et al.,* 2013). During glycerol consumption, electrons and reducing powers are also produced and subsequently serve as energy source for N_2-fixation. As a result, photosynthetic O_2 evolution is no longer occur, while respiration levels are significantly higher, causing the culture to eventually become anaerobic.

The most practical way of inducing *Cyanothece* 51142 H_2 production is thus by using the ASP2+C growth medium. The recipe of this medium (Table 5.7) is very similar to that of the ASP2 medium, which does not have any nitrate salts, but it also contains glycerol. From my experiences, it is important to put in glycerol content sufficient for inducing anaerobiosis, as too low level would then lead to re-initiation of photosynthesis and subsequent cessation in H_2 production. On the other hand, very high glycerol level (~ 75 mM) also results in slow growth rate (Alagesan, Gaudana *et al.,* 2013) and high associated nutrient cost (unless wasted glycerol, generated as by-product of bio-diesel production, is used instead). Having optimised the glycerol level, its final concentration within the starting culture (stock culture + medium) is 50 mM. For every H_2 production experiment, as the volume ratio of stock culture (200 ml) to ASP2+C growth medium (600 ml) was always fixed at 1 to 3, this makes up the total volume of all starting cultures as 800 ml. When

preparing glycerol content in the medium, the dilution factor of 0.75 needed to be taken into account. Numerically, the glycerol concentration of ~ 67 mM within the ASP2+C growth medium is required in order to achieve the final concentration of 50 mM within the starting culture.

Table 5.7: ASP2+C medium recipe

Component	Quantity
ASP2 salts	10 ml
P1 metals	1 ml
Iron solution	1 ml
Buffer solution	10 ml
NaCl	18 g
$MgSO_4$	2.44 g
Glycerol	4.94 ml

Dilute to 1 litre with deionised water, titrate to pH 7.4

5.7. Stock Culture Preparation

Cyanothece 51142 cells were scraped off an agar plate and re-suspended in a sterilised 50 ml Corning flask filled with autoclaved ASP2+N medium. This procedure was performed inside a laminar flow hood, a device that filters ambient air to minimise particulate concentrations. Before making cell transfer, the working surface of the sterile hood and the nitrile lab gloves were washed with 70% ethanol in order to ensure a sterile environment during the early stages of cyanobacterial growth. Reasonably, this is the period when the culture is most vulnerable to contamination. The 50 ml flask was kept under the optimal growth conditions recommended in the literature: at 30°C, with starting pH of 7.4 and under continuous cool-white fluorescent illumination of 46 μmol m^{-2} s^{-1} (Reddy, Haskell *et al.,* 1993). The mixing was provided by a mechanical shaker. After approximately 5 days of cultivation, the culture was scaled up to a volume of 200 ml. Once again, a sterile hood was used to transfer the contents of the 50 ml flask into a 200 ml flask, which was then topped up with freshly made and sterile ASP2+N medium. As the cell density of *Cyanothece* 51142 increased, the culture became greener and less transparent. The entire growth process lasted less than 2 weeks. At that point, fully grown stock cultures were ready to be used for experiments (200 ml for ICL flat-plate PBR and 400 ml for Sartorius PBR).

5.8. Analytical Techniques

5.8.1. Spectrophotometry

Spectrophotometry was used to determine the OD of *Cyanothece* 51142 culture by light absorption. ODs, measured in both absorbance units (AU) and signal (mV), have a linear relationship with the Chl content and the dry biomass concentration of that culture (Figures 5.1.A and B and Figures 5.2.A and B). A Lambda 40 UV / Vis Spectrometer from Perkin-Elmer Instruments running the UV WinLab software was used to measure OD of the culture at three distinct wavelengths of 620, 678 and 750 nm. The Chl content was estimated from obtained ODs using Equation 5.4. Using Equation 5.5, the corresponding dry biomass content can be calculated from the Chl concentration. Cyanobacterial samples were analysed in a 1.5 ml cuvette and the instrument was autozeroed with the light absorbed measurement from a cuvette filled with ASP2 medium.

5.8.2. Ion Chromatography

Ion chromatography (IC) was used to quantitatively determine the change of macro-nutrients - nitrate (NO_3^{-1}), sulphate (SO_4^{-2}) and phosphate (PO_4^{-3}) concentrations, in the aqueous culture. This task was carried out using the 882 Compact IC Plus instrument with an 863 Compact Autosampler from Metrohm running the MagIC Net software. The separation column was a Metrosep A Supp 5, with the dimensions of 150.0 mm L x 4.0 mm ID. The concentrations of compounds eluting from the column were measured by means of a conductivity detector in units of microSiemens per centimetre ($\mu S\ cm^{-1}$). The sodium-based anion solution (liquid phase) consisted of 3.2 mM sodium carbonate (Na_2CO_3) and 1.0 mM sodium bicarbonate ($NaHCO_3$). Deionised water was used as the

rinse and 0.1 M sulphuric acid (H_2SO_4) as the regenerator. The liquid phase was pumped through the instrument using a peristaltic pump at a flow rate of 0.7 ml min^{-1}. The anion concentrations corresponded to the area occupied by their respective peaks. These areas were calibrated against standard concentration using CertiPUR Anion Multi-Element Standards from Merck at concentrations of 1, 10, 50, 100 and 150 ppm (1 ppm = 1 mg L^{-1}). Retention times, when the anions were eluted from the column, were 10.3, 13.8 and 16.2 minutes for NO_3^{-1}, SO_4^{-2} and PO_4^{-3}, respectively. For sample preparation, cyanobacterial samples were spun down in a mini-centrifuge at 13,000 rpm for 10 min – only the supernatant liquid was used for IC investigation. The purified liquid was diluted by a factor of seventy to avoid the column being overloaded. However, it was subsequently found that the PO_4^{-3} concentration present in the medium was not sufficiently high to be tracked by this technique. IC was therefore primarily used to measure the nitrate and sulphate uptake during cyanobacterial growth. In addition, the IC signal also showed a peak at 6.2 min, which was correspond to chloride (Cl^-). However, as Cl^{-1} was not my interested compound, its concentration was not calculated. A representative IC result, showing the Cl^{-1}, NO_3^{-1} and SO_4^{-2} conduction peaks, is presented in Figure 5.10. For both NO_3^{-1} and SO_4^{-2}, the linear relationship between anion concentration and its conduction peak area can be seen from Figures 5.11.A and B, respectively. Equations 5.19 and 5.20 were used to correlate NO_3^{-1} and SO_4^{-2} peaks area (µS cm^{-1} min) with their corresponding concentrations (mg L^{-1}).

$$\left[NO_3{}^{-1}\right]\,(\text{mg L}^{-1}) = 4.9 \cdot \text{Area of } NO_3{}^{-1}(\mu\text{s cm}^{-1}\text{min}) \qquad \text{Equation 5.19}$$

$$\left[SO_4{}^{-2}\right]\,(\text{mg L}^{-1}) = 3.9 \cdot \text{Area of } SO_4{}^{-2}(\mu\text{s cm}^{-1}\text{min}) \qquad \text{Equation 5.20}$$

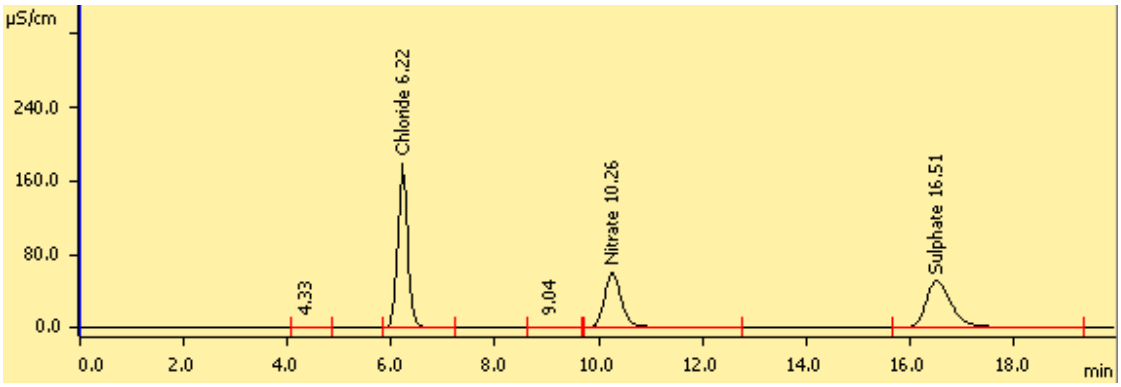

Figure 5.10: Representative ion chromatography (IC) results

Figure 5.11: IC calibration for anion

A) NO_3^{-1}

B) SO_4^{-2}

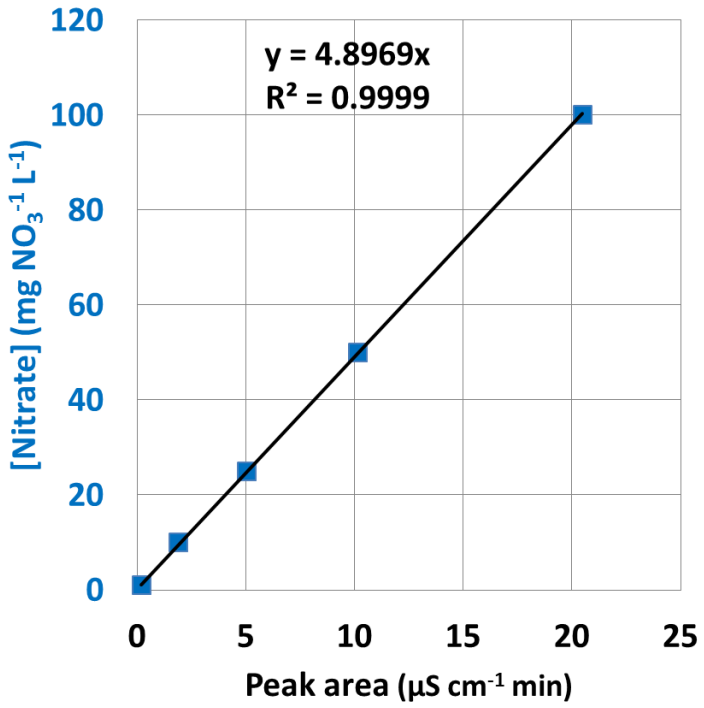

Figure 5.11.A: IC calibration for NO_3^{-1}

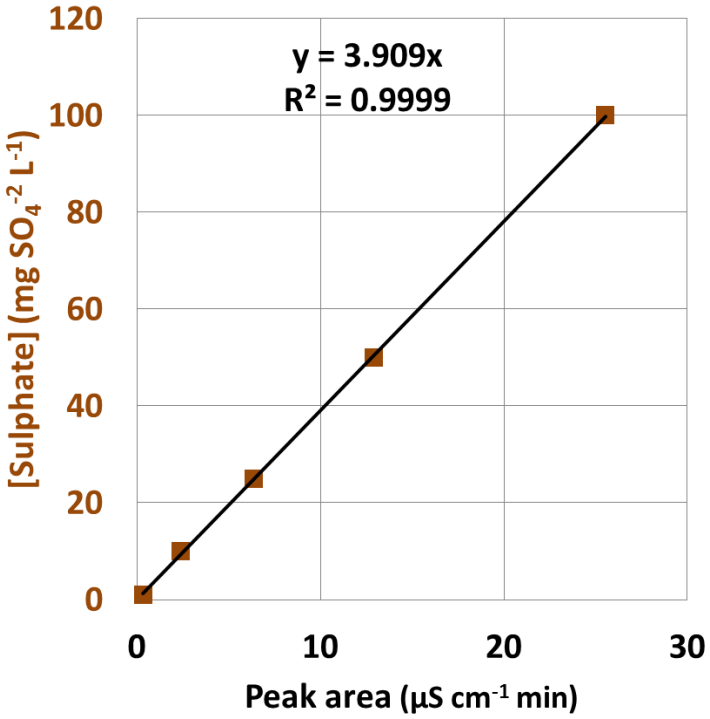

Figure 5.11.B: IC calibration for SO_4^{-2}

5.8.3. Nuclear Magnetic Resonance

Proton nuclear magnetic resonance spectroscopy (^{1}H NMR) was used to quantitatively determine the concentrations of glycerol as well as cellularly excreted fermentative products (ethanol and acetic acid) in the aqueous culture. NMR spectra were recorded on Bruker DRX-400 (^{1}H, 400.1 MHz) and AV-400 (^{1}H, 400.3 MHz) spectrometers, at 298 K. The spectra were processed using MestreNova software. The concentrations of my interested compounds corresponded to the area occupied by their respective peaks. These areas were calibrated against standard concentration using a non-reactive potassium hydrogen phthalate (KHP) at known concentration of 50 mM. The concentration was estimated using Equation 5.21, which takes into account both peak area and the number of proton giving the NMR signals. ^{1}H chemical shifts are reported as δ (in ppm) and referenced to the residual proton signal of the deuterated solvent (^{1}H: D_2O **δ** 4.70). The chemical shifts of KHP, glycerol, ethanol and acetic acid are tabulated in Table 5.8. For sample preparation, 5 ml of cyanobacterial samples, directly collected from the reactor under sterile condition, were spun down in a mini-centrifuge at 13,000 rpm for 10 min – only the supernatant liquid was used for NMR investigation. Equal volumes (200 µl) of the purified liquid, deuterium oxide (D_2O) and KHP were then injected into the NMR tube, which was gently shaken to provide homogenous mixing. The chemical shift of an individual compound in the sample was confirmed by running ^{1}H NMR of the purified compound.

$$\frac{[C_i]}{[C_{KHP}]} = \frac{A_i}{A_{KHP}} \cdot \frac{n_{KHP}}{n_i} \qquad \text{Equation 5.21}$$

In this equation, C_i, A_i and n_i are the concentration, the peak area and the number of protons giving the NMR signals of a particular compound, respectively. For KHP, its concentration = 50 mM, the area = 1 and n = 2.

Table 5.8: The chemical shifts of my interested compounds

Compounds	Chemical shifts	number of equivalent nuclei given the signals
Glycerol	3.44-3.58, 3.66-3.70	2
Acetic acid	1.95	3
Ethanol	1.08, 3.50-3.56	3
KHP	7.4 – 7.5, 7.6 – 7.7	2
D_2O	4.4 – 5.0	-

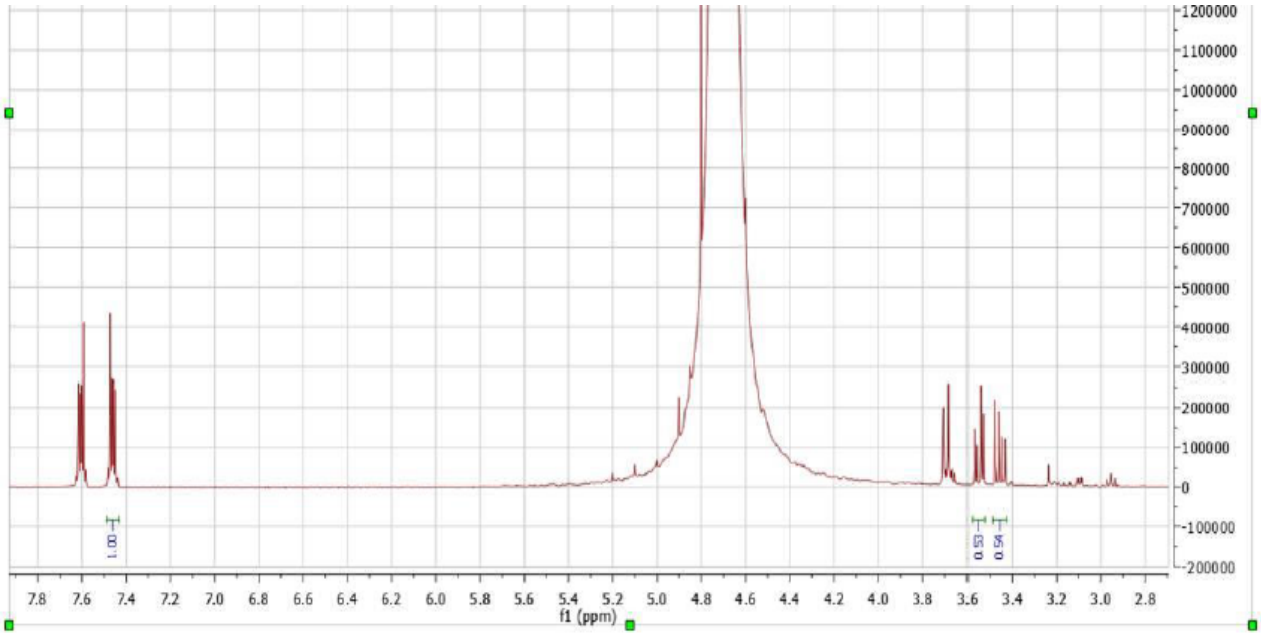

Figure 5.12: Representative NMR spectra. Two peaks on the far left belong to KHP, whereas ones on the far right are from glycerol.

5.8.4. Mass Spectrometry

The mass spectrometer (MS) was used to identify the chemical composition of a gaseous compound or sample by measuring the ionic mass-to-charge ratio of its constituent elements. Essentially, the MS contains 3 key internal units, which are 1) an ioniser to chemically fragment the compound into its charged particles, 2) a detector to capture those particles and 3) a suction pump that creates a vacuum system between the ioniser and the detector. Ions are separated on a mass basis; they impact the detector, inducing a current or a charge (Beckmann, Messinger *et al.,* 2009). In this thesis, a compact quadrupole Pfeiffer Vacuum Prisma MS running Windows Quadstar 422 software was used.

5.8.4.1. Injection Mass Spectrometry

Injection MS was used to identify the components of the gaseous product emitted by an anaerobic *Cyanothece* 51142 culture. An argon (Ar) carrier gas flow of 30 ml min^{-1} was fed into the MS, which was set to continuously scan across all mass-to-charge ratios and take measurements of the relevant atomic masses (H_2, water, N_2, O_2, Ar and CO_2; atomic mass = 2, 18, 28, 32, 40 and 44, respectively). Figure 5.13 shows a representative result of this scan; it represents the injection MS background measurement. A 1 ml gas-tight syringe was inserted through the septum at the top port of the ICL flat-plate PBR into the gas phase of the anaerobic *Cyanothece* 51142 culture and subsequently used to collect 1 ml of the gas sample from the head space of the reactor. The sample was then injected into the Ar carrier gas stream via a septum. This produced a number of peaks in the MS readings corresponding to the presence of particular atomic masses in the injection. The component volumes (ml) corresponded to the area occupied by their respective peaks (Ampere

second – A s). These areas were calibrated against known volumes of my interested gases supplied from BOC at volumes of 0.1, 0.2, 0.3, 0.4 and 0.5 ml. Their calibrations can be seen from Figures 5.14.A – D and Equations 5.22 - 25.

$$H_2 \text{ volume (ml)} = 9.68 \cdot 10^7 \cdot H_2 \text{ peak area (A s)} \qquad \text{Equation 5.22}$$

$$CO_2 \text{ volume (ml)} = 2.24 \cdot 10^9 \cdot CO_2 \text{ peak area (A s)} \qquad \text{Equation 5.23}$$

$$N_2 \text{ volume (ml)} = 1.19 \cdot 10^9 \cdot N_2 \text{ peak area (A s)} \qquad \text{Equation 5.24}$$

$$O_2 \text{ volume (ml)} = 2.13 \cdot 10^9 \cdot O_2 \text{ peak area (A s)} \qquad \text{Equation 5.25}$$

Once the volume is successfully estimated, it is possible to calculate the composition of an individual component present in the gas sample using Equation 5.26.

$$\text{Composition (\%)} = \frac{\text{Volume of gas present in syringe (ml)}}{\text{Total volume of gas sample (ml)}} \text{ x } 100 \qquad \text{Equation 5.26}$$

Injections were repeated three times to verify the consistency of the measurements. The syringe was dipped into acetone to sterilise it before injections were taken. It was important to use a heated (110°C) MS capillary to prevent any moisture in the injection from blocking the carrier gas path to the MS ioniser.

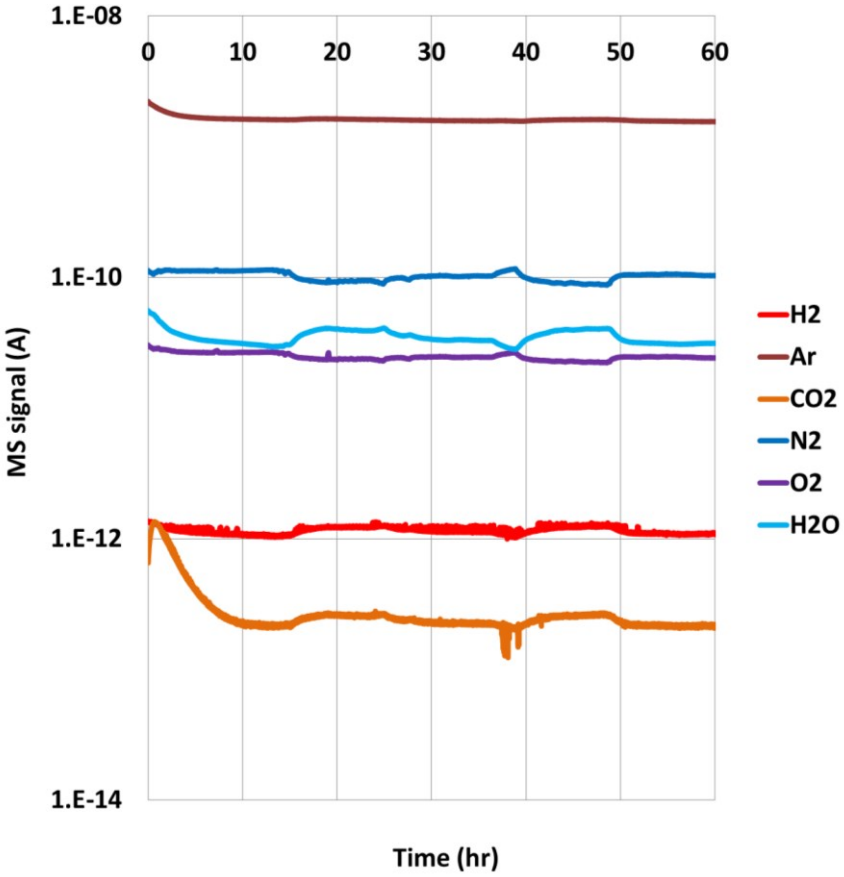

Figure 5.13: Representative results of an ion monitoring graph obtained from the mass spectrometer

Figure 5.14: Injection mass spectrometry calibration for gaseous component

A) H_2

B) CO_2

C) N_2

D) O_2

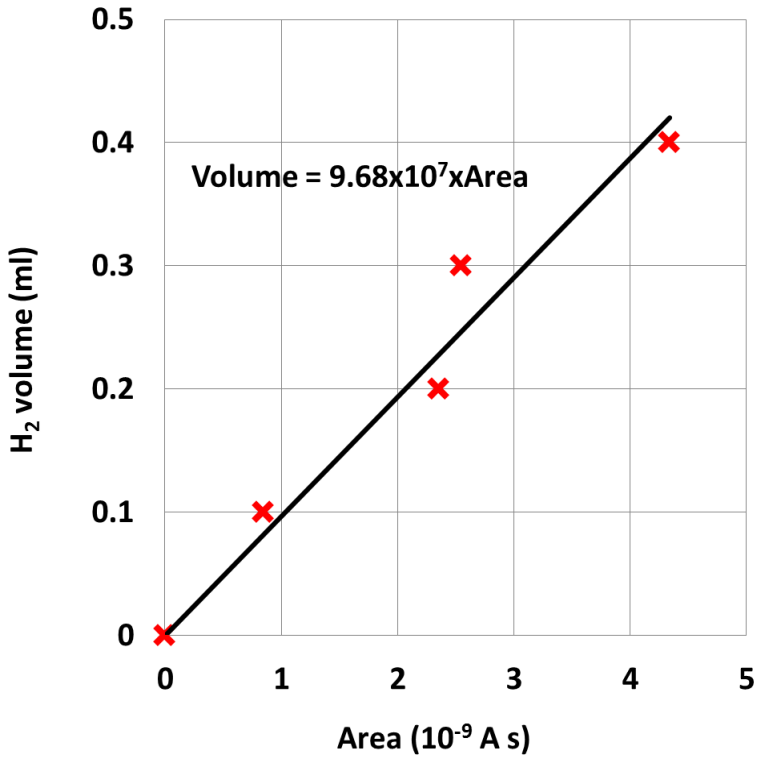

Figure 5.14.A: Injection mass spectrometry calibration for H_2

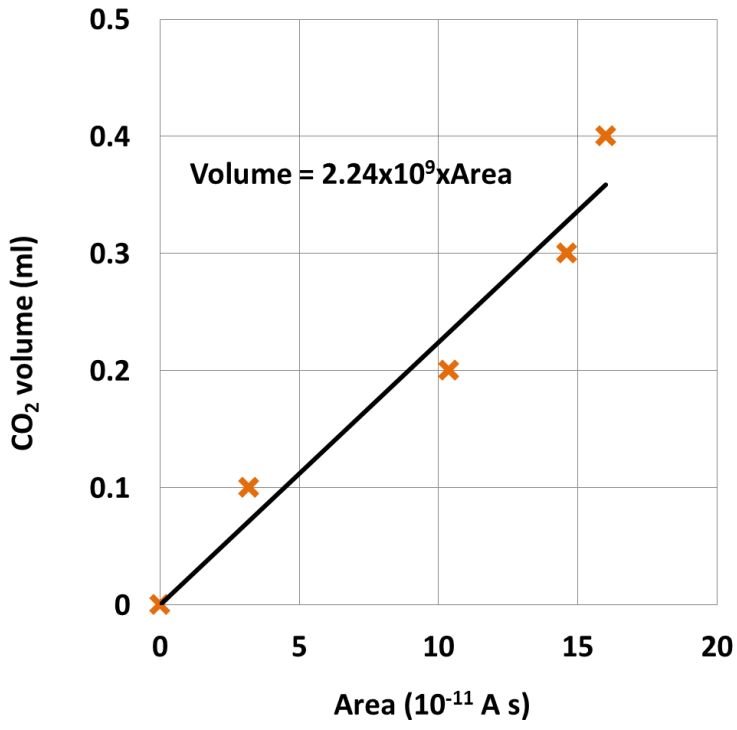

Figure 5.14.B: Injection mass spectrometry calibration for CO_2

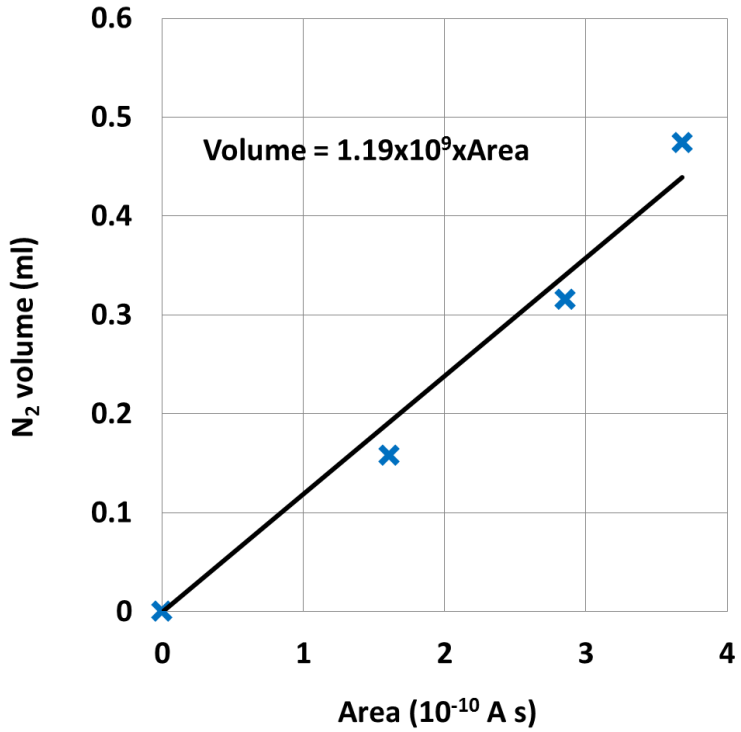

Figure 5.14.C: Injection mass spectrometry calibration for N_2

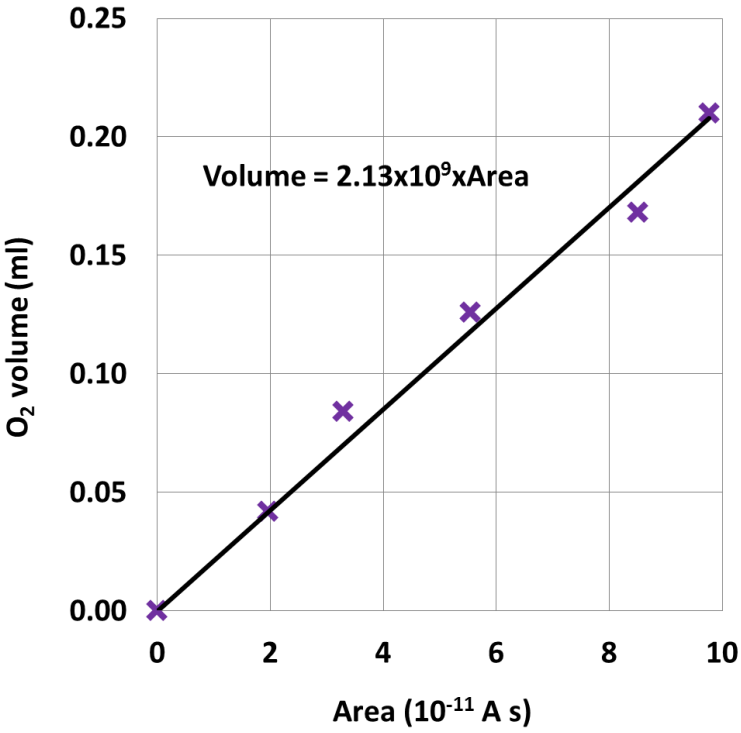

Figure 5.14.D: Injection mass spectrometry calibration for O_2

5.8.4.2. Membrane-Inlet Mass Spectrometry (MIMS)

MIMS was used to accurately and *in situ* measure the concentration of H_2 produced by the anaerobic *Cyanothece* 51142 culture (Tamburic, Zemichael *et al.,* 2011). This task was performed using the Aston Analytical Ultra-Trace MIMS System, which is incorporated into the primary compartment of the ICL flat-plate PBR (Figure 5.15). The mass spectrometer is a compact quadrupole Pfeiffer Vacuum Prisma, running Windows Quadstar 422 software. The membrane system serves as the only interface between the liquid cyanobacterial culture at atmospheric pressure and the vacuum chamber of a mass spectrometer. Driven by these partial pressure gradients, gaseous H_2 pervaporates through a thin polydimethylsiloxane (PDMS) membrane and is transported by an Ar carrier gas, via a heated capillary, into the inlet of the MS (Figure 5.16).

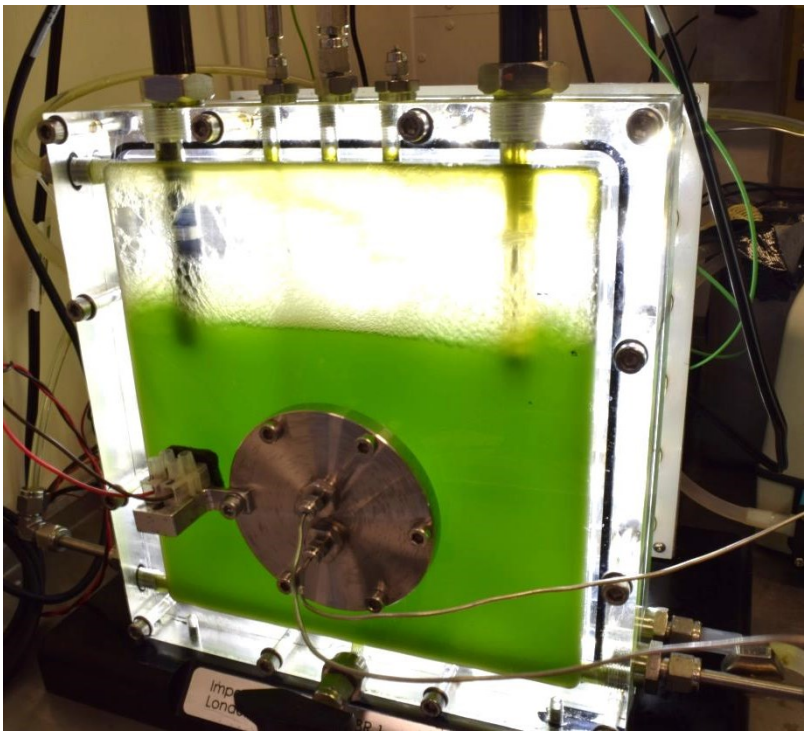

Figure 5.15: The membrane, incorporated into the front compartment of the ICL flat-plate PBR and directly attached to the liquid phase.

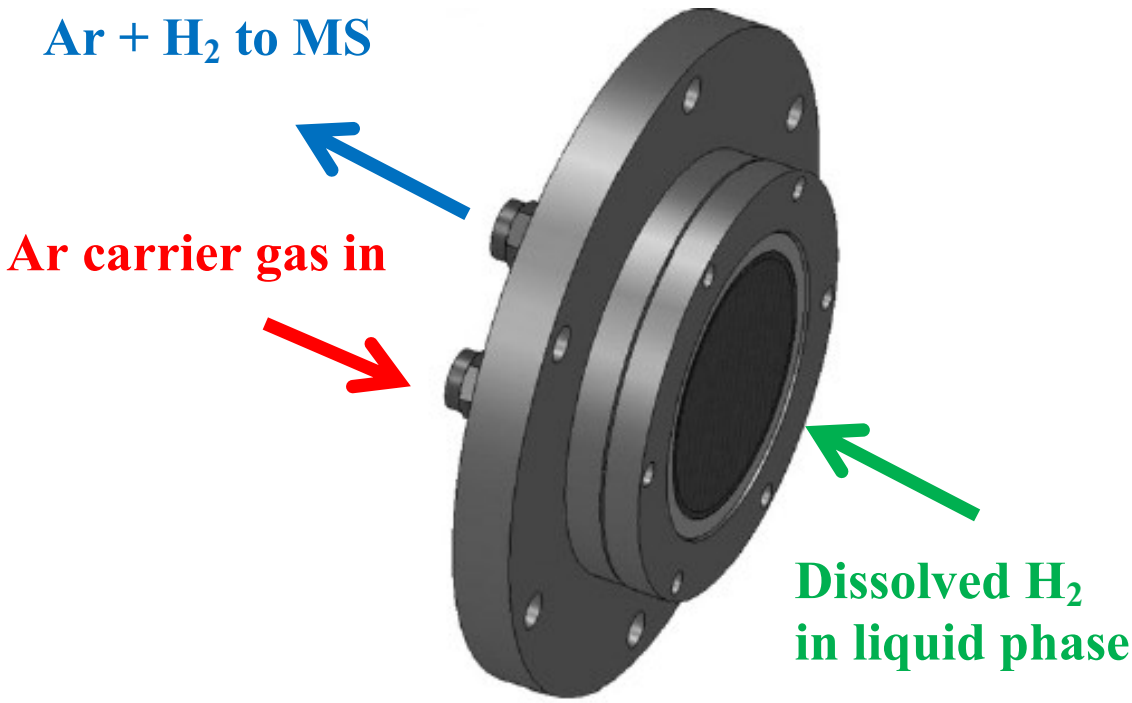

Figure 5.16: Schematic diagram of membrane system

The pervaporation of H_2 emitted by cyanobacterial culture through the membrane is a three-stage process. The process begins with an absorption of H_2 molecules onto the membrane surface; this is followed by the permeation of these H_2 molecules through the membrane material, before an eventual desorption of H_2 into the argon carrier gas stream on the other side (Lloyd, Thomas *et al.,* 2002). Numerically, the H_2 pervaporation rate through the membrane can be estimated using a modified form of Fick's First Law (Beckmann, Messinger *et al.,* 2009), as shown in Equation 5.27. As the pervaporation rate of 9.3 ml hr^{-1} (Tamburic, Zemichael *et al.,* 2011) is significantly higher than the *Cyanothece* 51142 H_2 production rate of 1.81 ml H_2 L^{-1} hr^{-1}, reported by Min and Sherman (Min and Sherman 2010), this implies capability of MIMS to measure any H_2 produced by the cyanobacteria.

$$\text{Pervaporation rate} = \frac{\text{Per}\cdot A\cdot \Delta P}{l} \qquad \text{Equation 5.27}$$

In this equation, Per is the H_2 permeability = $6x10^{-15}$ m^2 s^{-1} Pa^{-1}, A is the membrane area = $1.36x10^{-3}$ m^2, Δp is the partial pressure of H_2 on the gas and liquid side of the MIMS system = 1 atm = $1.01x10^5$ Pa and l is the membrane thickness = $3.2x10^{-4}$ m.

MIMS was calibrated by passing a known flow rate of H_2 from a gas cylinder through the membrane / reactor interface into the Ar carrier gas line. The H_2 flow rate was precisely controlled using a digital mass flow controller from Porter Instrument Company, Inc. The H_2 flow was varied between 30 and 76 ml hr^{-1}, with the corresponding MS signal measured (Figure 5.17.A), as the lowest controllable H_2 flow of the mass flow controller was restricted to 30 ml hr^{-1}. Equation 5.28 was used to correlate the mass spectrometer H_2 ion current output with its corresponding H_2 flow / production rate.

$$H_2(\text{ml hr}^{-1}) = 3.46 \cdot 10^{11} \cdot \text{Signal (A)} \qquad \text{Equation 5.28}$$

Figure 5.15: Membrane-inlet mass spectrometry calibration for H_2

A) H_2 measurement

B) H_2 calibration

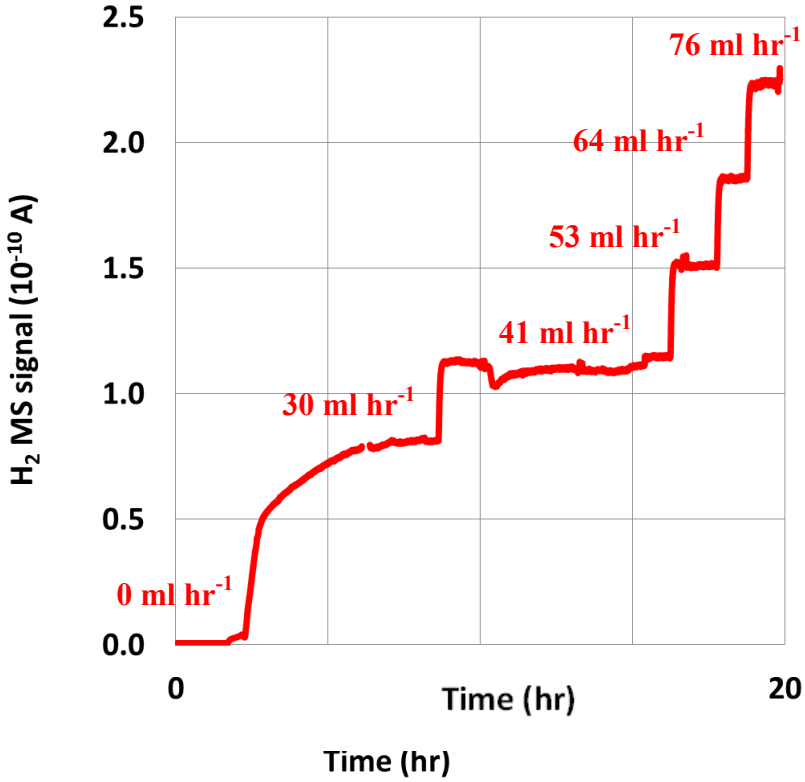

Figure 5.17.A: H_2 measurement

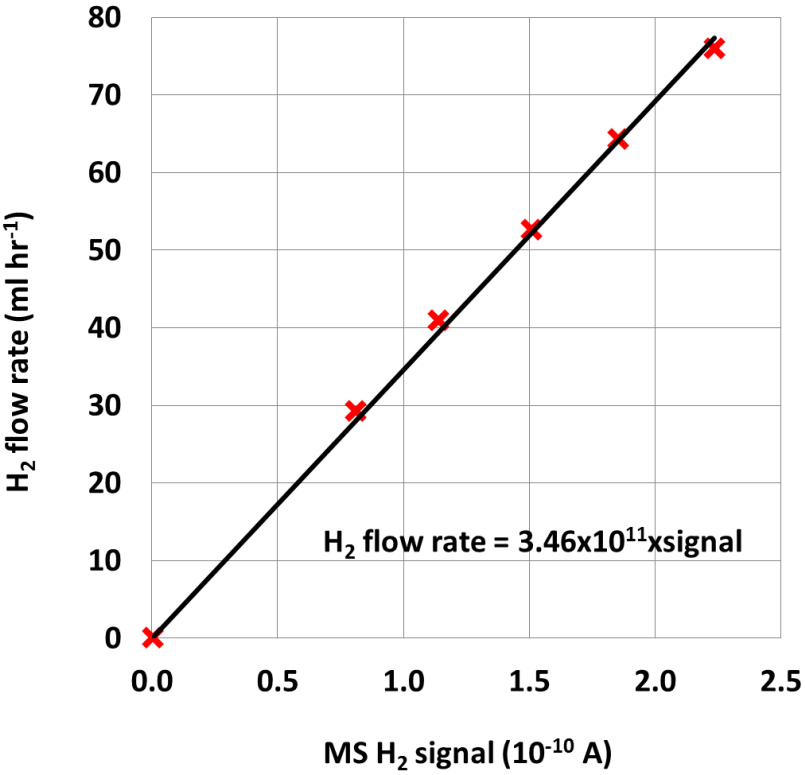

Figure 5.17.B: MIMS calibration for H_2

5.8.5. Water Displacement

Water displacement is one of the simplest techniques, which is conventionally used to measure the volume of gaseous H_2 evolved by green algae and cyanobacteria (Melis and Happe 2001, Tamburic, Zemichael *et al.,* 2011). For an experimental set-up, one free port at the top surface of the ICL flat-plate PBR was connected to an inverted measuring cylinder, which was initially filled with water, via H_2-impermeable stainless steel tube (Figure 5.18). Once cells enter the H_2 production phase, the formed gas flows through the metallic tube and is eventually captured at the top of the cylinder. The collected gas pushes the water downwards; consequently, the volume of gaseous H_2 produced was equated to the volume of displaced liquid water. In parallel, the injection mass spectrometry, section 5.8.4.1, was employed to confirm that the gas collected was actually H_2 as well as to determine its purity.

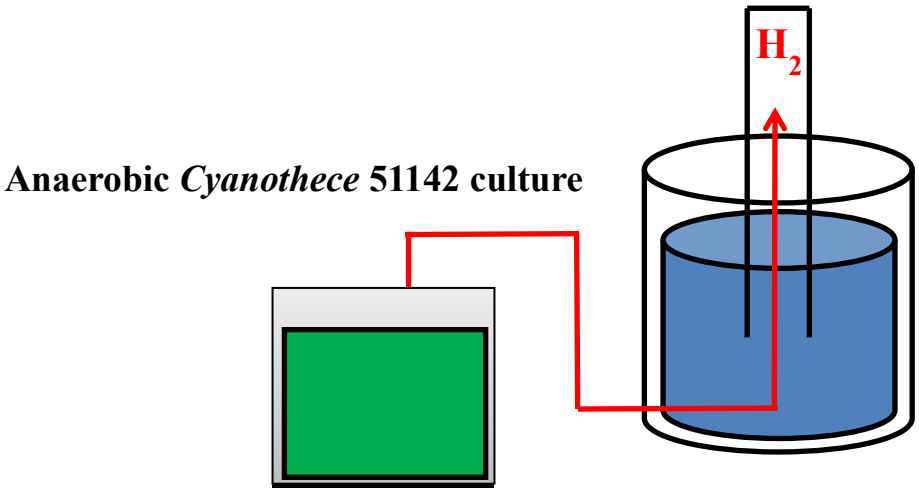

Figure 5.18: A schematic diagram representing the set-up water displacement system for H_2 measurement.

5.9. Mathematical Models

5.9.1. Logistic Model

5.9.1.1. Logistic Growth Model

A logistic growth function, Equation 5.29, is a common model of population growth, first published by Pierre-Francois Verhulst in 1838, to describe the self-limiting growth of a biological population (Verhulst 1838). It has been frequently and effectively used to fit kinetic parameters to algal growth and nutrient uptake data (Lemesle and Mailleret 2008, Tamburic, Zemichael *et al.,* 2012). In this equation, X_{max} represents the maximum dry biomass concentration (g L^{-1}) obtained in a particular experiment. μ_{max} is the maximum specific growth rate (hr^{-1}), which describes the number of cell divisions per unit time under the respective condition. t_0 is the inflexion point of the function (hr). X(t) is the dry biomass concentration at any specific time, t. A clear representation of individual logistic growth model's parameter can be seen from Figure 5.19. The gradient of the microbial growth profile at $t = t_0$ is considered as the maximum specific growth rate.

$$X(t) = \frac{X_{max}}{1+e^{-\mu max \cdot (t-t_0)}} \qquad \text{Equation 5.29}$$

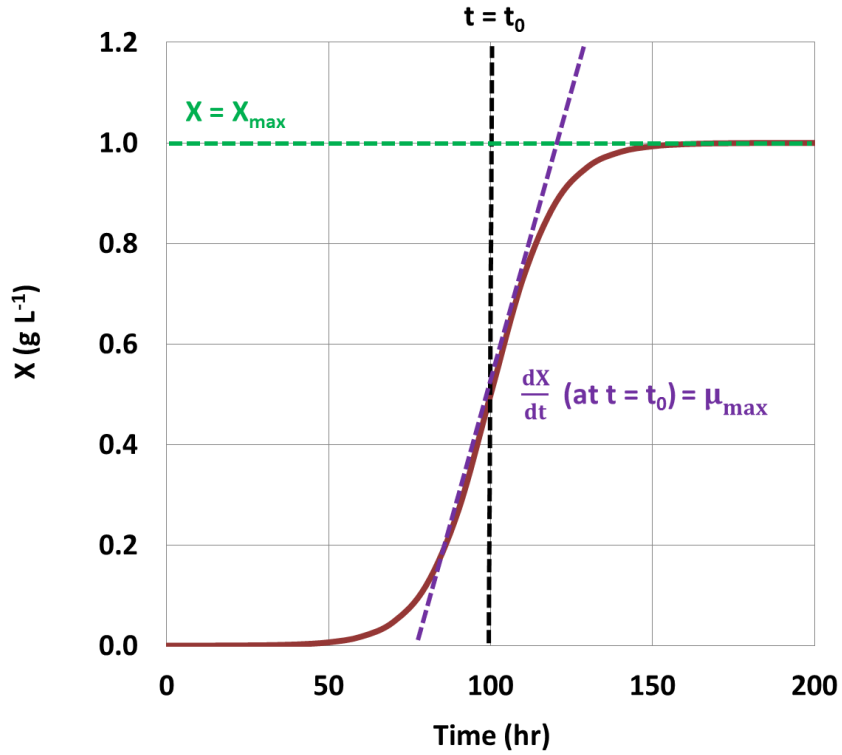

Figure 5.19: Representation of logistic model's parameters.

5.9.1.2. Logistic Nutrient Uptake Model

In the case of nutrient uptake, an inverted form of the logistic function, as expressed in Equation 5.30, was utilised, as it is able to reflect the observed decrease in nutrient concentration. [C_{max}] represents the total nutrient consumption (mg L^{-1}) observed in a particular experiment, which is equal to the difference between an initial and the final ([C_{final}]) concentrations. r_{max} is the maximum specific uptake rate (hr^{-1}). [C(t)] is the nutrient concentration at any specific time, t.

$$[C(t)] = \frac{[C_{total}]}{1+e^{r_{max}\cdot(t-t_0)}} + [C_{final}] \qquad \text{Equation 5.30}$$

In order to fit the logistic curve to discrete experimental data, the total least squares error between modelled and experimental data is minimised. By assigning initial values for the parameters of Equations 5.29 and 5.30 in this way, OD(t) and [C(t)] at any specific time can be consequently determined. Mathematical solutions to the logistic models will be described in more detail (with examples) in Results and Discussions Chapter I.

5.9.2. Aiba Light Model

The microalgal maximum specific growth rate increases with increasing light intensity up to the point of light saturation, at which the highest possible rate, $\mu_{max,s}$, is attained. Beyond the saturation intensity, the microbes start to experience photoinhibition effects and the subsequent growth rate will decline (Molina Grima, Fernández *et al.,* 1999). The Aiba model (Aiba 1982), Equation 5.31, has been developed to describe this behaviour. For this model, h(I) is a light intensity function (dimensionless), which takes into account for light saturation, k_s, (µmol m^{-2} s^{-1}) and photoinhibition, k_i, (µmol m^{-2} s^{-1}) effects. I is an average local light intensity (µmol m^{-2} s^{-1}), experienced by cells inside the photobioreactor.

$$h(I) = \frac{I}{k_s + I + \frac{I^2}{k_i}} \qquad \text{Equation 5.31}$$

5.9.3. Beer-Lambert Light Attenuation Model

The average intensity inside the PBR is always not the same as the incident intensity supplied by the light source, but actually depends on light path length and biomass concentration. This attenuation of light is usually expressed by Equation 5.32 (Barbosa, Zijffers *et al.,* 2005).

$$I_{out} = I_{in} \cdot \exp(-a_c \cdot X \cdot L) \qquad \text{Equation 5.32}$$

In this equation, I_{out} is the transmitted intensity (μmol m^{-2} s^{-1}), I_{in} is the incident intensity, a_c is the sum of a spectral-averaged absorption coefficient on a dry biomass concentration (g m^{-3}), X, and a volume-averaged reflection coefficient on bubble volume fraction (previously estimated as 0.126 m^2 g^{-1} (Zhang, Dechatiwongse *et al.,* 2015a) and L is light path length along bioreactor (0.025 m for an ICL flat-plate PBR and 0.023 m for a Sartorius tubular PBR). The average intensity can then be estimated as an integral of intensity over path length, as shown in Equation 5.33. In this equation, I_l is defined as a local light intensity along the path length of the bioreactor.

$$I = \frac{\int_0^L I_l \, dl}{L} = \frac{I_{in}}{a_c \cdot X \cdot L} \cdot (1 - e^{-a_c \cdot X \cdot L}) \qquad \text{Equation 5.33}$$

5.9.4. Arrhenius Temperature Model

Similar to light intensity, an increase in temperature generally enhances microbial photosynthesis and subsequent growth rates up to a critical temperature, above which these activities start to decline (Konopka and Brock 1978, Lester, Adams *et al.,* 1988, Torzillo and Vonshak 1994, Inoue, Taira *et al.,* 2001). An Arrhenius model (Topiwala and Sinclair 1971), Equation 5.34, describes this

character of microalgae as the result of two competing temperature-dependent processes – synthesis (1st term) and denaturation (2nd term). The synthetic term is a dominant process up to an optimum temperature, beyond which the denaturation significantly dominates.

$$h(T) = A \cdot \exp\left(-\frac{E_a}{R \cdot T}\right) - B \cdot \exp\left(-\frac{E_b}{R \cdot T}\right) \quad \text{Equation 5.34}$$

In this equation, h(T) represents a temperature function (dimensionless). E_a and E_b are activation energies (J mol^{-1}), whereas A and B are pre-exponential factors (dimensionless) for the synthesis and denaturation respectively. R is a universal gas constant = 8.314 J mol^{-1} K^{-1} and T is an absolute temperature (K).

5.9.5. Growth Model

5.9.5.1. Maximum Specific Growth Rate Model

Light intensity and temperature are known to strongly influence the growth of microalgae. It is possible to include the effects of these environmental effects into the growth using Equation 5.35. Here, $\mu_{max,s}$ is the maximum specific growth rate obtained by cells under the light-saturating condition (hr^{-1}), whereas μ_{max} represents the maximum specific growth rate under any specific conditions (hr^{-1}). $h(T)_G$ and $h(I)_G$ are the temperature and light intensity functions for the cyanobacterial growth process respectively (dimensionless).

$$\mu_{max} = \mu_{max,s} \cdot h(T)_G \cdot h(I)_G \quad \text{Equation 5.35}$$

In order to fit experimental data with Equation 5.35, temperature was initially fixed, so $h(T)_G$ became constant. The multiply of $\mu_{max,s}$ and $h(T)_G$ could then be considered as a new constant, called "U(T)". As parameters of Aiba model – k_s and k_i - are independent of U(T), the method of least squares can be carried out to determine their optimised values. Vice versa, parameters of the Arrhenius model and $\mu_{max,s}$ were determined by keeping incident light intensity constant. Again, $h(I)_G \cdot \mu_{max,s}$ was assigned as new constant, "U(I)". Similar procedure was then performed to determine values of E_a, E_b, A, B and U(I). Finally, because the value of $h(I)_G$ has already been determined, the value of $\mu_{max,s}$ can be worked out. Applications and examples of the specific growth rate model will be shown in Results and Discussions Chapter I.

5.9.5.2. Productivity Model

Although the maximum specific growth rate is commonly used to describe the growth of microorganisms, it is unable to indicate the biomass quantity of the culture. As a result, the biomass productivity, P, (g L^{-1} hr^{-1}) proves to be a better growth indicator, as it also takes into account the biomass content, X, (g L^{-1}) of the culture being produced at the inflexion point of the logistic function ($t = t_0$), as shown in Equation 5.36. It should be noted here that the value of X is in fact not constant, but dependent on light intensity, temperature and available nutrients.

$$P = \mu_{max,s} \cdot h(T)_G \cdot h(I)_G \cdot X \qquad \text{Equation 5.36}$$

The parameters of the productivity model were recovered in a similar way to their specific growth rate model counterparts. Applications and examples will be shown in Results and Discussions Chapter I.

5.9.6. H_2 Production Model

H_2 production can be described by Equation 5.37, which closely relates the gas production rate (ml H_2 L^{-1} hr^{-1}) with present dry biomass concentration (g L^{-1}). In addition to temperature, $h(T)_H$, and light intensity, $h(I)_H$, the equation also takes into account $Y_{H/X}$ - H_2 yield coefficient (ml H_2 g^{-1} hr^{-1}), which can be assumed as a function of carbon substrate and intracellular nitrogen concentration (Vatcheva, de Jong *et al.,,* 2006). In all of H_2 production studies, as glycerol (carbon) was added in an excessive quantity and nitrate (nitrogen) was also completely consumed before the start of H_2 production, it was reasonable to assume $Y_{H/X}$ as the constant.

$$R_{H_2} = Y_{H/X} \cdot h(T) \cdot h(I) \cdot X \qquad \text{Equation 5.37}$$

$Y_{H/X}$ and parameters of Aiba and Arrhenius models were optimised using the least-squares methodology in the similar way to that of the growth model. Mathematical solutions will be described in more detail (with examples) in Results and Discussions Chapter II.

5.9.7. A Two-stage Chemostat PBR System

A chemostat is the simplest operational mode of an open bioreactor system (other known operations are turbidostat, auxostat and retentostat), during which fresh medium is continuously fed into the reactor at the same rate as culture liquid is taken out, thereby keeping the total volume of the culture constant (Hoskisson and Hobbs 2005). In this thesis, a two-stage chemostat PBR system (Figure 5.19) was developed for the purpose of extending the duration of cyanobacterial H_2 production.

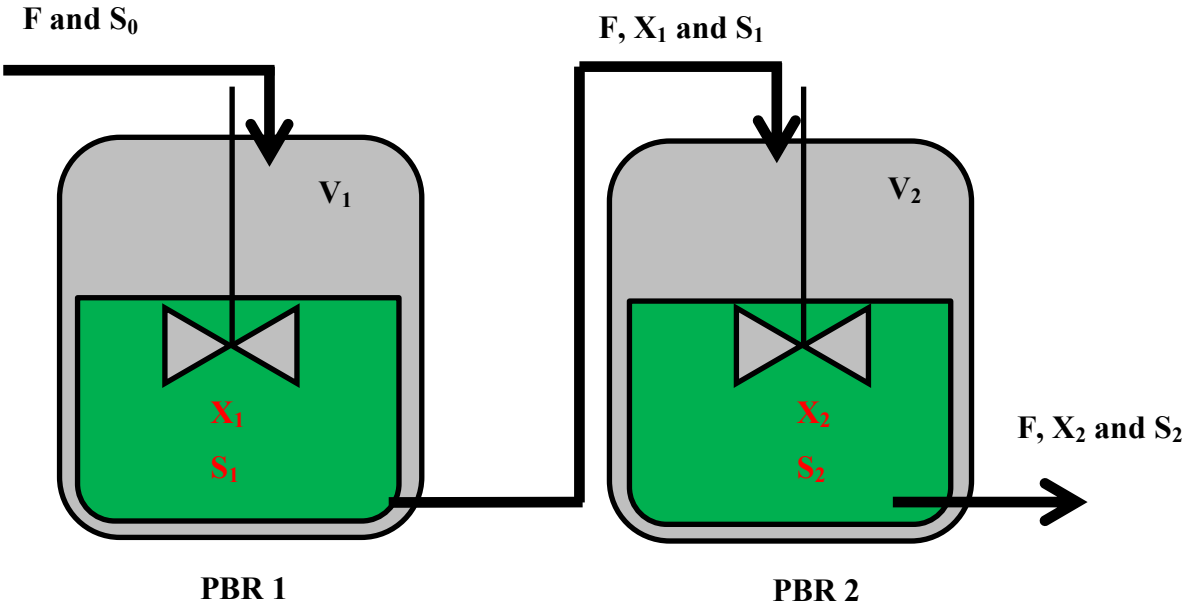

Figure 5.20: A schematic diagram representing a two-stage chemostat PBRs system Abbreviations: F is the flow rate of inflows and outflows of PBR. X_i is the dry biomass concentration. S_i is the substrate concentration. V_i is the liquid volume of PBR_i. Subscript "0" indicates that it is the property of the growth medium, whereas subscripts "1" and "2" refer to those of PBR 1 and 2 respectively.

5.9.7.1. Dilution rate

Dilution rate (D) is a very important parameter of the chemostat system, as it can be used to control the specific growth rate (μ) of microorganism. Theoretically, it is possible to increase the value of μ, by increasing D up to the critical dilution rate (D_c), beyond which the "wash-out condition" of cells will occur. The dilution rate is defined as the rate of medium flow (F) over the volume of culture in the bioreactor (V), as shown in Equation 5.38.

$$\text{Dilutaion rate (D)} = \frac{\text{Feed rate (F)}}{\text{Working volume of bioreactor (V)}} \qquad \text{Equation 5.38}$$

5.9.7.2. Biomass Balance

By applying the law of conservation of mass over an individual PBR, the rate of change in biomass is equal to the rate of biomass inflow + the rate of biomass generation (reproduction) – the rate of biomass outflow – the rate of biomass loss (death). Numerically, the mass balance describing the change of biomass within PBR 1 and 2 were shown in Equations 5.39 and 5.40 respectively. All terms have the units of g L^{-1} hr^{-1}. Here, X is the dry biomass concentration (g L^{-1}), μ is the specific growth rate (hr^{-1}), D is the dilution rate (hr^{-1}), μ_d is he specific decay rate (hr^{-1}) and t is the time (hr). Subscripts "1" and "2" refer to PBR 1 and 2 respectively.

$$\frac{dX_1}{dt} = (\mu_1 - D_1 - \mu_{d1}) \cdot X_1(t) \qquad \text{Equation 5.39}$$

$$\frac{dX_2}{dt} = (\mu_2 - \mu_{d2}) \cdot X_2(t) + (X_1 - X_2) \cdot D_2 \qquad \text{Equation 5.40}$$

5.9.7.3. Substrate Balance

In the case of substrate balance, the same principle of mass conservation remained applicable. The mass balance describing the change of substrate within PBR 1 and 2 were shown in Equations 5.41 and 5.42 respectively. In these equations, S is the substrate concentration (mg L^{-1}), R_s is the rate of substrate consumption by cells (mg L^{-1} hr^{-1}). Subscripts "0" refer to the property of the growth medium.

$$\frac{dS_1}{dt} = D_1 \cdot (S_0 - S_1) - R_{s1} \qquad \text{Equation 5.41}$$

$$\frac{dS_2}{dt} = D_2 \cdot (S_1 - S_2) - R_{s2} \qquad \text{Equation 5.42}$$

5.9.7.4. Gaseous Mass Transport

As proposed by Royce and Thornhill (Royce and Thornhill 1991), mass transfer properties of CO_2 and O_2 are linearly correlated as expressed in Equation 5.43. In this equation, $k_L{}^{CO_2}a$ (hr^{-1}) and $k_L{}^{O_2}a$ (hr^{-1}) are the volumetric gas–liquid mass transfer coefficients for CO_2 and O_2, respectively.

$$\frac{k_L{}^{CO_2}a}{k_L{}^{O_2}a} = 0.89 \qquad \text{Equation 5.43}$$

The mass balance for gaseous substrates can be constructed in a similar way to that of liquid / solid substrates (section 5.9.7.3), apart from the fact that an additional term of gaseous mass transport (the first term on the right hand side of Equation 5.44) need to be included in the balance.

$$\frac{d[CO_2]}{dt} = {k_L}^{CO_2}a \cdot ([CO_2{}^*] - [CO_2]) + D_1 \cdot ([CO_2]_0 - [CO_2]) - R_{CO_2} \qquad \text{Equation 5.44}$$

Here, CO_2 represents the gaseous compound. $[CO_2]$ is the steady-state dissolved CO_2 concentration (mg L^{-1}) in the liquid culture, whereas $[CO_2{}^*]$ is the theoretically saturated concentration of CO_2 (mg L^{-1}), which can be estimated using Henry's law (Equation 5.45). $[CO_2]_0$ is the dissolved CO_2 concentration present in the fed medium. Lastly, R_{CO_2} is the rate of CO_2 consumption by cells (mg L^{-1} hr^{-1}).

According to Henry's law (Battino and Clever 1966), at a constant temperature, the amount of a given gas that dissolves in a given type and volume of liquid is directly proportional to the partial pressure of that gas in equilibrium with that liquid. Mathematically, the previous statement can be expressed as Equation 5.45 (in the case of CO_2).

$$P_{CO_2} = [CO_2{}^*] \cdot H_{CO_2} \qquad \text{Equation 5.45}$$

Here, P_{CO_2} is the partial pressure of CO_2 above the liquid solution and H_{CO_2} is the Henry's constant of CO_2, which is also a function of liquid solvent and temperature.

By considering water as the liquid solvent, values of the Henry's constants for CO_2 and O_2 are as follows (Royce and Thornhill 1991):

$$H_{CO_2} = \exp\left(11.25 - \frac{395.9}{(T-175.9)}\right) \qquad \text{Equation 5.46}$$

$$H_{O_2} = \exp(12.74 - \frac{133.4}{(T-206.7)})$$ Equation 5.47

5.9.7.5. Delivery Rate

For any fed-batch or continuous flow processes, it is possible to quantify the delivery rate of key substrates e.g. nutrients and O_2 into a confined system using Equation 5.38. In this equation, F is the feed rate of liquid medium containing key substrates, S is the substrate concentration within the medium and V is the working volume of the PBR being fed.

$$\text{Delivery rate} = \frac{F \cdot S}{V}$$ Equation 5.48

For all of equations introduced in this section, their applications and mathematical solutions will be shown in more detail in Results and Discussions Chapter III.

6. Results and Discussion

I. Growth of *Cyanothece* sp. ATCC 51142

I.1. Introduction

The major reason behind my decision of choosing a *Cyanothece* 51142 strain as the studied microorganism came from the fact that this cyanobacterium is a wild-type strain, which has an exceptional ability to produce H_2 at the highest rate among all of previously investigated strains (Bandyopadhyay, Stoeckel *et al.,* 2010, Min and Sherman 2010).

As expressed in Equation 5.37 (all mathematical equations are listed and documented in section 5), the quantity of produced biohydrogen is closely related to the quantity of functioning *Cyanothece* 51142 cells, which in turn directly determines the number of light-harvesting complexes, oxygen-evolving centres, nitrogenase enzymes and other reaction centres that are critical to the H_2 production process. In addition to enhancing the gas production, the production of *Cyanothece* 51142 biomass also facilitates the accumulation of essential bioactive products such as proteins, vitamins and amino acids (Schneegurt, Arieli *et al.,* 1995). These may be extracted in parallel or at the end of the H_2 production process and used to produce an array of high-value nutrition and pharmaceuticals that introduce additional lines of income and subsequently improve on an economic viability of a biohydrogen production facility (Patel, Tamburic *et al.,* 2012).

Due to its remarkable H_2 production rate and desirable biochemical composition, a number of studies have been carried out in order to understand the growth of *Cyanothece* 51142. The effects of critical growth parameters, such as carbon and nitrogen sources (Schneegurt, Sherman *et al.,* 1997,

Feng, Bandyopadhyay *et al.,* 2010), illumination condition e.g. light / dark cycles, continuous light (Reddy, Haskell *et al.,* 1993, Schneegurt 1994, ColonLopez, Sherman *et al.,* 1997) and continuous dark (Schneegurt, Tucker *et al.,* 2000) and photobioreactor geometry (Alagesan, Gaudana *et al.,* 2013) have all been investigated. However, little attention has been paid to the growth dependence on cultivating parameters such as temperature and light intensity. Since both parameters directly affect photosynthesis, the fundamental energy-harnessing process, of *Cyanothece* 51142, an enhancement in physiological activities e.g. the cyanobacteiral growth is possible by understanding this missing knowledge.

The aim of this chapter is to fully understand influences of two cultivating parameters – temperature and light intensity - on *Cyanothece* 51142 growth and subsequently determine an optimal environmental condition, which can be employed for optimising cyanobacterial biomass productivity. In this chapter, a simple logistic growth model (Equation 5.29) was used to fit with the experimental growth data in order to extract important parameters of cyanobacterial growth kinetics. The comprehensive use of the model will be demonstrated through its excellent fitting capability with well-understood scenarios, such as the effect of carbon and nitrogen sources on *Cyanothece* 51142 growth, to its implementation in more complex and unknown situations, such as the growth under different light and temperature regimes. Eventually, obtained growth parameters were fitted to the developed growth model (Equations 5.35 and 5.36), which takes into account simultaneous effects of temperature (Equation 5.34), light intensity (Equation 5.31) and light attenuation (Equations 5.32 and 5.33) in order to gain insight on how these environmental parameters affect growth. The focus in all these experiments has been to grow *Cyanothece* 51142 cultures to high densities, ready to be exploited for subsequent H_2 production, as quickly and as economically as possible. It should be noted here that, due to time constraint, every experiment in this chapter was carried out only once.

I.2. Choice of Photobioreactor

All of growth experiments were carried out in the Sartorius tubular PBR, due to its major advantage of an automated parameter controlling system. The temperature of the aqueous culture is measured by a Pt100 Type 25-3 thermocouple and is controlled by means of a heated water jacket that encompasses the central vessel of the PBR. pH and dissolved oxygen concentration (pO_2) are measured by probes from Hamilton – Easyferm : Plus K8 160 pH electrode and OxyfermFDA 160 oxygen tension probe, respectively. The growth of the cyanobacterium is real-time monitored by the Sartorius Fundalux II OD probe, containing an LED that operates in the 870 - 910 nm wavelength range. The OD calibration was performed by directly extracting a 6 ml cyanobacterial sample from the tubular reactor at regular time intervals, and analysing its light-scattering properties at 620, 678 and 750 nm using a spectrophotometer. This OD measurement, initially in absorbance units, was converted to units of chlorophyll (Equation 5.4) and then dry biomass concentration (Equation 5.5). In addition, the PBR also provides a high level of operational flexibility, as it can be operated as an open system, allowing a continuous supply of gaseous CO_2 for autotrophic growth condition.

I.3. Growth Cycle of *Cyanothece* 51142

Commonly, the growth cycle of microorganism can be characterised into five distinct phases: i) lag (adaptation) ii) exponential (light and nutrient-sufficient) iii) linear (light-limited) iv) stationary (nutrient-limited) and v) cell death (Tomaselli 2004). Figure.I.1.A displays the nitrogen-replete photoautotrophic growth profile of *Cyanothece* 51142, which consists of all of the growth phases, except the death phase. In this study, the cyanobacterium *Cyanothece* 51142 was cultivated under continuous illumination of 207 μmol m^{-2} s^{-1} and constant temperature of 35 ^{o}C using the ASP2+N growth medium. A constant gas flow of 20 ml min^{-1} of sterile 10% volume CO_2 volume air^{-1} was continuously bubbled throughout the liquid phase in order to ensure that there is sufficient carbon

source available to facilitate the photoautotrophic growth of *Cyanothece* 51142. 1.5 g L^{-1} of $NaNO_3$ was also added into the medium to further enhance the cyanobacterial growth rate.

The first "lag phase" is the time during which microorganisms need to adapt themselves to the new cultivating environment after inocculation. As a result, during this period, a minimal change in the biomass concentration is observed for the first 20 hours. Following, the secondary "exponential growth phase" is clearly marked between 20 - 70 hour, during which simultaneous increase in the density of *Cyanothece* 51142 culture, from 0.2 to 2.4 g L^{-1}, and decrease in an available nitrate concentration, from 1244 to 100 mg NO_3^{-1} L^{-1}, are clearly seen. During this period, the rate of cyanobacterial reproduction proceeds at its maximum value, μ_{max}, which is an exponential function of time, as long as the cells have access to sufficient illumination and nutrients.

For the determination of μ_{max}, estimated values of both μ_{max} and the maximum biomass concentration (X_{max}) were initially assigned into the logistic growth model so that the culture concentration at each specific time can subsequently be calculated. The initial value of X_{max} can be directly read from the figure. Eventually, the parameter estimation using Solver add-on to the Excel program (Microsoft Corp., USA) was performed in order to search for the optimal combination of both parameter values, which results in the minimum sum of root squared deviations between the experimental and simulated biomass concentration data. In the case of nitrate uptake parameters, the same procedure was carried out to work out the maximum specific nitrate uptake rate (r_{max}) and its corresponding total consumption ($[C_{total}]$). The fitted functions are presented as black dotted lines in Figures I.1.B and C, where the magnitudes of μ_{max}, X_{max} , r_{max} and $[C_{total}]$ under this particular light intensity are 0.073 hr^{-1}, 3.2 g L^{-1} ,0.088 hr^{-1} and 1325 mg NO_3^{-1} L^{-1}, respectively. In order to investigate the reliability of obtained parameter values, the simple confidence bound analysis was executed. Specifically, both 5% upper and lower deviations in an original value of the maximum specific growth rate were selected as new inputs for the logistic model so that two additional growth

profiles can be subsequently stimulated. As the minimal degree of discrepancy between all three growth profiles was observed (Figure I.1.D), this thus ensures the confidence in the value of the determined rate.

As the culture becomes denser, the transport of light through its path length - the thickness of the PBR's body, becomes poorer (Posten 2009). This is due to an increasing effect of mutual shading phenomena, at which the cells closer to the illumination source begin to obstruct the cells behind them, thereby reducing their ability to photosynthesise and grow. Evidently, under the respective final biomass concentration of 3.2 g L^{-1}, an incident irradiance of 207 μmol m^{-2} s^{-1} is significantly reduced to an average value of 22.7 μmol m^{-2} s^{-1} (Figure I.1.E). In addition, after the mid-way of the path length (L > 11.3 mm), local light intensity becomes close to zero, implying that at least half of the PBR is under virtually dark conditions. Consequently, the growth rate decreases from its maximum value and becomes a linear function of time. Under this light-limited circumstance, the growth behaviour is considered to be under the "linear growth phase". As the cell density increases further, the availability of key nutrients - nitrate (in this case) - starts to become another limiting factor. Under nitrate-deprivation, from time = 95 hours, the growth rate is reduced to zero and the cyanobacterium culture begins to enter the "stationary phase", during which its concentration has reached and remained at a final stable value of 3.2 g L^{-1} based on this particular set of environmental conditions. The subsequent cessation of *Cyanothece* 51142 growth after nitrate depletion, observed in Figure I.1.A, agrees with many previous studies reported for algae and cyanobacteria (Nigam 2011, Cakmak, Angun *et al.,* 2012, Sinetova, Červený *et al.,* 2012). This is because nitrogen is commonly the second most important constituent of biomass - accounting for 8 - 9% of *Cyanothece* 51142 dry biomass (Schneegurt, Arieli *et al.,* 1995), after carbon and subsequently serves a key role in the cellular reproduction. In the absence of an extrinsic nitrogen source, microorganisms generally start to utilise their intracellular accumulated metabolites (Clark 2006), in this case proteins, which were previously synthesised from nitrate. As soon as these

metabolites are exhausted, the growth phase is transformed into an eventual death phase, where the rate of cell death becomes significant and greater than the rate of cellular reproduction. As the decay phase is found being absent in this particular experiment, it can be explained that dinitrogen (N_2), from a supplied mixture of CO_2 and air, can still provide an extracellular nitrogen source to the *Cyanothece* 51142 culture, thereby enabling a potentially long duration of stationary phase.

In addition to nitrogen, there are three other essential macro-nutrients – sulphur, carbon and phosphorus – required by microorganisms. The results obtained from ion chromatography show an excess sulphate concentration with a mean value of 1,900 mg SO_4^{-2} L^{-1} in the medium (Figure I.1.F), whereas CO_2 is continuously sparged through the aqueous phase of the PBR to ensure sufficient concentration of dissolved carbon. In the case of phosphorus, as mentioned in section 5.8.2 of Experimental Methods, the PO_4^{-3} concentrations present in the prepared samples were extremely low and could not be tracked by this technique. However, the study conducted by Sinetova and co-workers (Sinetova, Červený *et al.,* 2012) showed that there was no significant impact on cyanobacterial growth caused by the phosphorus starvation.

From Figure I.1.G, the actual concentration of dissolved O_2, which represents the sum of total photosynthetic rate (= the rate of photosynthetic O_2 evolution - the rate of O_2 consumption by cellular respiration) and rate of O_2 dissolution (= from sparging air into liquid culture – leaving the system), can be seen to decrease sharply after the lag phase and the culture entered the exponential phase. This is due to the fact that as the culture matures, the rate of cellular respiration increases, while the photosynthetic O_2 evolution is limited by the decreased degree of light penetration (Figure I.1.E). The onset of approximately 24 hr periodic oscillations of pH was clearly observed at a nitrate concentration of 400 mg L^{-1}, see Figure I.1.H. The magnitude of the variation between upper and lower pH for each cycle (labelled on the figure) increased as the nitrate concentration decreased. This phenomenon occurs due to the circadian behaviour of *Cyanothece* 51142, which periodically

performs photosynthesis and N_2-fixation in approximately 12 hr light – 12 hr dark cycles, respectively (Schneegurt 1994). In the presence of nitrate, between time = 60 – 100 hours, the nitrogenase enzymes, which catalyse the N_2-fixing reaction, are inactivated (Dutta 2005), consequently, the photosynthetic CO_2-fixation can be the sole cause of the pH variation during this time period. During the subjective light periods, CO_2 is photosynthetically fixed and lower dissolved gas concentration causes the pH to increase. Conversely, during the subjective dark cycles, the carbon fixation process temporally ceases thereby decreasing the pH. After time = 100 hour, when nitrate becomes depleted, the variation of pH is partially affected by the formation of NH_3, which acts as a weak base, during the subjective dark periods.

Figures I.1.A - H: Growth and nutrient kinetics of *Cyanothece* 51142, cultivated at 207 μmol m^{-2} s^{-1}, 35 °C, 20 ml min^{-1} of sterile 10 % volume CO_2 volume air^{-1} and 1.5 g $NaNO_3$ L^{-1} in ASP2 medium.

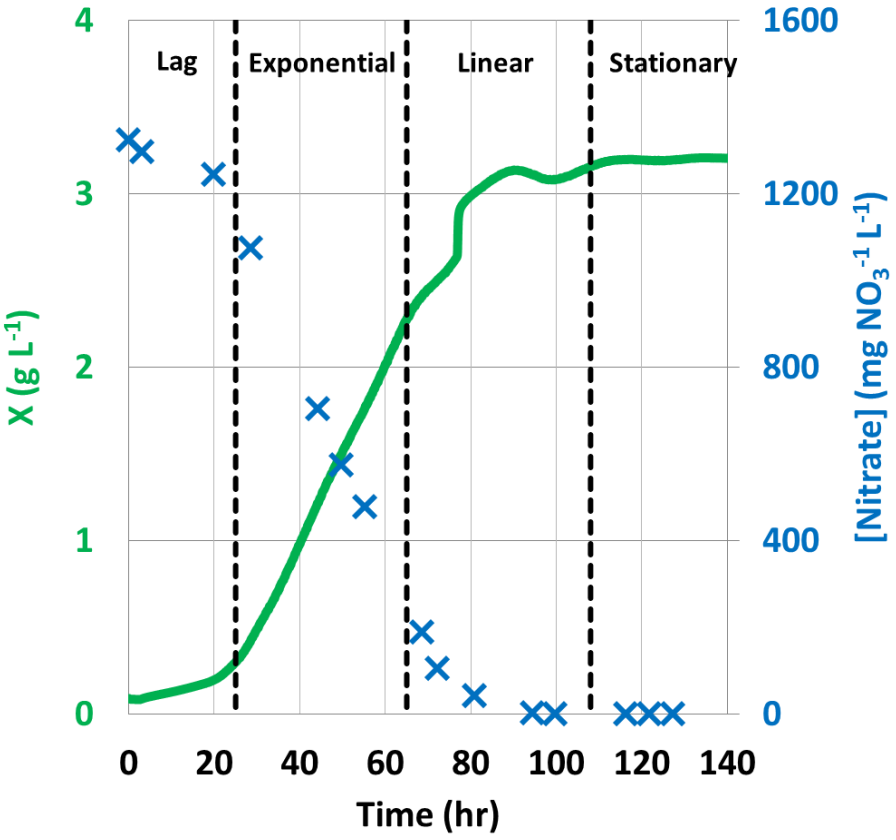

Figure I.1.A: Four common growth phases of the cyanobacterial culture. An increase in biomass concentration (green line) was observed in parallel with the decrease in NO_3^{-1} substrate (blue cross).

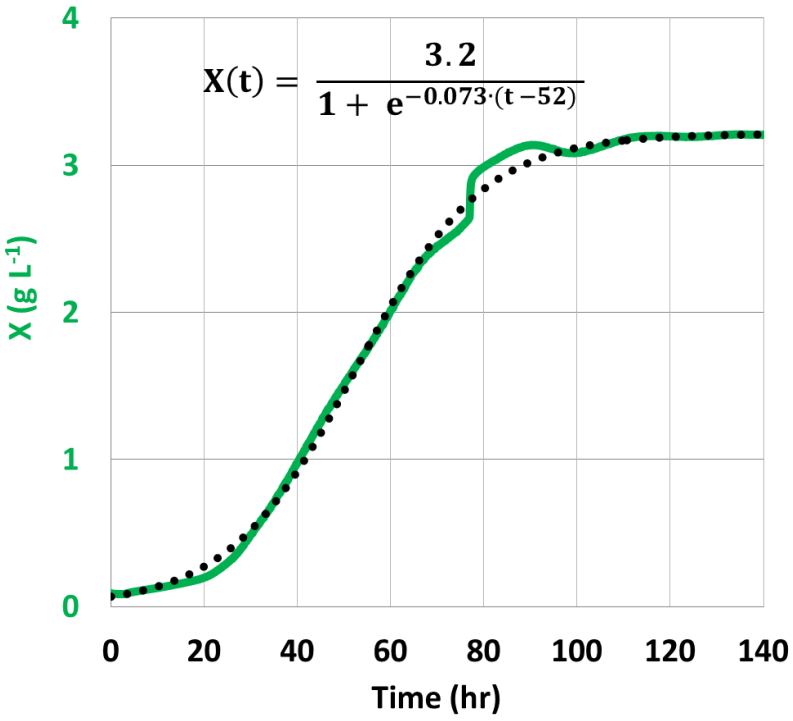

Figure I.1.B: *Cyanothece* 51142 growth can be well-described by a logistic function (black dotted line). μ_{max} and X_{max} are determined to be 0.073 $hr^{-1}$and 3.2 g L^{-1} respectively.

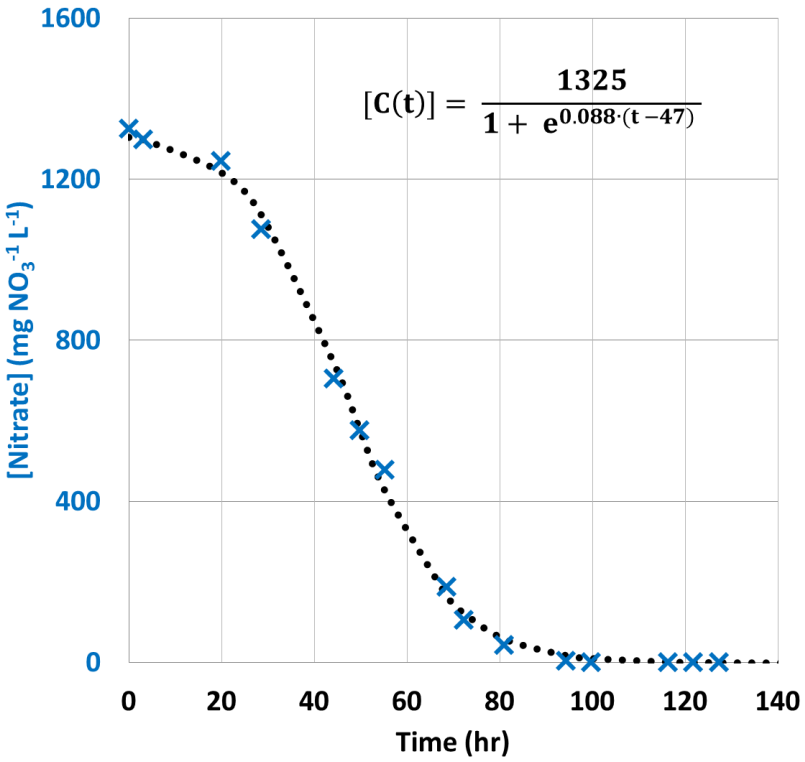

Figure I.1.C: *Cyanothece* 51142 nitrate uptake can also be well-described by an inverse form of the logistic function (black dotted line). r_{max} and X_{max} are determined to be 0.088 hr^{-1} and 1325 mg NO_3^{-1} L^{-1}, respectively.

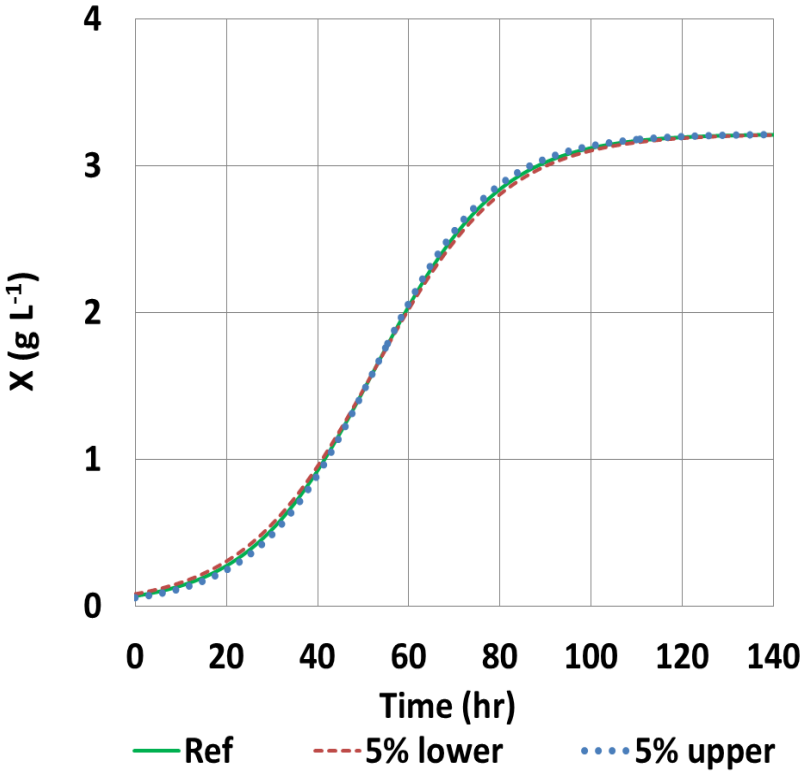

Figure I.1.D: Confidence bounds on the maximum specific growth rate determined using the logistic growth model

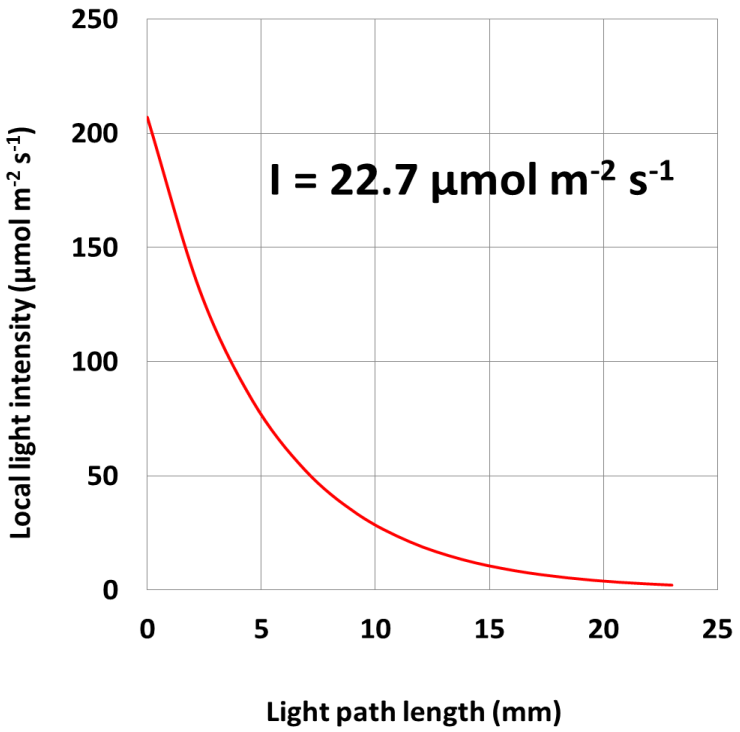

Figure I.1.E: Under very dense culture of 3.2 g L^{-1}, an incident irradiance of 207 µmol m^{-2} s^{-1} is significantly reduced along the thickness of the tubular PBR. An average light intensity inside the PBR is estimated to be only 22.7 µmol m^{-2} s^{-1}.

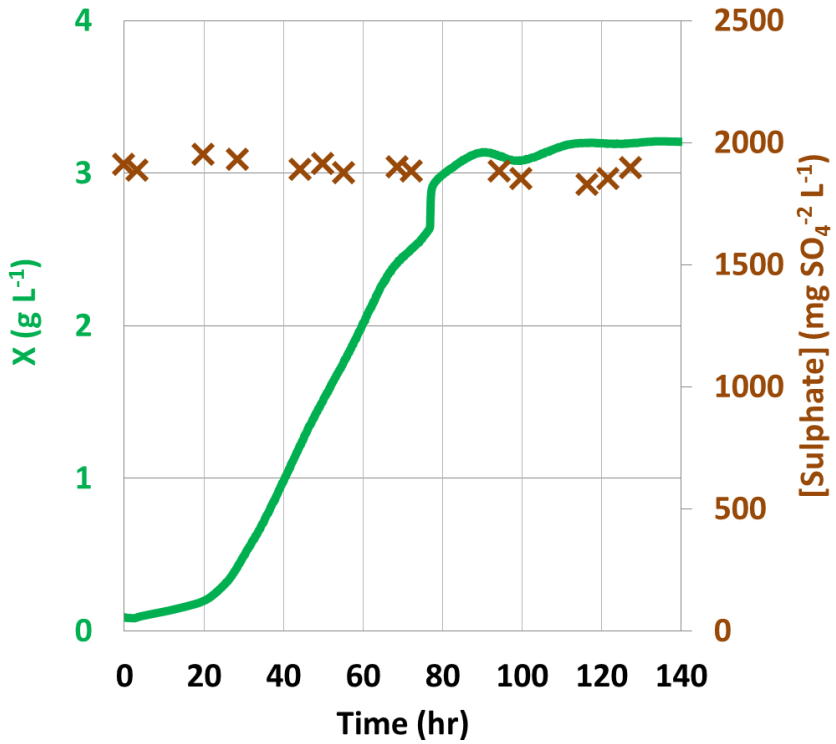

Figure I.1.F: Constant sulphate concentration profile (brown cross) throughout a whole growth experiment.

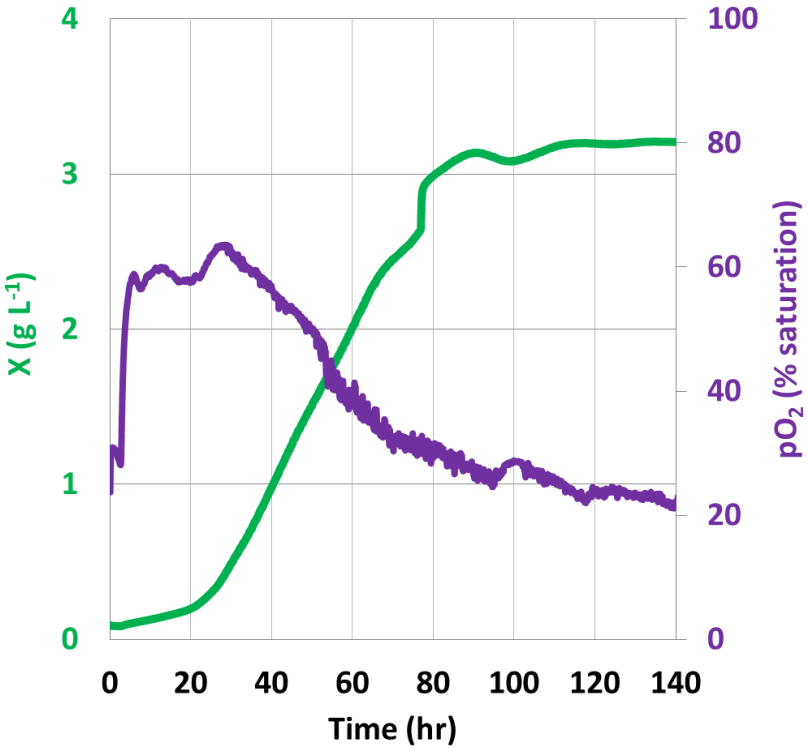

Figure I.1.G: A decreasing profile of dissolved O_2 (purple line) was due to an increasing culture density, which implies a greater rate of cellular respiration, whereas rate of photosynthetic O_2 production remains the same (under a fixed irradiance).

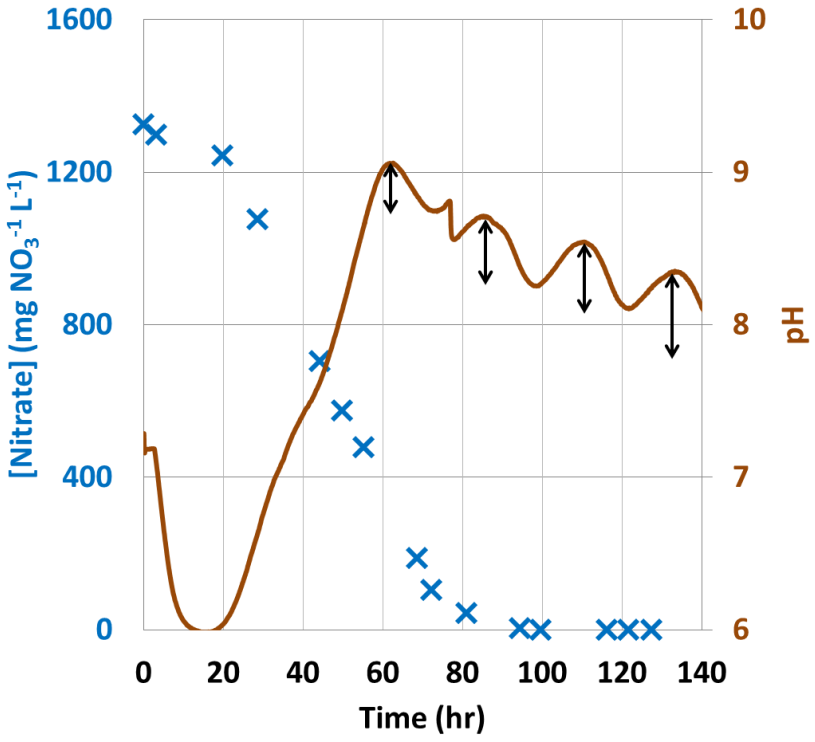

Figure I.1.H: An alternating pH profile (brown line) confirms the circadian behaviour of *Cyanothece* 51142, which periodically performs photosynthesis and N_2-fixation in approximately 12 hr light – 12 hr dark cycles, respectively.

I.4. Effect of Different Nitrogen Source

Nitrogen is one of four essential macro-nutrients, required for the biomass production of microorganisms. Its major utilisation includes the biosynthesis of intracellular proteins and nucleic acids. The cyanobacterium *Cyanothece* 51142 is able to grow using nitrogen salts such as ammonium (NH_4^{+1}) or nitrate (NO_3^{-1}) as well as unfixed N_2 (Feng, Bandyopadhyay *et al.,* 2010). However, 17 mM of NH_4^{+1} was previously reported to inhibit the cyanobacterial growth, due to its deleterious effect on the photosystems of cyanobacteria (Dai, Deblois *et al.,* 2008, Drath, Kloft *et al.,* 2008). Whereas, in the case of NO_3^{-1} and N_2, no negative effects has been found. Therefore, the investigation will be specifically focused on the latter two compounds.

In this section, the effects of NO_3^{-1} and N_2 on the growth process parameters - X, pO_2 and pH - of the *Cyanothece* 51142 culture will be discuessed. In both experiments, the cyanobacterial culture was cultivated, using the ASP2 growth medium under continuous illumination of 275 μmol m^{-2} s^{-1} and constant temperature of 35 ^oC. A 20 ml min^{-1} constant flow of sterile gas mixture of 10% volume CO_2 volume air^{-1} was continuously sparged through an aqueous cultural phase to ensure the autotrophic as well as diazotrophic (N_2-fixing) conditions. In the need of nitrogen-replete condition, 1.5 g L^{-1} of $NaNO_3$ was added into an existing medium to make the ASP2+N medium.

I.4.1. Atmospheric Nitrogen (N_2)

As shown in Figure I.2.A, under photoautotrophic nitrogen-fixing growth conditions, the *Cyanothece* 51142 culture experienced the first lag phase for approximately 30 hours, before proceeding into the secondary exponential phase, with μ_{max} of 0.031 hr^{-1} (0.744 day^{-1}), see Figure I.2.A. By comparing with previously reported values, under similar growth conditions, obtained rate is 2.4 and 2.66 times higher than those observed by Alagesan and colleagues (Alagesan, Gaudana *et*

al., 2013) and Feng and co-workers (Feng, Bandyopadhyay *et al.,* 2010), respectively. This can be the consequence of difference in 1) incident irradiance and 2) CO_2 concentration. As in Feng's experiment, only 50 μmol m^{-2} s^{-1} and ambient CO_2 were used to grow the *Cyanothece* 51142 culture, whereas Alagesan's study employed a slightly higher irradiance of 100 μmol m^{-2} s^{-1}, but their CO_2 supply was also from ambient air, whose concentration is as low as 0.04 % CO_2 volume air volume^{-1}. The light-limiting linear growth phase appears to take place, between time = 100 and 144 hours, after which the stationary phase is eventually attained. Under this particular cultivating condition, the cells are able to reach a final dry biomass concentration of 2.9 g L^{-1}. The logistic model, represented by a black dot line on the figure, was still demonstrated to have a sufficient capability to track most of the growth profile as well as extract key growth parameters under such condition. However, the model is unable to simulate periodically oscillating patterns in biomass concentration. A similar pattern is also observed for both of pO_2 and pH profiles (Figures I.2. B and C). All of these observations are expected and strongly confirm the circadian metabolic shift behaviour of *Cyanothece* 51142 (Reddy, Haskell *et al.,* 1993, Sherman, Meunier *et al.,* 1998, Welsh, Liberton *et al.,* 2008), where photosynthesis and N_2-fixation are temporally carried out during day and night times, respectively. In addition, as continuous light condition was maintained throughout an experimental time course, the result thus reassures the previously discovered unique biological character of *Cyanothece* 51142 to sustain its metabolic switch, regardless of illumination conditions (Schneegurt 1994, ColonLopez, Sherman *et al.,* 1997). However, it can be clearly observed that the duration spent between two adjacent pO_2 as well as pH peaks is increasing as experimental time proceeds. This behaviour may be explained through acclimatisation of the cyanobacterium with the new illuminating conditions.

Specifically, peaks of pO_2 suggest occurrences of photosynthetic CO_2 fixation during subjective light periods, when O_2 is simultaneously produced as by-products. As CO_2 is naturally an acidic compound, by photosynthetically fixing this inorganic carbon into its fixed organic form - glycogen

(Schneegurt, Sherman *et al.,* 1997) - means that there is a lower quantity of dissolved CO_2 available in the liquid phase, thereby causing the pH value to rise to the maximum value of 7.8. Concurrently increasing profiles of both pO_2 and pH can be evidently seen from Figures I.2.B and C, for example at time = 30 – 40 hour. In contrast, when the culture of *Cyanothece* 51142 enters into subjective darks, for example at t = 45 - 55 hour, the role of photosynthesis changes from active to become inactive (Colon-Lopez and Sherman 1998, Toepel, Welsh *et al.,* 2008). This metabolic shift is again confirmed by the same figures, when pH starts to decline and eventually reaches the minimum value of 6.3. This decrease in pH value is due to the temporary cessation of photosynthesis, which subsequently allows the greater quantity of unfixed CO_2 to be dissolved in the culture medium. At the same time, a declining profile of pO_2 is as well observed and suggests an active role of cellular respiration (ColonLopez, Sherman *et al.,* 1997). Cyanobacterial respiration causes two beneficial effects towards an enhancement of N_2-fixing reaction: i) significantly reducing intracellular O_2 levels and thereby inducing the necessary low-O_2 environment for the activation of nitrogenase enzyme (Fay 1992) and ii) converting previously synthesised glycogen into chemical energy, which is utilised to fuel an energy-dependent N_2-fixation process. Although an analytical technique to measure nitrogenase activity such as acetylene reduction assay (Reddy, Haskell *et al.,* 1993, Bandyopadhyay, Stoeckel *et al.,* 2010), was not present in my laboratory, at the time of conducting this experiment, the growing ability of the cyanobacterium can still serve as a key indicator of the happening N_2-fixation under this particular study.

Figures I.2. A - C: Growth kinetics of *Cyanothece* 51142, cultivated at 275 µmol m^{-2} s^{-1}, 35 $^{\circ}$C, 20 ml min^{-1} of sterile 10 % volume CO_2 volume air^{-1} in ASP2 medium.

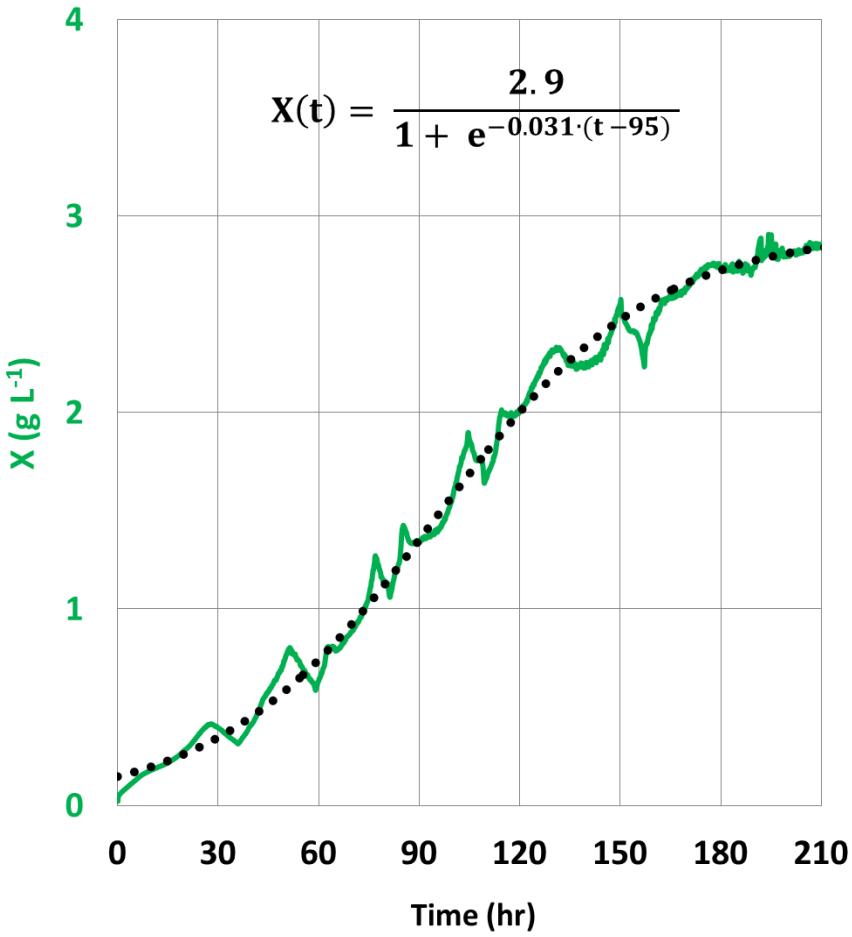

Figure I.2.A: Photoautotrophic nitrogen-fixing growth of *Cyanothece* 51142 culture. The profile can be well-described by a logistic function (black dotted line). μ_{max} and X_{max} are determined to be 0.031 hr^{-1} and 2.9 g L^{-1} respectively.

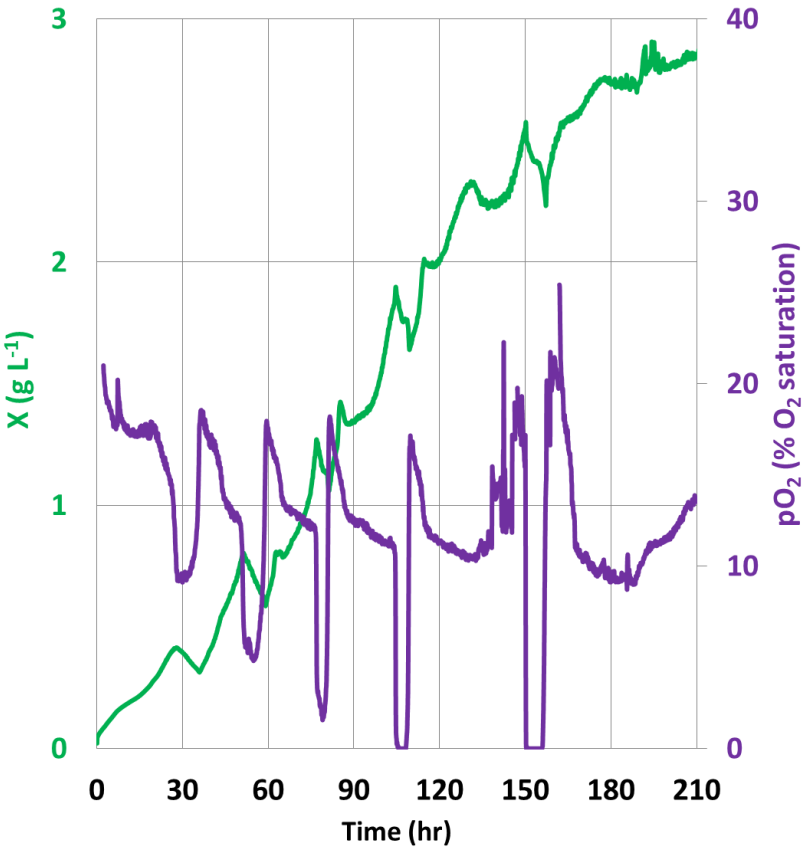

Figure I.2.B: Oscillating patterns in both biomass (green line) and pO_2 (purple line) profiles confirms circadian-regulated metabolic shift behaviour of *Cyanothece* 51142 strain.

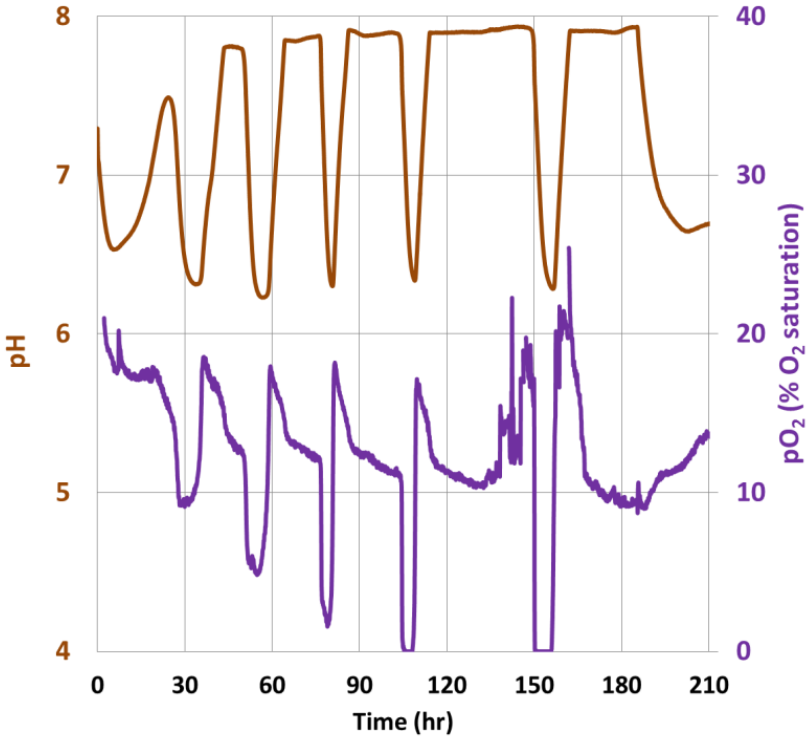

Figure I.2.C: A high level of coherence can be seen between pO_2 and pH (brown line) profiles

I.4.2. Nitrate Salt (NO_3^{-1})

In the presence of NO_3^{-1}, the nitrogenase activity is reported to become inactivated (Dutta 2005). This statement is confirmed by the photoautotrophic nitrogen-sufficient growth condition (Figures I.3.A, B and C), during which strong oscillating patterns no longer exist in any of biomass concentration, pO_2 and pH profiles. Although there are periodic variations in pH value from time = 50 hr onwards, their magnitudes (mean value of 0.5) are not as strong as the ones observed under nitrogen-fixing condition (mean value of 1.5) (section I.4.1). In fact, all of the parameters here possess similar profiles to those presented before in section I.3, as the same type of carbon and nitrogen substrates were used. Under this particular condition, the *Cyanothece* 51142 culture is able to reproduce with μ_{max} of 0.08 hr^{-1} (1.92 day^{-1}), and eventually reaches its final concentration of 3 g L^{-1} within 120 hours after its inocculation, see Figure I.3.B. This specific growth rate is approximately 2.6 times faster than that obtained under the nitrogen-fixing conditions. Similar enhancements were also reported by previous studies (Feng, Bandyopadhyay *et al.,* 2010, Alagesan, Gaudana *et al.,* 2013). This can be explained by the fact that the fixation of N_2 is a typically energy-demanding process; with supplement of nitrate salts, the reaction is inhibited and thereby allowing a greater quantity of chemical energy to be used for other biomass producing reactions. In comparison with previously obtained result in section I.3, the current growth rate is still slightly higher (1.1 fold). This increment is a result of the difference in intensities of incident light used between these two studies (207 µmol m^{-2} s^{-1} in section I.3 and 275 µmol m^{-2} s^{-1} in this section). The effect of irradiance upon the photoautotrophic growth of *Cyanothece* 51142 will be fully discussed later in section I.6.

Despite significant improvements in cyanobacterial growth rate, when N_2 was switched into nitrate, there was approximately no enhancement in cyanobacterial biomass concentration. Even when nitrate salts become depleted after time = 100 hr, the cells can still rely on N_2, from the supplied air,

as their replacement of nitrogen source. This circumstance thus disregards the nitrogen deficiency as the major cause for this observation. Similar to section I.3, mutual shading between cells, causing an inefficient internal light distribution, is mostly likely the true reason. As expressed in Equations 5.32 and 5.33, local light intensity is a function of biomass concentration and light path length. By using the same PBR and same incident light intensity, the same light attenuation effect will occur whenever the culture reaches the same biomass concentration. Under this photo-limitation condition, there is not enough solar energy for every single cell of the cyanobacterial culture, consequently the growth is restricted to a certain value of biomass concentration.

In the case of nitrate consumption, the specific uptake rate was found to be 0.079 hr^{-1}, which is again 1.2 higher than that measured in section I.3. This observation is highly reasonable, as when light intensity is increased from 207 to 275 μmol m^{-2} s^{-1}, growth rate is increased and there is subsequently a greater demand for nutrients to support this activity. As soon as the nitrogen substrate ran out at time = 100 hour, *Cyanothece* 51142 substitutes by activating its nitrogenase, as previously explained in section I.3.

Figures I.3.A - C: Growth kinetics of *Cyanothece* 51142, cultivated at 275 μmol m^{-2} s^{-1}, 35 ˚C, 20 ml min^{-1} of sterile 10 % volume CO_2 volume air^{-1} and 1.5 g $NaNO_3$ L^{-1} in ASP2 medium.

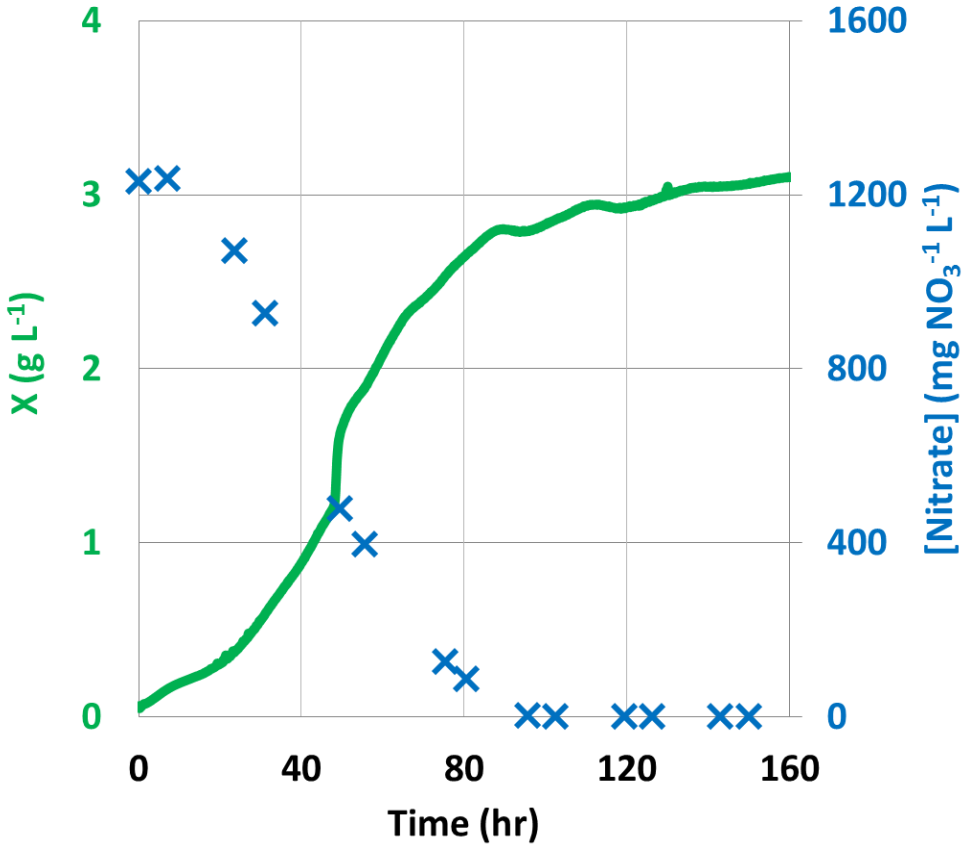

Figure I.3.A: Photoautotrophic nitrogen-replete growth profile (green line) of *Cyanothece* 51142 culture. With an increasing biomass concentration (green line), a simultaneously decrease in nitrate concentration (blue cross) is observed.

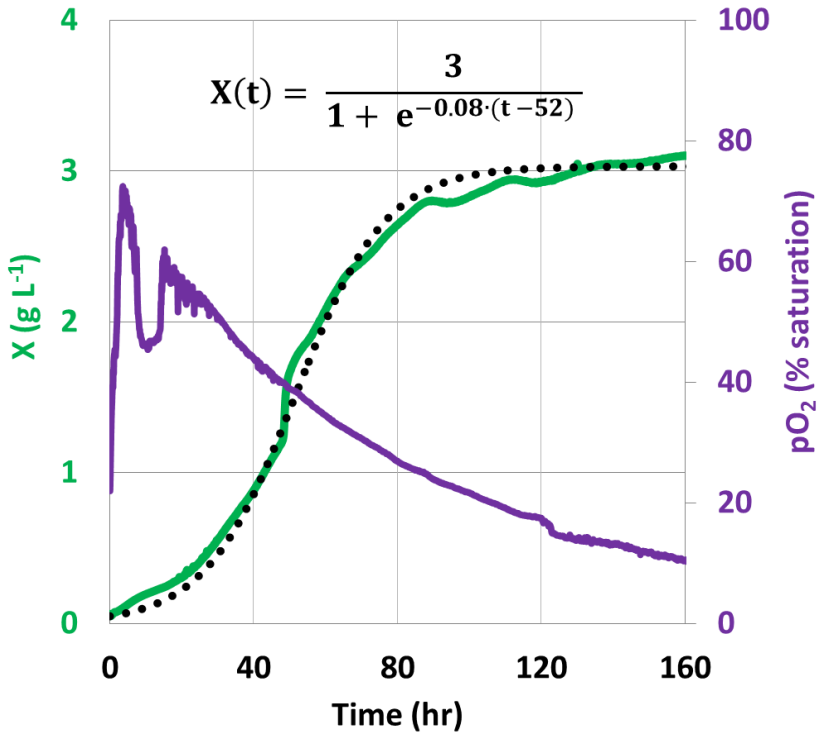

Figure I.3.B: Using logistic function, μ_{max} and X_{max} are determined to be 0.08 $hr^{-1}$and 3 g L^{-1} respectively. A continuous decline in pO_2 value (purple line) is due to an increasing respiration of growing culture.

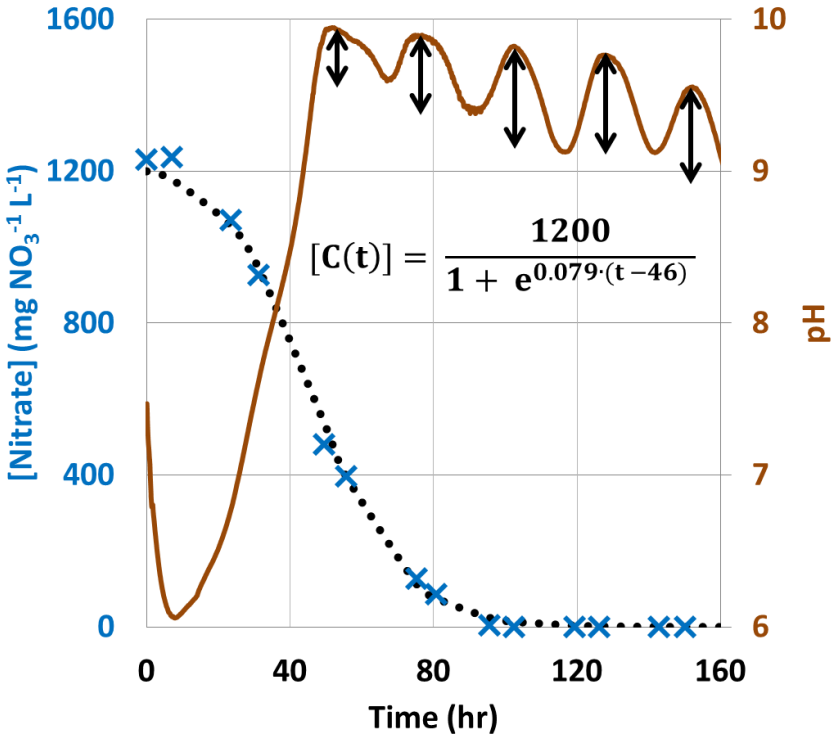

Figure I.3.C: In the case of nitrate uptake kinetics, r_{max} and $[C_{total}]$ are determined to be 0.079 hr^{-1} and 1200 mg NO_3^{-1} L^{-1}, respectively. The periodically oscillating profile of pH (brown line) is observed, but at much lower degree than that of nitrogen-fixing condition.

I.5. Effect of Different Carbon Source

Carbon is another essential nutrient, required for the cultivation of *Cyanothece* 51142, as it accounts for approximately 40% of the cyanobacterial biomass (Schneegurt, Arieli *et al.,* 1995). *Cyanothece* 51142 is able to grow using inorganic carbon - CO_2 - via photosynthetic fixation as well as under the supplement of various organic carbon substrates (Schneegurt, Sherman *et al.,* 1997). However, glycerol appears to be the only substrate capable of enhancing the cyanobacterial growth rate, with minimal adverse effect (Feng, Bandyopadhyay *et al.,* 2010). Therefore, this particular substrate is usually used as an additional carbon source to study the growth and the H_2 production of *Cyanothece* strains.

In this section, the effects of two carbon sources - CO_2 and glycerol on the growth process parameters - X, pO_2 and pH - of the *Cyanothece* 51142 culture will be discussed. In both experiments, the cyanobacterial culture was cultivated, using the ASP2 growth medium under continuous illumination of 275 μmol m^{-2} s^{-1} and constant temperature of 35 ^{o}C. For CO_2 experiments, a 20 ml min^{-1} constant flow of sterile gas mixture of 10% volume CO_2 volume air^{-1} was continuously bubbled through an aqueous cultural phase to provide carbon as well as nitrogen sources. In the case of glycerol experiments, the gaseous mixture of CO_2 and air was replaced by pure air in order to solely restrict the carbon-dependence of growth on glycerol substrate. Sterile glycerol was eventually added into the cyanobacterial culture to make the final concentration of 35 mM. It should be noted here that my decision of choosing glycerol concentration is based on previous studies (Bandyopadhyay, Stoeckel *et al.,* 2010, Alagesan, Gaudana *et al.,* 2013), which reported 30 and 50 mM as optimal concentrations, facilitating the growth and the H_2 production process of the *Cyanothece* 51142 strain, respectively. But, a substrate concentration of 75 mM was found to inhibit the growth of the cyanobacterial culture (Alagesan, Gaudana *et al.,* 2013).

I.5.1. Carbon Dioxide (CO_2)

As the same cultivating condition as section I.4.1 was employed to carry out the CO_2 experiment, all of results and discussions can be compared with that particular section.

I.5.2. Glycerol

When an organic carbon - glycerol in this case - is utilised as the sole carbon source to cultivate the cells, this particular condition is usually called "heterotrophic" growth condition. Figure I.4.A clearly shows an ability of the cyanobacterium *Cyanothece* 51142 to photoheterotrophically grow, in the presence of glycerol. It can be clearly seen that both cultures, cultivated under the provision of CO_2 and glycerol, enter the exponential phase at approximately the same time of 30 hours, the glycerol-supplemented culture apparently possesses the faster growth rate – steeper gradient. By fitting the experimental data with the logistic model (Figure I.4.B), μ_{max} of this particular study can be estimated and found to be 0.074 hr^{-1}, which is around 2.4 times higher than that of the photoautotrophic growth condition. This finding is again highly comparable with previous enhancement factor of 2, observed by Alagesan *et al.,* (Alagesan, Gaudana *et al.,* 2013) and Feng *et al.,* (Feng, Bandyopadhyay *et al.,* 2010). The biomass concentration was limited to the final value of 3.2 g L^{-1} - in the same range with other growth conditions in previous sections, because of mutual shading effects.

Similar to nitrogen-replete condition (section I.4.2), usual oscillating pH and pO_2 profiles disappear in the presence of glycerol (Figures I.4.C and D). This can be explained by proteome analyses of the *Cyanothece* 51142 strain conducted by Aryal *et al.,* (Aryal, Callister *et al.,* 2013), which shows a glycerol-induced inhibition of key enzymes of CBB cycles. This inhibition then leads to the significant reduction in activities of photosynthetic carbon fixation as well as its concurrent O_2

evolution. In addition to reducing photosynthesis-related activities, glycerol also induces higher levels of respiration and glycogen breakdown, both of which facilitate the nitrogen-fixing activities. Under this circumstance, the rate of O_2 consumption (via respiration) becomes greater than its production rate (via photosynthesis and O_2 dissolution from sparging air). As a result, the negative change of dissolved O_2 concentration with respect to time is quite expected and reflected by a continuous decline in pO_2 value (Figure I.4.C), since the beginning of the experiment until the time = 45 hours. Between time = 45 and 120 hours, the value of pO_2 was still maintained at virtually zero, as there was still glycerol substrate available to support high cellular respiration. As soon as glycerol was used up at time = 90 hour, a rapid rise in pO_2 value is observed. This observation suggests an initiation of O_2 production from photosynthetic activities as well as much lower respiratory level carried out by cells. By fitting the glycerol concentration profile with the logistic model, its maximum specific uptake rate is found to be 0.07 hr^{-1}.

In the case of pH (Figure I.4.D), its profile appears to be consistent with that of pO_2. Shortly after the establishment of anaerobic conditions at time = 45 hours, the pH starts to drop from its original value of 7.7 to eventually reach the new low value within a range of 6.7 – 7, before rising again after the depletion of glycerol. The first drop can be explained as the common cellular response to the low-O_2 environment, because, under anaerobic condition, microorganisms are able to ferment the organic substrate into a number of fermentative products and CO_2 (Heritage 1996, Catalanotti, Yang *et al.,* 2013). These excreted products are typically acidic in nature and their production subsequently causes the pH to decrease. In the case of the second pH rise, as soon as glycerol is used up, *Cyanothece* 51142 initiates photosynthetic activity and begins to photosynthetically fix CO_2, thereby eventually increasing the pH of the liquid phase.

Figures I.4.A - D: Growth kinetics of *Cyanothece* 51142, cultivated at 275 μmol m^{-2} s^{-1}, 35 ˚C, 20 ml min^{-1} of sterile air and 50 mM glycerol in ASP2 medium.

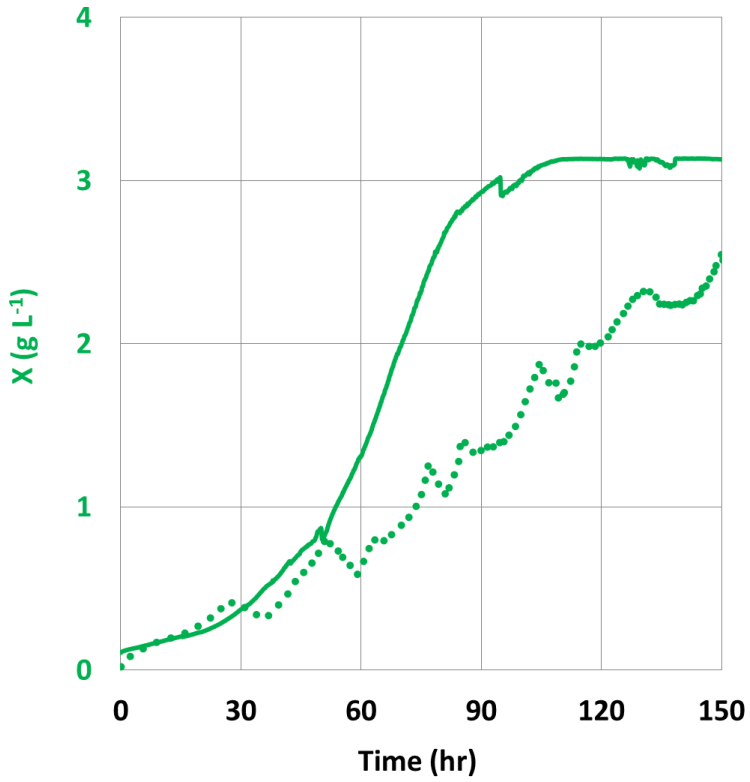

Figure I.4.A: Comparison between photoheterotrophic (green line) and photoautotrophic (green dotted line) growth profiles of *Cyanothece* 51142 culture.

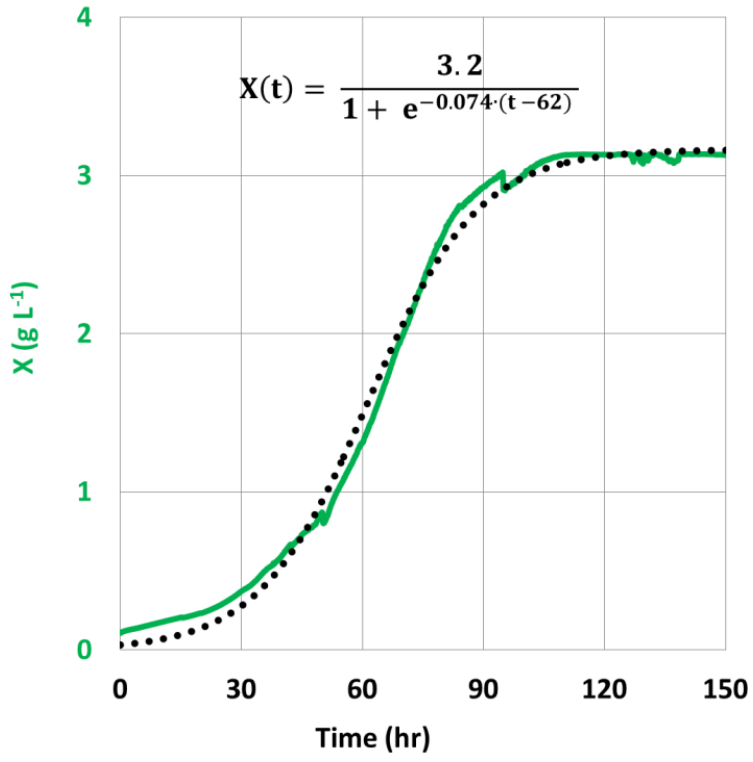

Figure I.4.B: Using logistic function (black dotted line), μ_{max} and X_{max} are determined to be 0.074 hr^{-1} and 3.2 g L^{-1} respectively.

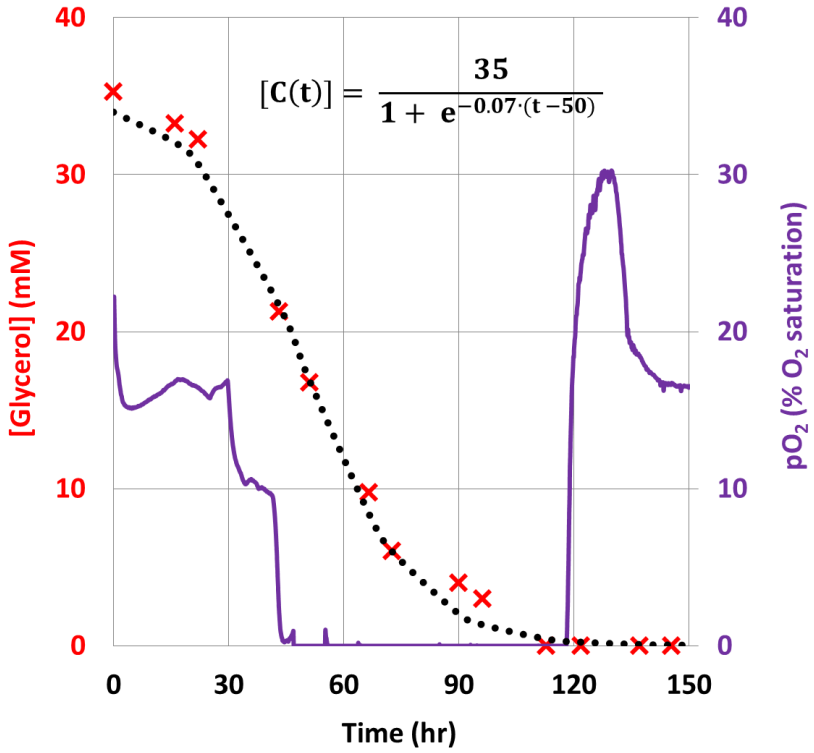

Figure I.4.C: In the case of glycerol uptake kinetics, r_{max} and $[C_{total}]$ are determined to be 0.07 hr^{-1} and 35 mM, respectively. In presence of glycerol (red cross), a continuous decline in pO_2 (purple line) is observed due to an enhanced respiration. After glycerol depletion at time = 120 hr, there is an instantaneous rise in pO_2, suggesting an initiation of photosynthesis.

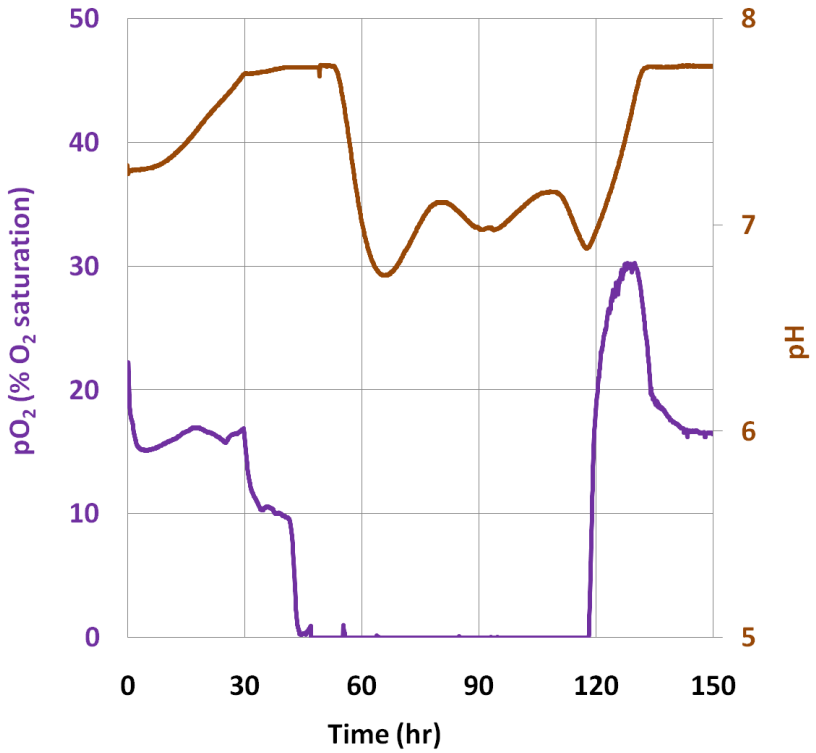

Figure I.4.D: Under anaerobic condition, the culture ferments glycerol to produce CO_2 and organic acids, which cause pH to decline. As soon as, photosynthesis is initiated at tie = 120 hr, CO_2 is subsequently fixed and pH starts to increase.

I.6. Effect of Light Intensity

Light intensity is undoubtedly one of the most important environmental parameters, affecting *Cyanothece* 5142 growth. In general, an increase in light intensity facilitates an increase in photosynthetic activity, thereby enhancing both the growth rate and the subsequent H_2 production rate of the microalgal cells (Hallenbeck and Benemann 2002). However, this relationship continues up to a critical irradiance, which after photoinhibition taking effect, replaces photo-saturation, and causes cell death (Nixon, Michoux *et al.,* 2010). As a result, the aim of this section is to investigate the effect of light intensity upon the growth kinetics of *Cyanothece* 51142 culture and subsequently locate an optimal light regime, facilitating maximal cyanobacterial biomass productivity.

Experimentally, the cyanobacterial culture was cultivated under continuous illumination of seven different light intensities at 23, 46, 92, 138, 207, 275 and 320 μmol m^{-2} s^{-1}. The medium was ASP2, with an addition of 1.5 g $NaNO_3L^{-1}$. Temperature was maintained at 35 $^{\circ}$C for every light intensity study. 20 ml min^{-1} of sterile 10 % volume CO_2 volume air^{-1} was sparged through the aqueous culture to provide photoautotrophic conditions. Similar to previous sections, key parameters of growth - maximum specific growth rate (μ_{max}) and maximum biomass concentration (X_{max}) - and nutrient uptake kinetics - maximum specific uptake rate (r_{max}) and total nutrient consumption ($[C_{total}]$), under each respective irradiance, were determined by fitting the experimental data to the logistic model (Equations 5.29 and 5.30 respectively). Eventually, the relationship between irradiance and determined parameters was modelled using Equation 5.35, which is capable of simultaneously describing two environmental factors - light intensity (Equations 5.31 – 5.33) and temperature (Equation 5.34).

It can be seen from Figure I.5.A - O that both growth and nitrate uptake profiles, under all of investigating light intensities, can be perfectly described by the logistic model. Key results from the

parameter evaluation are tabulated in Table I.1. It should be noted here that there was a variation in an initial NO_3^{-1} concentration, which may subsequently affect the value of X_{max}, as nitrogen is an essential constituent of biomass. However, due to an eventual light attenuation effect in every light intensity experiment, X_{max} was found to be limited to certain value, even there was the difference in the substrate concentration. Numerically, similar values of X_{max} were obtained under 138 (Figures I.5.G and H) and 207 μmol m^{-2} s^{-1} (Figures I.5.K and L), at which the initial NO_3^{-1} concentrations were determined to be 1,061 and 1,325 mg NO_3^{-1} L^{-1}, respectively. Plotting one specific rate against another for all of studied conditions yields a linear regression with $R^2 = 0.9439$ (Figure I.6), which implies that cyanobacterial growth is directly proportional to nitrate consumption.

Figures I.5.A - N: Fitting of growth and nitrate uptake kinetics of *Cyanothece* 51142, cultivated at 23, 46, 92, 138, 207, 275 and 320 μmol m^{-2} s^{-1}, 35 °C, 20 ml min^{-1} of sterile 10 % volume CO_2 volume air^{-1} and 1.5 g $NaNO_3$ L^{-1} in ASP2 medium.

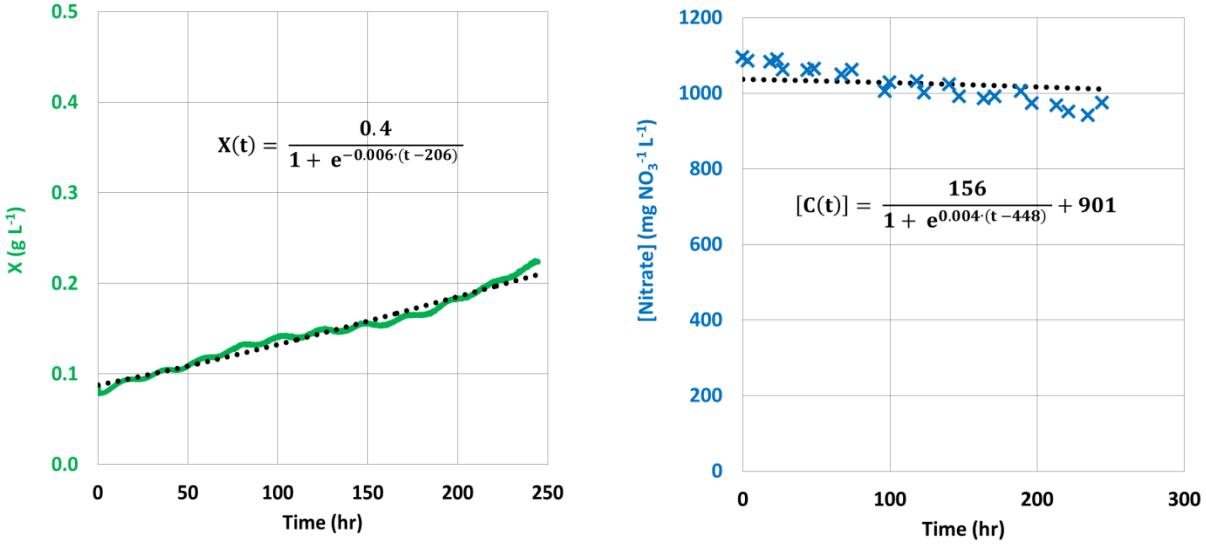

Figure 1.5.A and B: Fitting of growth and nitrate uptake data for 23 µmol m^{-2} s^{-1}

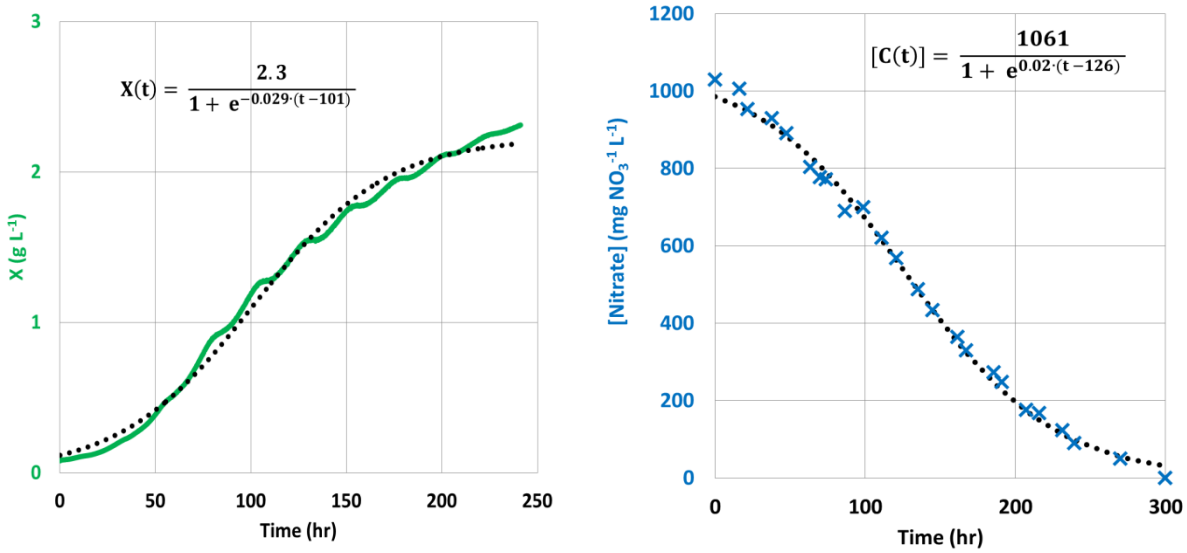

Figure 1.5.C and D: Fitting of growth and nitrate uptake data for 46 µmol m^{-2} s^{-1}

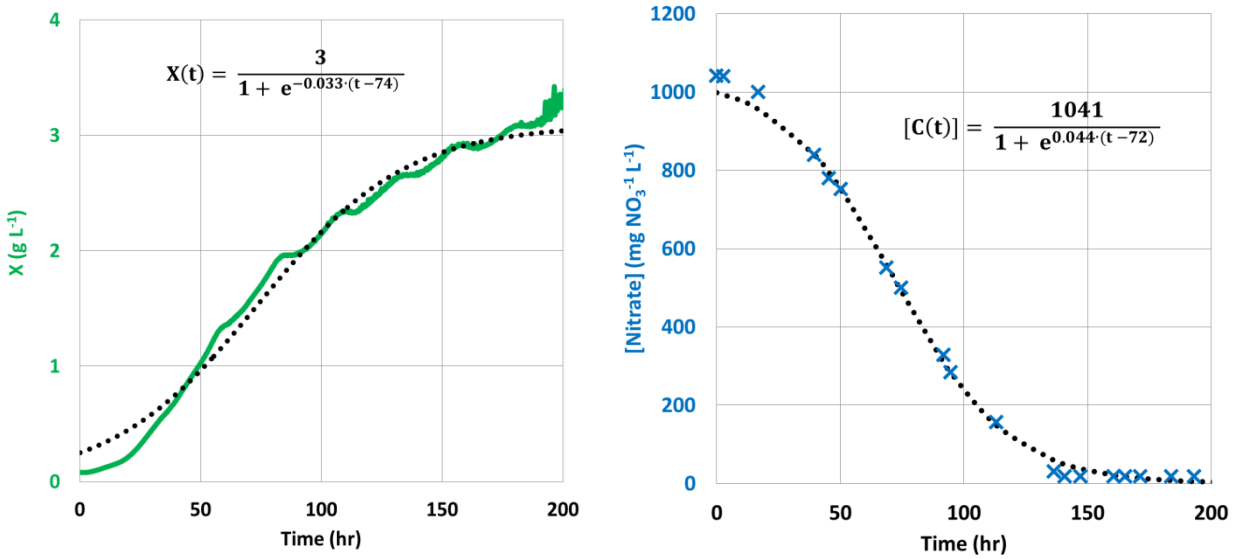

Figures I.5.E and F: Fitting of growth and nitrate uptake data for 92 µmol m^{-2} s^{-1}

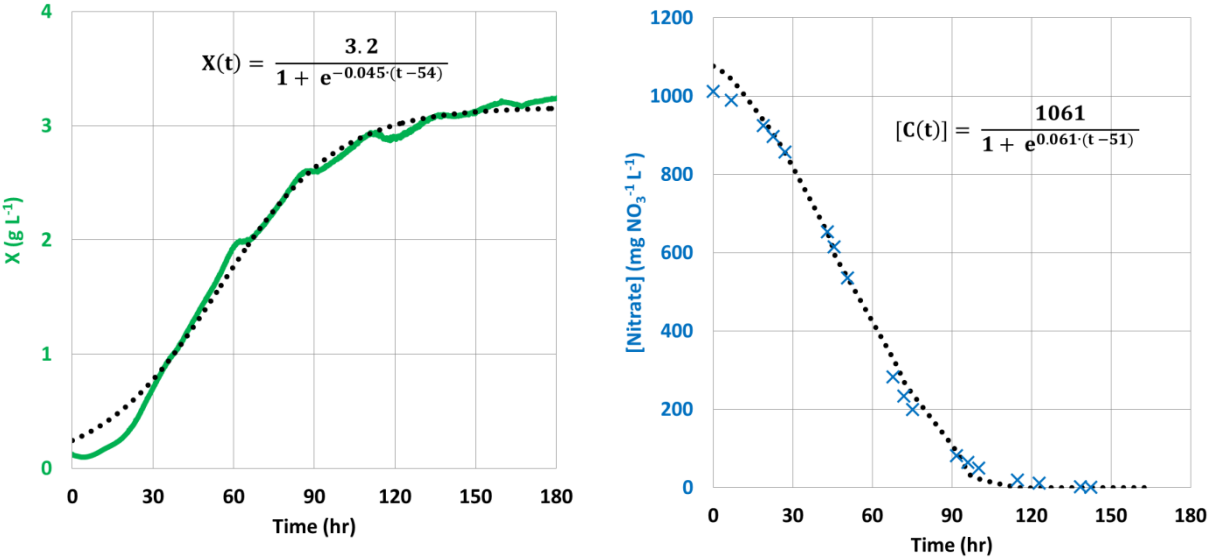

Figures I.5.G and H: Fitting of growth and nitrate uptake data for 138 µmol m^{-2} s^{-1}

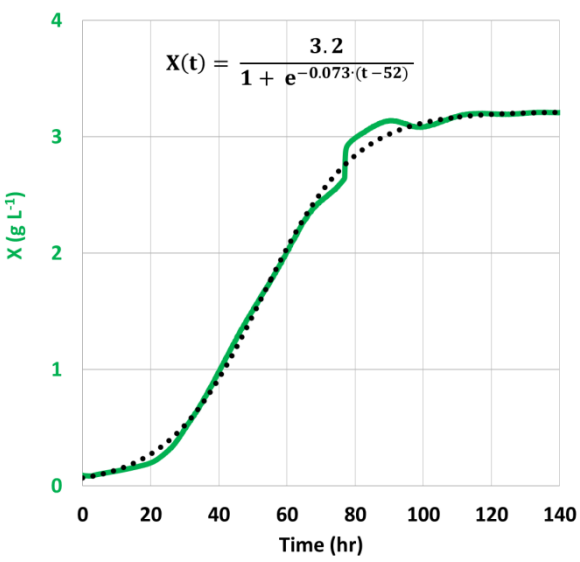

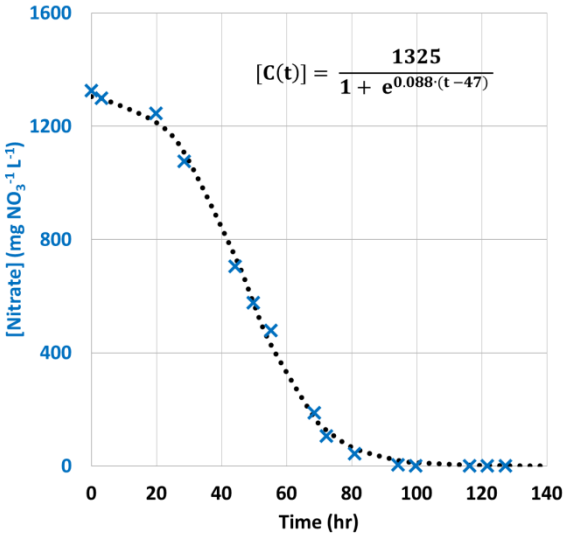

Figures I.5.I and J: Fitting of growth and nitrate uptake data for 207 µmol m^{-2} s^{-1}

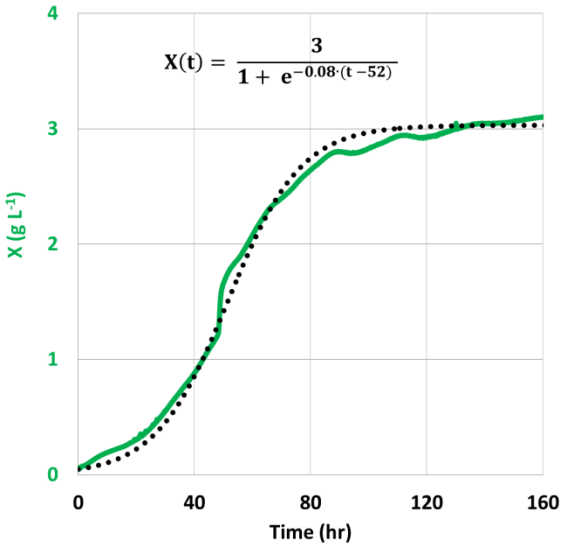

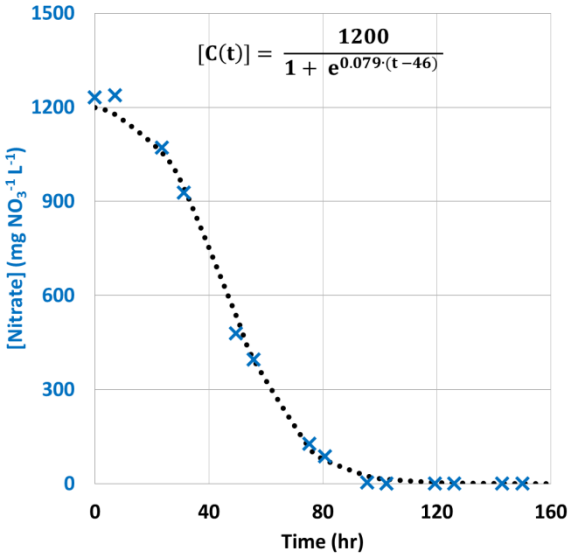

Figures I.5.K and L: Fitting of growth and nitrate uptake data for 275 µmol m^{-2} s^{-1}

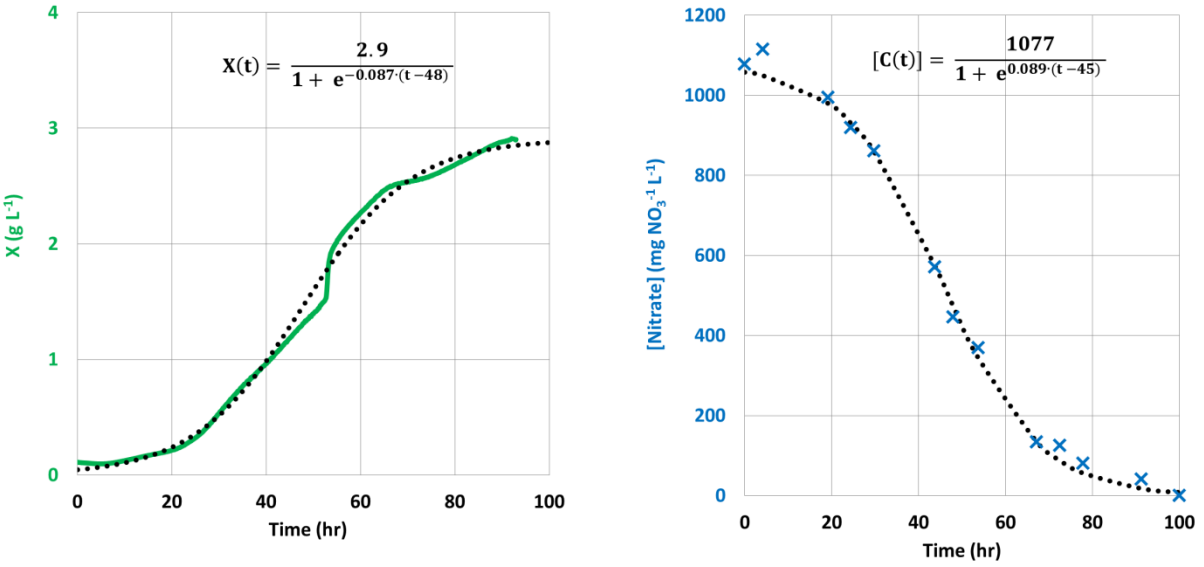

Figures I.5.M and N: Fitting of growth and nitrate uptake data for 320 µmol m^{-2} s^{-1}

Table I.1: Growth and uptake kinetics data under different studied light intensities

Light Intensity (µmol m^{-2} s^{-1})	μ_{max} (hr^{-1})	Maximum DBC (g L^{-1})	r_{max} (hr^{-1})	Total Nitrate Uptake (mg $NO_3^{-1}L^{-1}$)
23	~0.006	0.2	0.004	156
46	0.029	2.3	0.020	1061
92	0.033	3	0.044	1041
138	0.045	3.2	0.060	1061
207	0.073	3.2	0.089	1325
275	0.080	3	0.079	1230
320	0.087	2.9	0.089	1077

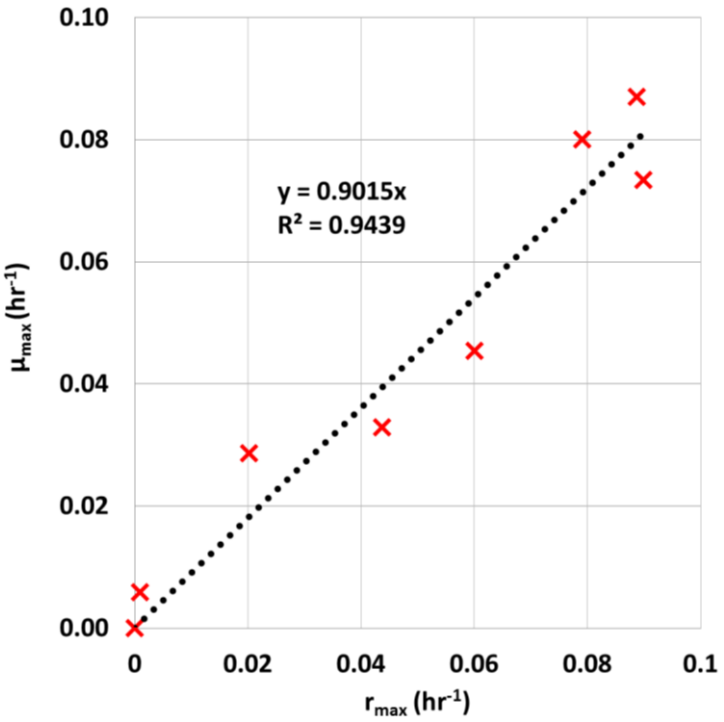

Figure I.6: As nitrogen is an important nutritional source required by *Cyanothece* 51142 culture, the maximum specific growth rate of the culture strongly shows a linear relationship with its maximum specific nitrate uptake rate under respective irradiance (each red cross represents adjacent light intensity, starting with 0 μE m^{-2} s^{-1} from left-end).

By plotting individual modelled growth profiles on the same x-axis (Figure I.7), the photo-dependence of *Cyanothece* 51142 growth behaviour can be clearly observed. The figure shows that the duration of the initial lag phase appears to be the same of approximately 24 hours, regardless of cultivating irradiance. However, as the cultures start to enter the exponential growth phase, the influence of different light intensities on the maximum specific growth rate can be clearly seen. At 23 μmol m^{-2} s^{-1}, there is virtually no grow in the *Cyanothece* 51142 culture, as its final biomass concentration at time = 200 hours still remains very low at 0.2 g L^{-1}. This particular observation is expected and due to an insufficient solar energy for driving the light-dependent photosynthetic process of the cyanobacterium. Without photosynthesis, the cells are unable to derive their carbon

source from supplied CO_2 and become incapable of reproducing. Under non-growing circumstance, there is thus a minimal demand of nitrate salts, whose concentration remains at high level - more than 1,000 mg NO_3^{-1} L^{-1} (Figure I.5.A and B). With increasing light intensity, both μ_{max} and X_{max} become enhanced (Figure I.8.A). Quantitatively, as the irradiance was increased from 23 to 46 μmol m^{-2} s^{-1}, μ_{max} and X_{max} were increased by factors of 7.25 and 10 respectively (calculated from data in Table I.1). Whist, from 46 to 92 μmol m^{-2} s^{-1}, these light-induced enhancement factors are reduced to 1.34 and 1.41 for μ_{max} and X_{max} respectively. Beyond 92 μmol m^{-2} s^{-1}, the final biomass concentration remains approximately the same at a mean value of 3.1 g L^{-1}, whereas μ_{max} continues to rise, with no sign of reaching a plateau yet. The constant biomass concentration profile is likely to be caused by poor light distribution inside the liquid culture, which is commonly induced by very dense culture (Posten 2009), rather than light-induced photoinhibition. It can be seen from Figure I.8.A that the relationship between light intensity and obtained growth rate was not perfectly described by the Aiba model, which takes into account the effect of light attenuation –average irradiances was used instead of incident irradiances. However, when the attenuation factor was excluded from the model, the quality of fitting was significantly improved (Figure I.8.B). These observations then imply the mutual shading between cells as the reason behind the discrepancy in Figure I.8.A. It should be noted here that the experimental data at very low intensity of 23 μmol m^{-2} s^{-1} was excluded from the simulation, as this particular intensity is too low to initiate an effective growth of cyanobacterium. Under a fixed temperature of 35 °C, the temperature function, $h(T)_G$, becomes another constant, making $h(I)_G$ an only variable in the Equation 5.35. Consequently, the multiplier between $\mu_{max,s}$ and $h(T = 35\ ^{\circ}C)_G$ can be considered as a new constant, called U(T = 35 °C), which represents the possible maximum specific growth rate, obtained at the light-saturating radiance and temperature of 35 °C. By minimising the sum of root squared deviations between the experimental and simulated growth rate data, the value of U(T = 35 °C) as well as two constants of Aiba model – photo-saturation constant (k_s) and photoinhibition constant (k_i) are estimated to be 0.944 hr^{-1}, 347 μmol m^{-2} s^{-1} and 10,068 μmol m^{-2} s^{-1}, respectively. Nevertheless, it should also be

noted here that there is a limited confidence in the value of obtained k_i, as its value was found to be far beyond the investigating light intensity range of this study. As a result, the experimental verification will need to be carried out in order to confirm its value. By knowing parameters of $h(T)_G$ (details will be explained in section I.7), the value of $h(T = 35\ ^{\circ}C)_G$ can be eventually calculated ~ 1. Consequently, it becomes possible to determine an absolute value of $\mu_{max,s}$, which is 0.52 hr^{-1}. This rate should not be confused with μ_{max}, which represents the maximum specific growth rate under any respective irradiance. Even at 320 μmol m^{-2} s^{-1}, the value of the photoinhibition term (I^2 / k_i ~10 μmol m^{-2} s^{-1}) is still insignificant compared to the light saturation constant, suggesting an insignificant effect of photoinhibition over a whole range of studied irradiances. This finding is consistent with previous studies (Janssen, Slenders *et al.,* 2001, Rosello-Sastre 2009), which show that the effect of photoinhibition on green algae and cyanobacteria is generally seen under intensities of the order of 500 – 700 μmol $m^{-2}s^{-1}$. An obtained value of k_s also implies that 347 μmol m^{-2} s^{-1} is an average light intensity, which changes the light condition from limitation into saturation.

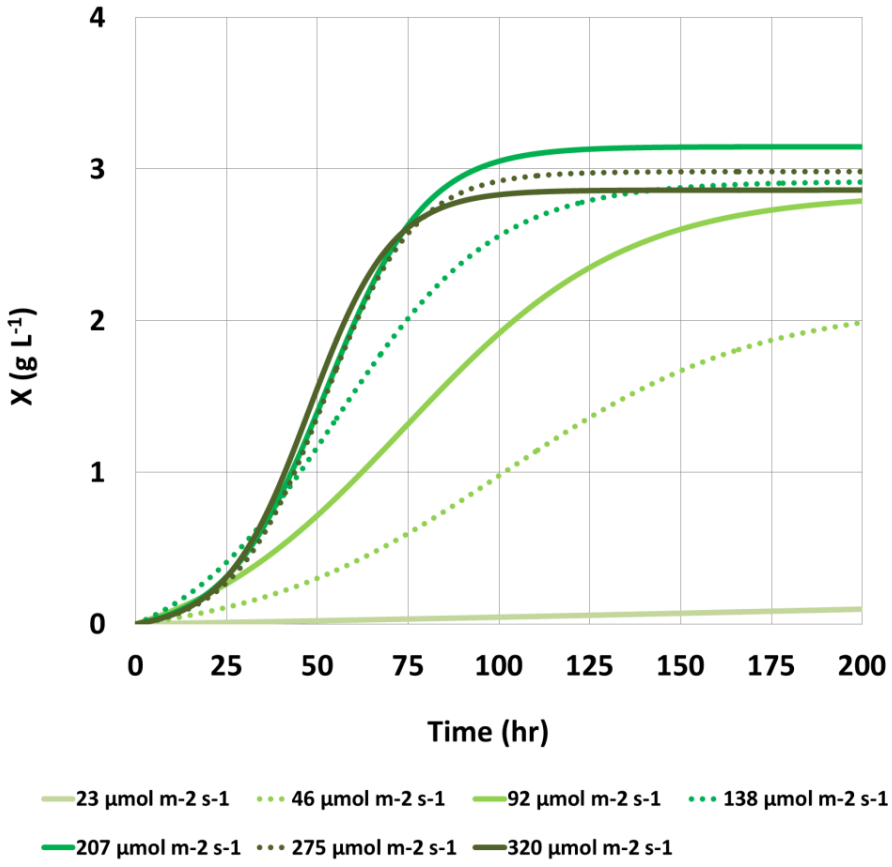

Figure I.7: *Cyanothece* 51142 photoautotrophic growth profiles under different light regimes.

Figures I.8.A and B: The non-linear relationship between μ_{max} and irradiance, described by an Aiba model. A) With light attenuation effect and B) without light attenuation effect.

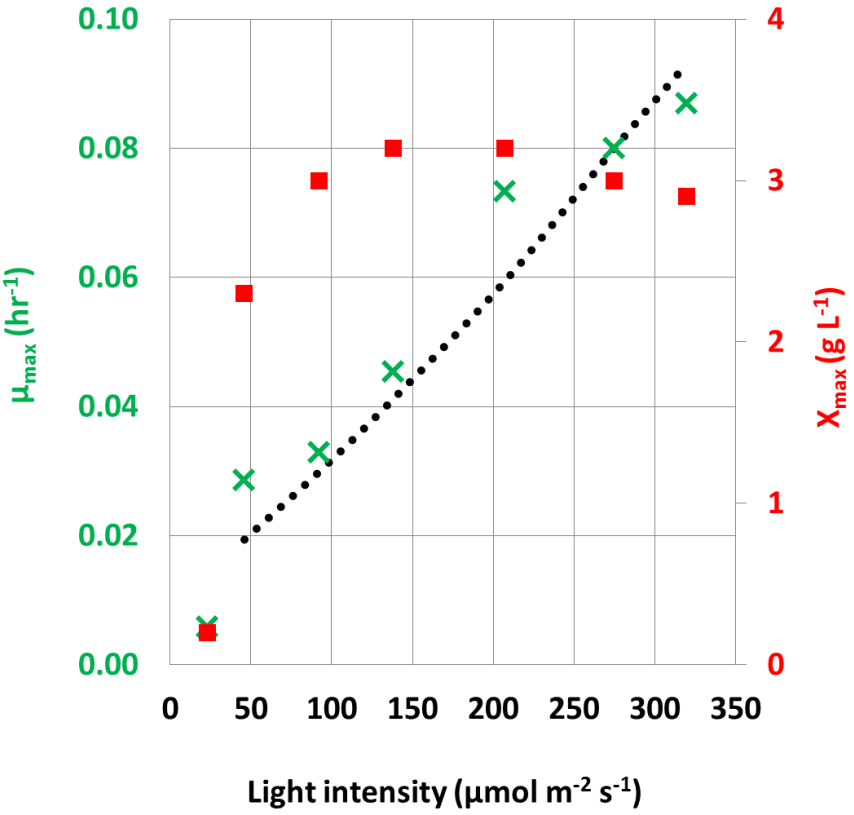

Figure I.8.A: The relationship between μ_{max} (green cross) and irradiance was not well-described by an Aiba model (black dotted line), when the light attenuation effect was taken into account. Due to mutual shading phenomena, after 92 μE m^{-2} s^{-1}, the final biomass concentration (red square) reaches a stable value of 3.1 g L^{-1}. Under 23 μE m^{-2} s^{-1}, there wass virtually no growth in *Cyanothece* 51142 culture.

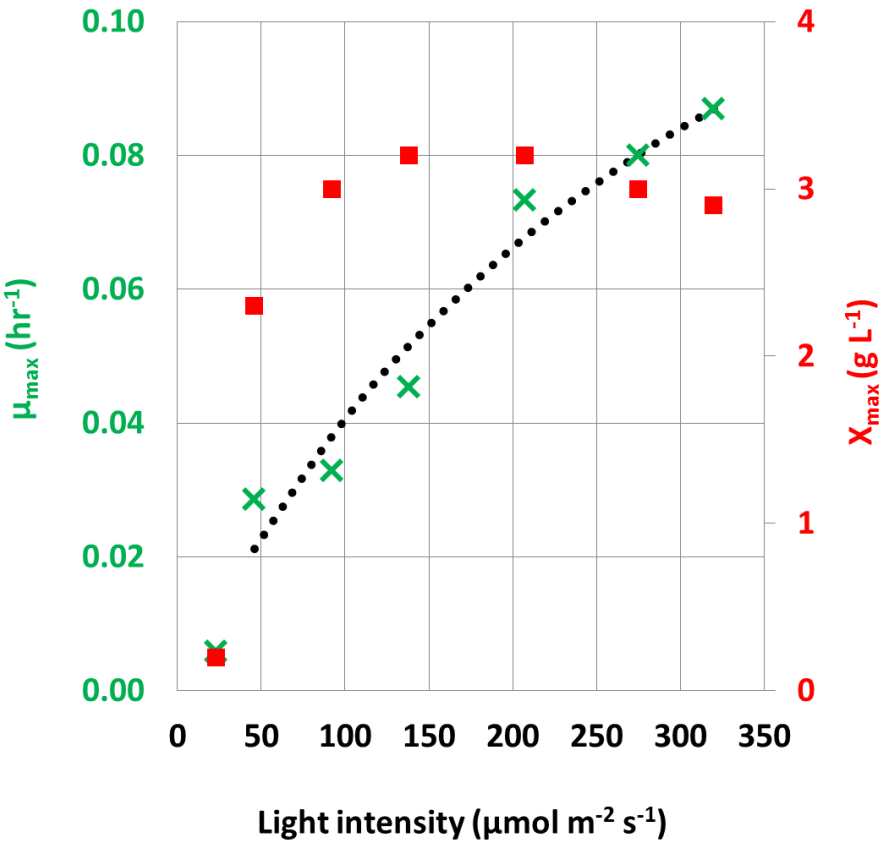

Figure I.8.B: The relationship between μ_{max} (green cross) and irradiance can be perfectly described by an Aiba model (black dotted line), when the light attenuation effect was excluded.

I.7. Effect of Temperature

Temperature is another key environmental parameter, which has a strong influence on the photosynthetic capability and nutrient uptake mechanism of microalgae (Reay, Nedwell *et al.,* 1999, Inoue, Taira *et al.,* 2001). Due to its direct influence on photosynthesis, there is a connection between temperature, light and photoinhibition. Under light saturating conditions, temperature becomes the controlling factor of the microalgal growth process and its increasing value generally enhances the growth rate up to a critical temperature, above which thermal-induced photoinhibitive effects start to occur and cause cell death (Konopka and Brock 1978, Lester, Adams *et al.,* 1988, Torzillo and Vonshak 1994).

In this section, the effect of cultivating temperature on the photoautotrophic growth of the *Cyanothece* 51142 strain will be discussed. In terms of experimental set-up, the cyanobacterial culture was cultivated under continuous illumination with a fixed intensity of 69 μmol m^{-2} s^{-1}. The medium was ASP2, with an addition of 1.5 g $NaNO_3L^{-1}$. The six investigated temperatures were 25, 30, 32, 35, 37 and 40°C. 20 ml min^{-1} of sterile 10 % volume CO_2 volume air^{-1} was sparged through the aqueous culture to provide photoautotrophic conditions.

Table I.2 shows all parameters of the growth kinetics that were determined using the logistic models, whereas Figures I.9.A - F confirms the good quality of fitting between experimental and simulated data. As previous experimental work on the continuously-illuminated batch growth of *Cyanothece* 51142 normally used a fixed temperature of 30 °C, whilst varying light intensity and quality, there was the difficulty in comparing obtained results against any benchmark. Nevertheless, the maximum specific growth rate at 30 °C is 0.032 $hour^{-1}$, whereas the rates from Feng and Sinetova's publications (Feng, Bandyopadhyay *et al.,* 2010, Sinetova, Červený *et al.,* 2012) are

0.025 hour^{-1} and 0.052 hour^{-1}, respectively. This can be explained that my rate is slightly higher than Feng's due to the use of marginally higher irradiance (69 µmol m^{-2} s^{-1} versus 46 µmol m^{-2} s^{-1}). Nevertheless, it is lower than Sinetova's, which is probably due to their use of red (λ_{max} ~ 627 nm) light emitting diodes, whose wavelength overlaps with absorption wavelengths of chlorophyll a (650 – 700 nm) and phycocyanin (620 nm), the two light harvesting pigments within cyanobacteria.

Figures I.9.A - F: Fitting of growth and nitrate uptake kinetics of *Cyanothece* 51142, cultivated under 25, 30, 32, 35, 37 and 40 ˚C, 69 µmol m^{-2} s^{-1}, 20 ml min^{-1} of sterile 10 % volume CO_2 volume air^{-1} and 1.5 g $NaNO_3$ L^{-1} in ASP2 medium.

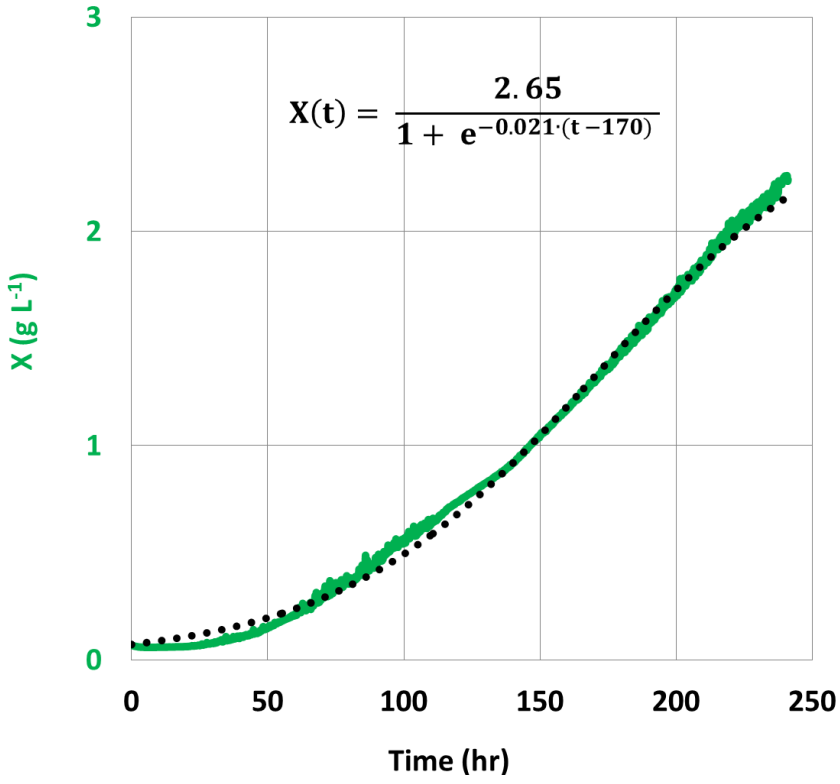

Figures I.9.A: Fitting of growth data for 25 ˚C

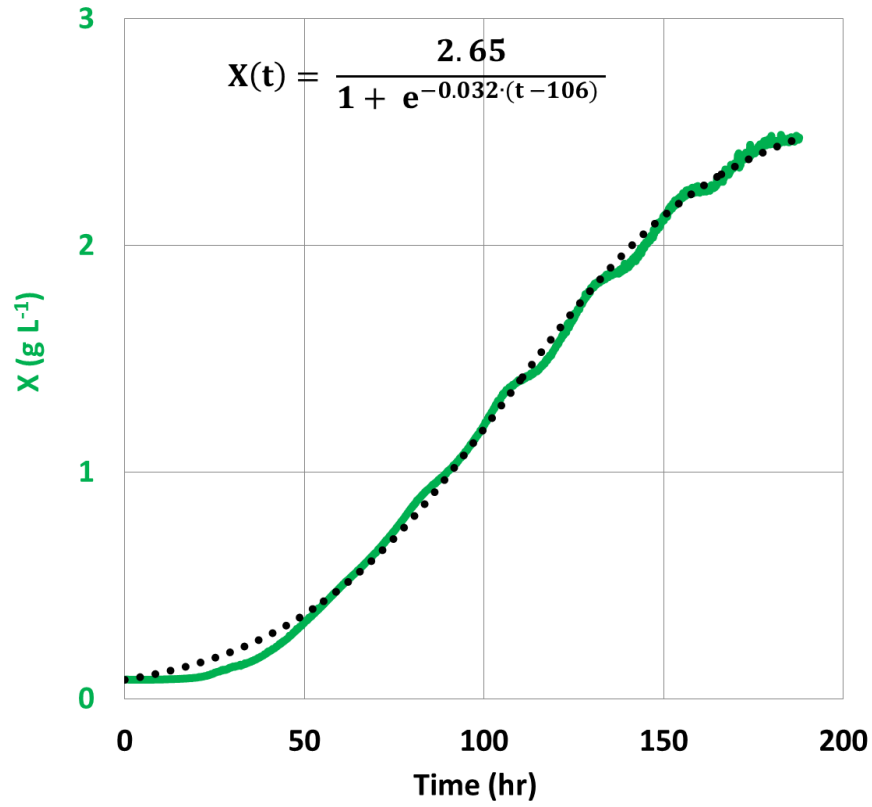

Figures I.9.B: Fitting of growth data for 30 ˚C

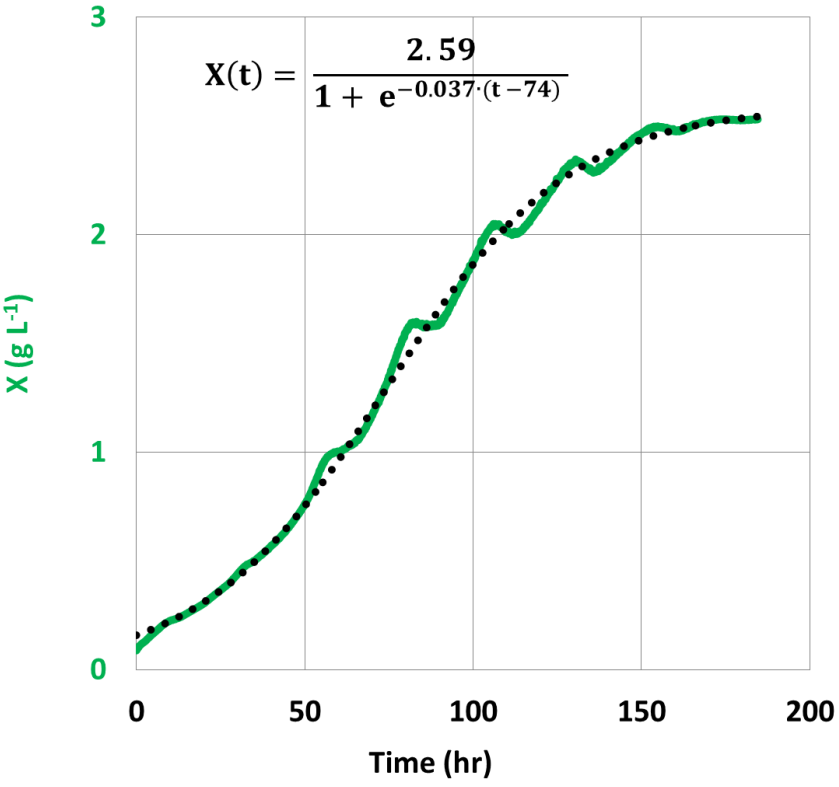

Figures I.9.C: Fitting of growth data for 32 ˚C

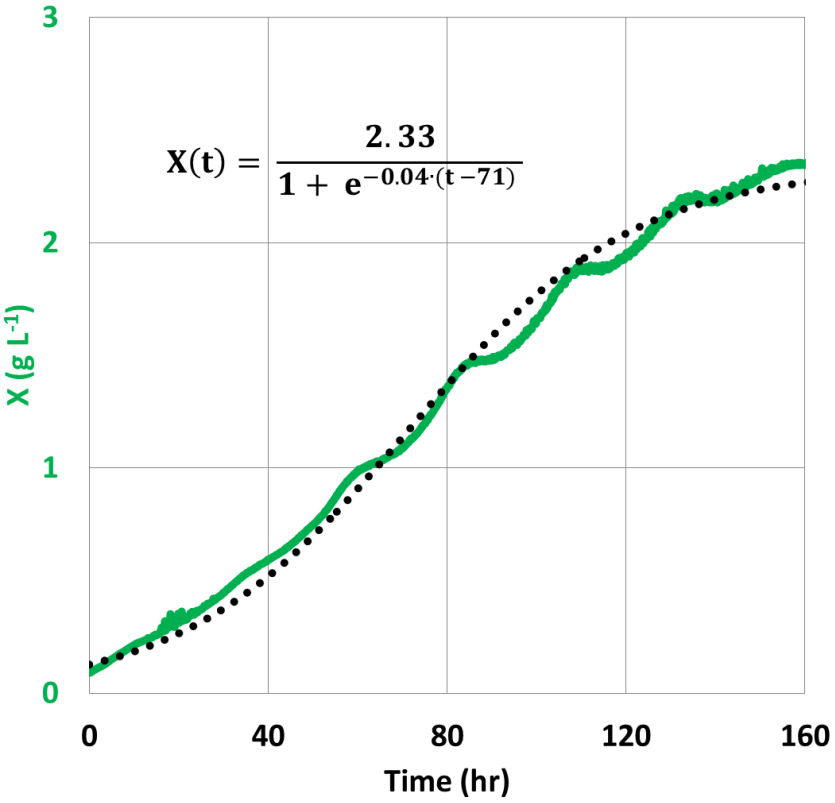

Figures I.9.D: Fitting of growth data for 35 ˚C

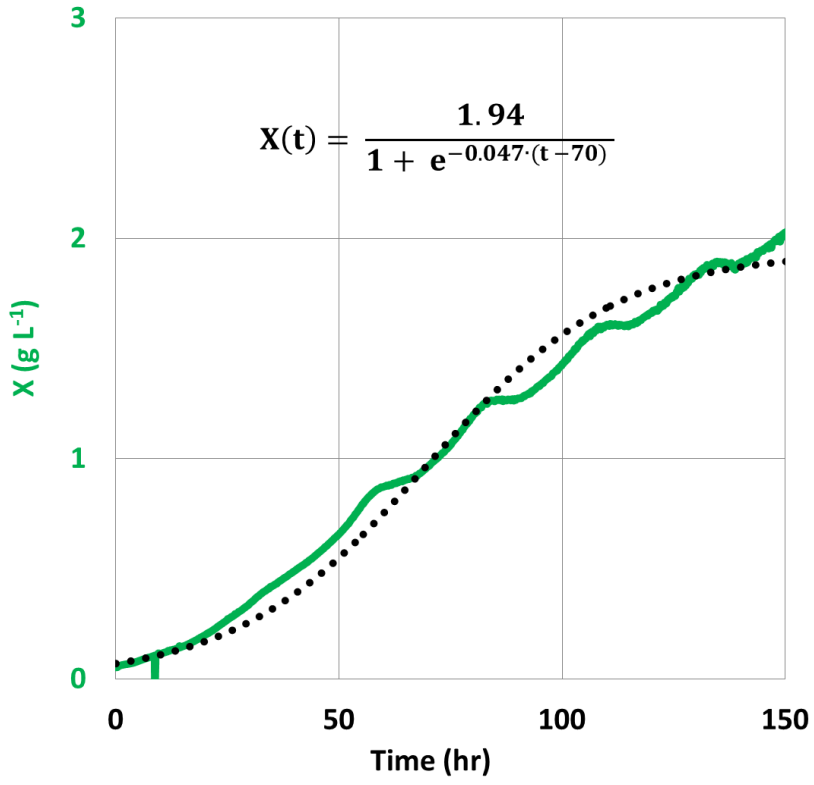

Figures I.9.E: Fitting of growth data for 37 ˚C

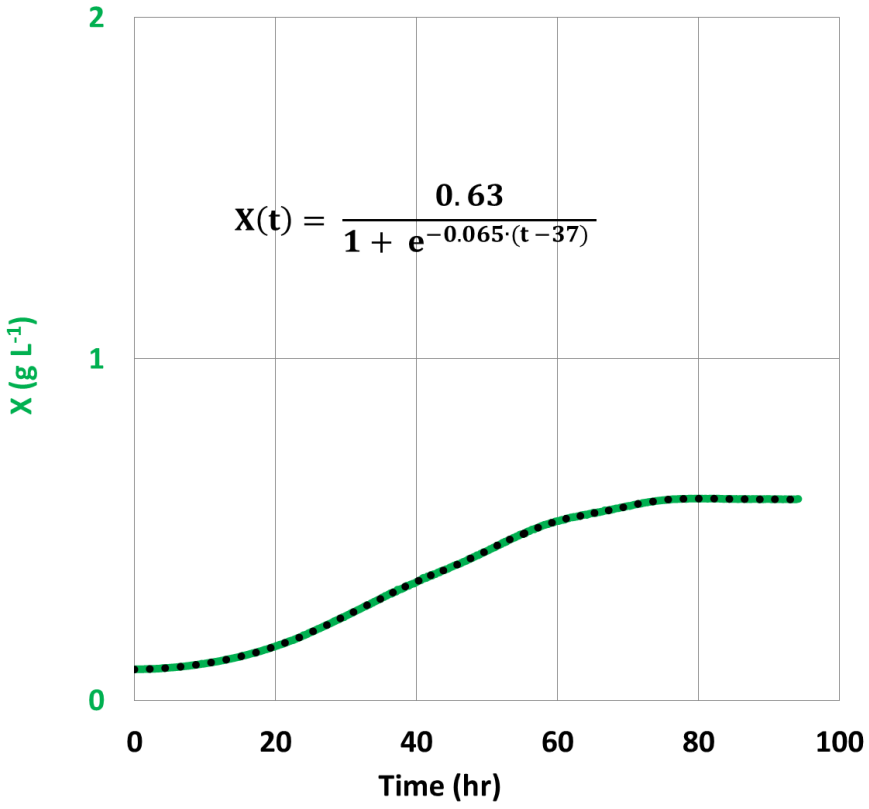

Figures I.9.F: Fitting of growth data for 40 ˚C

Table I.2: Growth and uptake kinetics data under different studied temperatures

Temperature (˚C)	μ_{max} (hr^{-1})	Maximum DBC ($g\ L^{-1}$)	Productivity ($g\ L^{-1}hr^{-1}$)
25	0.021	2.65	0.028
30	0.032	2.65	0.048
32	0.037	2.59	0.048
35	0.040	2.33	0.047
37	0.047	1.94	0.046
40	0.065	0.63	0.021

By plotting all growth profiles in the same figure (Figure I.10), the temperature influence on *Cyanothece* 51142 growth can be clearly illustrated. Among all of studied temperatures, although the culture, cultivated under 40 °C, possesses the fastest maximum specific growth rate – 0.065 hr^{-1}, its final biomass concentration of 0.63 g L^{-1}, on the other hand, happens to be lowest. The slowest growth is observed for the cells grown under 25 °C, as their reproduction was still in progress even when the time reached 200 hours. Even the final concentration has not been attained under this particular condition; it was estimated as 2.65 g L^{-1} using extrapolation of a logistic model. Under 30 and 32 °C, cyanobacterial cultures are able to eventually attain an approximately similar final concentration of 2.60 – 2.65 g L^{-1}, whereas at 35 °C, the concentration drops to 2.33 g L^{-1} and continues falling further to 0.63 g L^{-1} at 40 °C. From Figure I.11, the relationship between the maximum specific growth rate and the temperature is seen to be virtually linear with every 10 °C rise in temperature resulting in an approximately doubled specific growth rate (calculated from data in Table I.3). This finding is in fact a typical Arrhenius type correlation observed for many chemical and biochemical reactions (Alagappan and Cowan 2004): as the temperature increases, the rates of biochemical reaction or enzymatic activity increase. The slow growth rate of the cyanobacterium, observed at 25 °C, can be explained by two potential reasons: i) suppressed repair cycle of protein D_1, which can lead to a lower PSII activity and subsequently a photoinhibition scenario (Gombos 1994, Kanervo, Tasaka *et al.,* 1997) or ii) slow rate of cellular nutrient uptake (Reay, Nedwell *et al.,* 1999). However, as a steady pO_2 profile, with eventual saturation at 34 $\%O_2$ saturation, is observed (Figure I.12) – this suggests an insignificant reduction in photosynthetic activity and thereby disregarding photoinhibition effect as the major cause. Therefore, the conclusion is that, under low temperature, as consumption ability of the cells becomes reduced, the growth rate is subsequently lower.

In the case of the biomass concentration, a constant profile of final biomass concentration of 2.6 g L^{-1} is observed under temperatures between 25 and 32 °C, beyond which it is replaced by a

continuously declining trend. In contrast to low temperature cultivation, low biomass concentration, produced by the culture cultivated at 40 °C, is due to high temperature-induced damage of the photosynthetic apparatus of the cyanobacterium, as high temperature is found to cause a detachment of the Mn-stabilising extrinsic 33 kDa protein from the PS II core complex (Yamane, Kashino *et al.,* 1998). Evidently, the O_2 level of the culture cultivated at 40 °C was seen to sharply decrease by more than 50% of its initial value within 80 hours after the inocculation (Figure I.12), dissimilar to that obtained at 37 °C, which eventually levelled off at 27 %O_2 saturation with again an expected circadian-periodic character (Schneegurt 1994). A similar reduction in photosynthetic activity induced by thermal stress has also been previously reported in a mesophilic cyanobacterium, *Synechocystis* sp. PCC6803 (Inoue, Taira *et al.,* 2001). With greater degree of damage to the photosynthetic apparatus, the cyanobacterium is incapable of utilising the same amount of solar energy, thus becoming more susceptible to undergoing photoinhibition at a much lower light intensity. This can be clearly demonstrated by the result from the light study (section I.6.), which shows that there is no photoinhibition up to 320 μmol m^{-2} s^{-1} at the cultivation temperature of 35 °C, whereas photoinhibition is prominent at 40 °C for illumination as low as 69 μmol m^{-2} s^{-1}. Figure I.12 also displays a high degree of coherence between pO_2 and pH experimental results, as the decreasing photosynthetic activity commonly leads to an increasing level of unfixed dissolved CO_2, which in turn causes the culture to become more acidic. The high acidity – an eventual pH of 5 - can be clearly seen for the culture cultivated at 40 °C.

From the temperature study, it can be suggested that even though the growth rate can be enhanced by an increase in culture temperature, the biomass yield is in fact limited to a low value by certain temperatures. As a result, the biomass productivity (P), which is defined as the product of the maximum specific growth rate and the dry biomass concentration being accumulated at $t = t_0$ (i.e. inflexion point of the logistic model) (Table I.3), is a better indicator to locate the optimum temperature for photoautotrophic growth of the *Cyanothece* 51142 strain. From Table I.2 and

Figure I.13, the highest productivity of 0.047 g L^{-1} $hour^{-1}$ is observed at a temperature of 35 °C, whereas the lowest productivities of 0.021 g L^{-1} hr^{-1} is obtained at 40 °C. In order to determine parameters of the Arrhenius's temperature model, the sum of root squared deviations between experimental and simulated productivity data, using Equation 5.36, is minimised. As constants of the Aiba model are already known from section I.6, the values of $h(I)_G$, under incident irradiance of 69 µmol m^{-2} s^{-1} and different biomass concentrations, can be subsequently calculated (data not shown). As a result, the rest of the unknown parameters can be determined as follows, for reproduction: E_a = 40.0 kJ mol^{-1} and A = 6.07×10^6 and for denaturation: E_b = 381.8 kJ mol^{-1} and B = 1.30×10^{59}. These obtained values are observed to be consistent with previously reported values taken from literature and the comparison can be seen from Table I.3. The models (black dotted line on Figure I.13) are also found to provide a good representation of the temperature versus biomass productivity relationship.

Table I.3: Comparison of Aiba and Arrhenius' parameters, obtained during growth phase, between my and literature values.

Definition	Symbol	My value	Literature value	References
Activation enery for synthetic process	E_a (kJ mol^{-1})	40.0	[37.5, 122.5]	(Topiwala and Sinclair 1971, Hardy, Burns *et al.,* 1973, Béchet, Shilton *et al.,* 2013, Brauer, Stomp *et al.,* 2013)
Activation enery for denaturation process	E_b (kJ mol^{-1})	381.8	[127.5, 654]	
Pre-exponential factor for synthetic process	A (no unit)	$6.07x10^6$	[$3.2x10^5$, $1.70x10^{21}$]	
Pre-exponential factor for denaturation process	B (no unit)	$1.30x10^{59}$	[$5.57x10^{19}$, $1.92x10^{101}$]	
Photo-saturation coefficient	k_s (µmol m^{-2} s^{-1})	347	[70, 250]	(Gons, Hoogveld *et al.,* 2006, Béchet, Shilton *et al.,* 2013, Cabello, Morales *et al.,* 2014)
Photoinhibition coefficient	k_i (µmol m^{-2} s^{-1})	10,068	[2770, 53600]	

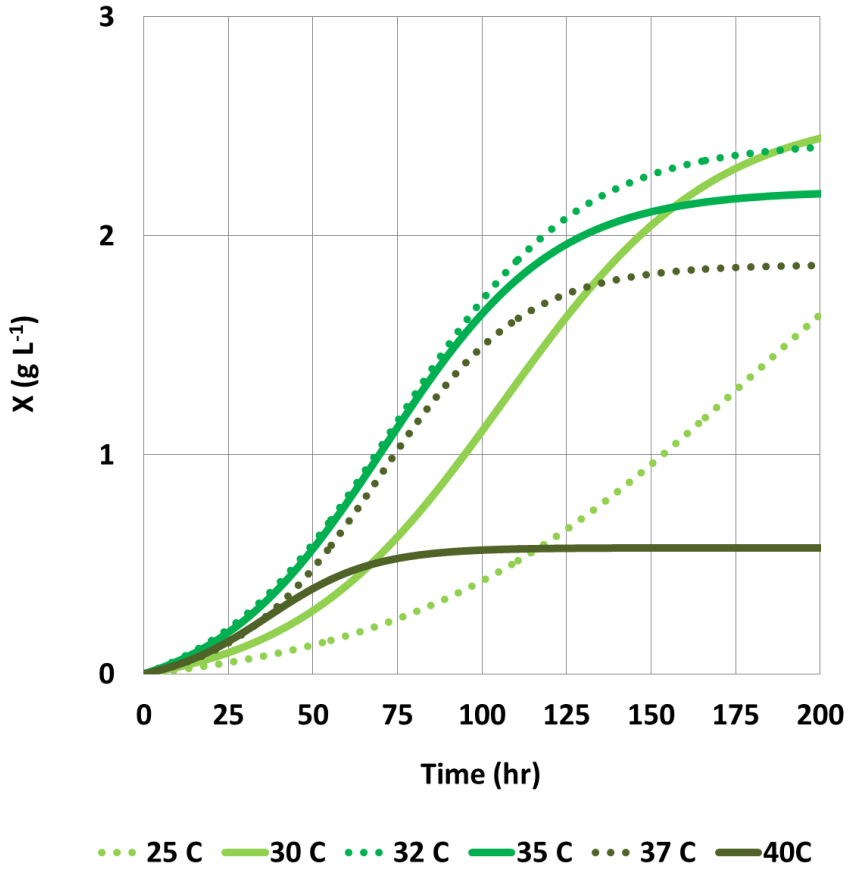

Figure I.10: *Cyanothece* 51142 photoautotrophic growth profiles under different temperature regimes.

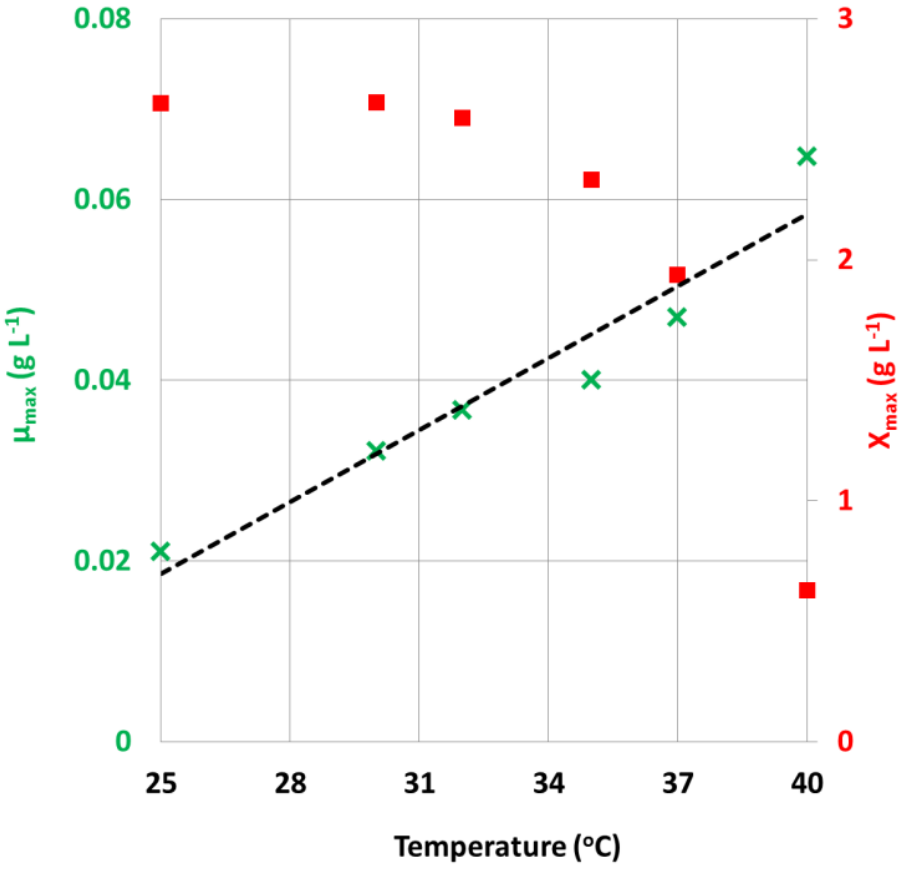

Figure I.11: For every 10 ˚C increase in temperature, μ_{max} (green cross) of *Cyanothece* 51142 cultures is enhanced by approximately 2-folds. However, high-temperature induced photoinhibition causes the final biomass concentration (red square) to significantly drop after 32 ˚C.

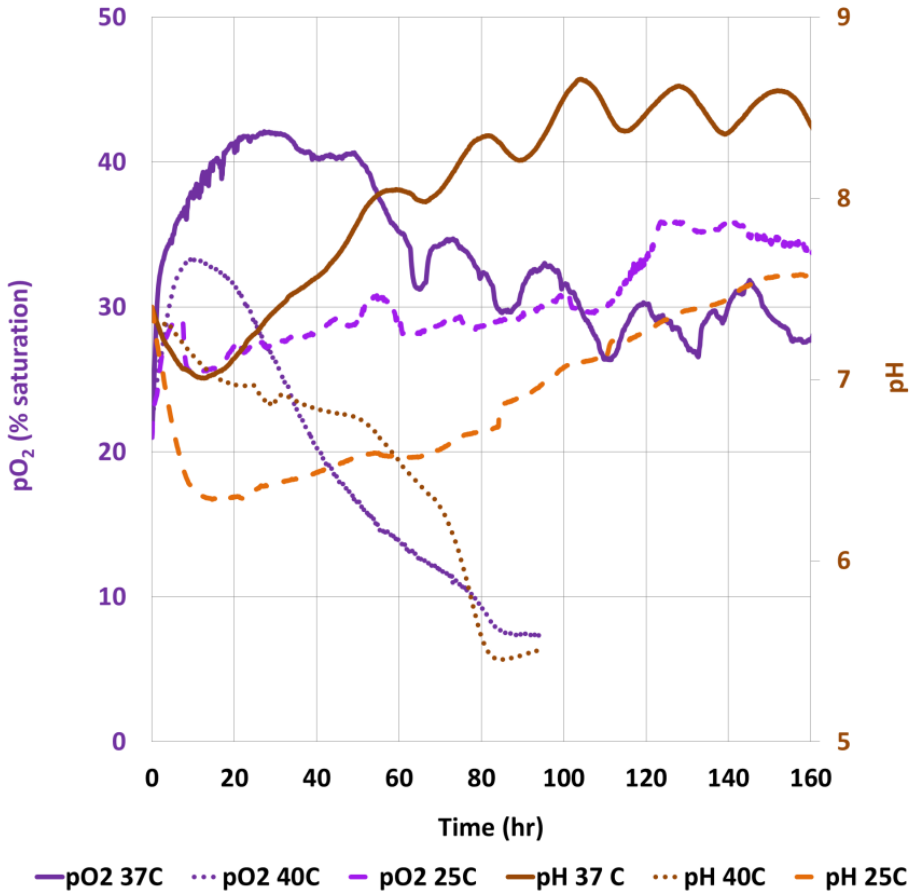

Figure I.12: Photosynthetic activity of *Cyanothece* 51142 culture is significantly reduced when the cultivating temperature is maintained at 40 ˚C. Under this particular temperature, pH also continues to decrease; this is because of a greater quantity of unfixed CO_2 present in the system.

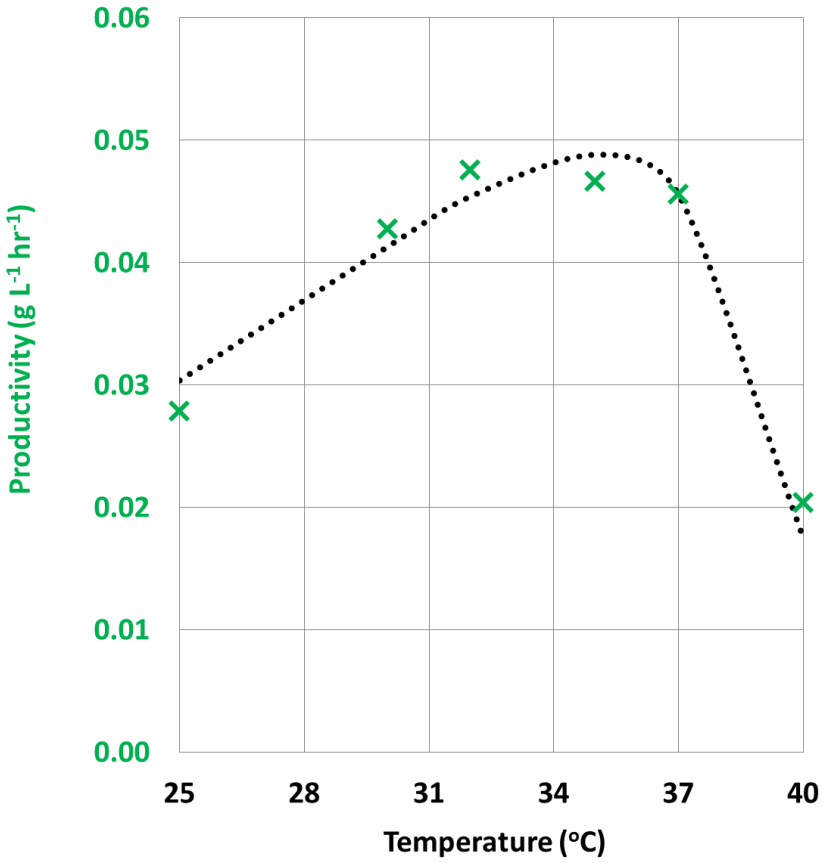

Figure I.13: The relationship between biomass productivity (green cross) and temperature can be well-described by an extended Arrhenius model (black dotted line). Under low-temperature, the productivity is limited by low nutrient consumption capability. Whist, at high temperature, photoinhibition occurs and causes the growth cessation.

I.8. Summary

In this chapter, the effect of different cultivating factors – nitrogen and carbon sources and light intensity and temperature - upon the growth of the *Cyanothece* 51142 culture was investigated. By achieving growing dense and healthy culture, the system can be anaerobically exploited for facilitating the subsequent H_2 production. A logistic growth model is found to accurately describe the growth of cells from an initial lag phase up to the stationary phase, regardless of the growth conditions, and subsequently utilised to determine the parameters of the growth kinetics. Mathematical models, coupling together three equations: Arrhenius temperature, Aiba light intensity and Beer-Lambert light attenuation, were developed to evaluate environmental influences that are important for optimising the cyanobacterial growth. Under photoautotrophic growth conditions, the maximum specific growth rate can be two-fold enhanced, when an ambient air is replaced by nitrate salts. In the case of carbon source, photoheterotrophic growth conditions, where glycerol is provided, facilitate approximately 2.4 times faster maximum specific growth rate than photoautotrophic conditions alone. In the presence of either nitrate or glycerol, circadian-regulated metabolic shift behaviour of the *Cyanothece* 51142 strain disappears, as these substrates inhibit the activity of nitrogenase-mediated nitrogen and photosynthetic carbon fixations, respectively. However, as soon as substrates become depleted, cells are able to regain their fixing capabilities and sustain them even under continuous illumination condition. The final biomass concentration, in all cases, is limited within a range of 2.8 – 3 g L^{-1}, due to eventual photo-limitation inside the PBR. This poor light penetration is caused by mutual shading phenomena between cells, which commonly occur under very dense cultures. In contrast to biomass concentration, the maximum specific growth rate is found to continue increasing with rising incident light intensity. Within the investigated range – up to 320 μmol m^{-2} s^{-1}, the cyanobacterium is able to grow without experiencing photoinhibition. An average light intensity, at which light-limiting is transformed into light-saturating regimes, is located at 347 μmol m^{-2} s^{-1}. In the case of temperature, an optimal

condition, facilitating the highest biomass productivity of approximately 0.05 g L^{-1} $hour^{-1}$, is found at 35 ˚C. Therefore, a fixed temperature of 35 ˚C was used whenever possible in subsequent experiments. Under sub-optimal temperatures, the *Cyanothece* 51142 growth is limited by lower nutrient consumption rates, whereas, under over-optimal temperatures, thermal-induced photoinhibition begins to take effect, evidently at temperature of 40 ˚C, and result in low biomass productivity.

II. Hydrogen Production of *Cyanothece* 51142

II.1. Introduction

H_2 production by *Cyanothece* 51142 is predominantly catalysed by nitrogenase enzymes (Min and Sherman 2010), whose function becomes activated under nitrogen-fixing and anaerobic conditions (Fay 1992). Commonly, the sparging of inert gases – Ar and N_2 – is used to induce necessary anaerobiosis within cyanobacterial cultures (Borodin, Tsygankov *et al.,* 2000, Bandyopadhyay, Stoeckel *et al.,* 2010). However, when it comes to the scale up of biohydrogen processes, such external interference is likely not to be a feasible option, as it would lead to a more complex processing operation together with higher associated costs. In addition, the activity of nitrogenase is also directly influenced by cultivating conditions of light intensity and temperature (Dutta, De *et al.,* 2005), as illumination provides a primary energy source, facilitating an energy-intensive N_2-fixation process, whereas the latter typically controls the rate of any biochemical reactions inside the cells. Up to now, the relationships between these two environmental parameters and H_2 production rate of *Cyanothece* 51142 is still missing and thus becomes the aim of investigations in this chapter.

This chapter will start by demonstrating glycerol as a more effective and economically feasible anaerobic-inducer for air-incubated batch *Cyanothece* 51142 cultures (Dechatiwongse, Maitland *et al.,* 2015). The reason behind this success was that this particular substrate can enhance cyanobacterial respiratory as well as inhibit photosynthetic O_2 evolution (Aryal, Callister *et al.,* 2013), thereby promoting the eventual removal of O_2 inside the system. H_2 production rates and yields were measured by MIMS in the ICL flat-plate PBR. The purity of H_2 production was verified by injection mass spectrometry.

Concurrent production of fermentative products was identified and subsequently quantified using NMR. In order to investigate environmental influences upon the gas producing ability of *Cyanothece* 51142 strain, its H_2 production properties, following glycerol-induced anaerobic conditions, under different light intensity and temperature regimes were analysed and compared. Specifically, the developed H_2 production model (Equation 5.37), taking into account the quantity of available biomass in the PBR system as well as simultaneous effects of temperature (Equation 5.34), light intensity (Equation 5.31) and light attenuation (Equations 5.32 and 5.33), was used to fit with experimental H_2 production data so that important parameters of the model can be computationally determined. All derived kinetic parameters will be utilised for the development and design of a novel continuous flow PBR system, which can be found in Results and Discussions Chapter III, which permits a significant improvement in both H_2 and biomass productivity. It should be noted here that the batch H_2 production experiment under 35 ^{o}C and 92 μmol m^{-2} s^{-1} (section II.3) was repeated and its results were found to be reproducible, whereas the rest of experiments in this chapter were carried out only once.

II.2. Choice of Photobioreactor

All of H_2 production experiments were carried out in the dual compartment ICL flat-plate PBR, whose full description can be found in Experimental Methods (section 5), due to its explicit design for gas measurements. The temperature of the culture is measured by a K-type thermocouple supplied by Omega and controlled by means of hot water recirculation in the secondary compartment. Two probes from Consort BVBA – the SP01T pH electrode and the SZ10T galvanic pO_2 electrode are used for *in situ* measurement of pH and dissolved O_2 concentration, respectively. The cyanobacterial growth is monitored using a photodiode

operating with an absorption bandwidth of 650 – 700 nm. In addition, a membrane-inlet mass spectrometry (MIMS) system was also incorporated into the reactor for *in situ* measurement of dissolved H_2 gas in the aqueous phase. For data quantification, Equation 5.7 was employed to convert obtained electrical signals into the corresponding dry biomass concentration, whereas, in the case of H_2 production, Equation 5.28 was used.

II.3. Batch Hydrogen Production of *Cyanothece* 51142

In order to induce anaerobiosis inside the air-incubated *Cyanothece* 51142 culture, without the use of inert gas sparging, organic glycerol was used as sole carbon source for the batch cultivation of this microbe. Figure II.1.A shows experimental profiles of the growth and the H_2 production phases obtained from batch cultivation of *Cyanothece* 51142 under constant condition of 35 ^{o}C and 92 μmol m^{-2} s^{-1} in the ASP2 growth medium. Glycerol was added into the medium to the final concentration of 50 mM, as high rates of H_2 production were previously reported under this particular concentration (Bandyopadhyay, Stoeckel *et al.,* 2010). Sterile pure air was sparged throughout the liquid culture for 5 minutes before the PBR was completely sealed in order to provide saturated O_2 and N_2 for respiration and N_2-fixation respectively.

From Figure II.1.A, under photoheterotrophic growth conditions, the culture progressed through all five common growth phases (similar to other microorganisms) (Tomaselli 2004) – from the initial lag phase up to an eventual death phase. As generally expected, during the lag phase of approximately 10 hours, a minimal change in dry biomass concentration of the culture is observed, as cells are adapting to the new environment. Simultaneously, approximately constant levels of glycerol and NO_3^{-1} concentrations are seen (Figures II.2.A

and B), due to minimal nutrient requirement by the cells.

Figures II.1.A and B: Growth and H_2 production profiles of batch *Cyanothece* 51142 culture, cultivated at 92 μmol m^{-2} s^{-1}, 35 ˚C, 50 mM glycerol in air-saturated ASP2 growth medium. A) Experimental data and B) Fitting with the logistic growth model

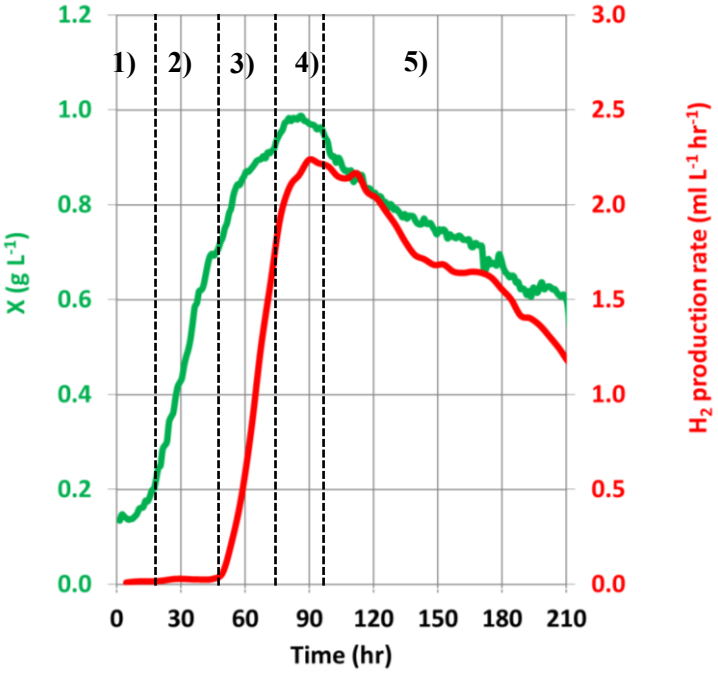

Figure II.1.A: A whole H_2 production consists of two interconnected sub-stages – 1) the growth stage, for first 70 hr, and 2) the H_2 production stage, beginning from time = 55 hr. Abbreviations: 1) initial lag, 2) exponential 3) linear 4) stationary and 5) death phases.

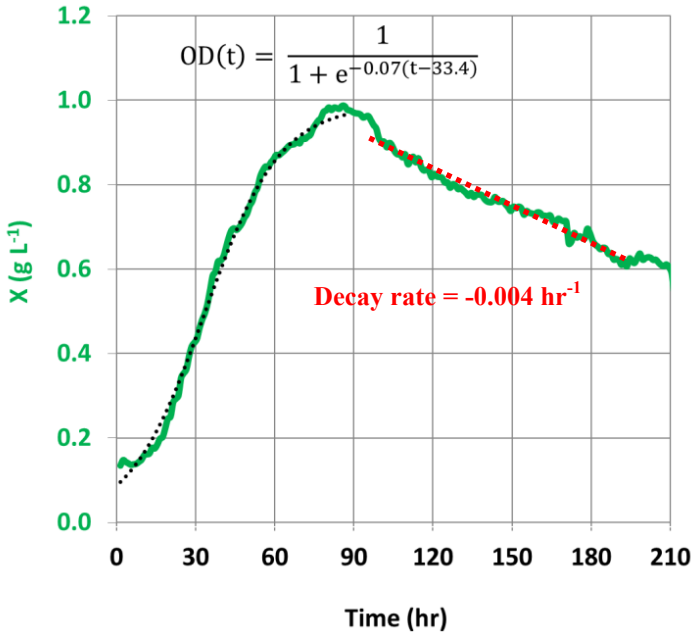

Figure II.1.B:Using logistic model (black dotted line), μ_{max} of *Cyanothece* 51142 culture, cultivated under 92 µmol m^{-2} s^{-1}, 35 ˚C, was determined as 0.07 hr^{-1}. The decay rate (red dotted line), during terminal death phase, was calculated as linear gradient of the natural log of the growth profile over time and subsequently found to be -0.004 hr^{-1}.

With sufficient provision of light, nutrients and O_2, *Cyanothece* 51142 then enters the secondary exponential phase, at time = 10 – 60 hr, during which its maximum specific growth rate (μ_{max}) is estimated as 0.07 hr^{-1} using a logistic growth model (Equation 5.29), as shown in Figure II.1.B. By comparing the obtained rate with other previously reported values, under similar growth conditions, my rate is approximately 1.65-fold higher than that reported by Feng and co-workers – 1.02 day^{-1} (Feng, Bandyopadhyay *et al.,* 2010). This significant increment is most likely due to an almost 2 times difference in incident light intensity between mine (92 µmol m^{-2} s^{-1}) and Feng's system (50 µmol m^{-2} s^{-1}). As the culture matures, there is a greater demand of key macro-nutrients, which can be seen from the simultaneous decreases in glycerol and nitrate (Figures II.2.A and B), which serve as carbon and nitrogen sources, respectively. As time proceeds, nitrate eventually becomes depleted at time = 50, whereas glycerol remains in excess at the final concentration of 25 mM. Again, by fitting experimental data to the logistic nutrient uptake model (Equation 5.30), the maximum specific uptake rate of nitrate is determined to be 0.2 hr^{-1}. By multiplying this rate with its initial substrate concentration (130 ppm), the total nitrate consumption rate, under this particular condition, is calculated as 26 ppm hr^{-1}. It should be noted here that the ASP2 medium, used to inocculate the *Cyanothece* 51142 culture, was in fact free of NO_3^{-1}, consequently, the initial NO_3^{-1} detection of ~ 130 ppm was most likely due to carried-over ions from the stock medium. In the case of glycerol, carbon-sufficiency is confirmed, its total uptake rate being simply determined by calculating the linear gradient of its concentration profile over time and subsequently found to be 0.38 mM hr^{-1}. Even being deprived of NO_3^{-1} source since t = 50 hr, *Cyanothece* 51142 was able to continue its growth until t = 75 hr (Figure II.1.A), when the stationary growth phase was finally attained, as the culture could still utilise either dissolved N_2 from initially sparged air or intracellular nitrogen reserve such as proteins as its replacement of nitrogen source . In addition to carbon and nitrogen, sulphur

and phosphorus are two other essential macro-nutrients. An excess of sulphate was supplied as shown by the concentration profile (Figure II.2.C), which remains at a relatively constant level of 2,000 mg SO_4^{-2} L^{-1}. For phosphate, as mentioned in section 5.8.2 of Experimental Methods, the quantity of the compound is too low to be detected by the IC technique. A previous study, conducted by Sinetova and colleagues (Sinetova, Červený *et al.,* 2012), reports on the insignificant effect of phosphorus starvation upon *Cyanothece* 5142 growth. Despite the sufficiency of macro-nutrients in the broth, the cyanobacterial culture still entered the terminal death phase, which starts to take place at time = 95 hr.

Figures II.2.A - C: Growth and macro-nutrient uptake profiles of batch *Cyanothece* 51142 culture, cultivated at 92 μmol m^{-2} s^{-1}, 35 ˚C, 50 mM glycerol in air-saturated ASP2 growth medium. A) Glycerol uptake, B) Nitrate and C) Sulphate

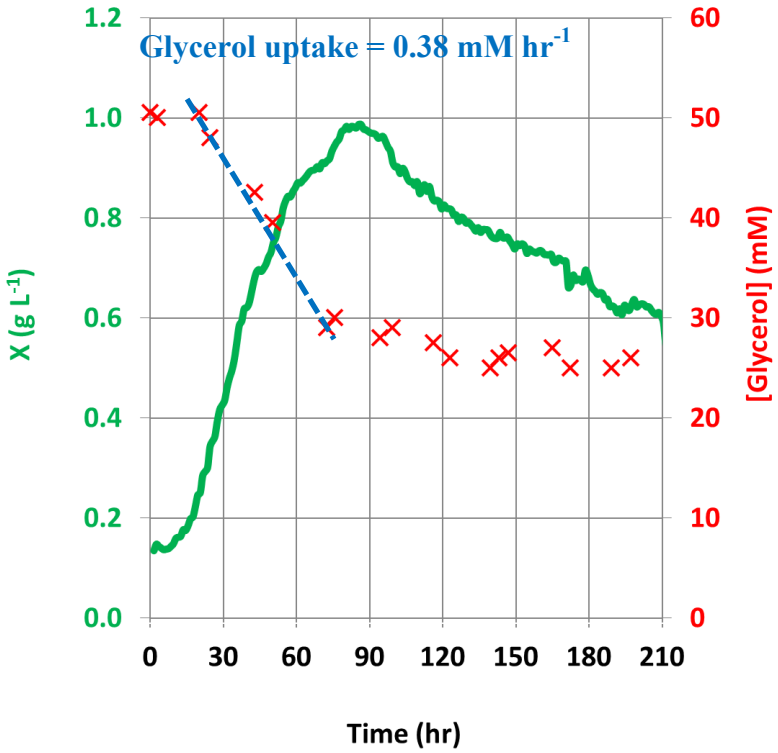

Figure II.2.A: As *Cyanothece* 51142 culture matures, there is a greater demand glycerol. This substrate serves as carbon source for biomass production as well as chemical energy and reducing power for H_2 production. The total uptake rate of glycerol was estimated as 0.38 mM hr^{-1} using a linear regression.

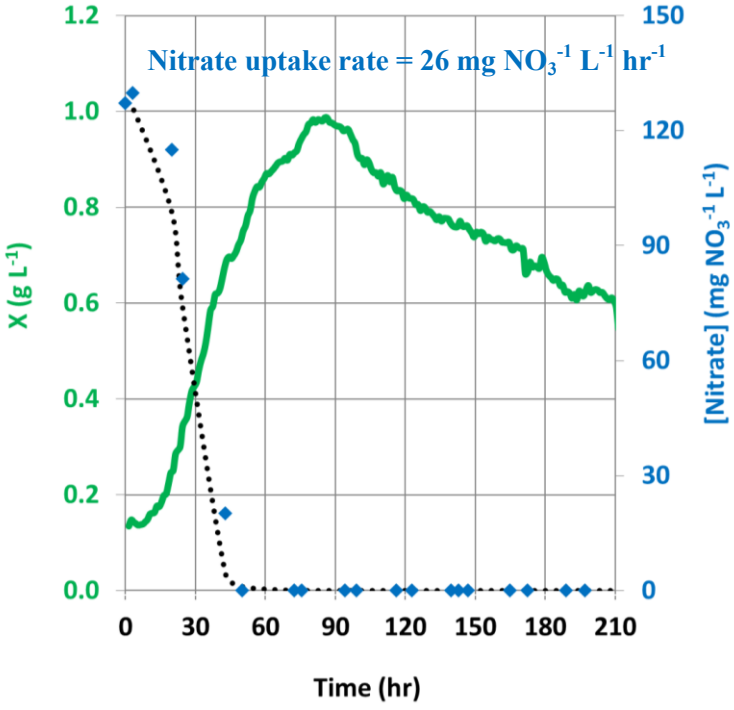

Figure II.2.B: Similar to glycerol, NO_3^{-1} is also required by the culture as its source of nitrogen. An intrinsic uptake rate was determined by fitting experimental data with a logistic model.

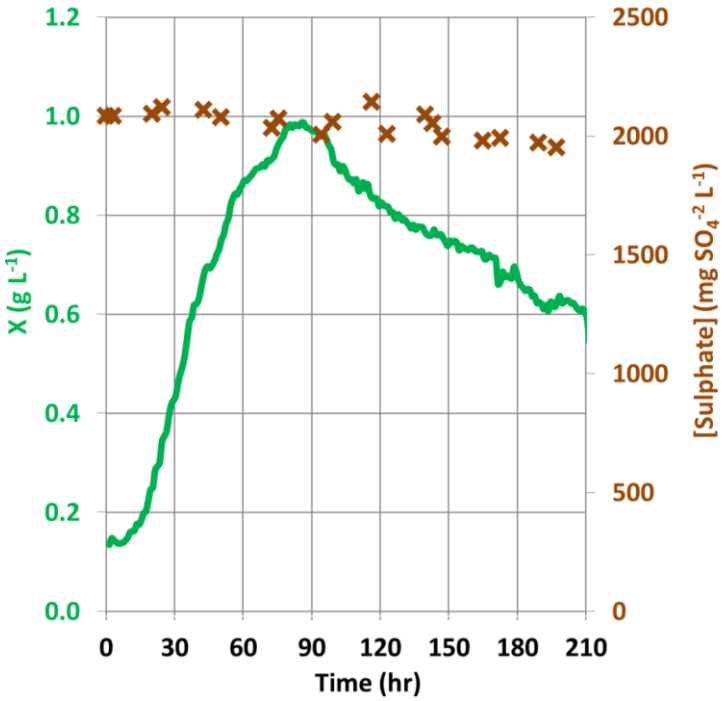

Figure II.2.C: An excessive quantity of sulphate is confirmed by its high level of approximately 2,000 mg SO_4^{-2} L^{-1}

Apart from light and macro-nutrients, dissolved O_2 (pO_2) is another important parameter, as it is required during cellular respiration, an essential metabolism performed by microorganisms to convert starch back into chemical energy. The energy is then utilised to fuel biochemical reactions, supporting the growth as well as the H_2 production process. Due to enhanced respiration, induced by glycerol, the pO_2 value begins to decrease, at time = 40 hr, before eventually reaching zero at time = 60 hr (see Figure II.3). Similar to glycerol, the O_2 consumption rate is also estimated from the linear gradient of its concentration profile as 1.47 $\%O_2\ hr^{-1}$ (~ 0.082 mg O_2 L^{-1} hr^{-1}, this conversion was made using Equation 5.13). Although the declining pO_2 profile is expected, there is an initial rise in its concentration, observed at an early stage of the exponential phase (time = 20 – 40 hours). As glycerol was the only available carbon source in the experiment, it is reasonable to conclude that this O_2 production is not derived from photosynthetic CO_2 fixation process. In fact, it has been reported that,

upon nitrate consumption, cyanobacteria are able to alternatively produce O_2 via photolysis of water (Flores, Frias *et al.,* 2005). Evidently, an occurrence of this scenario is confirmed by a decrease of NO_3^{-1} concentration (Figure II.2.B), which appears to take place in parallel to the increase of pO_2.

As soon as the level of pO_2 becomes zero at time = 60 hours, the onset of H_2 production was detected *in situ* by MIMS system (Figure II.3). This observation was also confirmed by the gas composition results obtained from the injection mass spectrometry (Figure II.4), which show a clear increase in H_2 mol% as soon as O_2 mol% reaches the value of zero. Under anaerobic conditions, a significant decrease in N_2 mol% is also observed and thus confirms an activation of N_2-fixation (Fay 1992). In parallel with an increase in H_2 composition, the trace quantity of CO_2 – (means composition of 3 mol%) was also detected. This concurrent production of CO_2 is commonly expected, as in the absence of the O_2 terminal electron acceptor, microbes can ferment the gas and organic compounds from their organic substrate, glycerol in this case, for the purpose of maintaining their redox balance and conserving energy (Catalanotti, Yang *et al.,* 2013). An existence of organic products inside the broth is confirmed by Figures II.5.A and B, which shows co-production of acetic and ethanol (both at low concentrations of less than 5 mM), after the establishment of anaerobiosis. This observation is in good agreement with a previous study conducted by Welsh and colleagues, which revealed the ability of *Cyanothece* 51142 to excrete ethanol, lactate and acetate (Welsh, Liberton *et al.,* 2008). As the NMR analysis did not find lactic acid, its absence can be hypothesised as the consequence of an extremely low concentration of this particular compound, which may be below the detection limit of the technique.

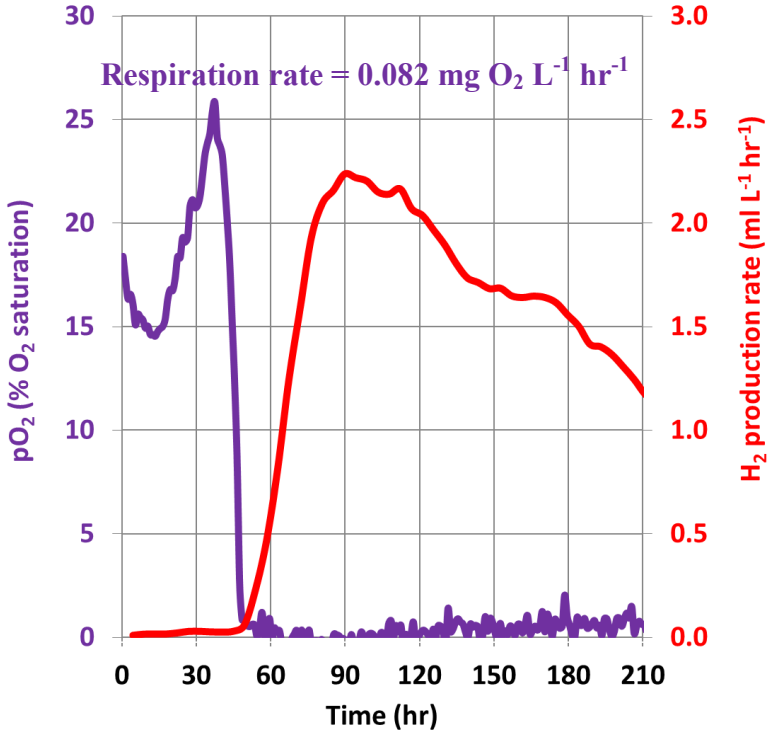

Figure II.3: A decreasing profile of dissolved O_2 was due to an enhanced cellular respiration of the culture. As soon as pO_2 became virtually zero, an onset of H_2 production was detected by MIMS.

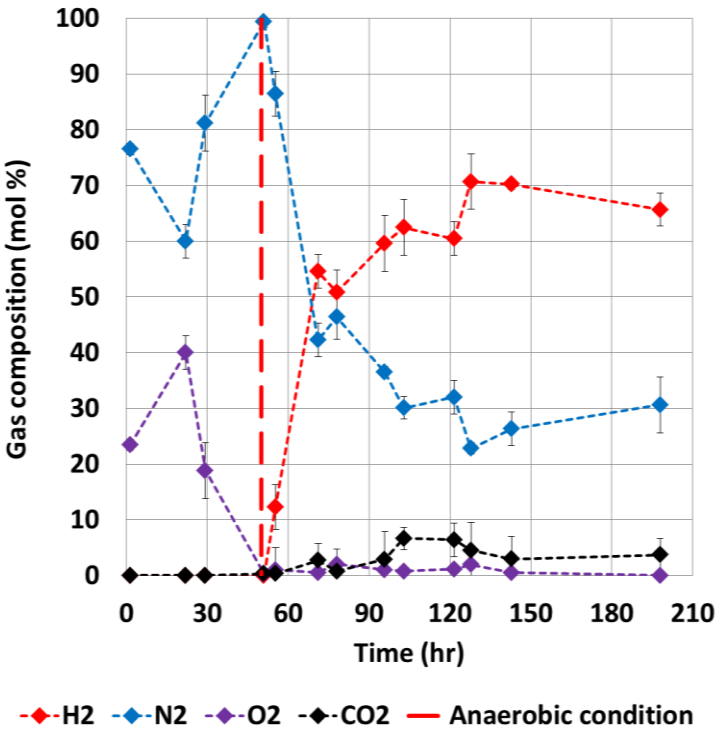

Figure II.4: Gas composition within the headspace of the ICL flat-plate PBR, used to cultivate batch *Cyanothece* 51142 culture at 35 ^{o}C and 92 µmol m^{-2} s^{-1}

Figures II.5.A and B: Nuclear magnetic resonance analysis of the supernatant liquid collected from *Cyanothece* 51142 samples. A) Concentration profile and B) Compound identification.

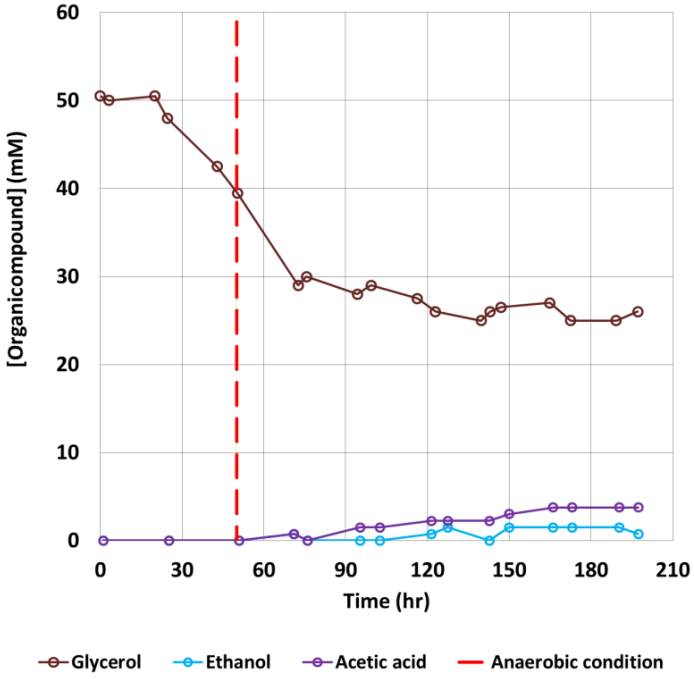

Figure II.5.A: Concentration profile of organic carbon compounds within the supernatant liquid collected from *Cyanothece* 51142 samples.

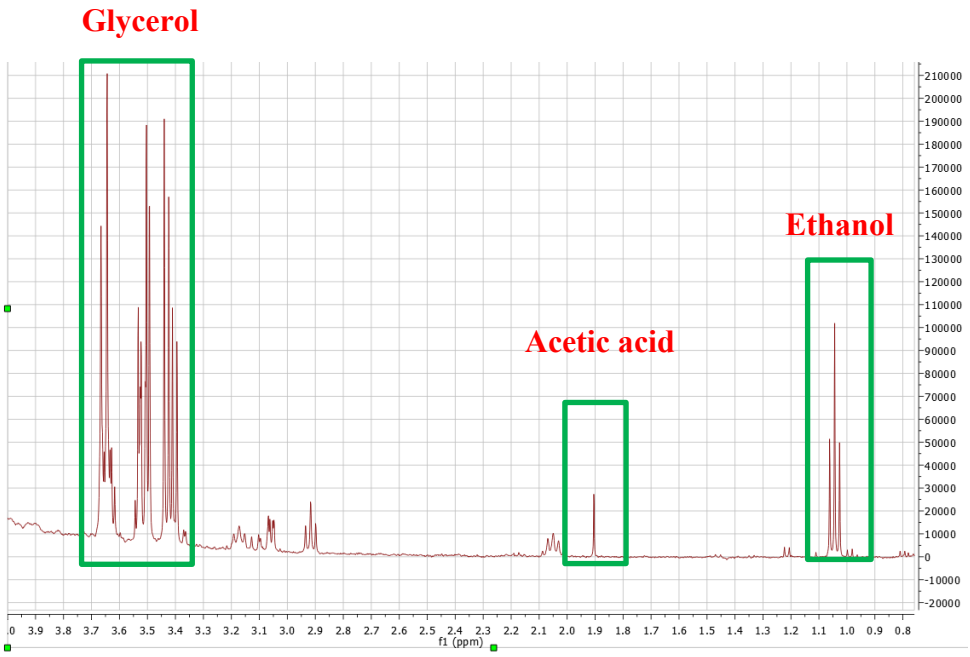

Figure II.5.B: Identification of organic carbon compounds within the liquid supernatant, collected during H_2 production phase of the *Cyanothece* 51142 culture

Once being established at time = 60 hr, well-sustained anaerobic conditions were observed throughout the whole experiment as long as glycerol is present in the growth medium (Figures II.2.A and II.3) and thus reassuring an effectiveness of the glycerol-induced anaerobiosis approach. Under this continuously low-O_2 environment, an uninterrupted profile of H_2 production rate is clearly observed, as shown in Figure II.1.A. The figure also shows a high degree of coherence between the gas production rate and the cyanobacterial growth: as biomass concentration of the culture increases, the H_2 formation rate rises. This observation is expected, since when the culture develops, there are a greater number of H_2-producing cells inside the system. The rate eventually reached its maximum value of approximately 2.2 ml H_2 L^{-1} hr^{-1}, during the stationary growth phase (time = 70 – 95 hr), when the *Cyanothece* 51142 culture attained its final biomass concentration of 1 g L^{-1}. However, both concentration and rate were seen to decline after time = 95 hr, indicating the beginning of the death phase. During this terminal phase, the decay rate can be estimated by calculating the negative gradient of the natural log of the growth profile over time and subsequently found to be -0.004 hr^{-1}, as shown in Figure II.1.B. The main reason for the occurrence of the death phase is commonly due to unfavourable cultivating environments, such as i) depletion of essential macro-nutrients, ii) accumulation of cellularly excreted inhibitory by-products and iii) insufficient access to O_2 (in the case of green algae and cyanobacteria) (Heritage 1996) – which subsequently exert a high level of stress upon cells. In this current study, the first case can be disregarded, as sufficient sources of essential nutrients were confirmed (Figures II.2.A and C and Figure II.4). However, as an excretion of fermentative products – CO_2 and organic acids was confirmed using MS and NMR analysis (Figures II.4 and II.5.A), these compounds are acidic in nature and subsequently turn the aqueous environment into a much more acidic one. From Figure II.6, pH was seen to decrease from 7.5 to the minimum value of 3.5 at the same time as the culture moves into the death phase. Generally, the optimal range of pH to

facilitate the growth of cyanobacteria is between 7.7 – 9.4 (Wicks and Thiel 1990). In addition to the secondary case, a prolonged duration of anaerobic condition is another potential cause, as *Cyanothece* 51142 requires O_2 to metabolise intracellular glycogen to obtain chemical energy via cellular respiration. In absence of O_2, the cyanobacterium is unable to produce enough ATP to sustain its physiological activities and eventually die.

In order to compare the obtained H_2 productivity with other benchmarks, an initial rate – the cumulative yield of gas production during the first 24 hours after its onset, is commonly used, instead of the maximum rate. By using the estimation methodology, as shown in Figure II.7, the initial rate of 2.13 ml H_2 L^{-1} hr^{-1} is comparable with the value of 33 ± 5 μmol H_2 mg Chl^{-1} hr^{-1} ~ 1.81 ml H_2 L^{-1} hr^{-1}, reported by Min and Sherman under similar growth conditions (Min and Sherman 2010). Nevertheless, according to Bandyopadhyay and co-workers (Bandyopadhyay, Stoeckel *et al.,* 2010), it is possible to obtain a striking initial rate of up to ~ 25 ml H_2 L^{-1} hr^{-1} – approximately 12-fold higher than mine – by growing the *Cyanothece* 51142 culture under true light / dark cycles, before changing into continuous illumination when H_2 production was initiated. This significant difference may be explained by the fact that even the function of nitrogenase enzymes is diurnal, regardless of illumination condition (ColonLopez, Sherman *et al.,* 1997, Schneegurt, Tucker *et al.,* 2000) – its activity is found to become only half of its normal rate, when the cyanobacterial culture is cultivated under continuous light instead of light dark cycles (Toepel, Welsh *et al.,* 2008). Fundamentally, under continuous illumination, there is a 2-fold reduction in *Cyanothece* 51l42 respiratory rate (Toepel, Welsh *et al.,* 2008), which then resulted in lower levels of biochemically generated ATP for facilitating N_2-fixing reaction. In addition, by using Equation 5.11 proposed by Giannelli and co-workers (Giannelli, Scoma *et al.,* 2009), the solar-to-H_2 energy conversion (SHEC) efficiency of *Cyanothece* 51142 culture, cultivated under this studied

condition, is calculated to be 0.72 %. This estimation agrees with most studies, which report an efficiency of less than 1% for H_2 photoproduction processes using green algae and cyanobacteria (Masukawa, Kitashima *et al.,* 2012).

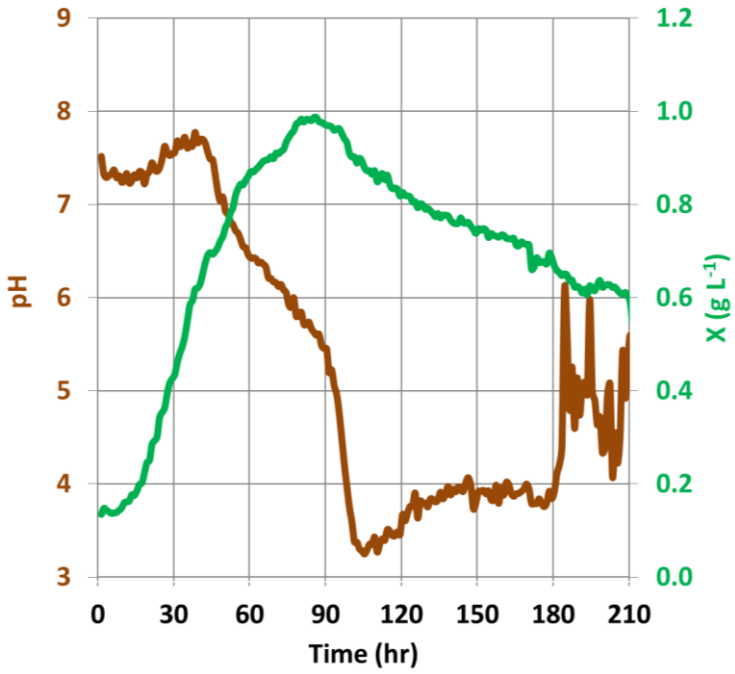

Figure II.6: pH profile of the batch *Cyanothece* 51142 H_2 production. The continuous decline in pH value was observed as soon as the system became anaerobic at time = 60 hr.

An initial rate of H_2 production was estimated based on the gradient of H_2 yield accumulated over time during the first 24 hours after the onset of gas evolution at time = 60 hours (Figure II.7).

The rate was estimated to be $\frac{300-0\ \text{ml}}{203-62\ \text{hr}}$ = 2.13 ml H_2 L^{-1} hr^{-1}, using the working volume of the flat-plate PBR of 800 ml.

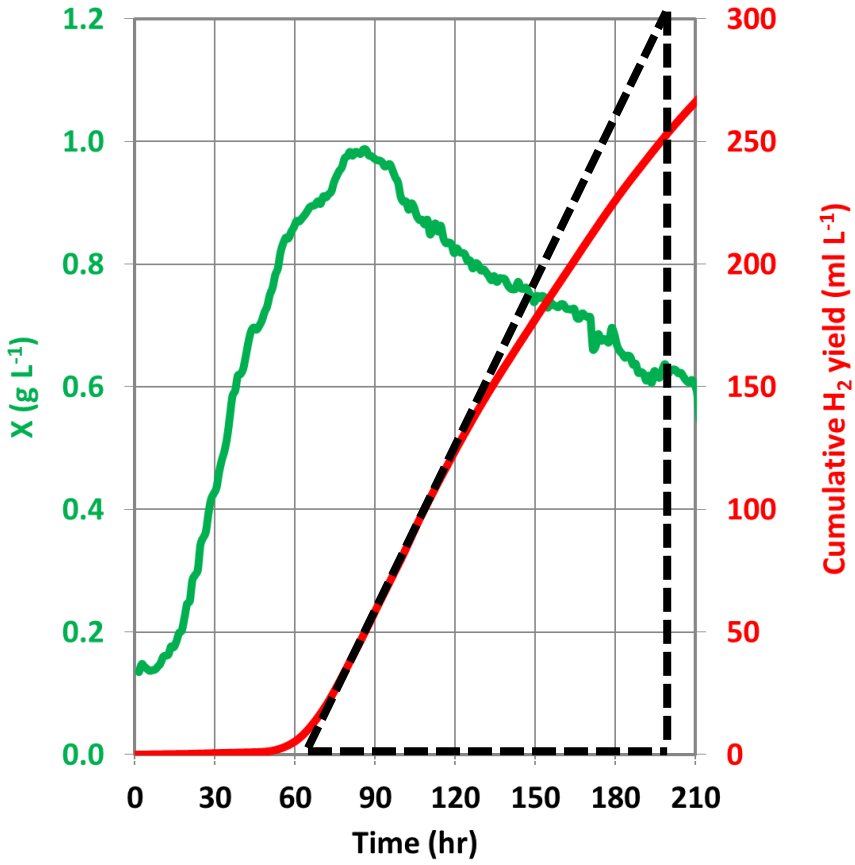

Figure II.7: Cumulative H_2 yield of *Cyanothece* 51142 culture, cultivated at 35 ^{o}C and 92 µmol m^{-2} s^{-1}

By carrying out the batch *Cyanothece* 51142 H_2 photoproduction, it is clear that an overall gas formation process consists of two interconnected sub-stages – the primary growth and the secondary gas production itself. Key parameters of the growth and nutrient uptake kinetics, determined under this studied condition, are tabulated in Table II.1.

Table II.1: Parameters of *Cyanothece* 51142 growth, nutrient uptake and respiration kinetics, under photoheterotrophic growth, 35 ^{o}C and 92 μmol m^{-2} s^{-1} conditions

Definition	Symbol	Value	Unit
Maximum specific growth rate	μ_{max}	0.07	hr^{-1}
Specific decay rate	μ_d	-0.004	hr^{-1}
Respiration rate	r_{Oxygen}	0.082	mg O_2 L^{-1} hr^{-1}
Nitrate uptake rate	$r_{Nitrate}$	26	mg NO_3^{-1} L^{-1} hr^{-1}
Glycerol uptake rate	$r_{Glycerol}$	0.38	mM hr^{-1}

II.4. Effect of Light Intensity

N_2-fixation is well-known to be an energy-demanding biological process. Consequently, light is an important factor to be examined, as it serves as the primary energy source for the reaction. The relationship between nitrogenase activity and irradiance can be characterised into three distinct phases: i) photo-limitation, ii) photo-saturation and iiiii) photo-inhibition, which are similar to those of photosynthesis (Staal, Lintel-Hekkert *et al.,* 2001, Staal, Hekkert *et al.,* 2002, Ariosa, Carrasco *et al.,* 2006). Light-saturating regime can start at any irradiances up to 200 – 300 μmol m^{-2} s^{-1} (Fernandez-Valiente, Quesada *et al.,* 2001, Staal, Hekkert *et al.,* 2002, Ariosa, Carrasco *et al.,* 2006), whereas the inhibiting phenomenon is previously reported to occur at an extreme irradiance of 1400 μmol m^{-2} s^{-1} (Ariosa, Carrasco *et al.,* 2006). For *Cyanothece* 51142, the effect of three different light regimes (30, 100 and 200 μmol m^{-2} s^{-1}) over hydrogenase-mediated H_2 production via proton-electron recombination reaction of *Cyanothece* 51142 has been investigated by Min and Sherman (Min and Sherman 2010). However, as nitrogenases are the predominant enzymes, catalysing H_2 evolution for this cyanobacterium (Min and Sherman 2010), it is desirable to understand the effect of light intensity on the nitrogenase-catalysed hydrogen production rate and this forms the basis of this section.

Since the growth condition in section II.3 was demonstrated to effectively facilitate nitrogenase-mediated H_2 production of *Cyanothece* 51142, it was subsequently employed as an initial cultivating condition for every of light intensity study. Experimentally, the cyanobacterial culture was cultivated under continuous illumination of 92 μmol m^{-2} s^{-1} and constant temperature of 35 $^{\circ}$C. The growth medium was an air-saturated ASP2+C (50 mM of glycerol). Shortly after the onset of H_2 evolution was detected by MIMS system, irradiance

was changed from its original value into a new set value (46, 92, 138, 230 and 320 µmol m^{-2} s^{-1}) in order to examine its direct effect on the gas-producing mechanism. A set of the growth, the H_2 production and the pO_2 experimental profiles, under each respective irradiance, can be seen in Figure II.8.A – H. The time, when light intensity was altered, is represented as a black dotted line on the graph. It should be noted here that the results, under 92 µmol m^{-2} s^{-1}, are previously presented and discussed in section II.3 and their presentation shall not be repeated here. Due to the implementation of the same initial growth conditions, the later discussion will be with emphasis on the subsequent H_2 production phase.

Figures II.8.A - H: Growth, H_2 production and pO_2 profiles of batch glycerol-supplemented, air-saturated *Cyanothece* 51142 culture, cultivated under incident irradiances of 46, 138, 230 and 320 µmol m^{-2} s^{-1}

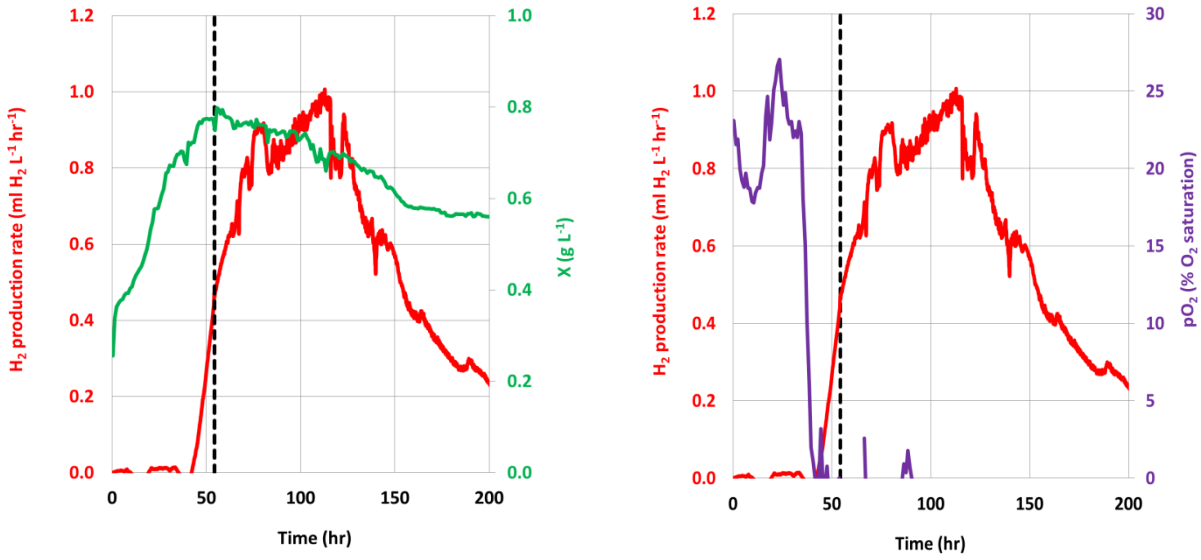

Figures II.8.A and B: *Cyanothece* 51142 growth, H_2 production rate and pO_2 for 46 µmol m^{-2} s^{-1}

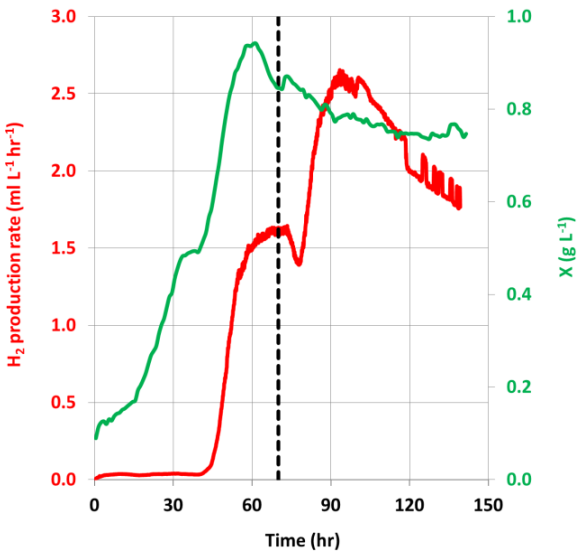

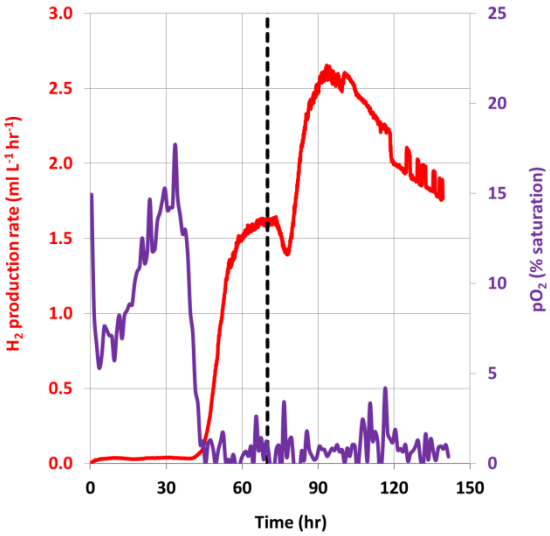

Figures II.8.C and D: *Cyanothece* 51142 growth, H_2 production rate and pO_2 for 138 µmol m^{-2} s^{-1}

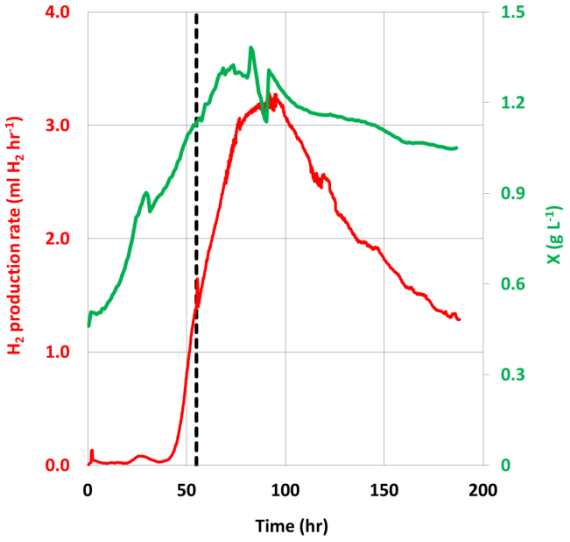

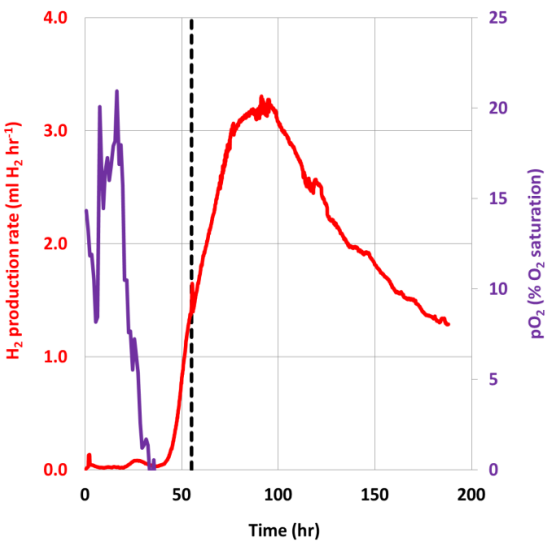

Figures II.8.E and F: *Cyanothece* 51142 growth, H_2 production rate and pO_2 for 230 µmol m^{-2} s^{-1}

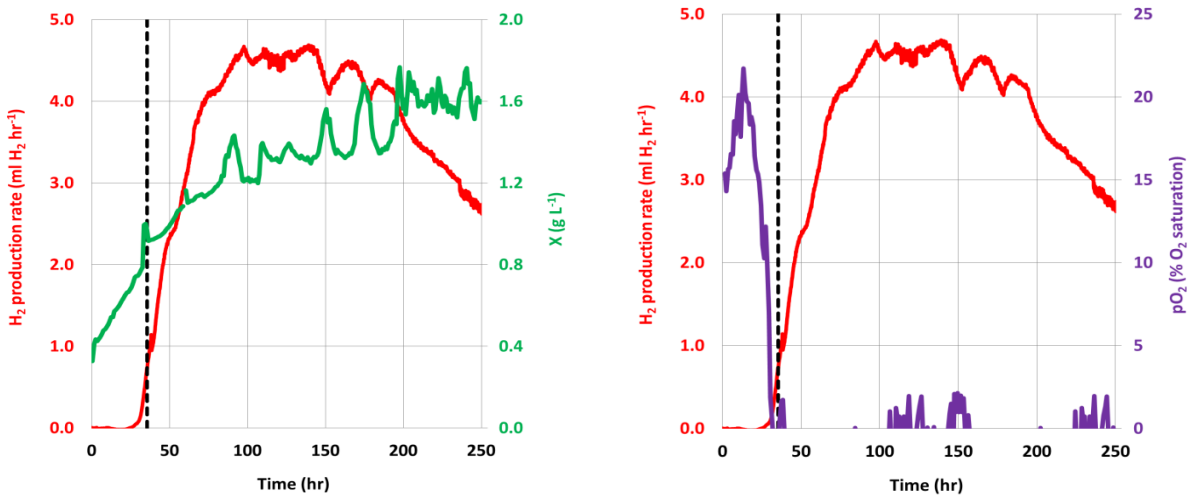

Figures II.8.G and H: *Cyanothece* 51142 growth, H_2 production rate and pO_2 for 320 µmol m^{-2} s^{-1}

In order to make a clear comparison, all of the obtained H_2 production rate as well as yield profiles are plotted on the same x-axis, as illustrated in Figures II.9 and II.10, respectively. Numerical values of both parameters as well as their corresponding SHEC efficiencies are tabulated in Table II.2. It should also be noted here that every light experiments were carried out, apart from the dark condition (0 µmol m^{-2} s^{-1}), at which a complete cessation of gas production is widely reported. This is due to the oxidation of nitrogenase-produced H_2 by dark-induced uptake hydrogenases and subsequently the resulting production rate can be reasonably assumed to be zero (Bandyopadhyay, Stoeckel *et al.,* 2010, Min and Sherman 2010). From both figures, a strong light-dependence of the H_2 production is confirmed, as an increasing light intensity leads to subsequent increases in the maximum gas production rate and cumulative yield. Quantitatively, as incident irradiance is doubled from 46 into 92 µmol m^{-2} s^{-1}, the rate is found to be enhanced by approximately the same factor of 2.2 (calculated from data in Table II.2). However, this proportional enhancement is no longer observed under higher light intensity regimes, as when irradiance is increased from 46 to 320 µmol m^{-2}

s^{-1} (7-fold increment), the hydrogen production rate is only increased by a factor of 4.6, suggests an increasing, but non-linear relationship between H_2 production rate and light intensity. In contrast, with increasing irradiance, the SHEC efficiency becomes enhanced but only up to 92 μmol m^{-2} s^{-1}, after which its value starts to decline. As the efficiency is defined as the ratio of output to input energies (Equation 5.11), an increase in incident light intensity means that a greater amount of electrical energy is required to generate the higher power of illumination. In addition, as the *Cyanothece* 51142 culture matures, individual cell has less access to sufficient light source, due to an increasing mutual shading phenomena (Posten 2009). The significance of this light-limiting scenario is confirmed by photograph of the culture cultivated within the ICL flat-plate PBR, Figure II.11.A (Zhang, Dechatiwongse *et al.,* 2015b), which clearly shows that only cells closer to an illuminated exposure surface have access to illumination, whereas the majority of cells, located near the front surface and in the middle of the PBR are shaded behind. By employing Equation 5.32, light attenuation effects inside the PBR for both 230 and 320 μmol m^{-2} s^{-1} can be simulated (Figures II.11.B and C). It can be seen from both figures that, as the cultures mature and eventually reach their final concentration, there are significant reductions in average light intensity – from 132 (dilute culture) to 60 (fully grown culture) μmol m^{-2} s^{-1} and 183 to 68 μmol m^{-2} s^{-1}. As there is usually a significant variation in the value of local light intensity within the PBR, as shown in Figures II.11.A, B and C, the term of 'average light intensity', which represents the sum of local light intensity at individual distance along the PBR's body, was used instead.

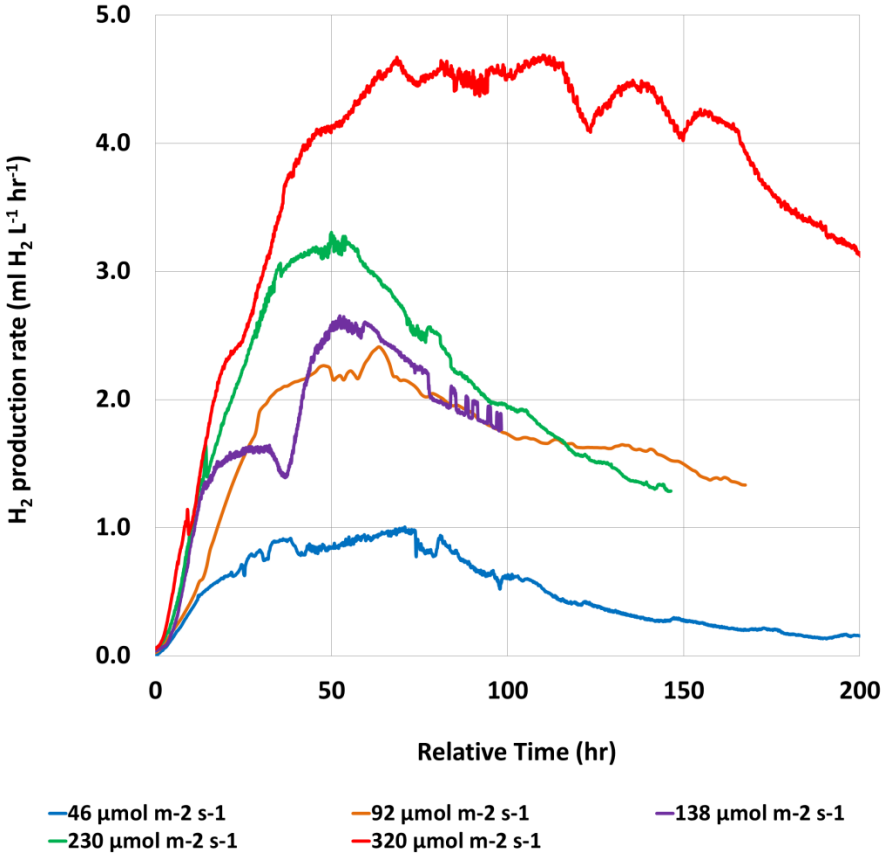

Figure II.9: H_2 production rate of *Cyanothece* 51142 culture, cultivated under 35 ^{o}C and a light intensity range of 46, 92, 138, 230 and 320 µmol m^{-2} s^{-1}. The onset of H_2 production was standardised to the same starting time.

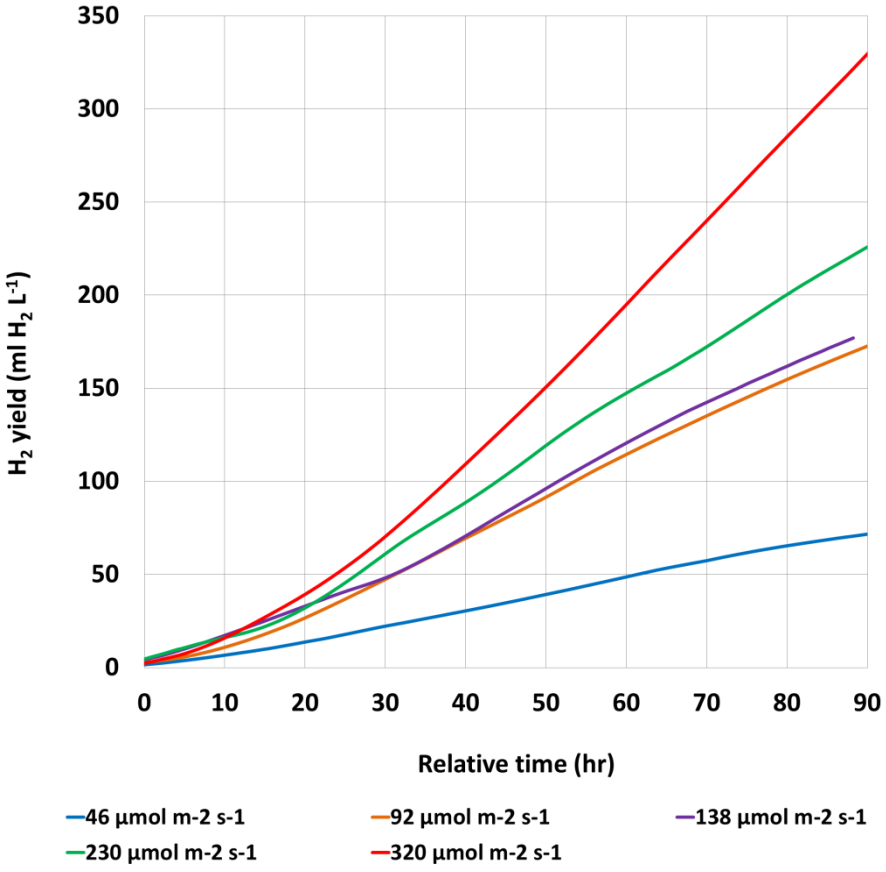

Figure II.10: Corresponding H_2 production yield of *Cyanothece* 51142 culture, cultivated under 35 ^{o}C and a light intensity range of 46, 92, 138, 230 and 320 µmol m^{-2} s^{-1}.

Table II.2: H_2 production of *Cyanothece* 51142 under cultivating light intensities of 0, 46, 92, 138, 230 and 320 µmol m^{-2} s^{-1}

Light intensity (µmol m^{-2} s^{-1})	Maximum H_2 productivity (ml H_2 L^{-1} hr^{-1})	H_2 yield over first 90 hours after its onset (ml L^{-1})	SHEC efficiency (%)
0	~0	-	-
46	~1.0	71	0.595
92	2.2	172	0.716
138	2.5	191	0.528
230	3.1	221	0.371
320	4.6	325	0.387

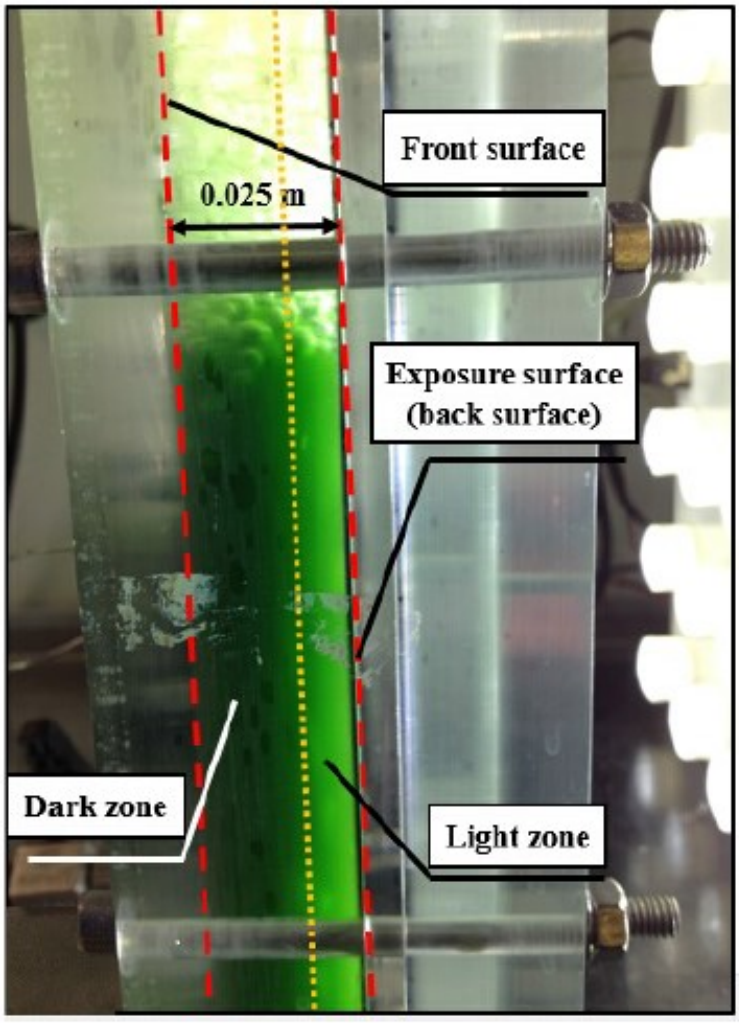

Figure II.11.A: Photograph of a very dense culture (~1.2 g L^{-1}), cultivated under 230 µmol m^{-2} s^{-1} and 35 °C in the ICL flat-plate PBR. Poor light penetration, caused by cellular mutual shading, at which only the culture, located near light source, can harvest solar energy (Zhang, Dechatiwongse *et al.,* 2015b).

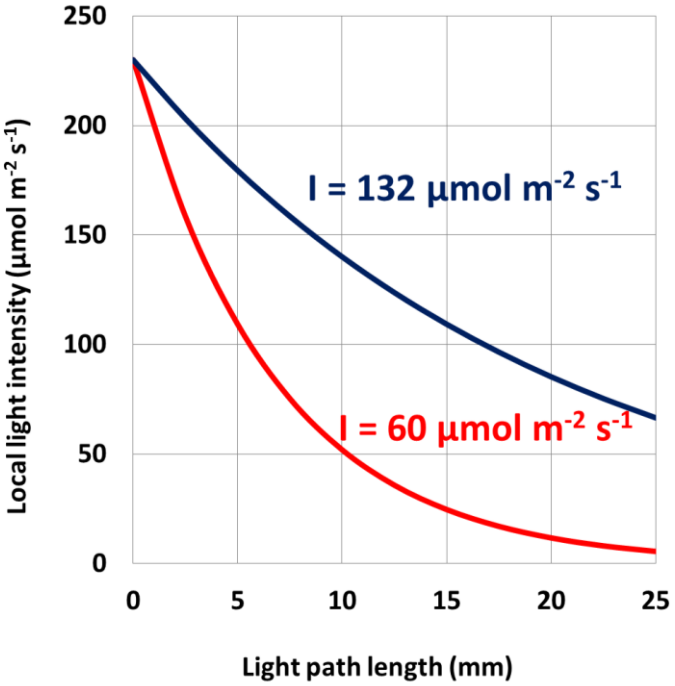

Figure II.11.B: Computational validation of mutual shading phenomena under an incident light intensity of 230 µmol m^{-2} s^{-1}. The blue line represents local light intensity profile, under an initial biomass concentration of ~ 0.4 g L^{-1}, whereas the red one is for the profile, under a very dense culture of ~ 1.2 g L^{-1}.

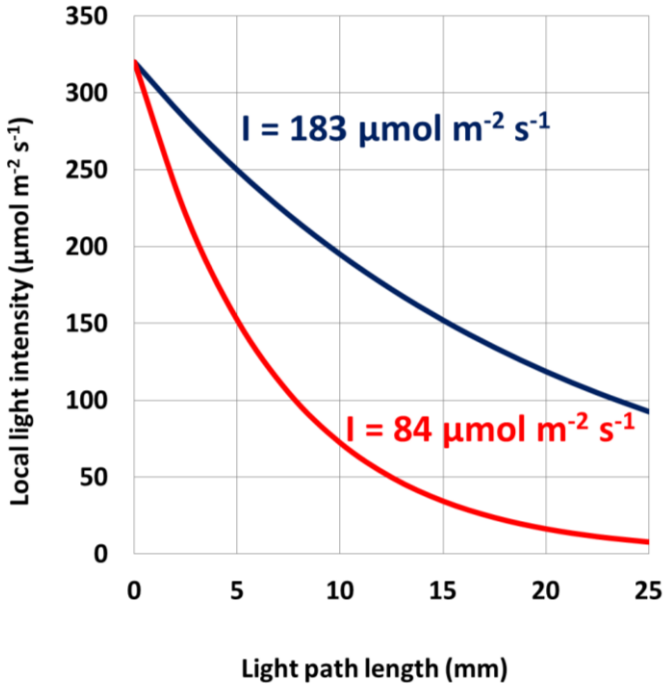

Figure II.11.C: Computational validation of mutual shading phenomena under an incident light intensity of 320 µmol m^{-2} s^{-1}.

In order to obtain an in-depth understating behind this correlation, the parameter estimation of the H_2 production model (Equation 5.37), which simultaneously takes into account effects, influenced by environmental parameters – temperature (Equation 5.34) and light intensity (Equation 5.31) - as well as available biomass (Equation 5.32), was performed. In addition, the model also introduces a H_2 yield coefficient ($Y_{H/X}$), which can be assumed as a function of carbon substrate and intracellular nitrogen concentration (Vatcheva, de Jong *et al.,* 2006). In all of H_2 production studies, as glycerol (carbon) was added in excess and nitrate (nitrogen) was also completely consumed before the start of H_2 production, it was reasonable to assume $Y_{H/X}$ as a constant. The parameter estimation was based on the concept of the least-squares methodology, which is to minimise the difference between experimental data and simulation results. Input experimental data were particularly selected during the *Cyanothece* 51142 stationary growth phase, where biomass concentration was constant and the maximum H_2 production rate was attained. By fixing the cultivating temperature at 35 ^{o}C, $h(T = 35\ ^{o}C)_H$, in Equation 5.37, becomes constant. The product of $Y_{H/X}$ and $h(T = 35\ ^{o}C)_H$ can then be considered as a new constant, called "$Y(T = 35\ ^{o}C)$". As parameters of Aiba model, Equation 5.31 – k_s and k_i - are independent of $Y(T = 35\ ^{o}C)$, the estimation process can be carried out to determine their values as 124 and 10,561 μmol m^{-2} s^{-1} respectively. Again, it should be noted here that there is a limited confidence in the value of obtained k_i, as its value was found to be far beyond the investigating light intensity range of this study. As a result, the experimental verification will need to be carried out in order to confirm its value. By knowing parameters of $h(T)_H$ (will be explained in Section II.5), the value of $h(T = 35\ ^{\circ}C)_H$ can be calculated as 6.95. Consequently, it becomes possible to determine an absolute value of $Y_{H/X}$, which is 1.23 ml H_2 g^{-1} hr^{-1}. Although it is difficult to compare this value with others, it has been previously found that H_2 production rate is not sensitive to the change of $Y_{H/X}$, which means that the uncertainty of this parameter will not induce significant errors on

the current model (Zhang, Dechatiwongse *et al.,* 2015b).

The non-linear photo-dependence of H_2 production is found to be well-described by the model, as shown in Figure II.12. The obtained parameters for the Aiba model also suggest that, up to 320 μmol m^{-2} s^{-1}, the H_2-producing behaviour of *Cyanothece* 51142 culture is dominantly influenced by light-saturated condition. This is because even under the highest studied irradiance, the photoinhibition term (I^2 / k_i) is still insignificant (numerically estimated as = 320^2 / 10,561 ~ 9.7 μmol m^{-2} s^{-1}), comparing to the value of k_s (124 μmol m^{-2} s^{-1}). Therefore, it can be interpreted that, within the investigated range, there exist only two distinct regimes of light-limitation and saturation, with the transition point between these two regimes at an average light intensity of 124 μmol m^{-2} s^{-1}. In comparison with the previous light study on photoautotrophic growth (Dechatiwongse, Srisamai *et al.,* 2014) (section I.6), the N_2-fixation was found to be saturated at approximately 3 times lower irradiance than that of the growth (347 μmol m^{-2} s^{-1}). This finding agrees with previous studies on other cyanobacteria such as *Aphanizomenon* (Osmond, Cooper *et al.,* 1985), *Anabaena* and *Microchaete* (Ariosa, Carrasco *et al.,* 2006), and suggests that N_2-fixation is more efficient in terms of solar energy utilisation than photosynthesis under low light condition.

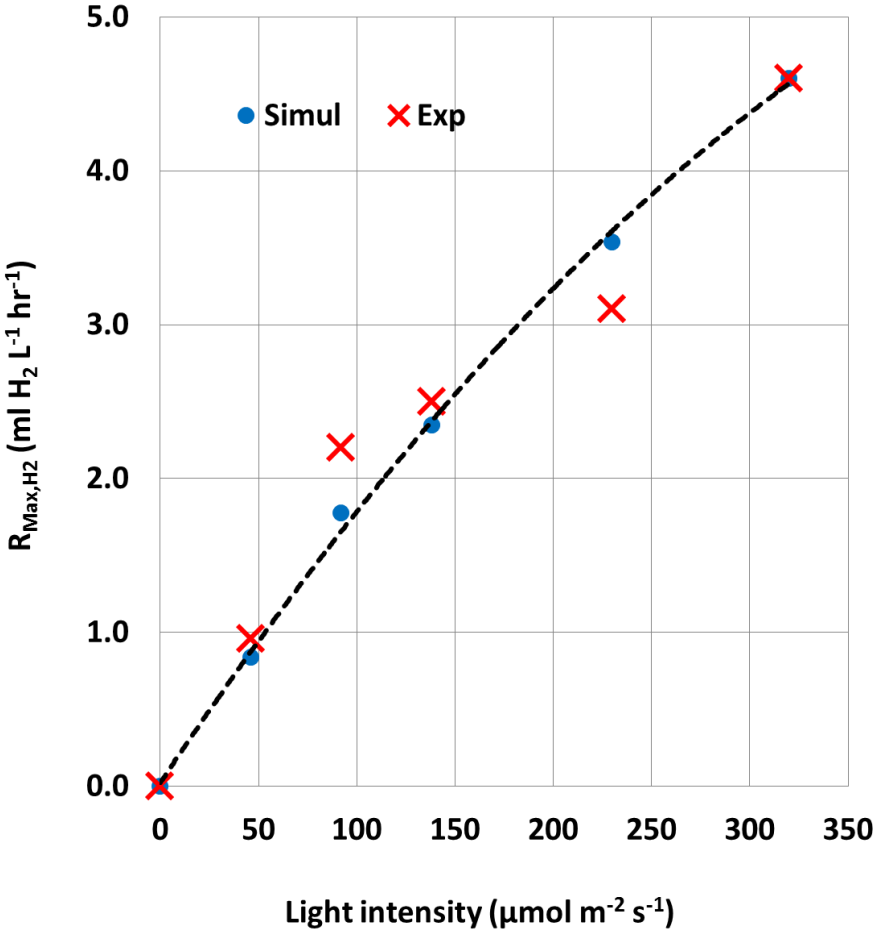

Figure II.12: The maximum H_2 production rate can be enhanced with an increasing incident irradiance up to 320 µmol m^{-2} s^{-1}. The photo-dependence of H_2 production was also well-described by Aiba model (black dashed line).

II.5. Effect of Temperature

Like most of biochemical reactions, the relationship between temperature and N_2-fixing activity is also one of the Arrhenius types, Equation 5.34 (Waughman 1977, Prevost, Antoun *et al.,* 1987, Brauer, Stomp *et al.,* 2013) – the total rate of reaction being the result of two competing temperature-dependent synthetic and denaturation processes. Generally, the rate can be enhanced with increasing temperature up to the optimal value, beyond which it becomes thermally inhibited. Rationally, high temperatures promote high level of cellular respiration, which in turn effectively converts an intracellular environment from aerobic into anaerobic conditions. However, it is very important for the cultivating temperature not to be above the critical point in order to avoid the thermal-induced denaturation process. There is a large range of critical temperatures, varying from strain to strain (Dutta 2005). In the case of *Cyanothece* 51142, although the optimal temperature to facilitate cyanobacterial growth was previously located to be 35 ^{o}C, with a photoinhibition being observed at 40 ^{o}C (Dechatiwongse, Srisamai *et al.,* 2014), the thermal conditions, which facilitates optimal H_2-evolving activity, are still undetermined.

In order to facilitate H_2 production by *Cyanothece* 51142, the same initial growth conditions as the light study, section II.4, was employed for all of investigating temperatures. Experimentally, the cyanobacterial culture was cultivated under continuous illumination of 92 μmol m^{-2} s^{-1} and constant temperature of 35 $^{\circ}$C. The growth medium was an air-saturated ASP2+C (50 mM of glycerol). As soon as the onset of H_2 evolution was detected by the MIMS system, temperature was changed from its original value to a new set value (20, 25, 30, 35, 40, 47 and 55 ^{o}C) in order to examine its direct effect on the gas-producing capability. A set of growth, H_2 production and pO_2 experimental profiles, under each respective

irradiance, can be found in Figure II.13.A – L. The time, when light intensity was altered, is again represented as a black dotted line on the graph. It should be noted here that the results, at 35 ^{o}C, were previously presented and discussed in Section II.3 and their presentation shall not be repeated here. Due to the implementation of the same initial growth conditions, the discussion will focus particularly made on the H_2 production phase.

Figures II.13.A - L: Growth, H_2 production and pO_2 profiles of batch glycerol-supplemented, air-saturated *Cyanothece* 51142 culture, cultivated under temperatures of 20, 25, 30, 35, 40, 47 and 55 ^{o}C.

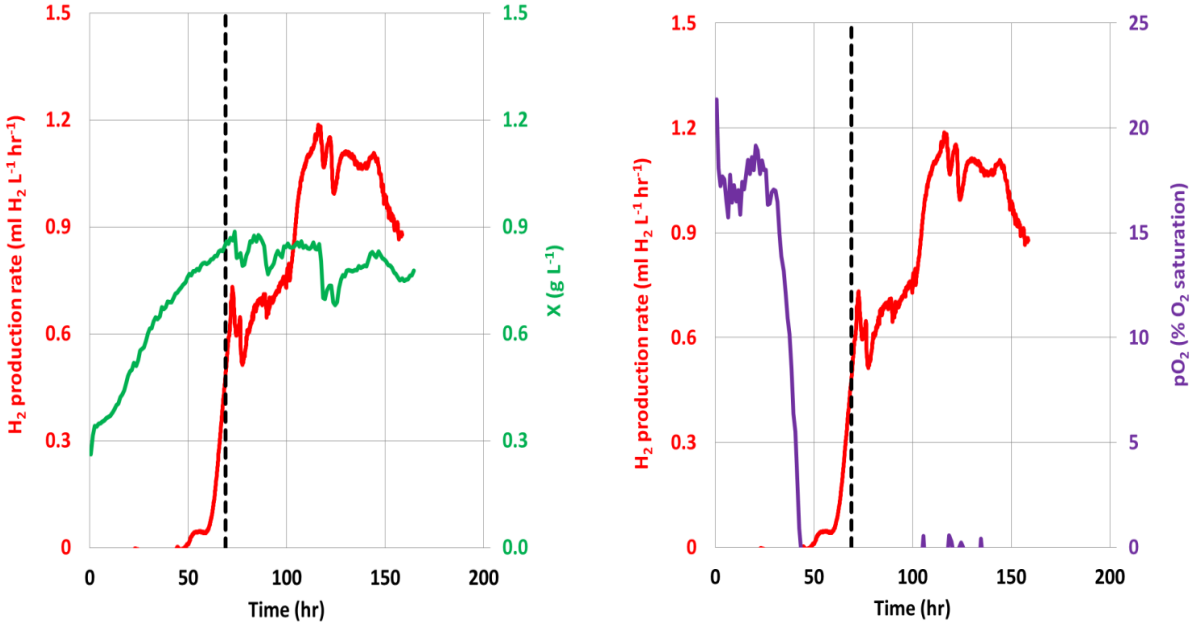

Figures II.13.A and B: *Cyanothece* 51142 growth, H_2 production rate and pO_2 for 20 ^{o}C

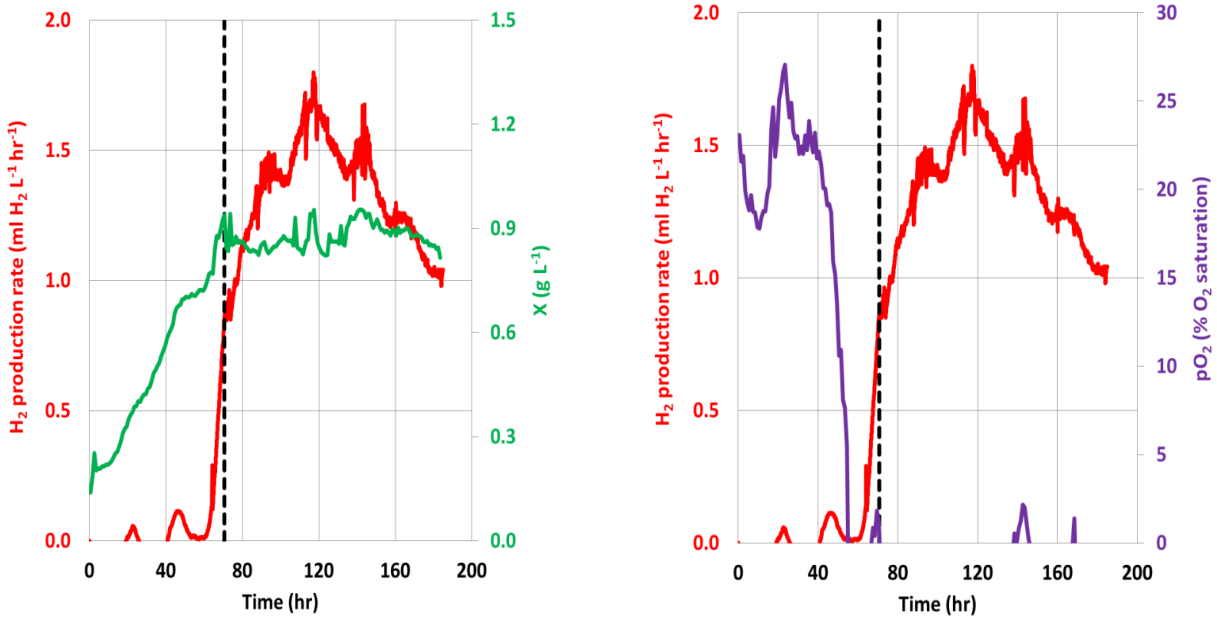

Figures II.13.C and D: *Cyanothece* 51142 growth, H_2 production rate and pO_2 for 25 ^{o}C

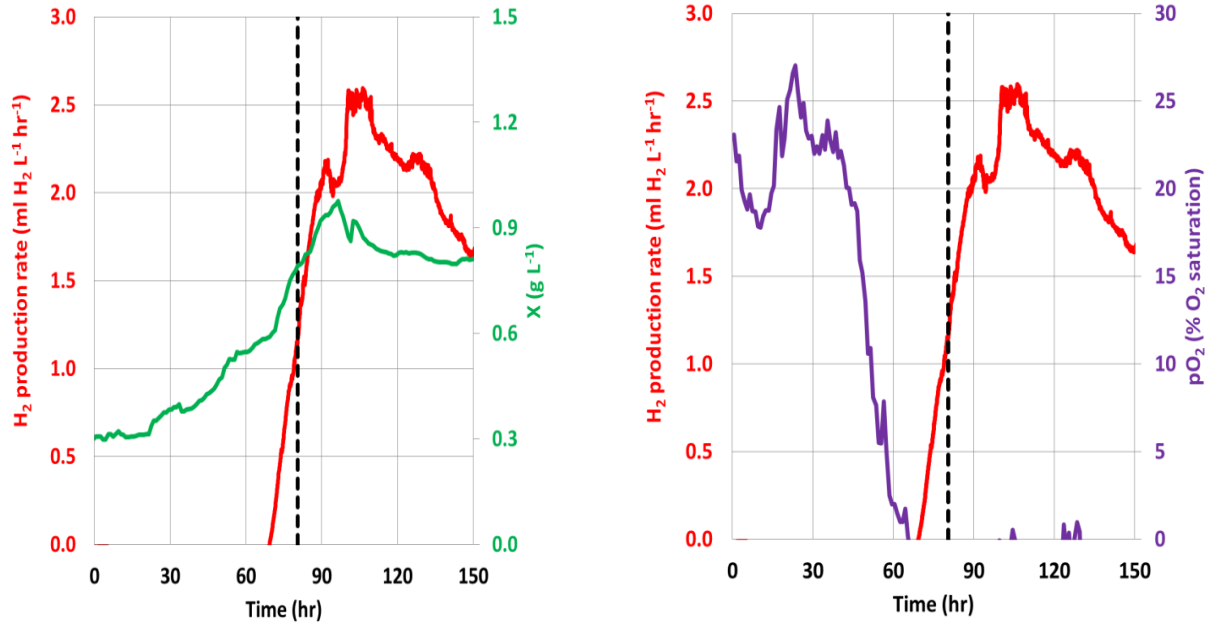

Figures II.13.E and F: *Cyanothece* 51142 growth, H_2 production rate and pO_2 for 30 ^{o}C

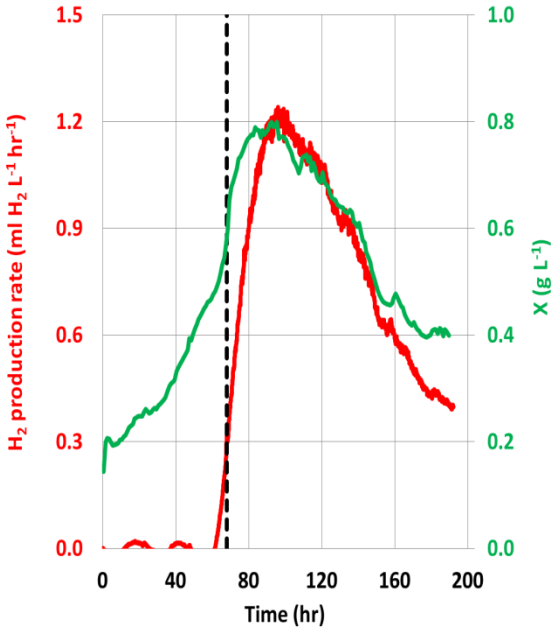

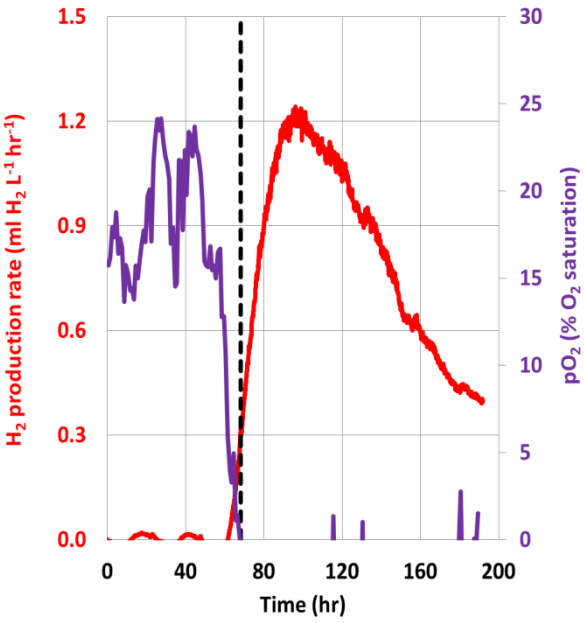

Figures II.13.G and H: *Cyanothece* 51142 growth, H_2 production rate and pO_2 for 40 ^{o}C

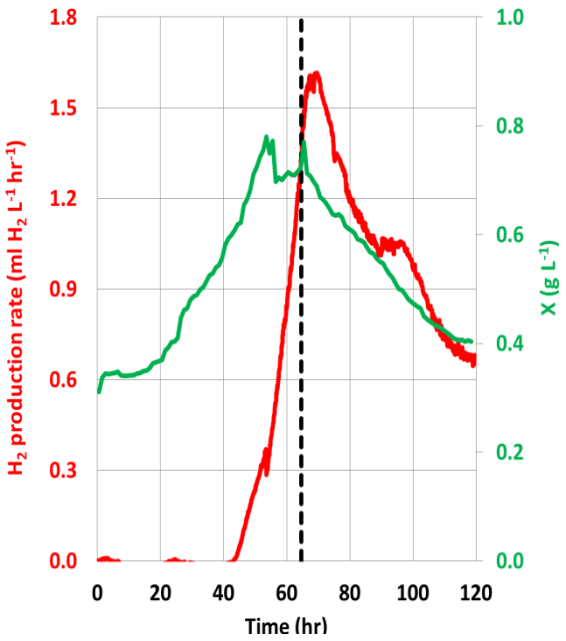

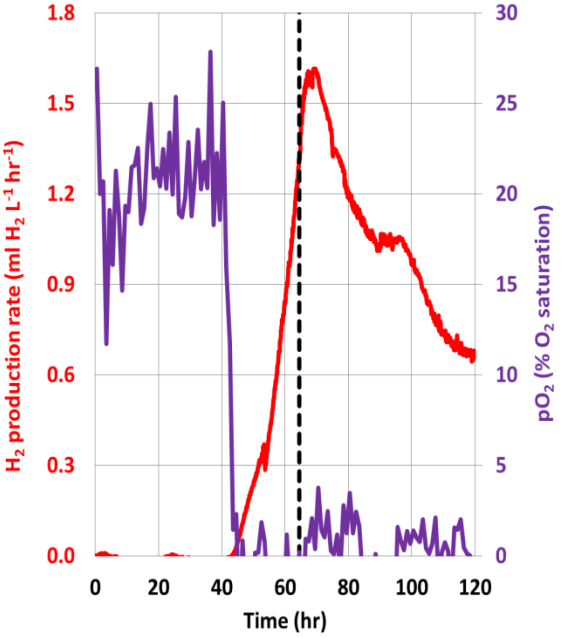

Figures II.13.I and J: *Cyanothece* 51142 growth, H_2 production rate and pO_2 for 47 ^{o}C

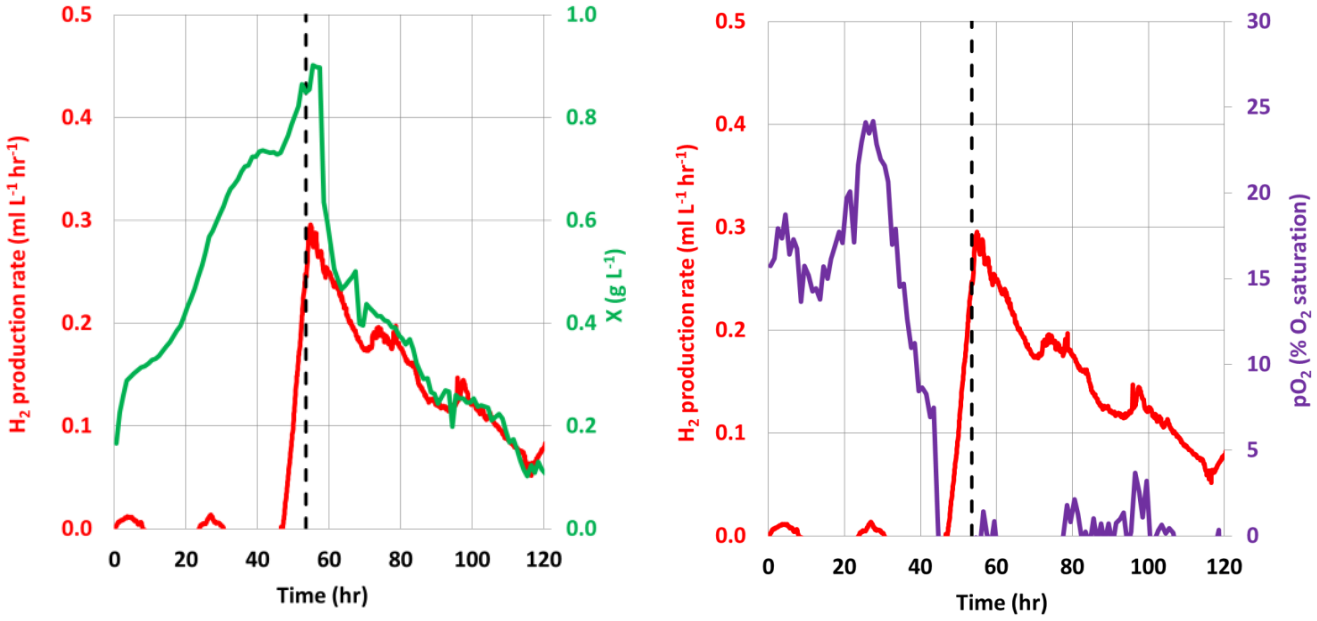

Figures II.13.K and L: *Cyanothece* 51142 growth, H_2 production rate and pO_2 for 55 ^{o}C

In order to make a clear comparison, all of the obtained H_2 production rate as well as yield profiles are plotted on the same x-axis, as illustrated in Figures II.14 and II.15, respectively. Numerical values of both parameters as well as their corresponding SHEC efficiencies are tabulated in Table II.3.

Table II.3: H_2 production of *Cyanothece* 51142 under cultivating temperature of 20, 25, 30, 35, 40, 47 and 55 ^oC

Temperature (^oC)	Maximum H_2 productivity (ml H_2 L^{-1} hr^{-1})	H_2 yield over first 70 hours after its onset (ml L^{-1})	SHEC efficiency (%)
20	1.1	60	0.321
25	1.6	94	0.503
30	2.5	141	0.754
35	2.1	128	0.685
40	1.2	72	0.385
47	0	-	-
55	0	-	-

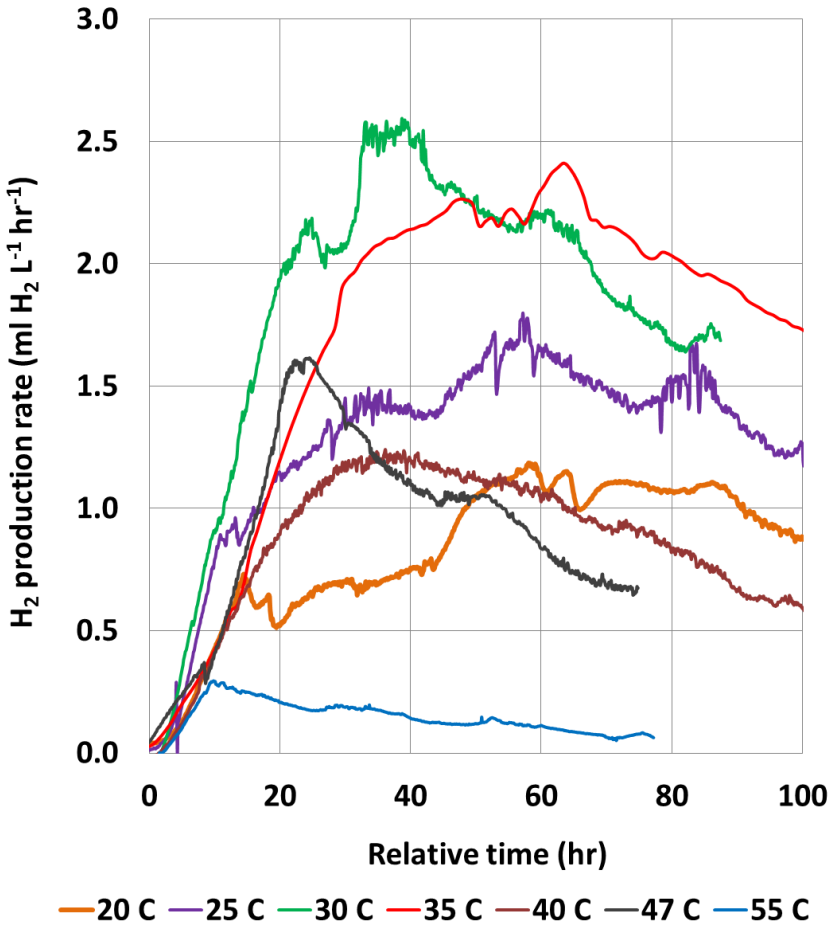

Figure II.14: H_2 production rate of *Cyanothece* 51142 culture, cultivated under 92 µmol m^{-2} s^{-1} and a temperature range of 20, 25, 30, 35, 40, 47 and 55 ^{o}C. The onset of H_2 production was standardised to the same starting time so that an initial and the maximum rate between different temperature regimes can be compared.

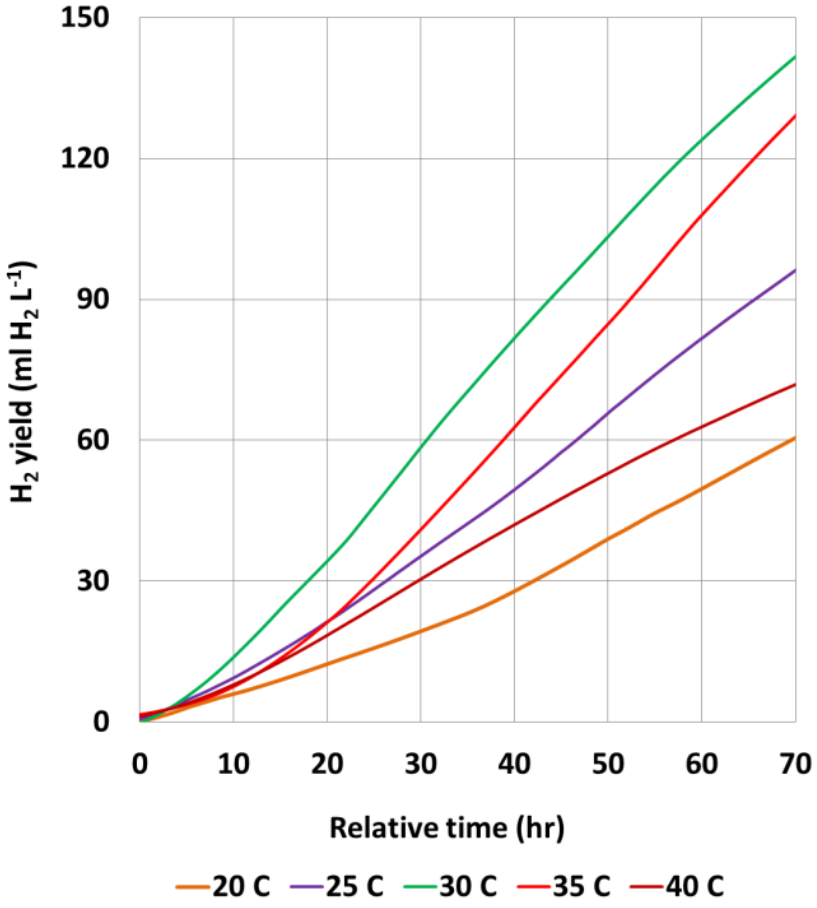

Figure II.15: Corresponding H_2 production yield of *Cyanothece* 51142 culture. Data for 47 and 55 ^{o}C are not present here, as the rate declined immediately after the temperature change and should not be taken into this comparison.

Having carried out the temperature study, the relationship between H_2 production rate and temperature for the cyanobacterium *Cyanothece* 51142 was first time revealed, as shown in Figure II.16.A. It can be seen from the figure that the highest maximum production rate of 2.5 ml H_2 L^{-1} hr^{-1} (also equivalent to the highest efficiency of 0.754% under a fixed irradiance of 92 μmol m^{-2} s^{-1}, see Table II.3) was obtained at a cultivating temperature of 30 ^{o}C. The complete inhibition of the gas production was experimentally observed at and beyond 47 ^{o}C. In addition, by plotting experimental data against N_2-fixation activity of *Cyanothece* sp. Miami BG043511 measured by Brauer and co-workers (Brauer, Stomp *et al.,* 2013), it appears that both results display a comparable pattern over the same temperature range. This high level of coherence can be the consequence of the same genus between my studied strain and Brauer's, but it clearly suggests the reliability of obtained result. In addition, an Arrhenius type character of the cyanobacterial gas production was confirmed from a good quality of fitting between experimental (red squared point) and modelled data (black solid line), as illustrated in Figure II.16.B. Computationally, parameters of the Arrhenius temperature model were determined by keeping incident light intensity constant as 92 μmol m^{-2} s^{-1}. As the values of $Y_{H/X}$ and the Aiba model constants have already been known from the light study, section II.4, the number of unknown parameters in Equation 5.37 was subsequently reduced from seven to four. By minimising the deviations between experimental H_2 production rates and those obtained from the equation, parameters of both synthetic (E_a = 73.7 kJ mol^{-1} and A = 8.13×10^{13}) and denaturation (E_b = 121.1 kJ mol^{-1} and B = 5.88×10^{21}) processes were successfully estimated and are found to be located within a range of previously reported values (Hardy, Burns *et al.,* 1973, Alagappan and Cowan 2004, Lombard, Labeyrie *et al.,* 2009, Brauer, Stomp *et al.,* 2013), tabulated in Table II.4.

Figures II.16.A and B: Influence of temperature upon the maximum H_2 production rate of *Cyanothece* 51142. A) Comparison between my and Brauer's experimental data and B) Fitting of obtained results with Arrhenius' function.

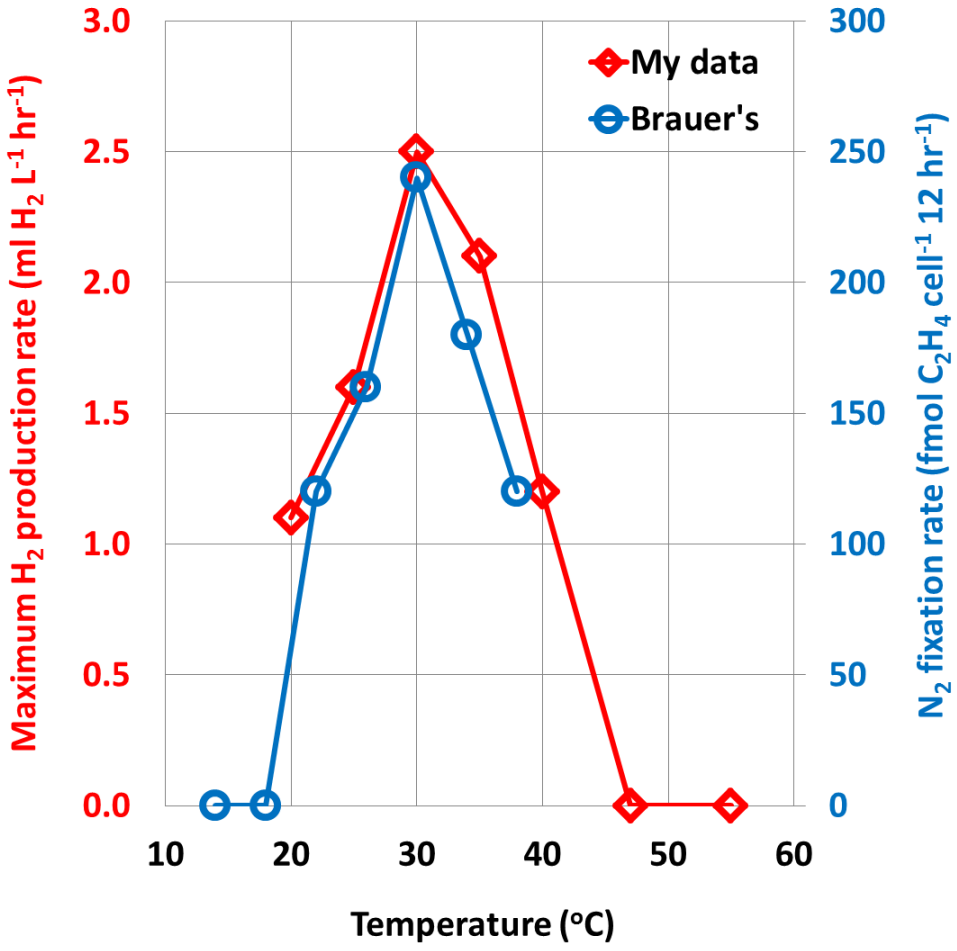

Figure II.16.A: The maximum H_2 production rate is enhanced with an increasing temperature up to an optimal value of 30 ˚C, after which the temperature-induced denaturation process starts to take an effect. The obtained H_2 production rate – temperature relationship is highly comparable with Brauer's N_2-fixation rate – temperature (Brauer, Stomp *et al.,* 2013).

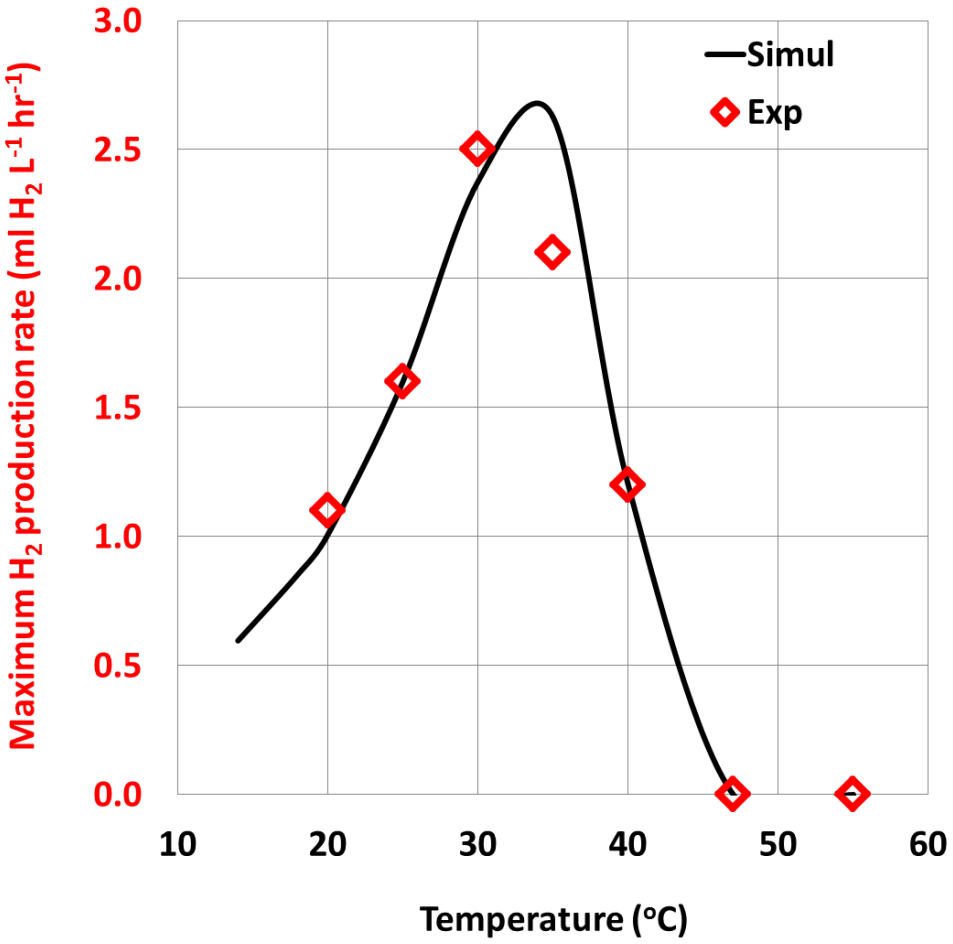

Figure II.16.B: The thermal influence on H_2 production of *Cyanothece* 51142 can be well-described by an Arrhenius' function (black solid line) (Topiwala and Sinclair 1971), whose parameters were determined as following; E_a = 73.7 kJ mol^{-1}, A = 8.13×10^{13}, E_b = 121.1 kJ mol^{-1} and B = 5.88×10^{21}.

Table II.4: Comparison of Aiba and Arrhenius' parameters, obtained during H_2 production phase, between My and literature values.

Definition	Symbol	My value	Literature value	References
Activation enery for synthetic process	E_a (kJ mol^{-1})	73.7	[37.5, 122.5]	(Topiwala and Sinclair 1971, Hardy, Burns *et al.,* 1973, Béchet, Shilton *et al.,* 2013, Brauer, Stomp *et al.,* 2013)
Activation enery for denaturation process	E_b (kJ mol^{-1})	121.1	[127.5, 654]	
Pre-exponential factor for synthetic process	A (no unit)	8.13×10^{13}	[$1.13x10^{7}$, $7.79x10^{21}$]	
Pre-exponential factor for denaturation process	B (no unit)	5.88×10^{21}	[$6.93x10^{19}$, $2.36x10^{101}$]	
Photo-saturation coefficient	k_s (µmol m^{-2} s^{-1})	124	[70, 250]	(Gons, Hoogveld *et al.,* 2006, Béchet, Shilton *et al.,* 2013, Cabello, Morales *et al.,* 2014)
Photoinhibition coefficient	k_i (µmol m^{-2} s^{-1})	10,561	[610 ,53600]	

II.5.1. Over-optimal Temperature

Beyond the optimal temperature of 30 ^{o}C, the H_2-producing capability of *Cyanothece* 51142 was clearly seen to be reduced with rising temperature. Quantitatively, the reductions in the maximum gas productivity are ~ 16% at 35 ^{o}C and then 52% at 40 ^{o}C, before an eventually complete inhibition starts to occur at 47 ^{o}C. Clearly, the rate of H_2 production depends on quantities of two properties: i) nitrogenase enzymes and ii) biomass concentration of cyanobacterial cultures. As the temperature study on *Cyanothece* 51142 growth, previously discussed in section I.7, indicated 35 ^{o}C as an optimal temperature, facilitating the maximum biomass productivity, this implies an insignificant influence of denaturation process under this specific temperature. Therefore, the thermal-induced reduction of nitrogenase expression appears to be an apparent reason, as shown by Brauer and co-workers (Brauer, Stomp *et al.,* 2013). However, as significant reduction in biomass concentration was observed under 40 ^{o}C (also shown in section I.7 of this thesis), it becomes most likely that, beyond 40 ^{o}C, the reduced H_2 production is jointly influenced by an increasing effect of denaturation process, which is initiated under higher temperatures (Topiwala and Sinclair 1971).

The thermal-induced damage upon light-harvesting pigments of *Cyanothece* 51142 culture was confirmed by light absorption spectra obtained from spectrophotometry (Figure II.17). The obtained results show an apparent decomposition of phycocyanin, located around peak of 620 nm, and chlorophyll a, located around peak of 680 nm, on the 2nd day after the temperature alteration to new values of 55 ^{o}C. In contrast, under investigated temperatures of 20 and 35 ^{o}C - peak areas and/or heights of spectra were found to increase, suggesting no thermal-induced damages within this temperature range. A similar observation was also made when plotting a normalised growth profile of every temperature on the same x-axis (Figure

II.18). The normalised biomass concentration (X_s) is defined as the ratio of subsequent biomass concentration at any specific time, after the change in the cultivating temperature, to its initial value, measured at the time before the change was made. From the figure, an adaptive ability of *Cyanothece* 51142 to survive in the new thermal environment was demonstrated from the cultures cultivated under 25 and 30 ^{o}C, as their starting concentrations (close to 1) were maintained for more than 100 hours. The same figure also confirms an increasing and strongly temperature dependent character of the denaturation reaction, as the rate of reduction in biomass concentration is seen to increase as the temperature is increased to 55 ^{o}C. Numerically, it took only 8 hours for the original biomass concentration of the culture cultivated at 55 ^{o}C to be reduced by half, whereas, at 40 ^{o}C, an approximately duration of 100 hours was required for the same magnitude of reduction.

II.5.2. Sub-optimal Temperature

For the sub-optimal temperature regimes, even the cultures cultivated at 20 and 25 ^{o}C eventually reached approximately the same final biomass concentration as at 30 ^{o}C (~ 0.8 – 0.9 g L^{-1}, Figures II.13.A, C and E), however, they still produced H_2 at 56 and 36% lower rates, compared to the optimal value. This inconsistent correlation between the gas production rate and the final biomass concentration suggests that the decreased hydrogen productivity appears to be caused by internal rather external properties of the cells. As respiration is an enzymatic process, it decreases at low temperatures and is eventually not fast enough to consume all of the intracellular O_2 (Staal, Meysman *et al.,* 2003, Stal 2009), which is necessary to create the appropriate environment for the full activity of the nitrogenase enzyme. However, from obtained experimental results, very well-sustained anaerobic conditions were observed instead, even under low temperature regimes of 20 and

25 ^{o}C (see Figures II.13.B and D), which mean that O_2-induced deactivation of nitrogenase may not be a major cause. In fact, these observations can be explained by the concept of an internal energy re-allocation, raised by Brauer and co-workers (Brauer, Stomp *et al.,* 2013), which states that it is still possible for N_2-fixing cyanobacteria to attain and maintain anaerobic conditions by spending a larger quantity of stored chemical energy to compensate for the low temperature-induced reduction in cellular respiration rate. However, as a consequence, this means that there will be a lower portion of available chemical energy, that can be utilised for driving N_2-fixation. As the quantification of glycerol using NMR (Figure II.19) shows that there was no significant difference in the total consumption of this substrate among all of studied temperatures, this thus implies that similar quantities of chemical energies and equivalent reducing powers, were derived from glycerol. Both NMR analysis together with pO_2 data then serve as strong evidences to support Brauer's explanation.

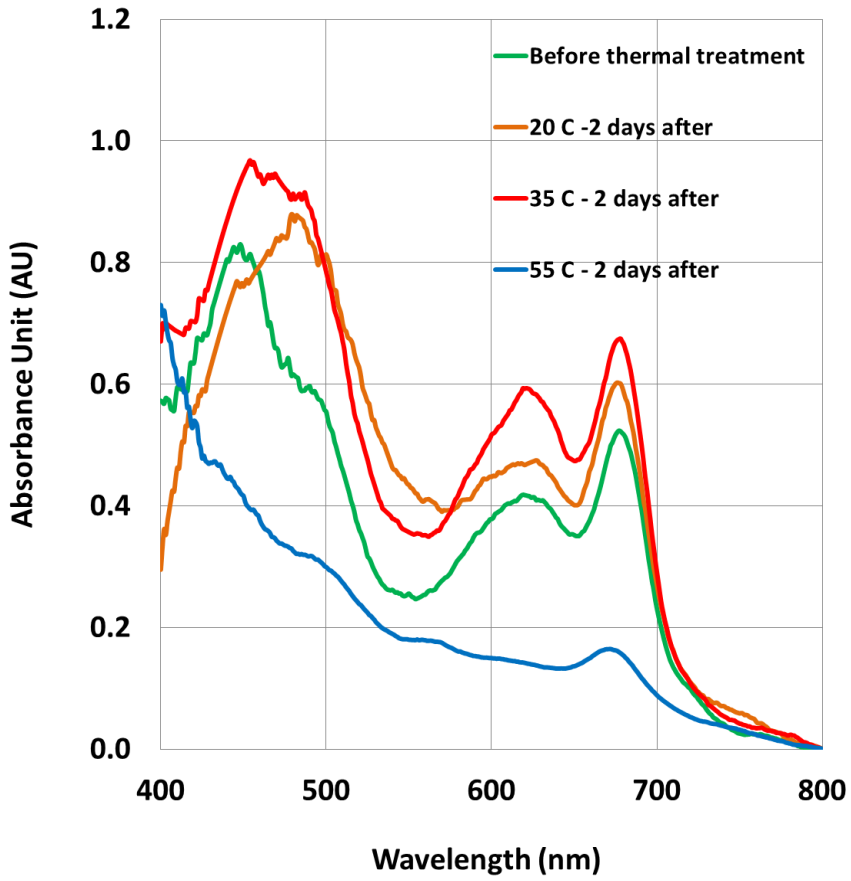

Figure II.17: An apparent thermal-induced decomposition of light-harvesting apparatus - phycocyanin (620 nm) and chlorophyll a (680 nm) was observed on the 2nd day after the temperature alteration into 55 ^{o}C. In contrast, under investigated temperatures of 20 and 35 ^{o}C - peak areas and/or heights of spectra were found being increased, thereby suggesting none of thermal-induced damages during this temperature range.

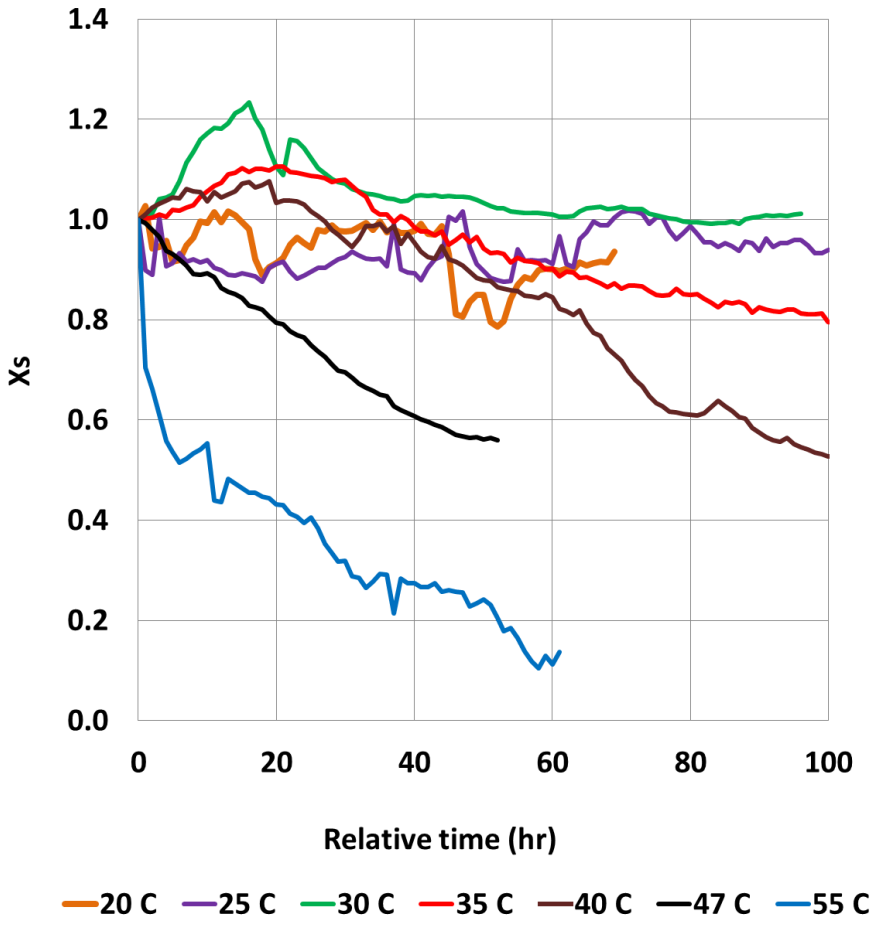

Figure II.18: Normalised biomass concentration X_s, is defined as ratio of subsequent concentration at any specific time after the change in temperature, over the concentration, at the time before making the change. Under low temperature regime (20, 25 and 30 ˚C), X_s remains close to 1, implying an adaptability of cells into the new thermal environment, whereas the rate of X_s decay was found enhancing as the temperature moves towards 55 ˚C.

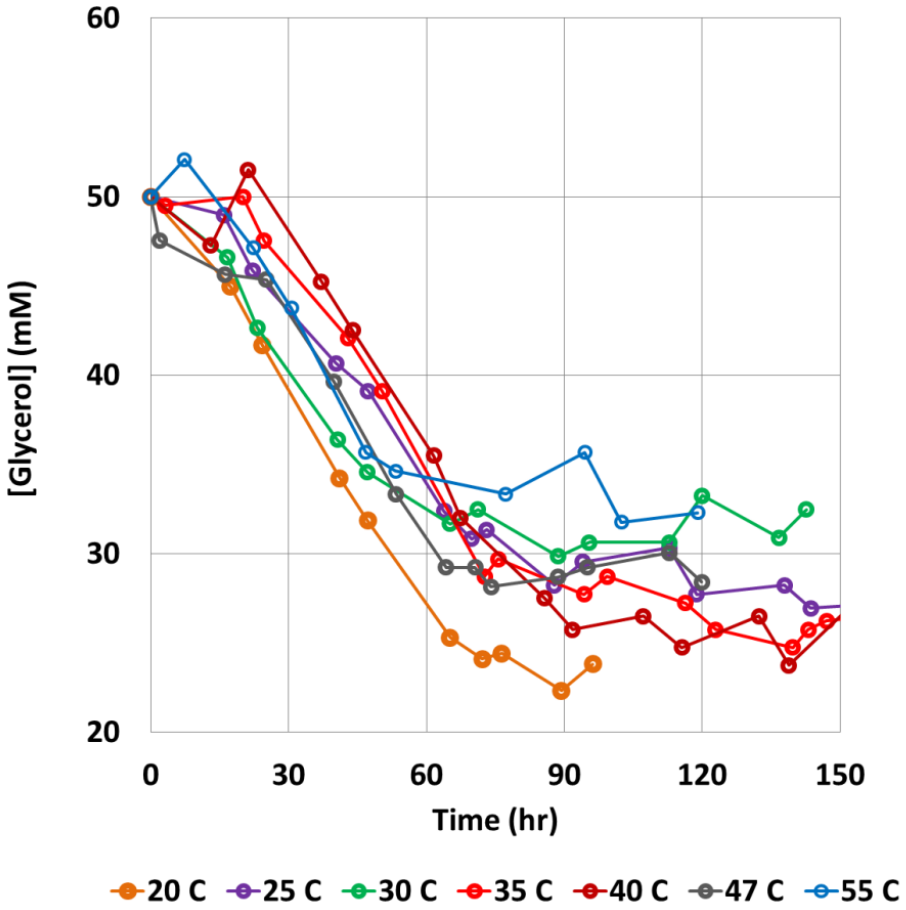

Figure II.19: Temperature effect - glycerol concentration profile: As there was no such significant difference in final substrate concentration (~22 – 25 mM), this implies the same chemical energy and reducing power gained by the culture under every of investigated temperature.

II.6. Summary

In this chapter, biohydrogen generation by the batch cyanobacterial culture, cultivated within a novel ICL flat-plate PBR, was facilitated under very well-controlled condition. The biological response of H_2 production process to individual changes in temperature and light intensity was subsequently monitored. Glycerol was demonstrated as an effective anaerobic-inducer onto cyanobacterial cultures for all of experiments. Under 35 ^oC and 92 μmol m^{-2} s^{-1}, the obtained H_2 production rate of 2.13 ml H_2 L^{-1} hr^{-1} (X = 1 g L^{-1}) and its corresponding solar-to-H_2 energy conversion efficiency of 0.716% are comparable to previously conducted studies. Uptake kinetics of key substrates – glycerol and nitrate – as well as cellular respiration were successfully computed using logistic models. Unfavourable cultivating conditions – i) depletion of essential macro-nutrients, ii) excretion of fermentative products and iii) prolonged duration of anaerobic condition – are likely to be prominent factors, driving cells into the terminal death phase. Having carried out light studies, the maximum H_2 production rate was observed to be enhanced with an increasing intensity up to an incident irradiance of 320 μmol m^{-2} s^{-1}. Within this intensity range, cells are able to grow and produce H_2 without experiencing any apparent effects of photo-inhibition. In contrast to the gas production rate, the solar-to-H_2 energy conversion efficiency decreases beyond 92 μmol m^{-2} s^{-1}, as more intense light conditions promote cellular biomass production, which in turn enhances the effect of light attenuation within the PBR system. By fitting experimental data to the developed H_2 production models, an average irradiance, at which the culture moves from photo-limitation into saturation, is located at 124 μmol m^{-2} s^{-1} under specifications of the ICL flat-plate PBR. In the case of temperature, its influence on *Cyanothece* 51142 gas production can be well-described by an Arrhenius type correlation, with an optimal temperature located at 30 ^oC. At low temperatures, H_2 production appears to be intrinsically

limited by the lower quantity of chemical energy available for driving the N_2-fixting reaction, whereas, at high temperatures, combined effects of thermal-induced reductions in nitrogenase expression (numerically beyond 30 ^{o}C) and thermal damages upon cyanobacterial light-harvesting apparatus (numerically beyond 40 ^{o}C) become prominent inhibitors.

III. Extended Hydrogen Production by using a Two-stage Continuous Flow Photobioreactor System

III.1. Introduction

One of the main limitations of biological H_2 photoproduction process is the short duration of anaerobic gas production. Regardless of species, under batch cultivation, cultures can only survive for 5 - 7 days (Kosourov, Tsygankov *et al.,* 2002) and their gas production rate generally declines within 24 hours after reaching its maximum value (Melnicki, Bianchi *et al.,* 2008, Tamburic, Zemichael *et al.,* 2012). This H_2 production duration needs to be significantly extended in order for large-scale biohydrogen production facilities to become viable.

Simultaneous conditions of anaerobiosis and nitrate-depletion are required for activation of H_2 production of the *Cyanothece* 51142 strain, as the function of the nitrogenase enzymes, catalysing gas producing reaction, is known to be rapidly inhibited in the presences of either O_2 or fixed nitrogen compounds such as nitrate or ammonium salt (Dutta, De *et al.,* 2005). However, nitrogen-deprivation causes significant biochemical stress to the cells and eventually drives them towards the death phase. In response to experiencing anaerobic conditions, microorganisms are also known to excrete a number of inhibitory by-products – organic acids as well as CO_2, which possess an acidic character and subsequently cause undesirable physiological conditions in the culture (Heritage 1996, Catalanotti, Yang *et al.,* 2013). As the rate of H_2 production is strongly dependent on the number of active *Cyanothece* 51142 cells within the system (Equation 5.37), prolonged duration of gas

production can potentially be achieved by maintaining high concentration of healthy cells, while keeping levels of both nitrate and dissolved O_2 close to zero. In principle, nitrate and O_2 enriched solutions could be precisely delivered into the liquid culture to match the cellular demands of both substrates. With adequate quantities of O_2 and nitrate, cells should be able to instantaneously use up both provided substrates for sustaining their reproduction process whilst retaining necessary conditions for H_2 production. Due to the inherent limitations of closed batch cultivation systems, where replenishment is not particularly feasible, a number of attempts have been made by applying the concept of chemical engineering process design in order to design novel PBR operation modes such as constantly- (Tamburic, Dechatiwongse *et al.,* 2013) and inconstantly-fed-batches (Kim, Kim *et al.,* 2010) and continuous processes (Lichtl, Bazin *et al.,* 1997, Fedorov, Kosourov *et al.,* 2005). Among all processes, a chemostat, which adopts the operational mode of an open continuous flow bioreactor system, appears to offer the most promising outcome, as it enables a substantial extension of the biological H_2 photoproduction period from a few days up to some months (Lichtl, Bazin *et al.,* 1997, Fedorov, Kosourov *et al.,* 2005).

The aim of this chapter is to report the successful experiments that have led to the extension of the duration of biohydrogen production by *Cyanothece* 51142 using a two-stage chemostat PBR system (Dechatiwongse, Maitland *et al.,* 2015). A series of two sequential PBRs are employed to independently handle incompatible demands by cells during two distinct phases – the growth and the H_2 production. The primary PBR mainly serves as an aerobic growth reactor, in which the *Cyanothece* 51142 biomass concentration will be maximised by the continuous provision of all essential macro-nutrients as well as trace elements. On the other hand, anaerobic and nitrate-depleting conditions will be strictly maintained within the secondary PBR for the full activation of cyanobacterial H_2 production. In order to maintain

the high level of biomass in the secondary PBR, old and nutrient-starved cells will be replaced by fully grown cells of the primary PBR. This cell feed will need to contain a nutrient concentration that is sufficient to nourish the *Cyanothece* 51142 cells without raising nitrate and O_2 levels too high and stopping the anaerobic H_2 production. Due to the required long operational period of the system, this experiment was carried out only once.

III.2. Choice of Photobioreactor

As the growth and the H_2 production of the *Cyanothece* 51142 strain possess incompatible requirements for their optimal conditions (section II.3), satisfying one process's requirement will result in physiologically unsatisfactory conditions for the other. Due to an inter-connection between these two processes, it becomes very difficult to handle this biological incompatibility within one confined system.

III.2.1. Design of a Two-Stage Continuous Flow System

In order to simultaneously handle these incompatible constraints, the concept of physical separation between the growth and the subsequent H_2 production processes was employed by using a system of two sequential PBRs, as schematically illustrated in Figure III.1.

The tubular Sartorius PBR (section I.2) was used as the primary growth reactor, in which the *Cyanothece* 51142 culture was cultivated under photoautotrophic growth conditions. A constant flow of 12.5 ml min^{-1} of sterile 20% volume of CO_2 in He was continuously sparged through the aqueous culture to provide required carbon source, facilitating the photoautotrophic growth of the cyanobacterium. With provision of CO_2 as sole carbon

source, the cyanobacterium is able to carry out photosynthetic carbon fixation and thus concurrent photosynthetic O_2 evolution. This O_2 production by cells constantly replenishes the system with O_2 substrate. In order to replenish the rest of the macro-nutrients (nitrogen, sulphur and phosphorus) and trace elements, the freshly prepared and sterile modified ASP2+N growth medium, containing 4 g $NaNO_3$ L^{-1}, was constantly supplied into the reactor via an Ismatec Reglo peristaltic pump. Theoretically, it is possible to maintain the final cell concentration, obtained during the stationary growth phase, as long as the minimum nutrient demand of the *Cyanothece* 51142 culture, under that particular condition, is met by the medium feed. These cellular demands are based on the nutrient uptake data, previously determined from the study of batch photoautotrophic growth cultivation (see section I.6).

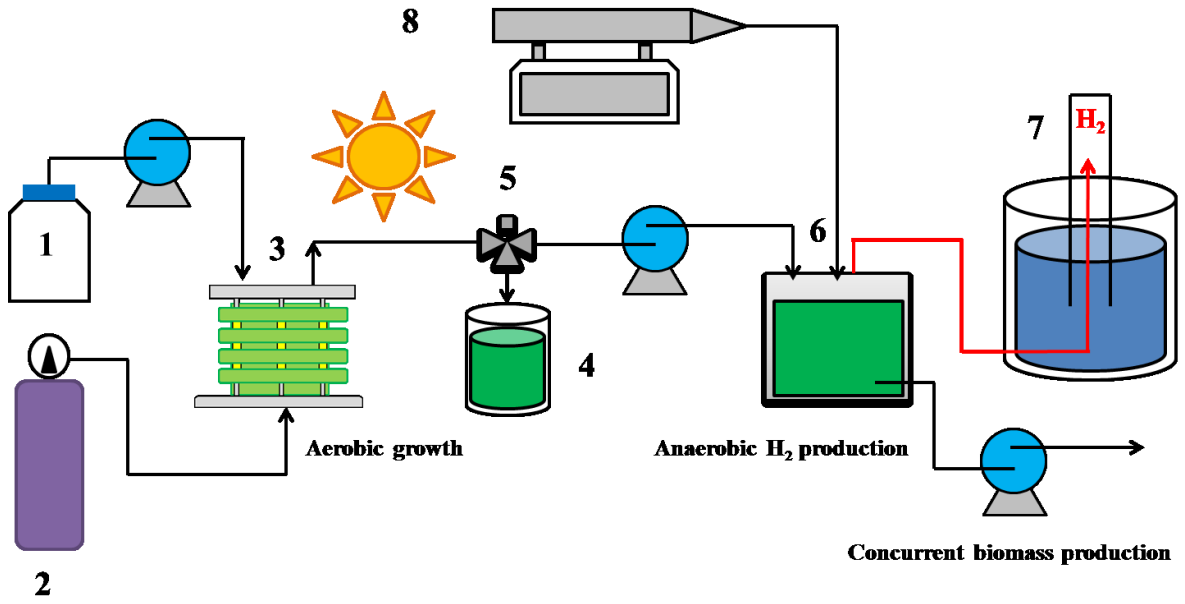

Figure III.1: Schematic process diagram of a two-stage chemostat photobioreactor system (Dechatiwongse, Maitland *et al*. 2015). Following numbers are; 1) ASP2+N medium 2) 20% volume of CO_2 in He gas cylinder 3) primary growth PBR 4) biomass tank 5) 3-way valve 6) secondary H_2-production PBR 7) water displacement system and 8) glycerol-fed dosing pump.

For the secondary H_2 production reactor, the ICL flat-plate PBR (section II.2) was employed, due to its gas-tight feature. Similar to section II.3, the *Cyanothece* 51142 culture was cultivated under photoheterotrophic growth condition using ASP2+C medium, which contains glycerol at a concentration of 50 mM. This initial provision of glycerol enhances the cellular respiration rate, which eventually turns an air-saturated into a completely anaerobic condition. In addition to being an anaerobic inducer, glycerol also has another benefit of serving as carbon source and subsequently promoting the growth of *Cyanothece* 51142 (Feng, Bandyopadhyay *et al.,* 2010). A peristaltic pump was used to replace dying cells, in the flat-plate PBR, with growing cells from the tubular PBR, whereas the replenishing of glycerol was executed by the use of a separate dosing pump. It is very important that the transfer rate of cells (and medium), enriched with NO_3^{-1} and dissolved O_2 from the primary reactor, is carefully chosen in such a way that delivery rates of these two substrates are still below rates of consumption in the secondary reactor. This is to ensure that there will be no accumulation of either NO_3^{-1} or pO_2, which would otherwise compromise gas evolution. Liquid culture is finally taken out through the drainage line at the same rate as the delivery rate in order to avoid an overflow scenario as well as to remove toxic substances excreted by cells under anaerobic conditions.

III.2.2. Experimental Operation of a Two-Stage Continuous Flow System

The experimental set-up of a two-stage continuous flow reactor system at the Department of Chemical Engineering, Imperial College London is shown in Figure III.2.

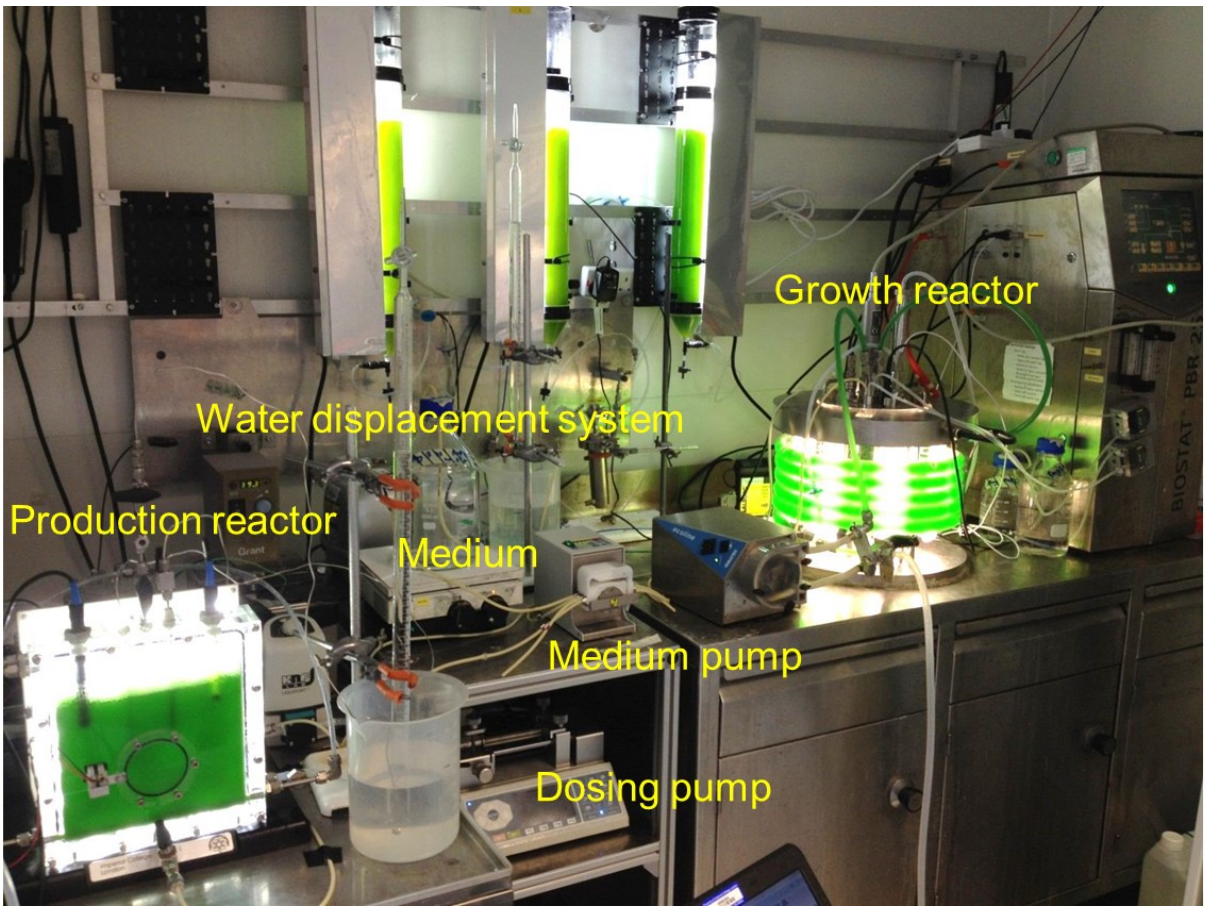

Figure III.2: Experimental set-up of a two-stage chemostat system at Department of Chemical Engineering, Imperial College London

Initially, the two reactors were started independently and operated as batch PBRs. Only once the cultures in both vessels entered the exponential growth phase, the peristaltic pump was initiated to start supplying the growth medium into the primary PBR. This is to avoid an occurrence of "wash-out" condition during the lag-phase ($\mu \sim 0$), during which any dilution rate will be greater than μ. To maintain a constant liquid level within the growth PBR, the culture was removed from the reactor, at the same rate as the medium being fed in, and later collected into a biomass collection tank. As soon as H_2 evolution was detected in the secondary PBR, the direction of a 3-way valve was changed in such a way to deliver cells into that bioreactor, instead of the collection tank. Eventually, the drainage of the flat-plate PBR was fully opened and the liquid was pumped out at the same rate as the cells being fed in. Under this arrangement, the entire system could then be regarded to be operating under "chemostat" control.

For both reactors, the cultures of *Cyanothece* 51142 were cultivated under continuous illumination with a fixed light intensity of 92 μmol m^{-2} s^{-1} and constant temperature of 35 $^{\circ}$C. This selection is based on results from Results and Discussions: Chapters I and II, which show that, under these cultivating conditions, the cyanobacterium is able to grow and produce H_2, without experiencing any photo- or thermal inhibitions. The control of pH inside the primary tubular PBR is possible by means of an automated acid / base pumping system and its value was maintained at pH of 7. During chemostat operation, the glycerol dosing pump was initiated to constantly provide the carbon substrate source for the H_2-producing cells inside the flat-plate PBR. During this particular study, the pumping rate of the peristaltic pump was fixed at 0.2 ml min^{-1}. The detailed explanation for this selection will be provided later in sections III.3.1 and 2.

In contrast to the batch operation (section II.3), the measurement of H_2 production was executed using a classical water displacement method, as the measuring stability of the MIMS technique was found to be severely compromised by cell transfer into / out of the secondary PBR (data not shown). For the set-up of this technique, one free port at the top of the ICL flat-plate PBR was connected to an inverted measuring cylinder, which was initially filled with water, via H_2-impermeable stainless steel tube. Once cells enter the H_2 production phase, the formed gas flows through the metallic tube and is eventually captured at the top of the cylinder. The collected gas pushes the water downwards; consequently, the volume of gaseous H_2 produced was equated to the volume of displaced liquid water. In parallel, injection mass spectrometry was employed to confirm that the gas collected was actually H_2 as well as to quantitatively determine its purity.

III.3. Performance of a Two-Stage Continuous Flow System

III.3.1. Primary Growth PBR

Using the described chemostat system, an active culture of *Cyanothece* 51142 was successfully maintained for 750 consecutive hours (~31 days), see Figure III.3. The chemostat-cultivated cyanobacterium displayed similar growth behaviour to the batch microbial growth cycle (Tomaselli 2004), with exceptions of a significantly extended stationary phase as well as an unobserved death phase.

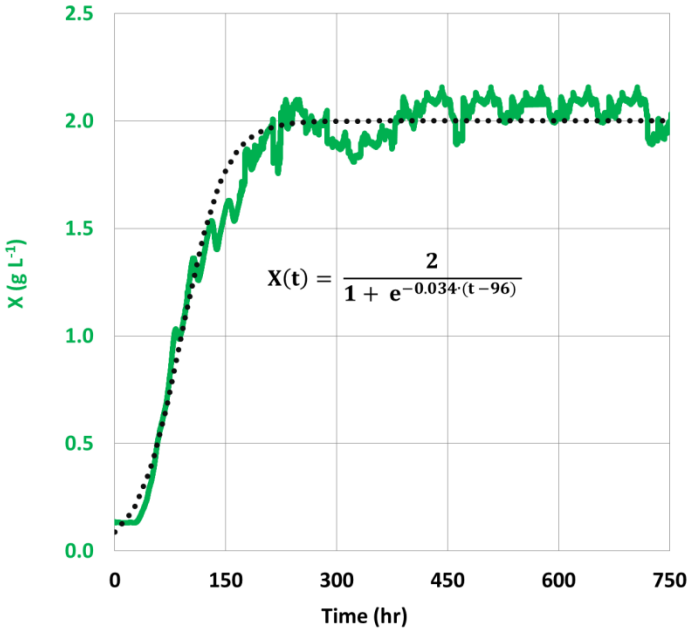

Figure III.3: The chemostat growth profile of *Cyanothece* 51142 can be perfectly described by logistic model. Under this particular study, μ_{max} was found to be 0.034 hr^{-1}, which is comparable to that previously determined from batch cultivation under the same growth condition.

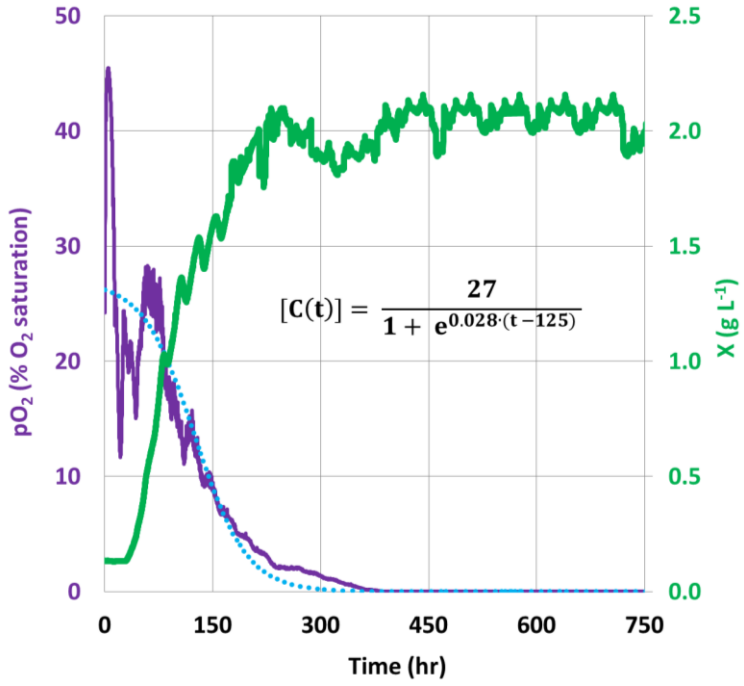

Figure III.4: A steady-state condition was confirmed by a constant profile of dry biomass concentration from time = 300 hr onwards. The specific O_2 consumption rate was determined to be 0.028 hr^{-1}, by fitting the pO_2 profile with a logistic nutrient uptake model (the light blue dotted line).

After the initial lag phase of approximately 24 hr, in the presence of sufficient light, nutrients and O_2, the *Cyanothece* 51142 culture started to enter its secondary exponential growth phase. At that time, the peristaltic pump was started to feed the ASP2+N growth medium into the primary tubular PBR with the flow rate of 0.2 ml min^{-1}. As the working volume of the PBR is 2,900 ml, using Equation 5.38, this feed rate is equivalent to the dilution rate (D) of 0.0041 hr^{-1}. Under nitrogen-replete and photoautotrophic growth condition, previously determined maximum specific growth rate of growing batch *Cyanothece* 51142 culture is 0.033 hr^{-1}, when an irradiance of 92 μmol m^{-2} s^{-1} is applied (section I.6). As the growth rate is much greater than the dilution rate (around 8 times), currently used feed rate will not lead to a "wash out" situation and was subsequently employed. In this particular study, the cells are able to reach a mean dry biomass concentration of 2 g L^{-1} and a maximum specific growth rate of 0.034 hr^{-1}. Similar to previous chapters, the value of these two growth parameters were determined by fitting the growth profile to a logistic model (Equation 5.29). As the μ_{max} obtained from both, batch and chemostat, processes are very similar, this thus confirms the reliability and reproducibility of the first growth reactor.

During the first 80 hours the pO_2 profile shows an oscillating pattern, after which a steady decline occurs, see Figure III.4. The former observation was expected, due to the previously reported circadian behaviour of *Cyanothece* 51142 strain, during which photosynthetic carbon fixation and its concurrent O_2 evolution are periodically performed in an approximately 12 hour cycle during subjective light periods (Schneegurt 1994, Bandyopadhyay, Elvitigala *et al.,* 2013). For the latter observation, it can be explained as the consequence of a mutual shading effect (Figure III.5), which is eventually induced under dense culture conditions, as discussed before in section I.3. In this scenario, most of cells have insufficient access to light source and thereby experiencing light-limitation.

Consequently, the activity of light-dependent photosynthesis (and its O_2 production) becomes significantly reduced. However, the rate of cellular respiration does not remain the same, but rises as the culture matures. Eventually, the rate of O_2 consumption will surpass the rate of its production, thus inducing a net decline of pO_2 in the aqueous phase. With insufficient O_2 substrate, the cyanobacterium is not able to effectively carry out an aerobic respiration to regain chemical energy from its photosynthetically fixed carbon – glycogen for *Cyanothece* 51142 strain (Schneegurt, Sherman *et al.,* 1997) - and therefore its growth rate is subsequently reduced.

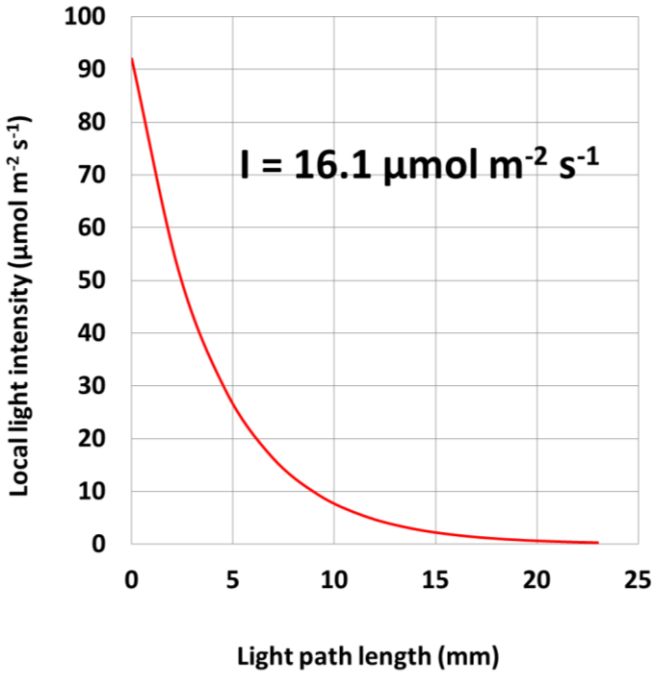

Figure III.5: With a steady-state biomass concentration of 2 g L^{-1}, the mutual shading scenario was confirmed; more than half of cells within the primary PBR experienced light-limited conditions. Under this condition, an incident light intensity of 92 µmol m^{-2} s^{-1} was significantly reduced to an average value of 16.1 µmol m^{-2} s^{-1}.

In a scenario, where a decreasing rate of reproduction is equal to the rate of cellular loss – the sum of the rate of cellular death and the rate of cell outflow by pumping – the rate of biomass accumulation becomes zero and results in an eventual constant culture density. From section II.3, as an anaerobic-induced decay rate was previously estimated as 0.004 hr^{-1}, together with known dilution rate of 0.0041 hr^{-1}, this thus infers that, during the stationary growth phase of chemostat operation, the specific growth rate of the *Cyanothece* 51142 culture is approximately 0.0081 hr^{-1}, which is around 4.2 time lowers than its maximum value. The numerical calculation using Equation 5.39 is as follows:

$$\frac{dX_1}{dt} = (\mu_1 - D_1 - \mu_{d1}) \cdot X_1(t)$$

With steady biomass concentration, $\frac{dX_1}{dt} = 0$

The equation becomes, $0 = (\mu_1 - D_1 - \mu_{d1}) \cdot X_1(t)$

Rearrange, $\mu_1 = D_1 + \mu_{d1} = 0.0041 + 0.004 = 0.0081\ hr^{-1}$

In contrast to previous batch photoautotrophic cultivation (section I.6), during which a continuously declining profile of substrate concentrations is normally observed, under chemostat operation, the nitrate concentration increases at the beginning of the experiment up to time = 300 hr, after which its level remains approximately constant for the remaining time of the experiment, see Figure III.6.A. The initial increase in nitrate concentration can be explained by the fact that the culture is initially diluted and the delivery rate of nitrate is much higher than the total rate of nitrate loss (sum of rate of nitrate consumption by cells and

rate of nitrate outflow via pumping). As a consequence, the rate of change of nitrate concentration with respect to time becomes positive and drives the concentration up to its final value of 1,500 mg NO_3^{-1} L^{-1}. By having a steady biomass concentration, a constant consumption rate for nitrate is expected and confirmed by its constant concentration profile. Under such conditions, at which there is no change in biomass and NO_3^{-1} concentrations with respect to time, the chemostat-cultivated *Cyanothece* 51142 culture has achieved a physiological steady-state condition. Using Equation 5.41, the steady-state nitrate uptake rate is equal to the difference between nitrate delivery rate and its outflow rate and can be subsequently calculated as 5.81 mg NO_3^{-1} L^{-1} hr^{-1}. The numerical derivation of Equation 5.41 is as follows:

$$\frac{dS_1}{dt} = D_1 \cdot (S_0 - S_1) - R_{s1}$$

$$\text{Under steady} - \text{state condition,} \quad \frac{dS_1}{dt} = 0$$

$$\text{The equation becomes,} \quad 0 = D_1 \cdot (S_0 - S_1) - R_{s1}$$

$$\text{Rearrange,} \quad R_{s1} = D_1 \cdot (S_0 - S_1)$$

As D_1 = 0.0041 hr^{-1}, whereas S_0 and S_1 = 2,917 and 1,500 mg NO_3^{-1} L^{-1} respectively, R_s can be numerically worked out as 5.81 mg NO_3^{-1} L^{-1} hr^{-1}, which is equivalent to 0.094 mmol NO_3^{-1} L^{-1} hr^{-1}.

Unlike nitrate, the sulphate concentration remains approximately constant for a whole

experiment, with the mean value of 1,930 mg SO_4^{-2} L^{-1} (see Figure III.6.B). Using the same derivation of Equation 5.41, D = 0.0041 hr^{-1}, whereas S_0 and S = 1,952 and 1,930 mg SO_4^{-2} L^{-1}, the cellular consumption rate of sulphate, at steady-state, is estimated as 0.09 mg SO_4^{-2} L^{-1} hr^{-1} (0.00095 mmol SO_4^{-2} L^{-1} hr^{-1}). On a molar basis, the sulphate demand is around 100 times less than that of nitrate. Even the quantity of phosphate present in the medium is too low to be analysed by IC technique (as mentioned in section 5.8.2 of Experimental Methods), a non-inhibitive effect of phosphorus starvation on the growth of *Cyanothece* 51142 strain is previously confirmed by Sinetova's work (Sinetova, Červený *et al.,* 2012).

Figures III.6.A and B: Growth and macro-nutrient concentration dynamics of the cyanobacterium *Cyanothece* 51142, cultivated under the photoautotrophic growth condition in the primary tubular PBR. A) Nitrate and B) Sulphate

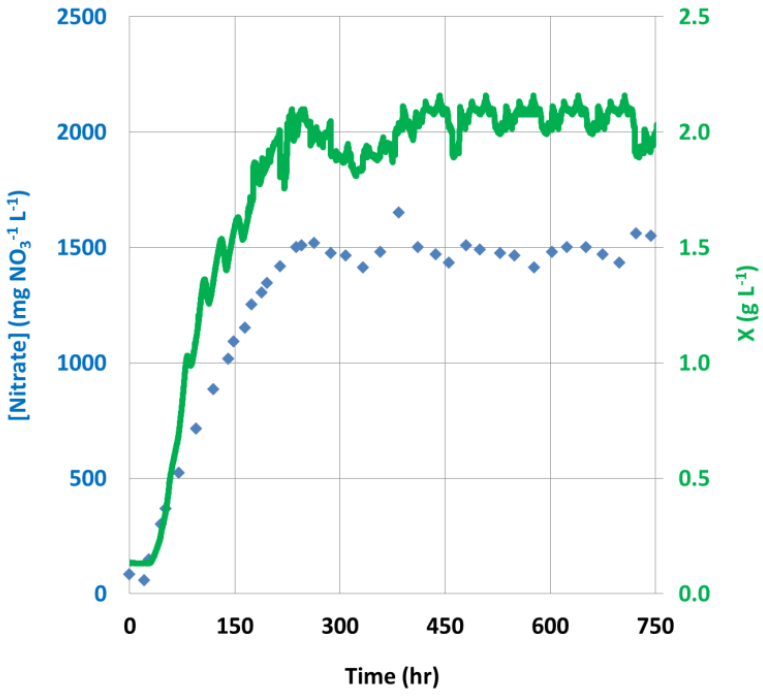

Figure III.6.A: By having a steady biomass concentration, a constant consumption rate for nitrate is expected and confirmed from time = 300 hours onwards. Under such conditions, the chemostat-cultivated culture achieved a physiological steady state condition.

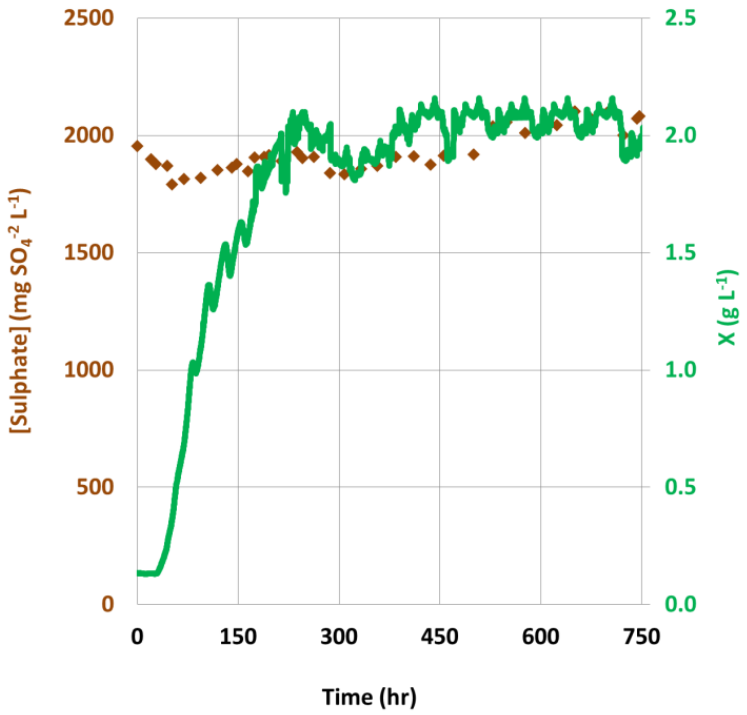

Figure III.6.B: Unlike nitrate, sulphate concentration remains approximately constant for a whole experiment, with the mean value of 1,930 mg SO_4^{-2} L^{-1}.

As nitrate is no longer a limiting substrate, in this particular study, it is possible that the carbon source (from CO_2 supply) may become limited instead. Although an analytical technique to directly measure dissolved CO_2 concentration (e.g. using pCO_2 electrode), was not present in my laboratory, at the time of conducting this experiment, the carbon availability within the primary growth PBR can be numerically estimated using Equations 5.43 – 5.47. As mass transfer properties of CO_2 and O_2 are correlated as proposed by Royce and Thornhill (Royce and Thornhill 1991) (Equation 5.43), the numerical approach will begin with an extraction of the volumetric gas–liquid mass transfer coefficient for oxygen ($k_L{}^{O_2}a$) from the pO_2 profile. Then, it becomes possible to estimate the CO_2 mass transfer coefficient ($k_L{}^{CO_2}a$) and the corresponding CO_2 flux flowing into the liquid culture. Calculations are shown below:

Due to its low solubility in water, it is commonly accepted that the rate-determining step for O_2 transport from air bubbles to the cells is primarily controlled by the liquid film resistances. Therefore, the overall O_2 mass transfer coefficient is approximately equal to the local coefficient in liquid phase (Garcia-Ochoa and Gomez 2009). Numerically, ${k_L}^{O_2}a$ can be estimated using Equation 5.44.

$$\frac{d[O_2]}{dt} = {k_L}^{O_2}a \cdot ([O_2{}^*] - [O_2]) + D_1 \cdot ([O_2]_0 - [O_2]) - R_{O_2}$$

Under steady-state conditions, $\frac{d[O_2]}{dt} = 0$

The fed medium is assumed to be air-saturated, so $[O_2]_0$ = 21% O_2 saturation ~ 1.22 g O_2 m^{-3} (unit conversion was made using Equation 5.13)

The steady-state dissolved O_2 concentration in the liquid culture ($[O_2]$) = 0 (see Figure III.4)

The theoretically saturated concentration of O_2 ($[O_2{}^*]$) was estimated to be 0.23 mol O_2 m^{-3} ~ 7.35 g O_2 m^{-3} using Henry's law (Equation 5.45 and 5.47) (see calculations in Appendixes).

The equation thus becomes, $0 = {k_L}^{O_2}a \cdot [O_2{}^*] + D_1 \cdot [O_2]_0 - R_{O_2}$

Rearrange, $${k_L}^{O_2}a = \frac{R_{O_2} - D_1 \cdot [O_2]_0}{[O_2{}^*]}$$

The maximum specific O_2 consumption rate was determined to be 0.028 hr^{-1}, by fitting the pO_2 profile with a logistic nutrient uptake model (Equation 5.30). The fitted data are

represented as the light blue dotted line onto Figure III.4. Given that a continuous decline in pO_2 value starts from time = 70 hr, the total quantity of O_2 uptake was chosen as 27 % O_2 saturation ~ 1.57 g O_2 m^{-3} (unit conversion was made using Equation 5.13). As a result, an estimation of the total O_2 uptake rate ($[R_{O_2}]$), which is the multiplier between the specific uptake rate and the total substrate consumed, can be executed as 0.044 g O_2 m^{-3} hr^{-1}. By substituting all obtained values into the mass balance (Equation 5.44), the value of ${k_L}^{O_2}a$ can eventually be worked out as 0.168 hr^{-1}.

Once ${k_L}^{O_2}a$ is known, the value of ${k_L}^{CO_2}a$ can be practically estimated, using Equation 5.43, as 0.149 hr^{-1}. To indicate whether the culture is under CO_2-limited or not, Equation 5.44 was re-employed to describe the CO_2 mass balance over the primary growth PBR.

$$\frac{dC_{CO_2}}{dt} = {k_L}^{CO_2}a \cdot ([CO_2{}^*] - [CO_2]) + D_1 \cdot ([CO_2]_0 - [CO_2]) - R_{CO_2}$$

Under steady-state conditions, $\frac{dC_{CO_2}}{dt} = 0$

Since there is virtually no CO_2 saturated in the fed medium, so $[CO_2]_0 = 0$

The equation thus becomes, $0 = {k_L}^{CO_2}a \cdot ([CO_2{}^*] - [CO_2]) - D_1 \cdot [CO_2] - R_{CO_2}$

Rearrange, $[CO_2] = \frac{{k_L}^{CO_2}a \cdot [CO_2{}^*] - R_{CO_2}}{D_1 + {k_L}^{CO_2}a}$

The theoretically saturated concentration of CO_2 ($[CO_2{}^*]$) was again calculated using Henry's law (Equation 5.45 and 5.46) and subsequently found to be 1,375 g CO_2 m^{-3} (see calculations

in Appendixes).

As the content of an elemental carbon is accounted for 40 % of *Cyanothece* 51142 (Schneegurt, Arieli *et al.,* 1995), it is possible to estimate a steady-state CO_2 consumption rate as follows:

$$R_{CO_2} = \mu_1 \cdot X_1(t) \cdot \frac{X_{C1}(t)}{X_1(t)} \cdot \frac{Mw_{CO_2}}{Mw_C}$$

Under steady-state, μ_1 is 0.0081 hr^{-1}, $X_1(t)$ = 2 g biomass L^{-1}, $\frac{X_{C1}(t)}{X_1(t)}$ = 0.4 g C b biomass^{-1}, Mw_{CO_2}= 44 g CO_2 mol^{-1} and Mw_C = 12 g C mol^{-1}. Consequently, R_{CO_2} is calculated to be 0.24 g CO_2 L^{-1} hr^{-1} ~ 237.6 g CO_2 m^{-3} hr^{-1}.

By replacing all of parameters with their known values, the value of dissolved CO_2 concentration ($[CO_2]$) within the liquid culture of the primary PBR was numerically found to be -183 g CO_2 m^{-3}, thereby indicating the carbon deficiency within the cyanobacterial culture. Therefore, it can be concluded that, for the chemostat experiment, the carbon-starvation appears to be the primary trigger, transforming the cyanobacterial growth behaviour from the exponential into the stationary phase at time = 300 hr. Nevertheless, this carbon scarcity only corresponds to 2.5 % of *Cyanothece* 51142 dry biomass and its subsequent effect on the cyanobacterial growth was unobserved (see calculation in Appendixes).

III.3.2. Secondary H_2 Production PBR

Before time = 70 hr, the secondary ICL flat-plate PBR was started up and operated as an independent batch system. Using a logistic model (Equation 5.29), the maximum specific

growth rate, between time = 20 and 70 hr, was subsequently determined as 0.076 hr^{-1} (black dotted line in Figure III.7), which is comparable to the rate, previously observed from the batch *Cyanothece* 51142 culture, cultivated under similar photoheterotrophic growth conditions – 0.07 hr^{-1} (section II.3). Noticeably, this photoheterotrophic growth rate is approximately 2-fold higher than the photoautotrophic rate, previously found in section III.3.1. The reason for this is the different type of utilised carbon substrate between both growth conditions. For photoheterotrophic growth, CO_2 was replaced by organic glycerol. These findings agrees with Feng's work (Feng, Bandyopadhyay *et al.,* 2010), which reports a similar growth enhancement. After implementation of chemostat operation for the flat-plate PBR at time = 70 hr - shortly after onset of anaerobiosis, the biomass concentration of the cyanobacterial culture continued to increase, albeit with approximately 4 times lower growth rate of 0.017 hr^{-1} (red dotted line on the same figure), before reaching the final value of 1.5 g L^{-1} at time = 300 hr. After complete consumption of pO_2 and nitrate, at time = 50 and 68 hours, respectively (Figures III.8.A and III.8.B), the growth of the *Cyanothece* 51142 culture reduces to its minimal value. As the observed secondary growth rate is very close to the dilution rate of the flat-plate PBR (0.015 hr^{-1}, calculated using Equation 5.38 and working PBR volume of 800 ml), this implies that an increase in biomass concentration, during the secondary exponential phase, is primarily due to the transfer of healthy and dense cells from the primary PBR. The marginal difference between the growth and dilution rates most likely derives from the fact that, even in the absence of NO_3^{-1} source, microorganisms can still grow by relying on N_2 from an initially sparged air (Reddy, Haskell *et al.,* 1993).

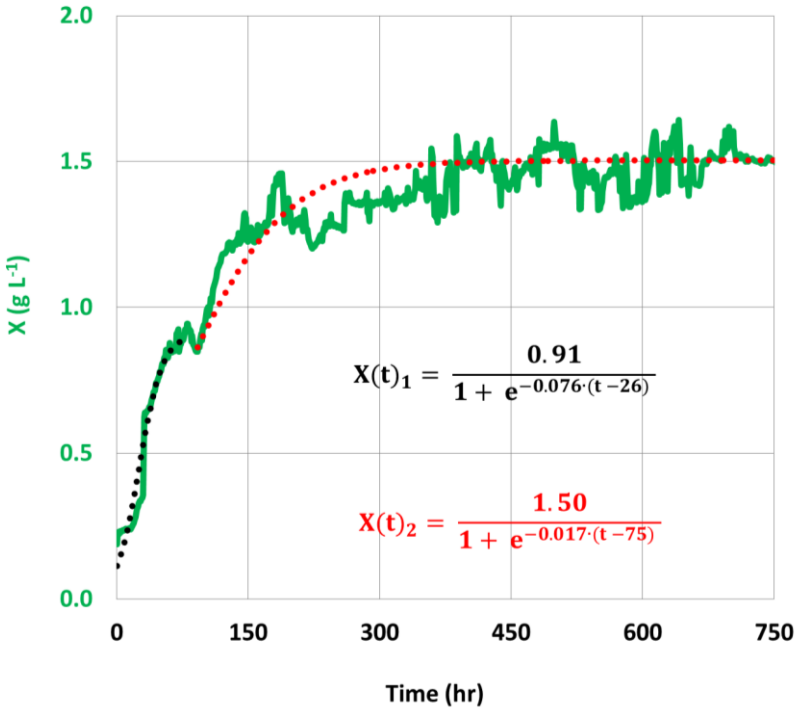

Figure III.7: Using a logistic model, μ_{max} of the batch *Cyanothece* 51142 culture is found to be 0.076 hr^{-1}, whereas that of the chemostat culture is estimated as 0.017 hr^{-1}. As the cyanobacterial growth rate is reduced to its minimal value under nitrate depletion and anaerobic conditions, the latter rate is approximately equal to the dilution rate of the flat-plate system (D = 0.015 hr^{-1})

Figures III.8.A - D: Growth, pO_2 and macro-nutrient concentration dynamics of the cyanobacterium *Cyanothece* 51142, cultivated under the photoheterotrophic growth condition in the secondary flat-plate PBR. A) pO_2, B) Nitrate, C) Sulphate and D) Glycerol.

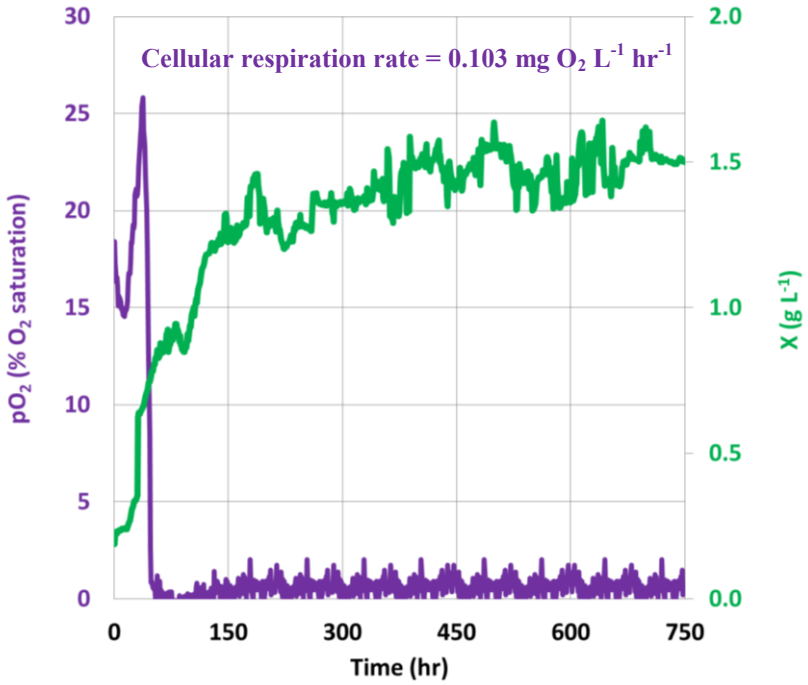

Figure III.8.A: By ensuring that delivery rate of cells, enriched with O_2, is below the cellular respiration rate of *Cyanothece* 51142 culture, it is possible to maintain anaerobic conditions inside the secondary PBR, throughout an experiment.

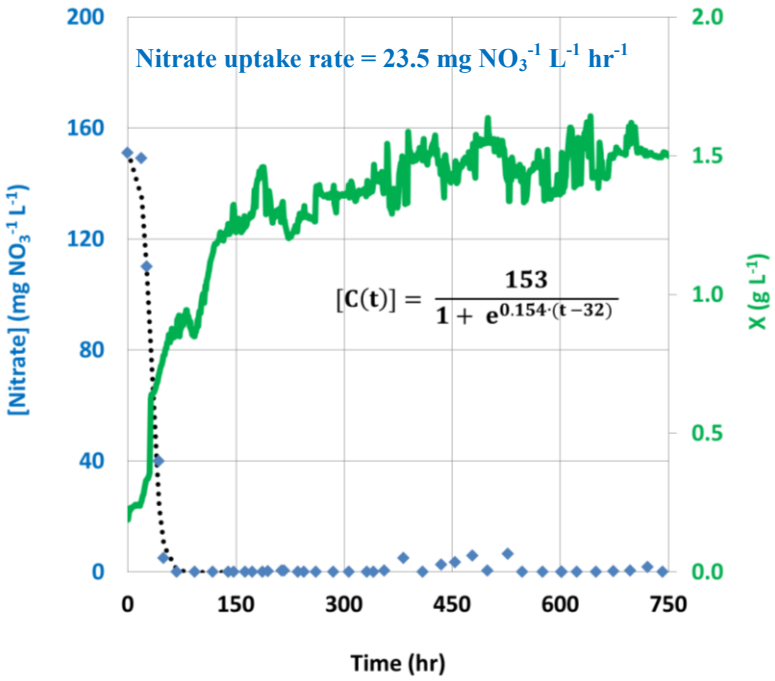

Figure III.8.B: By using a similar approach to the pO_2 profile, the nitrate concentration inside the flat-plate PBR was successfully controlled close to zero for the full activation of nitrogenase enzymes.

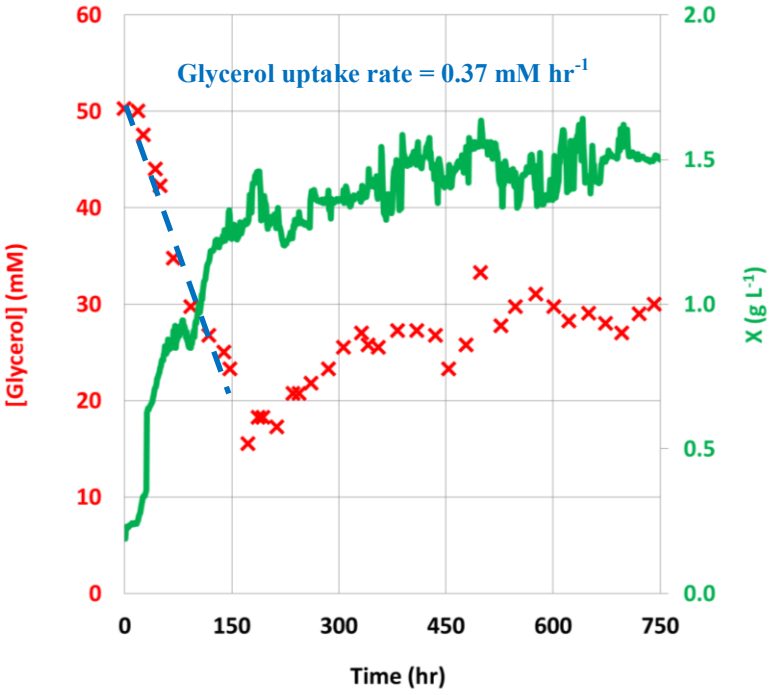

Figure III.8.C: Under batch operation, the glycerol uptake rate of *Cyanothece* 51142 culture was 0.37 mM hr^{-1}. By precisely delivering glycerol solution to match its demand, the constant concentration level of this substrate was eventually obtained from time = 300 hours onwards.

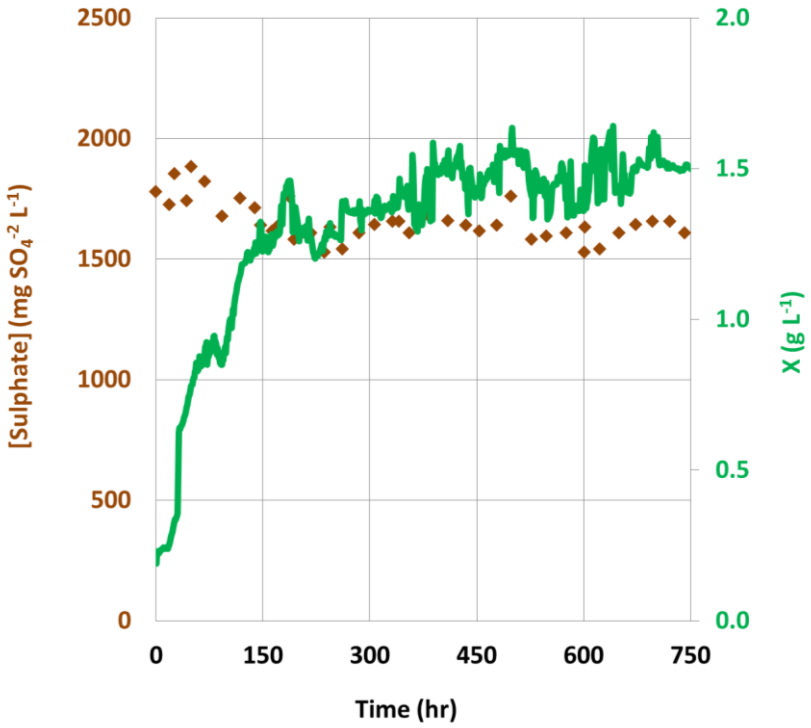

Figure III.8.D: Upon achieving steady-state conditions, sulphate concentration became constant at the mean value of 1,633 mg SO_4^{-2} L^{-1} hr^{-1}.

In contrast to a batch-cultivated culture (section II.3), for which cellular death started to take place at time = 95 hr, the chemostat-cultivated culture of *Cyanothece* 51142 was maintained healthy and active for more than 750 consecutive hours. Steady-state conditions appear to be established inside the secondary flat-plate PBR at time = 300 hours, after which there was no change in any properties of the culture with respect to time, see Figure III.8A - D. As cultures cultivated in the two distinct, but interconnected PBRs attained a steady-state environment at the same time, these observations thus demonstrate the high fidelity of my obtained experimental data. Remarkably, the final biomass concentration obtained from the chemostat system is also 1.5 times higher than that of the batch system. This improvement is due to the advantages of using a continuous flow operation, which allows i) replacement of nutrient-starved, old cells with fully grown, active cells and ii) replenishment of nitrate and dissolved

O_2 into the aqueous culture of the secondary PBR, which would be required by the cyanobacterium to grow and survive. However, as mentioned previously in section III.2.1, this operation is critically dependent on the correct pumping rate, which does not lead to the cumulative build-up of either substrate inside the system. Using Equation 5.48, it is possible to estimate the potential delivery rate for nitrate and dissolved O_2, providing that the concentration of both substrates inside the primary tubular PBR are known. The highest observed value was chosen as an input for each case – the nitrate concentration of 1,500 mg NO_3^{-1} L^{-1} and pO_2 of 45 $\%O_2$ saturation. It should be noted here that even though the pO_2 level of the primary PBR actually decreases, as time proceeds, it was decided to fix the input at its maximum level for ease of calculation. With a fixed pumping rate of 0.2 ml min^{-1} (= 12 ml hr^{-1}), this would result in corresponding nitrate and the O_2 delivery rates (into the flat-plate PBR) of 22.5 mg NO_3^{-1} $L^{-1}hr^{-1}$ and 0.675 $\%O_2$ hr^{-1} (~ 0.038 mg O_2 L^{-1} hr^{-1}) respectively. Calculations are shown below:

$$\text{Delivery rate, nitrate} = \frac{12\,\frac{\text{ml}}{\text{hr}} \cdot 1500\,\frac{\text{mg}}{\text{L}}}{800\ \text{ml}} = 22.5\ \text{mg}\ {NO_3}^{-1}\ \text{L}^{-1}\ \text{hr}^{-1}$$

$$\text{Delivery rate, dissolved oxygen} = \frac{12\,\frac{\text{ml}}{\text{hr}} \cdot 45\ \%\text{O}_2}{800\ \text{ml}} = 0.675\ \%\text{O}_2\ \text{hr}^{-1}$$

As both estimated values are still below their corresponding consumption rates by the cells – 26 mg NO_3^{-1} L^{-1} hr^{-1} and 0.082 mg O_2 L^{-1} hr^{-1} (previously determined in section II.3), this implies that no accumulation will occur and subsequently ensures that 0.2 ml min^{-1} is an appropriated pumping rate under these particular experimental conditions. Clear evidence, supporting these calculations, can be seen from Figures III.8.A and B, which display simultaneously well-maintained states of anaerobiosis and nitrate-depletion, once they were

established inside the system.

The mass balance of cells, cultivated in the secondary PBR, is described by Equations 5.40. Using this equation, it is possible to estimate the steady-state specific growth rate of *Cyanothece* 51142 culture as follows:

$$\frac{dX_2}{dt} = (\mu_2 - \mu_{d2}) \cdot X_2(t) + (X_1 - X_2) \cdot D_2$$

Under steady-state conditions, $\frac{dX_2}{dt} = 0$

The equation thus becomes, $0 = (\mu_2 - \mu_{d2}) \cdot X_2(t) + (X_1 - X_2) \cdot D_2$

After time = 300 hour, X_1 and X_2 become independent of time and their values can be fixed at mean values of 2 and 1.5 g L^{-1} respectively. Both dilution and decay rates were previously estimated as 0.015 and 0.0041 hr^{-1}, respectively. By substituting all known values into the derivative of Equation 5.40, μ_2 can be subsequently calculated as -0.0009 hr^{-1}. This negative value of μ implies that, during stationary phase, the culture of the secondary PBR did not reproduce and in fact its constant biomass concentration profile was induced by the right balance between the rate of healthy cells being fed into the flat-plate PBR and its corresponding loss rate, taking into account decay and outflow terms.

In terms of uptake kinetics, it can be seen from Figures III.8.A – C that, under batch operation - time before 70 hour, the cellular respiration rate as well as nutrient consumption rates of nitrate and glycerol are comparable to those previously determined in section II.3,

thereby confirming a high degree of reproducibility of results. An eventual substrate uptake rate, during steady-state conditions, can be determined using the chemostat substrate model (Equation 5.42), as shown below:

$$\frac{dS_2}{dt} = D_2 \cdot (S_1 - S_2) - R_{s2}$$

Under steady-state conditions, $\frac{dS_2}{dt} = 0$

The equation thus becomes, $0 = D_2 \cdot (S_1 - S_2) - R_{s2}$

Rearrange, $R_{s2} = D_2 \cdot (S_1 - S_2)$

For nitrate, as the concentration of this substrate inside the secondary PBR is virtually zero throughout a whole experimental duration, its steady-state total uptake rate is simply equal to the delivery rate of 22.5 mg NO_3^{-1} L^{-1} hr^{-1}. In the case of sulphate, the mean concentrations within the primary (1,930 mg SO_4^{-2} L^{-1}) and the secondary (1,633 mg SO_4^{-2} L^{-1} hr^{-1}) PBRs were chosen as S_1 and S_2 respectively. As a result, this yields the steady-state consumption rate of 4.46 mg SO_4^{-2} L^{-1}.

A separate dosing pump was employed to deliver concentrated glycerol solution directly into the liquid phase of the flat-plate PBR. Consequently, the chemostat substrate model was modified by replacing $D_2 \cdot S_1$ with a new constant called F_{gly}, which represents the glycerol feed rate.

The equation thus becomes, $R_{s2} = F_{gly} - D_2 \cdot S_2$

The mean glycerol concentration, during steady-state conditions, of 27.8 mM was chosen as S_2. Experimentally, glycerol was fed at the rate of 0.46 mM hr^{-1}, which is 1.2 times higher than its actual demand (0.38 mM hr^{-1}) to ensure carbon sufficiency. This marginal difference then explains an increase in the level of glycerol between time = 200 and 300 hour (Figure III.8.C), after which it was balanced by cellular consumption of this carbon substrate, which is calculated as 0.043 mM hr^{-1}.Under non-growth condition, all glycerol demand is subsequently utilised to support the H_2 production of *Cyanothece* 51142 culture.

III.3.3. Chemostat H_2 Production

Having been able to satisfy requirements, necessary to activate cyanobacterial H_2 production – simultaneous nitrate-depletion and anaerobic conditions, together with maintaining the final biomass concentration, the two-stage chemostat system then delivered a continuous production of H_2 for more than 680 hours (Figure III.9), which led to a final cumulative yield of 1750 ml H_2. In order to confirm the presence of H_2 in the produced gas, the technique of injection mass spectrometry was subsequently employed. From the analysis, a similar gas composition profile to the batch H_2 experiment (Figure II.4 in section II.3) was again observed (Figure III.10), with a clear H_2 signal as soon as the value of pO_2 reached zero. A mean CO_2 concentration of less than 3 mol% was again observed with the main gas constituent being H_2. Samples prepared from the *Cyanothece* 51142 culture were also analysed using NMR technique, which, however, did not show any excreted organic by-products as seen before in batch cultivation (see Figure III.11). This observation thus suggests that these compounds, with already low concentration, are being washed out of the

system.

During steady-state conditions (after time = 300 hour), H_2 production rate, estimated from the gradient of H_2 yield over time, eventually reached 2.6 ml H_2 hr^{-1} ~ 3.3 ml H_2 L^{-1} hr^{-1}, which is around 1.5-fold higher than the maximum productivity previously obtained in the batch process (see section II.3). Noticeably, this increment is the same factor as the enhancement in the final biomass concentration and can be explained by the linear dependence of gas production upon the quantity of biomass present in the PBR (Equation 5.37). By comparing with other benchmarks, the rate is approximately 5.7 times higher than the steady-state rate, observed from a two-stage chemostat-green algal *C. reinhardtii* PBR system (Fedorov, Kosourov *et al.,* 2005), but 6.6-fold lower than the optimal productivity (~ 22 ml L^{-1} hr^{-1}) of a single-stage chemostat-*Nostoc flagelliforme* PBR (Lichtl, Bazin *et al.,* 1997). However, as perturbation studies have not been executed in this chemostat system, the rates reported here are by no means optimal. It is proposed that it could be possible to enhance the rate further by employing an optimal dilution rate for the secondary PBR as well as cultivating the cyanobacterial culture in the primary PBR under alternating light / dark cycles. The former approach will ensure an optimal length of residence time for the cyanobacterial H_2-producing mechanism to take place, whereas the maximum levels of nitrogenase activities will be induced by the latter (Toepel, Welsh *et al.,* 2008).

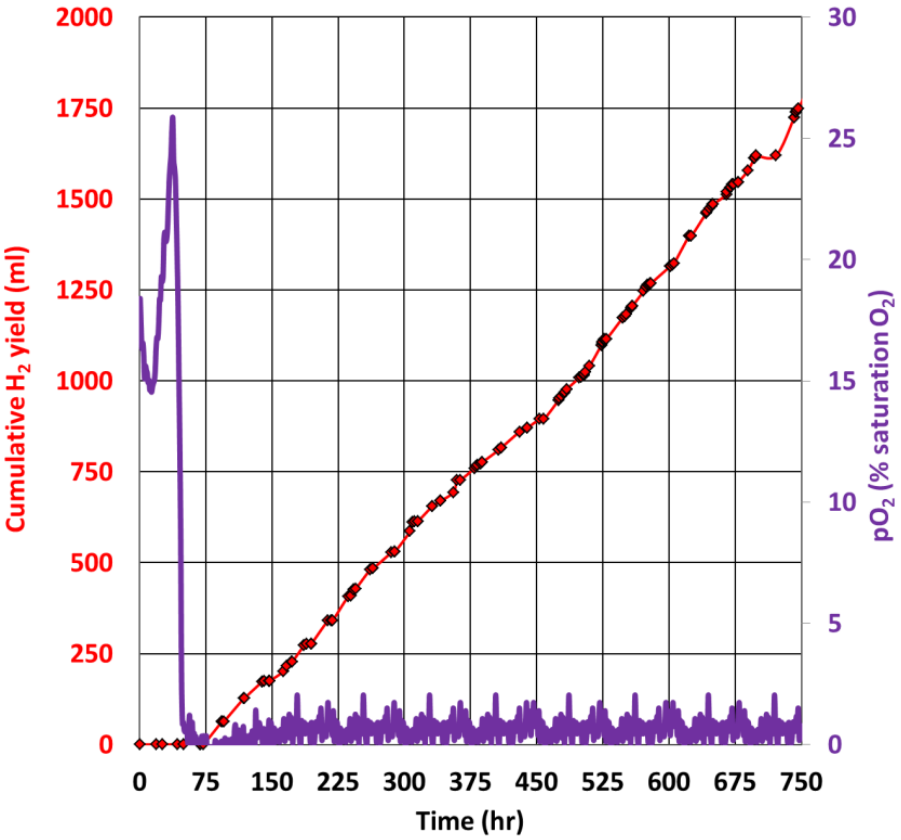

Figure III.9: More than 27-day continuous H_2 production by the cyanobacterium *Cyanothece* 51142, cultivated in a two-stage chemostat bioreactor system. The onset of gas evolution was observed as soon as anaerobic conditions were established inside the flat-plate PBR.

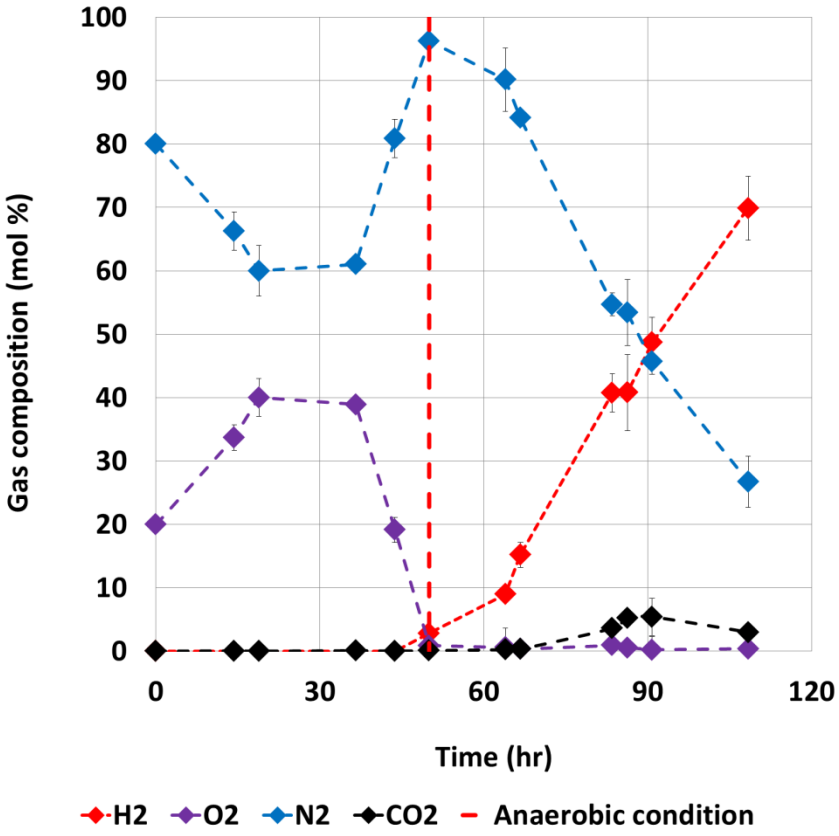

Figure III.10: Gas composition within the headspace of the ICL flat-plate PBR, used to cultivate chemostat *Cyanothece* 51142 culture at 35 ^{o}C and 92 µmol m^{-2} s^{-1}

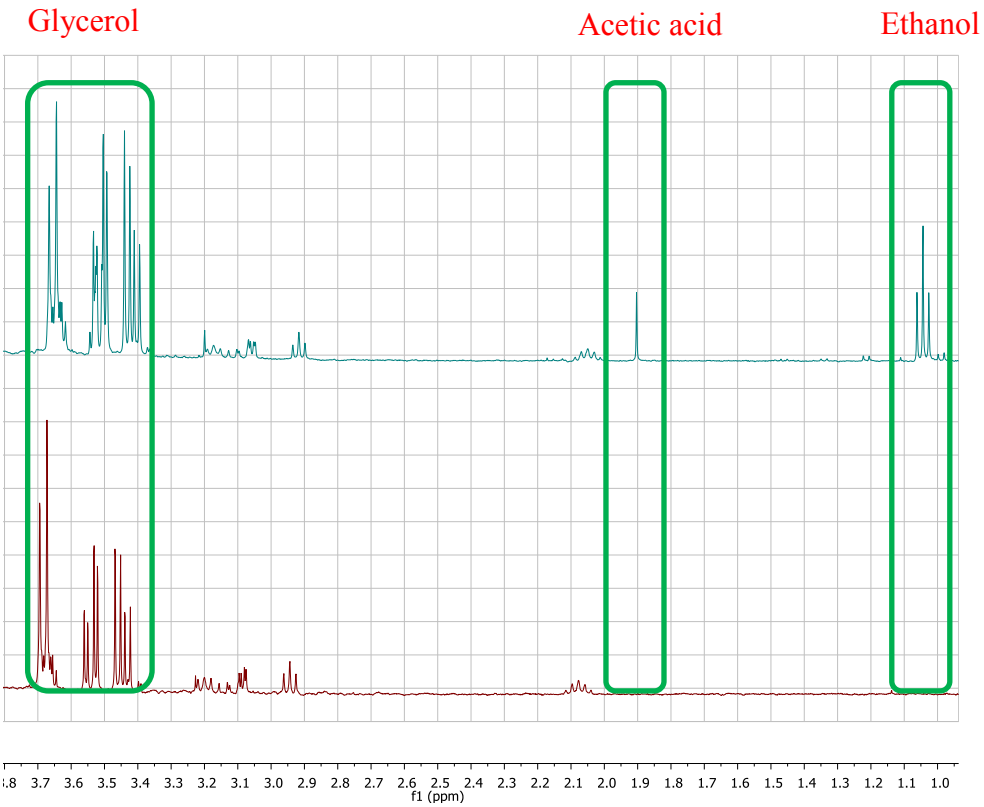

Figure III.11: Identification of organic carbon compounds within the liquid supernatant of *Cyanothece* 51142 cultures, collected during H_2 production phase from the flat-plate PBR;
Top) batch operation
Bottom) chemostat operation, under steady-state conditions

Using the perfect gas law (Equation 5.8), it is possible to convert the volumetric productivity (3.3 H_2 ml L^{-1} hr^{-1}) into its corresponding mass (0.26 mg H_2 L^{-1} hr^{-1}) as well as molar productivity (0.13 mmol H_2 L^{-1} hr^{-1}). The latter corresponds to a percentage steady-state conversion of (mole H_2 produced / mole glycerol fed) of ~ 28.3%. As the rate of cell transfer into the secondary PBR was ~24 mg biomass hr^{-1}, this suggests that each g of fed biomass can produce ~ 8.5 mg of H_2. For calculations, please see Appendixes.

In order to examine the overall performance of the system, both, its generated H_2 yield and productivity were compared with those obtained from the single-stage batch system (as presented in section II.3) and a theoretical multi-stage batch H_2 production systems, as shown in Figure III.12. It should be noted here that the latter process was not experimentally carried out, but its yield was simply assumed as multi-factor extrapolation of the single-stage batch system, taking into account a lag-time of 2 days (due to cleaning and re-setting up the system). Considering the experimental duration of 750 hours, from Figure III.12 and Table III.1, the chemostat system showed at least a 2 and 6.4-fold higher yield than multi-stage (864 ml H_2) and single-stage batch (272 ml H_2) systems, respectively. This significant improvement is the consequence of i) the success in prolonging the duration of the stationary growth phase of the culture inside the chemostat PBRs, ii) use of highly active cells, from the primary growth PBR, as H_2 producers, instead of repetitively using old cells as in the batch systems, iii) sufficient provision of organic glycerol, which serves as growth carbon source as well as energy contributors for the H_2 formation reaction and finally iv) no lag time required for re-setting up and cleaning the system. The same figure also suggests the great reliability of the water displacement system, as initial gas production rates, measured during time = 70 – 90 hour, are virtually the same in both batch and chemostat systems. Nevertheless, the divergence in gas yield and production rate between all scenarios appears to take place at

time = 200 hour and continues to become even more significant afterwards. This increasing deviation can be reasoned as it is due to the death phase in batch cultures which do not maintain their gas-producing capability.

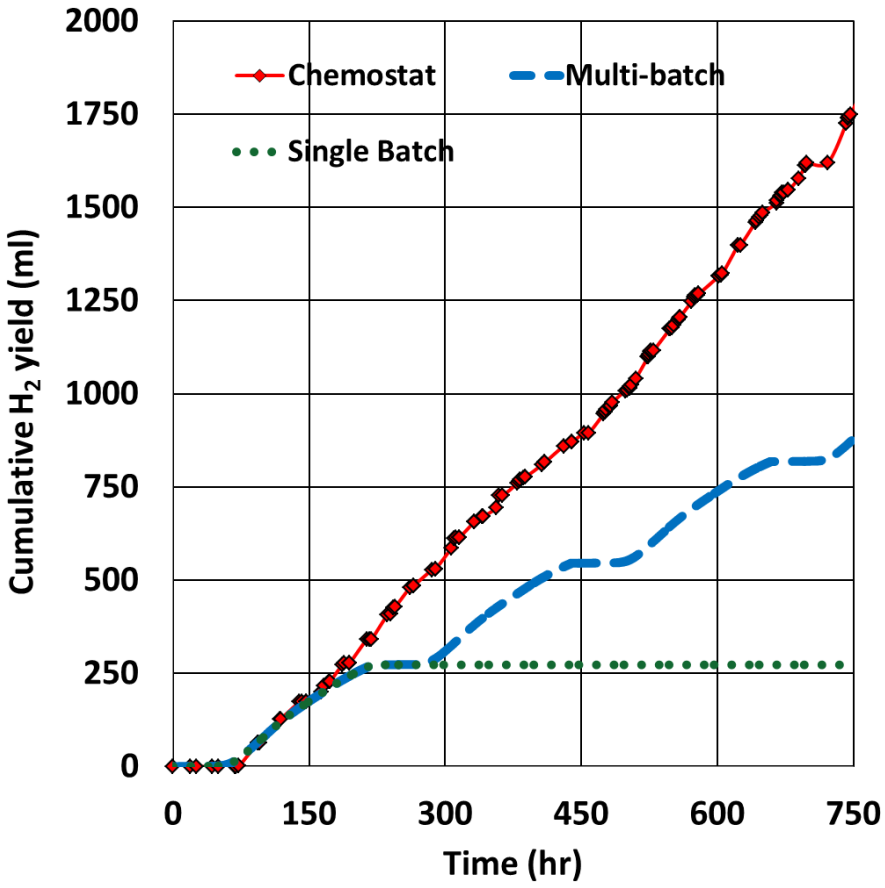

Figure III.12: Graphical comparison in cumulative H_2 yield profile between the chemostat, hypothetical multi-stage and single-stage batch systems

Table III.1: Numerical comparison in H_2 yield between the chemostat, hypothetical multi-stage and single-stage batch systems over the experimental duration of 750 hours

Processed PBR(s)	H_2 yield (ml)	Enhancement factor
Single-stage batch	272	1.00
Multi-stage batch	864	3.18
Chemostat	1750	6.43

III.3.4. Chemostat Biomass Production

From the *Cyanothece* 51142 growth profile of the secondary flat-plate PBR (Figure III.7), the rate of liquid culture leaving the PBR can be calculated by multiplying the known pumping rate with the respective biomass concentration. Consequently, the total cumulative biomass yield, collected from the PBR, can be estimated as the area under the biomass production rate versus time graph. As shown in Figure III.13, as soon as chemostat operation (steady-state) was established, time = 70 hour, a continuously increasing yield of biomass with respect to time is obtained. In contrast, a step-wise pattern would be produced by both multi-stage and single-stage batch processes. This significant difference is due to the nature of the continuous flow system, which permits continuous collection of cyanobacterial biomass from the system, whereas, in closed batch processes, it can only be feasible at the end of each operation cycle. Similar to section III.3.3, the yield of multi-stage batch processes was simply assumed to be an extrapolation of the single-stage one, taking into account a lag-

time of approximately 2 days (due to cleaning and starting up the system). It should also be noted here that, due to unfavourable growth conditions inside the secondary PBR, cellular reproduction becomes inhibited. Therefore, the biomass production solely comes from the growth of *Cyanothece* 51142 culture, cultivated in the primary PBR.

Considering the total experimental duration of 750 hours, the chemostat system (3.88 g L^{-1}) can be expected to offer at least a 2.5 to 7.3-fold increase in performance when comparing to multi-stage (1.58 g L^{-1}) and single-stage (0.53 g L^{-1}) batch PBRs, respectively (see Table III.2). There are two major reasons, which contribute towards this significant improvement. The first reason is the continuity of the chemostat system, which essentially eliminates the cleaning and start-up period of a batch processes. Another reason is the ability of the two-stage configuration to physically separate the aerobic growth from its incompatible anaerobic H_2 production, thereby allowing favourable cultivation conditions for each process to be established independently.

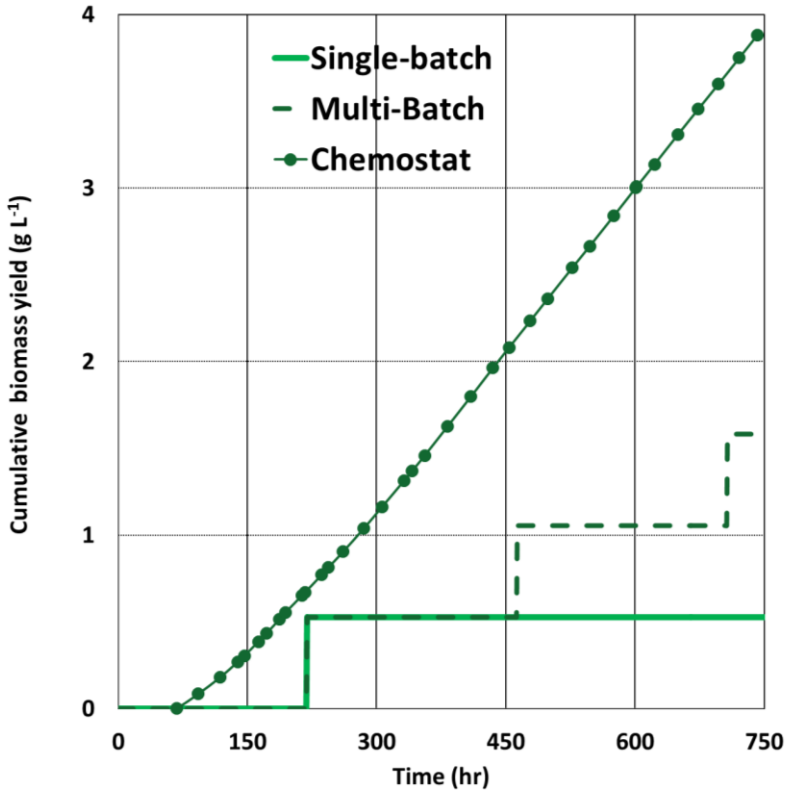

Figure III.13: Graphical comparison in cumulative biomass yield profile between the chemostat, hypothetical multi-stage and single-stage batch systems

Table III.2: Numerical comparison in biomass yield between the chemostat, hypothetical multi-stage and single-stage batch systems after 750 hours

Processed PBR(s)	Biomass yield (g L^{-1})	Enhancement factor
Single-stage batch	0.53	1.00
Multi-stage batch	1.58	2.98
Chemostat	3.88	7.32

III.4. Summary

Due to physiologically incompatible requirements between an aerobic cyanobacterial growth and its sequential anaerobic H_2 photoproduction, a two-stage chemostat PBR system was designed and developed so that these two inter-connected biological processes can be independently and effectively handled. Based on nutrient kinetics previously determined in section II.3, a dilution rate of 0.015 hr^{-1} was identified to replenish the culture cultivated in the secondary H_2 production PBR, with all essential substrates, while not interrupting the H_2 synthesis reaction. With the implementation of the two-stage chemostat, the growth and the H_2 production of *Cyanothece* 51142 has been successfully extended from a cycle of 7 - 10 days in normal batch mode to a duration of more than 1 month. At time = 70 hour, after the start of the experiment the entire system was operated under chemostat control. The physiological steady-state was achieved at time = 300 hour. The dry biomass concentration, accumulated in the primary growth and the secondary H_2-production PBRs, reached final values of 2 and 1.5 g L^{-1} respectively. By comparing the performance of the two-stage chemostat with that of a single-stage batch system, over the experimental duration of 750 hours, the chemostat displayed greatly enhanced productivities - more than 6.4 and 7.3 times higher H_2 (1750 ml H_2) and biomass yields (3.88 g L^{-1}). During steady-state, the H_2 production rate of the system eventually reached 2.6 ml H_2 hr^{-1} ~ 3.3 H_2 ml L^{-1} hr^{-1}, which is around 1.5-fold higher than the maximum rate for a batch process. This rate corresponds to the molar conversion of glycerol into H_2 of ~28.3%. Glycerol was demonstrated to be an effective anaerobic-inducer for an air-incubated *Cyanothece* 51142 culture. The presence of this substrate also allowed anaerobic conditions to be continuously maintained. Concurrent to H_2 production, at an industrial scale, further downstream processing of biomass, collected from the process, may be carried out to generate multiple streams of revenue from selling

HVPs e.g. vitamins, pharmaceuticals and human nutrition.

7. Conclusion and Future Work

7.1. Conclusion

The aim of this thesis was to quantify the growth and H_2 production kinetics of the N_2-fixing cyanobacterium *Cyanothece* 51142 and subsequently develop a continuous and practical cyanobacterial H_2 production process. This aim was realised by addressing three key objectives: the quantification of *Cyanothece* 51142 growth kinetics (Chapter I), the quantification of *Cyanothece* 51142 H_2 production kinetics (Chapter II), and the design, development and operation of a two-stage chemostat PBR system to extend the H_2 production capacity (Chapter III).

Overall, the thesis aim and objectives were successfully accomplished. *Cyanothece* 51142 growth was measured under different growth conditions – photoautotrophic and photoheterotrophic, nitrogen sources, light intensities, and temperatures. Anaerobic H_2 production was successfully initiated by the use of glycerol-supplemented and air-incubated *Cyanothece* 51142 cultures. Using a membrane-inlet mass spectrometry system, H_2 production was continuously and *in situ* measured under different light intensities and temperatures. Techniques for measuring the corresponding nitrate, sulphate and glycerol uptake were developed and used to accurately determine important parameters of these key nutrients kinetics. The environmental influence upon *Cyanothece* 51142 growth and its H_2 production was also investigated and corresponding optimal cultivating conditions were subsequently identified. The practical measurement techniques and methodologies developed during this thesis may be used in the future to investigate the growth and H_2 production of

various microalgal strains, in many different PBRs, and under different environmental conditions. By understanding the underlying biological mechanisms and corresponding requirements during both growth and H_2 production, this led to the design of a novel two-stage chemostat PBR system. The developed system proved effective at simultaneously facilitating *Cyanothece* 51142 growth and H_2 production at laboratory scale during continuous operation for 750 hours (~ 31 days), without any losses in its performance. With its excellent ability to overcome inherent limitations of closed batch processes, the chemostat enabled superior H_2 and biomass production rates and yields.

Objective I: Evaluate *Cyanothece* 51142 growth kinetics (Chapter I)

Some of the key parameters that affect *Cyanothece* 51142 growth kinetics were investigated and optimised (Dechatiwongse, Srisamai *et al.,* 2014). These include the light intensity, temperature, nitrogen source and growth condition – photoautotrophic and photoheterotrophic. The *Cyanothece* 51142 strain was shown to grow effectively using 10 % volume CO_2 volume air^{-1} – 10% CO_2 and 71% N_2 within the supplied gas mixture - as its carbon and nitrogen sources respectively. Even under continuous illumination, the cyanobacterium maintained its periodically alternating growth, pH and pO_2 profiles, confirming light-independence of the metabolic shift behaviour (Schneegurt 1994, ColonLopez, Sherman *et al.,* 1997). The cyanobacterial growth rate at least doubled when CO_2 was replaced by glycerol or nitrate salt was supplied instead of N_2. In the presence of glycerol or nitrate, the oscillating behaviour of cells no longer exists, suggesting their inhibitive nature. However, as soon as a cyanobacterial culture has consumed all of these substrates, it reinstates a diurnal cycle. With increasing light intensity, from 23 to 320 μmol m^{-2} s^{-1}, the photoautotrophic specific growth rate of *Cyanothece* 51142 strain consistently increases with no sign of photoinhibition, while there was little effect on the final biomass concentration of the culture, beyond 92 μmol m^{-2} s^{-1}. The latter is most likely due to the significant light attenuation, induced by the dense culture. The transition from photo-limitation into a saturation regime was determined to be at an average irradiance of 347 μmol m^{-2} s^{-1}. In terms of temperature, the optimal value to cultivate *Cyanothece* 51142 under photoautotrophic growth conditions was found to be 35 °C and clear evidence of photoinhibition was detectable at 40 °C.

Objective II: Evaluate *Cyanothece* 51142 H_2 production kinetics (Chapter II)

Anaerobic H_2 production by *Cyanothece* 51142 was reproducibly induced by a photoheterotrophic growth procedure – glycerol supplemented and air-incubated cultivation. Specifically, glycerol was shown to effectively enhance the cellular respiration and eventually impose successful anaerobic conditions. Air incubation was employed to ensure a minimal level of nitrate salts and thereby facilitating diazotrophic conditions. The H_2 production rates of cyanobacterial cultures were *in situ* and continuously measured using a membrane-inlet mass spectrometry system. Under incident irradiance up to 320 μmol m^{-2} s^{-1}, the final cyanobacterial biomass concentration and the H_2 production rate were observed to be enhanced as light intensity increases. Clear evidence for photo-limitation was observed at 92 μmol m^{-2} s^{-1}, beyond which the solar-to-H_2 conversion efficiency started to decrease, as mutual shading restricted the quantity of photons to be effectively captured and utilised by *Cyanothece* 51142. In the case of temperature, an optimal temperature was shown to be 30 ^{o}C, whereas an instantaneous cessation in H_2 production, caused by thermal-induced photoinhibition, was seen at 47 ^{o}C. The results also imply the limitation of chemical energy available for driving N_2-fixation as the major reason for a lower H_2 production rate at low temperature. Regardless of cultivating conditions, the duration of cyanobacterial H_2 photoproduction in a single batch PBR is very short - only 7 – 10 days and remains one of the critical issues to be resolved before a commercial biohydrogen facility could be conceived.

Objective III: Extend H_2 production by two-stage chemostat PBR system (Chapter III)

The insufficient duration of single batch H_2 production was addressed by the design of a novel two-stage chemostat PBR system for the cultivation of *Cyanothece* 51142 (Dechatiwongse, Maitland *et al.,* 2015). In this system, the two incompatible biological requirements – aerobic growth and anaerobic H_2 production – were independently and effectively satisfied using two physically separated but interconnected PBRs. The system proved effective at demonstrating continuous cyanobacterial H_2 production for 31 consecutive days, delivering the steady-state H_2 production rate of 3.3 ml H_2 L^{-1} hr^{-1} and a total yield of 1750 ml H_2. Biomass is also a valuable by-product of *Cyanothece* 51142, containing high levels of proteins and vitamins (Schneegurt, Arieli *et al.,* 1995). Due to the very nature of chemostat operation, the continuous collection of cyanobacterial biomass was feasible and eventually produced a total yield of 3.88 g L^{-1}. This novel approach was compared with two other methods of H_2 production by either single- or multi-stage batch processes. Under similar growth conditions and over the same experimental duration, the former system results in the maximum H_2 production of 2.2 ml H_2 L^{-1} hr^{-1}, the total H_2 and biomass yields of 272 ml H_2 and 0.53 g L^{-1} respectively. By extrapolating experimental results, it can be hypothesised that *Cyanothece* 51142 cultures could produce 864 ml H_2 and 1.58 g L^{-1} under multi-stage batch conditions, comprising a series of consecutive single-stage batch processes. As the performance of a two-stage chemostat PBR system proves superior to its counterparts based on the relevant H_2 and biomass production criteria, this should be the method of choice for future laboratory H_2 production experiments as well as for scaled-up applications for biological H_2 photoproduction.

7.2. Future Work

7.2.1. Perturbation Studies

As mentioned previously in section III.3.3, the conditions used to operate the two-stage chemostat system are still unoptimised. As a result, perturbation studies, which involve temporary changes in environmental conditions that could subsequently lead to pronounced alterations of the function of the biological system, are to be carried out. By achieving the steady-state condition, it becomes possible to make a temporary step change in one environmental parameter, while keeping the rest constant so that an individual effect of that particular parameter upon the performance of the system – new values of steady-state H_2 and biomass production rates – can be clearly identified and quantified. These newly determined experimental data can then be incorporated into my existing data set in order to re-evaluate parameter constants of both growth and H_2 production models (sections 5.9.2 – 5.9.6). The more experimental data, the higher confidence in the parameter estimation process. Environmental parameters to be investigated include light intensity (ColonLopez, Sherman *et al.,* 1997, Toepel, Welsh *et al.,* 2008, Alagesan, Gaudana *et al.,* 2013) and temperature (Brauer, Stomp *et al.,* 2013) as these two have direct influences on *Cyanothece* 51142 biomass and H_2 productions. For example, the value of k_i (photoinhibition term), previously determined in sections I.6 and II.4 should be re-evaluated through an experimental verification rather than the computational extrapolation. The experiment can be simply executed by practically employing step changes in light intensity upon the chemostat-cultivated cultures until the photoinhibition phenomenon begins to take place. Dilution rate is also one of key operating parameters, as it determines the quantity of nutrients and / or

biomass fed into the PBRs. Theoretically, an optimal dilution rate is one, which would compromise between the length of residence time and the replenishment of healthy cells and necessary nutrients, carried from the primary PBR. Specifically, the slower the dilution rate, the longer duration for the cyanobacterial cells to be kept within the secondary PBR for H_2 production. However, this change also implies the decreased rate of cell and nutrient transfer, which could then result in a delay in replacing old and starved cells with new and heathy cells.

7.2.2. Optimisation and Control Studies

Once perturbation studies have been completed, the growth and H_2 production models with highly confident parameter constants can then be used to computationally predict the biological performance of the two-stage chemostat *Cyanothece* 51142 PBR system upon any given operating conditions. This simulation approach could be utilised to indicate whether the laboratory-scale biohydrogen photoproduction process is economically viable or not, before any further attempts in scaling-up could have been made. Simply, the profitability = revenue (from selling H_2 fuel and cyanobacterial biomass-based products) – capital costs (PBRs construction and materials, lands and other devices e.g. heaters, coolers, pumps and compressors) – operating costs (labour, nutrients and on-site power consumption). Given that are some certain conditions, which could result in the maximum profitability, these conditions may then be considered as 'potential optimum conditions'. Eventually, laboratory-scale testings have to be executed in order to verify the accuracy of developed models in predicting optimised conditions and their subsequent performance of the biological system.

Once optimum conditions have been computationally determined and subsequently verified,

it is also equally important for such conditions to be precisely and constantly maintained throughout an operational duration of the cultivation process in order to ensure consistent biomass and H_2 productions. As a result, a process control such as feedback control loop should be considered being incorporated into the existing PBR system. Essential variables, affecting the growth and H_2 production of the cyanobacterium *Cyanothece* 51142 such as temperature, pO_2, macro-nutrients and OD must be real time monitored. A set of controllers should be set in such a way to maintain these variables at or close to their optimal values (set points). Any above-threshold deviations between the set point and the measured variable should then automatically alert manipulated variables such as valve position or pumping speed to perform an immediate adjustment to lessen the deviation and eventually bring the value of measured variable back to the set point. At pilot or industrial scale, a whole complex system could be effectively controlled from a central control room by a small number of on-site staffs.

7.2.3. Genetic Modification

One of major challenges for large-scale microalgae-based biofuel productions is the low efficiency of solar capture and conversion processes (numerically, photosynthetic efficiency of less than 3% (Blankenship, Tiede *et al.,* 2011) and solar-to-H_2 conversion efficiency of less than 1% (Masukawa, Kitashima *et al.,* 2012)). The most promising way to lessen this barrier is through genetic modification (GM), which involves the direct manipulation of a wild-type organism's genome in order to genetically induce modified physical or metabolic properties. As the genome of the wild-type cyanobacterium *Cyanothece* 51142 has been successfully sequenced (Welsh, Liberton *et al.,* 2008), it becomes possible to genetically engineer this cyanobacterial strain and subsequently create a mutant strain. As previously

mentioned in section 3.4.6, GM attempts could include: i) truncation of the antennae sizes in the photosynthetic apparatus of microalgae in order to improve the light penetration within the cell culture (Polle, Kanakagiri *et al.,* 2003, Melis 2009), ii) removal of uptake hydrogenases in order to prevent the biological oxidation of nitrogenase-produced H_2 (Lindblad, Christensson *et al.,* 2002) and lastly iii) elimination of some nonessential metabolic pathways, at which undesirable bio-products such as fermentative compounds are cellularly excreted (Doebbe, Rupprecht *et al.,* 2007, Burgess, Tamburic *et al.,* 2011). These approaches could be executed in a close collaboration with Professor Peter J Nixon's group, Department of Biochemistry, Imperial College London, which have an extensive expertise in the field of genetic manipulation. Once the cyanobacterium has been genetically modified, the performance of the newly created GM strain can be tested further using my laboratory facilities in the Department of Chemical Engineering, Imperial College London.

7.2.4. Scale-up

During the conduction of this thesis, a novel two-stage chemostat PBR system was developed and has been experimentally shown to be an effective PBR platform for biological H_2 photoproduction (Dechatiwongse, Maitland *et al.,* 2015). The next step is to construct and commission a scaled-up PBR in order to put these techniques into practice and investigate long-term H_2 production by *Cyanothece* 51142 cultures under outdoor conditions.

When it comes to the scale-up of biohydrogen production processes, most of the total associated cost is derived from the construction cost of bioreactors and the cost of nutrients, required during the operation (Melis 2002). In terms of reactor construction, an individual reactor unit of a two-stage chemostat PBR system could be economically manufactured from

high-density polyethylene in a process similar to the manufacture of commercial plastic bags. A working volume of these plastic bag PBRs should be in the order of 10 - 20 litres, which represents scale-up by a factor of 10 from most laboratory PBR systems. In order to minimise nutrient cost, industrially produced wastes of CO_2 and glycerol should be used as inexpensive carbon sources to facilitate the autotrophic and the heterotrophic growth conditions, respectively. Artificial seawater medium, previously used during laboratory cultivation, should be replaced by actual seawater, as the latter can provide an easily accessible, low-cost medium for a scaled up process. However, potential challenges could still include leaks caused by structural instability of the plastic bags, the formation of cyanobacterial films on surfaces and subsequent fouling of the system, a non-uniform mixing throughout the liquid phase, causing poor cyanobacterial growth rates and low biomass concentrations, difficulties in cleaning the system diligently enough to avoid contamination and the potential presence of toxic elements in the plastic, seawater or within CO_2 as well as glycerol feeds. As a result, one important recommendation is to begin with one plastic bag chemostat system in order to investigate its applicability to continuous H_2 production, using natural outdoor environments and inexpensive carbon sources, before expanding operations to a full scale, involving multiple chemostat units. Alongside this, a detailed cradle-to-grave economic analysis, based on experimental results of these scaled-up biohydrogen production facilities, is required. If economically viable, the project could then be taken up by industry, upgraded to pilot scale and eventually used in future commercial applications.

7.2.5. Cyanobacterial Biorefinery

Although cyanobacteria could offer a sustainable, renewable and clean route towards H_2 production, their current production rates are still too low to gain profit from operating an

industrial biohydrogen facility. This is due to current market values of H_2 and biomass, which are much lower than the cost of feedstock and process operation (Amos 2004), thereby making an overall process appear to be financially unsustainable. It thus becomes essential to employ a cyanobacterial biorefinery concept, in which H_2 is pursued in parallel with multiple value-added by-products, extracted from *Cyanothece* 51142 biomass. This multiproduct paradigm enables the maximum utilisation of materials associated with cyanobacterial growth and H_2 production in order to minimise waste and maximise the revenue of the process. In addition to a remarkable rate of H_2 production, the cyanobacterium *Cyanothece* 51142 has also been reported to accumulate a number of high value metabolites – proteins (55% of biomass dry weight), vitamin B_{12} as well as essential amino acids (Schneegurt, Arieli *et al.,* 1995). It appears to be a viable option, to carry out further downstream processing of biomass in order to produce an array of HVPs, which can then contribute significant revenue to support the economic viability of biohydrogen production (Bhavish, Tamburic *et al.,* 2012).

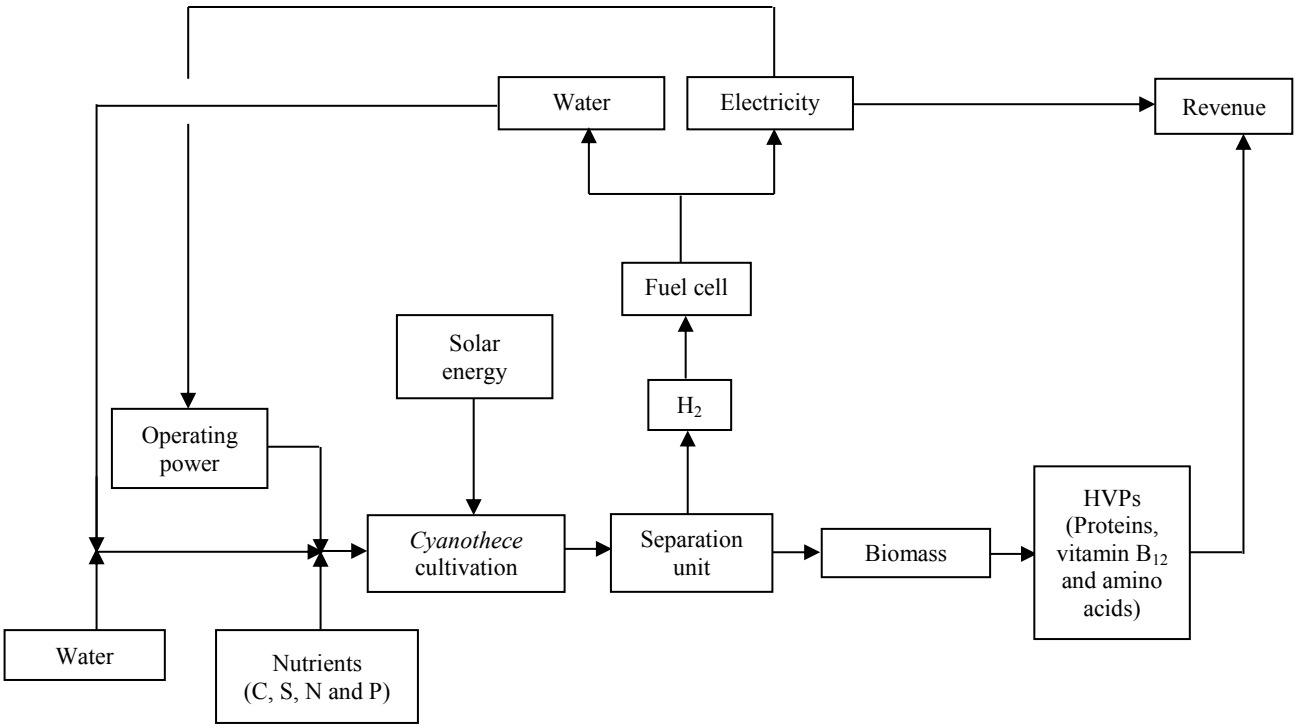

Figure III.14: Conceptual design of the microalgal biorefinery production process

As shown in Figure III.14, a conceptual process design of this microbial platform has been proposed in such a way that the economic viability and the environmental sustainability can be mutually achieved. Specifically, the cultivation of *Cyanothece* 51142 cultures, using the novel two-stage chemostat system, will be implemented in an outdoor, seaside location. This allows the direct utilisation of solar light as primary energy source, together with using seawater as the medium (Bharat Gami, Abhishek Naik *et al.,* 2011). As both sunlight and seawater are abundantly available and inexpensive, this use will promise the minimal cost of illumination and nutrients. It could also be possible to use wasted glycerol, by-product from an industrial bio-diesel production (Yang, Hanna *et al.,* 2012), as carbon source. Nevertheless, pre-treatment and sterilisation would be necessary in order to avoid potential toxicity and contamination, which could be induced by any impurities within sea water and glycerol. Besides, as cyanobacterial H_2 production is a strongly light-dependent process (Bandyopadhyay, Stoeckel *et al.,* 2010, Min and Sherman 2010), there is the requirement for an artificial light source during dark periods of natural light : dark cycles. The mainstream of revenue will come from the sale of proteins, vitamins and essential amino acids being extracted from cyanobacterial biomasses. On-site produced H_2 will directly be converted into electricity, by the use of a fuel cell system, to provide carbon-neutral distributed energy and if surplus, could be for sale as well. By-product water, produced from the fuel cell's conversion, can be directly fed back into the cultivation system to compensate the quantity of water losses though biomass collection as well as evaporation. Simultaneous to anaerobic H_2 production, cells also concurrently evolve CO_2, albeit at low quantity. This undesirable CO_2 will be recycled back into the primary growth PBR and subsequently used by cells as carbon source for its photoautotrophic growth. In addition, remaining opportunities, including an integration of this system with wasted water treatment (Markou and Georgakakis 2011) or other renewable energy-generating technologies (Subhadra 2010) are possible and can enhance the

status of algal-derived biofuels from concept into reality.

8. References

Aiba, S. (1982). Growth kinetics of photosynthetic microorganisms. Microbial Reactions, Springer Berlin Heidelberg. **23:** 85-156.

Akkerman, I., M. Janssen, J. Rocha and R. H. Wijffels (2002). "Photobiological hydrogen production: photochemical efficiency and bioreactor design." International Journal of Hydrogen Energy **27**(11–12): 1195-1208.

Alagappan, G. and R. M. Cowan (2004). "Effect of temperature and dissolved oxygen on the growth kinetics of *Pseudomonas putida* F1 growing on benzene and toluene." Chemosphere **54**(8): 1255-1265.

Alagesan, S., S. B. Gaudana, S. Krishnakumar and P. P. Wangikar (2013). "Model based optimization of high cell density cultivation of nitrogen-fixing cyanobacteria." Bioresource Technology **148**: 228-233.

Allakhverdiev, S. I., V. D. Kreslavski, V. Thavasi, S. K. Zharmukhamedov, V. V. Klimov, T. Nagata, H. Nishihara and S. Ramakrishna (2009). "Hydrogen photoproduction by use of photosynthetic organisms and biomimetic systems." Photochemical & Photobiological Sciences **8**(2): 148-156.

Amos, W. A. (2004). Updated cost analysis of photobiological hydrogen production from *Chlamydomonas reinhardtii* green algae National Renewable Energy Laboratory (NREL) - Milestone Completion Report.

Andersson, B. and S. Styring (1991). Photosystem II: molecular organization, function, and acclimation. Current Topics in Bioenergetics. C. P. Lee, Academic Press**:** 1-81.

Ariosa, Y., D. Carrasco, A. Quesada and E. Fernandez-Valiente (2006). "Incorporation of different N sources and light response curves of nitrogenase and

photosynthesis by cyanobacterial blooms from rice fields." Microbial Ecology **51**(3): 394-403.

Aryal, U. K., J. Stockel, R. Krovvidi, M. Gritsenko, M. Monroe, R. Moore, D. Koppenaal, R. Smith, H. Pakrasi and J. Jacobs (2011). "Dynamic proteomic profiling of a unicellular cyanobacterium *Cyanothece* ATCC51142 across light-dark diurnal cycles." BMC Systems Biology **5**(1): 194.

Aryal, U. K., S. J. Callister, S. Mishra, X. Zhang, J. I. Shutthanandan, T. E. Angel, A. K. Shukla, M. E. Monroe, R. J. Moore, D. W. Koppenaal, R. D. Smith and L. Sherman (2013). "Proteome analyses of srains ATCC 51142 and PCC 7822 of the diazotrophic cyanobacterium *Cyanothece* sp under culture conditions resulting in enhanced H_2 production." Applied and Environmental Microbiology **79**(4): 1070-1077.

Aryal, U. K., J. Stöckel, E. A. Welsh, M. A. Gritsenko, C. D. Nicora, D. W. Koppenaal, R. D. Smith, H. B. Pakrasi and J. M. Jacobs (2011). "Dynamic proteome analysis of *Cyanothece* sp. ATCC 51142 under constant light." Journal of Proteome Research **11**(2): 609-619.

Atsumi, S., W. Higashide and J. C. Liao (2009). "Direct photosynthetic recycling of carbon dioxide to isobutyraldehyde." Nat Biotech **27**(12): 1177-1180.

Bandyopadhyay, A., T. Elvitigala, M. Liberton and H. B. Pakrasi (2013). "Variations in the rhythms of respiration and nitrogen fixation in members of the unicellular diazotrophic cyanobacterial genus *Cyanothece*." Plant Physiology **161**(3): 1334-1346.

Bandyopadhyay, A., J. Stoeckel, H. Min, L. A. Sherman and H. B. Pakrasi (2010). "High rates of photobiological H_2 production by a cyanobacterium under aerobic conditions." Nature Communications **1**(139).

Barbir, F. (2005). "PEM electrolysis for production of hydrogen from renewable energy sources." Solar Energy **78**(5): 661-669.

Barbosa, M. J., Hadiyanto and R. H. Wijffels (2004). "Overcoming shear stress of microalgae cultures in sparged photobioreactors." Biotechnology and Bioengineering **85**(1): 78-85.

Barbosa, M. J., J. W. Zijffers, A. Nisworo, W. Vaes, J. van Schoonhoven and R. H. Wijffels (2005). "Optimization of biomass, vitamins, and carotenoid yield on light energy in a flat-panel reactor using the A-stat technique." Biotechnology and Bioengineering **89**(2): 233-242.

Baroli, I. and A. Melis (1996). "Photoinhibition and repair in *Dunaliella salina* acclimated to different growth irradiances." Planta **198**(4): 640-646.

Bartels, J. R., M. B. Pate and N. K. Olson (2010). "An economic survey of hydrogen production from conventional and alternative energy sources." International Journal of Hydrogen Energy **35**(16): 8371-8384.

Battino, R. and H. L. Clever (1966). "The Solubility of Gases in Liquids." Chemical Reviews **66**(4): 395-463.

Béchet, Q., A. Shilton and B. Guieysse (2013). "Modeling the effects of light and temperature on algae growth: State of the art and critical assessment for productivity prediction during outdoor cultivation." Biotechnology Advances **31**(8): 1648-1663.

Beckmann, K., J. Messinger, M. Badger, T. Wydrzynski and W. Hillier (2009). "On-line mass spectrometry: membrane inlet sampling." Photosynthesis Research **102**(2-3): 511-522.

Beer, L. L., E. S. Boyd, J. W. Peters and M. C. Posewitz (2009). "Engineering algae for biohydrogen and biofuel production." Current Opinion in Biotechnology **20**(3): 264-271.

Benemann, J. R. (1997). "Feasibility analysis of photobiological hydrogen production." International Journal of Hydrogen Energy **22**(10–11): 979-987.

Benemann, J. R. (1999). "Process analysis and economics of biophotolosys of water." InternationalEnergy Agency (IEA) - Agreement on the Production and Utilization of Hydrogen.

Berberoglu, H., J. Yin and L. Pilon (2007). "Light transfer in bubble sparged photobioreactors for H_2 production and CO_2 mitigation." International Journal of Hydrogen Energy **32**(13): 2273-2285.

Bernard, O. (2011). "Hurdles and challenges for modelling and control of microalgae for CO_2 mitigation and biofuel production." Journal of Process Control **21**(10): 1378-1389.

Bharat Gami, Abhishek Naik and B. Patel (2011). "Cultivation of *Spirulina* species in different liquid media." Journal of Algal Biomass Utilization **2**(3): 15-16.

Bilanovic, D., A. Andargatchew, T. Kroeger and G. Shelef (2009). "Freshwater and marine microalgae sequestering of CO_2 at different C and N concentrations – Response surface methodology analysis." Energy Conversion and Management **50**(2): 262-267.

Blankenship, R. E. (2008). The basic principles of photosynthetic energy storage. Molecular Mechanisms of Photosynthesis, Blackwell Science Ltd.

Blankenship, R. E., D. M. Tiede, J. Barber, G. W. Brudvig, G. Fleming, M. Ghirardi, M. R. Gunner, W. Junge, D. M. Kramer, A. Melis, T. A. Moore, C. C. Moser, D. G. Nocera, A. J. Nozik, D. R. Ort, W. W. Parson, R. C. Prince and R. T. Sayre (2011). "Comparing photosynthetic and photovoltaic efficiencies and recognizing the potential for improvement." Science **332**(6031): 805-809.

Borodin, V. B., A. A. Tsygankov, K. K. Rao and D. O. Hall (2000). "Hydrogen production by *Anabaena variabilis* PK84 under simulated outdoor conditions." Biotechnology and Bioengineering **69**(5): 478-485.

Borowitzka, M. A. (1999). "Commercial production of microalgae: ponds, tanks, tubes and fermenters." Journal of Biotechnology **70**(1–3): 313-321.

Boyle, N. and J. Morgan (2009). "Flux balance analysis of primary metabolism in *Chlamydomonas reinhardtii*." BMC Systems Biology **3**(1): 4.

Brauer, V. S., M. Stomp, C. Rosso, S. A. M. van Beusekom, B. Emmerich, L. J. Stal and J. Huisman (2013). "Low temperature delays timing and enhances the cost of nitrogen fixation in the unicellular cyanobacterium *Cyanothece*." Isme Journal **7**(11): 2105-2115.

Brentner, L. B., J. Peccia and J. B. Zimmerman (2010). "Challenges in developing biohydrogen as a sustainable energy source: implications for a research agenda." Environmental Science & Technology **44**(7): 2243-2254.

Buick, R. (1992). "The antiquity of oxygenic photosynthesis*:* evidence from stromatolites in sulphate-deficient Archaean lakes." Science **255**(5040): 74-77.

Burgess, S. J., B. Tamburic, F. Zemichael, K. Hellgardt and P. J. Nixon (2011). Chapter 3 - Solar-driven hydrogen production in green algae. Advances in Applied Microbiology. S. S. Allen I. Laskin and M. G. Geoffrey, Academic Press. **Volume 75:** 71-110.

Cakmak, T., P. Angun, Y. E. Demiray, A. D. Ozkan, Z. Elibol and T. Tekinay (2012). "Differential effects of nitrogen and sulphur deprivation on growth and biodiesel feedstock production of *Chlamydomonas reinhardtii*." Biotechnology and Bioengineering **109**(8): 1947-1957.

Cammack, R. (1999). "Bioinorganic chemistry: Hydrogenase sophistication." Nature **397**(6716): 214-215.

Cabello, J., M. Morales and S. Revah (2014). "Dynamic photosynthetic response of the microalga Scenedesmus obtusiusculus to light intensity perturbations." Chemical Engineering Journal **252**(0): 104-111.

Carrieri, D., K. Wawrousek, C. Eckert, J. Yu and P.-C. Maness (2011). "The role of the bidirectional hydrogenase in cyanobacteria." Bioresource Technology **102**(18): 8368-8377.

Carvalho, A. P., L. A. Meireles and F. X. Malcata (2006). "Microalgal Reactors: A review of enclosed system designs and performances." Biotechnology Progress **22**(6): 1490-1506.

Catalanotti, C., W. Yang, M. C. Posewitz and A. R. Grossman (2013). "Fermentation metabolism and its evolution in algae." Frontiers in plant science **4**: 150-150.

Chatzifragkou, A. and S. Papanikolaou (2012). "Effect of impurities in biodiesel-derived waste glycerol on the performance and feasibility of biotechnological processes." Applied Microbiology and Biotechnology **95**(1): 13-27.

Chen, C. Y., G. D. Saratale, C. M. Lee, P. C. Chen and J. S. Chang (2008). "Phototrophic hydrogen production in photobioreactors coupled with solar-energy-excited optical fibers." International Journal of Hydrogen Energy **33**(23): 6886-6895.

Chisti, Y. (2007). "Biodiesel from microalgae." Biotechnology Advances **25**(3): 294-306.

Chisti, Y. (2008). "Biodiesel from microalgae beats bioethanol." Trends in Biotechnology **26**(3): 126-131.

Chisti, Y. and U. J. Jauregui-Haza (2002). "Oxygen transfer and mixing in mechanically agitated airlift bioreactors." Biochemical Engineering Journal **10**(2): 143-153.

Christopher, K. and R. Dimitrios (2012). "A review on exergy comparison of hydrogen production methods from renewable energy sources." Energy & Environmental Science **5**(5): 6640-6651.

Clark, M. E., He, Q., He, Z., Huang, K. H., Alm, E. J., Wan, X. F., Hazen, T. C., Arkin, A. P., Wall, J. D., Zhou, J. Z. and Fields, M. W. (2006). "Temporal transcriptomic

analysis as Desulfovibrio vulgari Hildenborough transitions into stationary phase during electron donor depletion." Appl Environ Microbiol **72**: 5578–5588.

Colon-Lopez, M. S. and L. A. Sherman (1998). "Transcriptional and translational regulation of photosystem I and II genes in light-dark- and continuous-light-grown cultures of the unicellular cyanobacterium *Cyanothece* sp. strain ATCC 51142." Journal of Bacteriology **180**(3): 519-526.

ColonLopez, M., D. M. Sherman and L. A. Sherman (1997). "Transcriptional and translational regulation of nitrogenase in light-dark- and continuous-light grown cultures of the unicellular cyanobacterium *Cyanothece* sp. strain ATCC 51142." Journal of Bacteriology **179**(13): 4319-4327.

Cornet, J.-F. and C.-G. Dussap (2009). "A Simple and reliable formula for assessment of maximum volumetric productivities in photobioreactors." Biotechnology Progress **25**(2): 424-435.

Cournac, L., F. Mus, L. Bernard, G. Guedeney, P. Vignais and G. Peltier (2002). "Limiting steps of hydrogen production in *Chlamydomonas reinhardtii* and *Synechocystis* PCC 6803 as analysed by light-induced gas exchange transients." International Journal of Hydrogen Energy **27**(11–12): 1229-1237.

Dai, G., C. P. Deblois, S. Liu, P. Juneau and B. Qiu (2008). "Differential sensitivity of five cyanobacterial strains to ammonium toxicity and its inhibitory mechanism on the photosynthesis of rice-field cyanobacterium Ge-Xian-Mi (Nostoc)." Aquatic Toxicology **89**(2): 113-121.

Das, D. and T. N. Veziroğlu (2001). "Hydrogen production by biological processes: a survey of literature." International Journal of Hydrogen Energy **26**(1): 13-28.

Dasgupta, C. N., J. Jose Gilbert, P. Lindblad, T. Heidorn, S. A. Borgvang, K. Skjanes and D. Das (2010). "Recent trends on the development of photobiological processes and

photobioreactors for the improvement of hydrogen production." International Journal of Hydrogen Energy **35**(19): 10218-10238.

DBERR (2007). Meeting the energy challenge: a White Paper on energy. Department of Business, Enterprise and Regulatory Reform (DBERR).

Dechatiwongse, P., G. C. Maitland and K. Hellgardt (2015). "Demonstration of a two-stage aerobic / anaerobic chemostat for the enhanced production of hydrogen and biomass from unicellular nitrogen-fixing cyanobacterium." Algal Research **10**(0): 189 – 201.

Dechatiwongse, P., S. Srisamai, G. Maitland and K. Hellgardt (2014). "Effects of light and temperature on the photoautotrophic growth and photoinhibition of nitrogen-fixing cyanobacterium Cyanothece sp. ATCC 51142." Algal Research **5**(0): 103-111.

Dechatiwongse, P., D. Zhang, A. Del-Rio-Chanona, V. Vassiliadis, G. Maitland and K. Hellgardt "Effects of light intensity and temperature upon hydrogen production of nitrogen-fixing cyanobacterium *Cyanothece* sp. ATCC 51142 (in preparation)." Algal Research (provisional).

Degrenne, B., J. Pruvost and J. Legrand (2011). "Effect of prolonged hypoxia in autotrophic conditions in the hydrogen production by the green microalga Chlamydomonas reinhardtii in photobioreactor." Bioresource Technology **102**(2): 1035-1043.

Demirbas, A. (2007). "Progress and recent trends in biofuels." Progress in Energy and Combustion Science **33**(1): 1-18.

Dismukes, G. C., D. Carrieri, N. Bennette, G. M. Ananyev and M. C. Posewitz (2008). "Aquatic phototrophs: efficient alternatives to land-based crops for biofuels." Current Opinion in Biotechnology **19**(3): 235-240.

Doebbe, A., J. Rupprecht, J. Beckmann, J. H. Mussgnug, A. Hallmann, B. Hankamer and O. Kruse (2007). "Functional integration of the HUP1 hexose symporter gene into the

genome of *C. reinhardtii*: Impacts on biological H2 production." Journal of Biotechnology **131**(1): 27-33.

Drath, M., N. Kloft, A. Batschauer, K. Marin, J. Novak and K. Forchhammer (2008). "Ammonia triggers photodamage of photosystem II in the cyanobacterium *Synechocystis* sp strain PCC 6803." Plant Physiology **147**(1): 206-215.

Dutta, D., D. De, S. Chaudhuri and S. K. Bhattacharya (2005). "Hydrogen production by Cyanobacteria." Microbial Cell Factories **4**(36).

US EPA (2010). "Light-duty automotive technology, carbon dioxide emissions and fuel economy trends: 1975 through 2010." US Environmental Protection Agency (US EPA).

Eroglu, E. and A. Melis (2011). "Photobiological hydrogen production: Recent advances and state of the art." Bioresource Technology **102**(18): 8403-8413.

Esper, B., A. Badura and M. Rögner (2006). "Photosynthesis as a power supply for (bio-)hydrogen production." Trends in Plant Science **11**(11): 543-549.

Evans, G. (2007). "Liquid transport biofuels - technology status report." Internation Biofuels Strategy Project.

Fay, P. (1992). "Oxygen relations of nitrogen fixation in cyanobacteria." Microbiological Reviews **56**(2): 340-373.

Fedorov, A. S., S. Kosourov, M. L. Ghirardi and M. Seibert (2005). "Continuous hydrogen photoproduction by Chlamydomonas reinhardtii." Applied Biochemistry and Biotechnology **121**: 403-412.

Feng, X., A. Bandyopadhyay, B. Berla, L. Page, B. Wu, H. B. Pakrasi and Y. J. Tang (2010). "Mixotrophic and photoheterotrophic metabolism in *Cyanothece* sp ATCC 51142 under continuous light." Microbiology-Sgm **156**: 2566-2574.

Fernandez-Valiente, E., A. Quesada, C. Howard-Williams and I. Hawes (2001). "N-2-fixation in cyanobacterial mats from ponds on the McMurdo Ice Shelf, Antarctica." Microbial Ecology **42**(3): 338-349.

Flores, E., J. E. Frias, L. M. Rubio and A. Herrero (2005). "Photosynthetic nitrate assimilation in cyanobacteria." Photosynthesis Research **83**(2): 117-133.

Fouchard, S., J. Pruvost, B. Degrenne and J. Legrand (2008). "Investigation of H_2 production using the green microalga *Chlamydomonas reinhardtii* in a fully controlled photobioreactor fitted with on-line gas analysis." International Journal of Hydrogen Energy **33**(13): 3302-3310.

Gaffron, H. (1939). "Reduction of CO_2 with H_2 in green plants." Nature **143**(1): 204 - 205.

Gaffron, H. and J. Rubin (1942). "Fermentative and photochemical production of hydrogen in algae." The Journal of General Physiology: 19–240.

Garcia-Ochoa, F. and E. Gomez (2009). "Bioreactor scale-up and oxygen transfer rate in microbial processes: An overview." Biotechnology Advances **27**(2): 153-176.

Ghirardi, M. L., A. Dubini, J. P. Yu and P. C. Maness (2009). "Photobiological hydrogen-producing systems." Chemical Society Reviews **38**(1): 52-61.

Giannelli, L., A. Scoma and G. Torzillo (2009). "Interplay between light intensity, chlorophyll concentration and culture mixing on the hydrogen production in sulphur-deprived *Chlamydomonas reinhardtii* cultures grown in laboratory photobioreactors." Biotechnology and Bioengineering **104**(1): 76-90.

Gombos, Z., Wada, H. and Murata, N. (1994). "The recovery of photosynthesis from low-temperature photoinhibition is accelerated by the unsaturation of membrane lipids: a mechanism of chilling tolerance." Proc Natl Acad Sci U S A **91**(19): 8787-8791.

Gons, H. J., H. L. Hoogveld, S. G. H. Simis and M. Tijdens (2006). "Dynamic modelling of viral impact on cyanobacterial populations in shallow lakes: implications of burst size." Journal of the Marine Biological Association of the United Kingdom **86**(03): 537-542.

Gomez, L. D., C. G. Steele-King and S. J. McQueen-Mason (2008). "Sustainable liquid biofuels from biomass: the writing's on the walls." New Phytologist **178**(3): 473-485.

Green, M. A., K. Emery, Y. Hishikawa and W. Warta (2010). "Solar cell efficiency tables (version 36)." Progress in Photovoltaics: Research and Applications **18**(5): 346-352.

Greenbaum, E. (1988). "Energetic efficiency of hydrogen photoevolution by algal water splitting." Biophysical Journal **54**(2): 365-368.

Grima, E. M., F. G. A. Fernandez, F. G. Camacho and Y. Chisti (1999). "Photobioreactors: light regime, mass transfer, and scaleup." Journal of Biotechnology **70**(1-3): 231-247.

Grossman, A. R., C. Catalanotti, W. Yang, A. Dubini, L. Magneschi, V. Subramanian, M. C. Posewitz and M. Seibert (2011). "Multiple facets of anoxic metabolism and hydrogen production in the unicellular green alga *Chlamydomonas reinhardtii*." New Phytologist **190**(2): 279 - 288.

Hallenbeck, P. C., M. Abo-Hashesh and D. Ghosh (2012). "Strategies for improving biological hydrogen production." Bioresource Technology **110**: 1-9.

Hallenbeck, P. C. and J. R. Benemann (2002). "Biological hydrogen production; fundamentals and limiting processes." International Journal of Hydrogen Energy **27**(11–12): 1185-1193.

Hallenbeck, P. C. and D. Ghosh (2009). "Advances in fermentative biohydrogen production: the way forward?" Trends in Biotechnology **27**(5): 287-297.

Hammarström, L., J. R. Winkler, H. B. Gray and S. Styring (2011). "Shedding light on solar fuel efficiencies." Science **333**(6040): 288.

Hankamer, B., F. Lehr, J. Rupprecht, J. H. Mussgnug, C. Posten and O. Kruse (2007). "Photosynthetic biomass and H_2 production by green algae: from bioengineering to bioreactor scale-up." Physiologia Plantarum **131**(1): 10-21.

Hannon, M., J. Gimpel, M. Tran, B. Rasala and S. Mayfield (2010). "Biofuels from algae: challenges and potential." Biofuels **1**(5): 763-784.

Hansel, A. and P. Lindblad (1998). "Towards optimization of cyanobacteria as biotechnologically relevant producers of molecular hydrogen, a clean and renewable energy source." Applied Microbiology and Biotechnology **50**(2): 153-160.

Hardy, R. W. F., R. C. Burns and R. D. Holsten (1973). "Applications of the acetylene-ethylene assay for measurement of nitrogen fixation." Soil Biology and Biochemistry **5**(1): 47-81.

Hejazi, M. A. and R. H. Wijffels (2004). "Milking of microalgae." Trends in Biotechnology **22**(4): 189-194.

Hemmes, H., D. A. and G. R. (1986). "Thermodynamic properties of hydrogen at pressures up to 1 Mbar and temperatures between 100 and 1000K." Journal of Physics C; Solid State Physics **19**.

Heritage, J., Evans, E. G. V. and Killington, R. A. (1996). Introductory Microbiology. Cambridge Cambridge University Press.

Hoffert, M. I., K. Caldeira, G. Benford, D. R. Criswell, C. Green, H. Herzog, A. K. Jain, H. S. Kheshgi, K. S. Lackner, J. S. Lewis, H. D. Lightfoot, W. Manheimer, J. C. Mankins, M. E. Mauel, L. J. Perkins, M. E. Schlesinger, T. Volk and T. M. L. Wigley (2002). "Advanced technology paths to global climate stability: energy for a greenhouse planet." Science **298**(5595): 981-987.

Horner, J. K. and M. A. Wolinsky (2002). "A power-law sensitivity analysis of the hydrogen-producing metabolic pathway in Chlamydomonas reinhardtii." International Journal of Hydrogen Energy **27**(11): 1251-1255.

Hoskisson, P. A. and G. Hobbs (2005). "Continuous culture - making a comeback?" Microbiology-Sgm **151**: 3153-3159.

Howarth, D. C. and G. A. Codd (1985). "The uptake and production of molecular hydrogen by unicellular cyanobacteria." Journal of General Microbiology **131**(7): 1561-1569.

IEA (2011). "Key world energy statistics." International Energy Agency (IEA).

Inoue, N., Y. Taira, T. Emi, Y. Yamane, Y. Kashino, H. Koike and K. Satoh (2001). "Acclimation to the growth temperature and the high-temperature effects on photosystem II and plasma membranes in a mesophilic cyanobacterium, *Synechocystis* sp PCC6803." Plant and Cell Physiology **42**(10): 1140-1148.

IPCC (2007). Climate change 2007 - the physical science basis. Climate change 2007: The physical science basis, contribution of working group I to the fourth assessment report of the intergovernmental panel on climate change (IPCC).

Iwai, M., K. Takizawa, R. Tokutsu, A. Okamuro, Y. Takahashi and J. Minagawa (2010). "Isolation of the elusive supercomplex that drives cyclic electron flow in photosynthesis." Nature **464**(7292): 1210-1213.

James, B. D., G. N. Baum, P. Julie and K. N. Baum (2009). "Technoeconomic analysis of photoelectrochemical (PEC) hydrogen production." Directed Technologies.

Janssen, M. (2002). Cultivation of microalgae: effect of light/dark cycles on biomass yield, Wageningen University: Wageningen, The Netherlands.

Janssen, M., L. de Bresser, T. Baijens, J. Tramper, L. Mur, J. H. Snel and R. Wijffels (2000). "Scale-up aspects of photobioreactors: effects of mixing-induced light/dark cycles." Journal of Applied Phycology **12**(3-5): 225-237.

Janssen, M., M. Janssen, M. de Winter, J. Tramper, L. R. Mur, J. Snel and R. H. Wijffels (2000). "Efficiency of light utilization of *Chlamydomonas reinhardtii* under medium-duration light/dark cycles." Journal of Biotechnology **78**(2): 123-137.

Janssen, M., P. Slenders, J. Tramper, L. R. Mur and R. H. Wijffels (2001). "Photosynthetic efficiency of *Dunaliella tertiolecta* under short light/dark cycles." Enzyme and Microbial Technology **29**(4-5): 298-305.

Janssen, M., J. Tramper, L. R. Mur and R. H. Wijffels (2003). "Enclosed outdoor photobioreactors: Light regime, photosynthetic efficiency, scale-up, and future prospects." Biotechnology and Bioengineering **81**(2): 193-210.

Jo, J. H., D. S. Lee and J. M. Park (2006). "Modeling and optimization of photosynthetic hydrogen gas production by green alga *Chlamydomonas reinhardtii* in sulphur-deprived circumstance." Biotechnology Progress **22**(2): 431-437.

Kanervo, E., Y. Tasaka, N. Murata and E. M. Aro (1997). "Membrane lipid unsaturation modulates processing of the photosystem II reaction-center protein D1 at low temperatures." Plant Physiology **114**(3): 841-849.

Kim, B. W., H. N. Chang, I. K. Kim and K. S. Lee (1992). "Growth-kinetics of the photosynthetic bacteriumchlorobium-thiosulfatophilium in a fed-batch reactor." Biotechnology and Bioengineering **40**(5): 583-592.

Kim, J. P., K.-R. Kim, S. P. Choi, S. J. Han, M. S. Kim and S. J. Sim (2010). "Repeated production of hydrogen by sulfate re-addition in sulphur deprived culture of *Chlamydomonas reinhardtii*." International Journal of Hydrogen Energy **35**(24): 13387-13391.

Kirchman, D. L. (2012). Process in Microbial Ecology. Oxford, Oxford University Press.

Koku, H., İ. Eroğlu, U. Gündüz, M. Yücel and L. Türker (2003). "Kinetics of biological hydrogen production by the photosynthetic bacterium *Rhodobacter sphaeroides* O.U. 001." International Journal of Hydrogen Energy **28**(4): 381-388.

Konopka, A. and T. D. Brock (1978). "Effect of temperature on blue-green algae (cyanobacteria) in lake Mendota." Applied and Environmental Microbiology **36**(4): 572-576.

Kosourov, S., A. Tsygankov, M. Seibert and M. L. Ghirardi (2002). "Sustained hydrogen photoproduction by *Chlamydomonas reinhardtii*: Effects of culture parameters." Biotechnology and Bioengineering **78**(7): 731-740.

Kosourov, S. N. and M. Seibert (2009). "Hydrogen photoproduction by nutrient-deprived *Chlamydomonas reinhardtii* cells immobilized within thin alginate films under aerobic and anaerobic conditions." Biotechnology and Bioengineering **102**(1): 50-58.

Krassen, H., S. Stripp, G. von Abendroth, K. Ataka, T. Happe and J. Heberle (2009). "Immobilization of the [FeFe]-hydrogenase CrHydA1 on a gold electrode: Design of a catalytic surface for the production of molecular hydrogen." Journal of Biotechnology **142**(1): 3-9.

Kruse, O., J. Rupprecht, J. H. Mussgnug, G. C. Dismukes and B. Hankamer (2005). "Photosynthesis: a blueprint for solar energy capture and biohydrogen production technologies." Photochemical & Photobiological Sciences **4**(12): 957-970.

Kunjapur, A. M. and R. B. Eldridge (2010). "Photobioreactor design for commercial biofuel production from microalgae." Industrial & Engineering Chemistry Research **49**(8): 3516-3526.

Lange, B. M., T. Rujan, W. Martin and R. Croteau (2000). "Isoprenoid biosynthesis: The evolution of two ancient and distinct pathways across genomes." Proceedings of the National Academy of Sciences of the United States of America **97**(24): 13172-13177.

Laurinavichene, T. V., A. S. Fedorov, M. L. Ghirardi, M. Seibert and A. A. Tsygankov (2006). "Demonstration of sustained hydrogen photoproduction by immobilized, sulphur-deprived *Chlamydomonas reinhardtii* cells." International Journal of Hydrogen Energy **31**(5): 659-667.

Lee, Y.-K. and C.-S. Low (1991). "Effect of photobioreactor inclination on the biomass productivity of an outdoor algal culture." Biotechnology and Bioengineering **38**(9): 995-1000.

Lemesle, V. and L. Mailleret (2008). "A mechanistic investigation of the algae growth "Droop" model." Acta Biotheoretica **56**(1-2): 87-102.

Lester, W. W., M. S. Adams and A. M. Farmer (1988). "Effects of light and temperature on photosynthesis of the nuisance alga *Cladophora glomerata* (L.) Kutz from Green Bay, Lake Michigan." New Phytologist **109**(1): 53-58.

Levin, D. B., L. Pitt and M. Love (2004). "Biohydrogen production: prospects and limitations to practical application." International Journal of Hydrogen Energy **29**(2): 173-185.

Lewis, N. S. and D. G. Nocera (2006). "Powering the planet: Chemical challenges in solar energy utilization." Proceedings of the National Academy of Sciences **103**(43): 15729-15735.

Li, Z., S. Wakao, B. B. Fischer and K. K. Niyogi (2009). "Sensing and responding to excess light." Annual Review of Plant Biology **60**(1): 239-260.

Lichtl, R. R., M. J. Bazin and D. O. Hall (1997). "The biotechnology of hydrogen production by *Nostoc flagelliforme* grown under chemostat conditions." Applied Microbiology and Biotechnology **47**(6): 701-707.

Lindblad, P., K. Christensson, P. Lindberg, A. Fedorov, F. Pinto and A. Tsygankov (2002). "Photoproduction of H_2 by wildtype *Anabaena* PCC 7120 and a hydrogen uptake

deficient mutant: from laboratory experiments to outdoor culture." International Journal of Hydrogen Energy **27**: 1271 – 1281.

Lloyd, D., K. L. Thomas, G. Cowie, J. D. Tammam and A. G. Williams (2002). "Direct interface of chemistry to microbiological systems: membrane inlet mass spectrometry." Journal of Microbiological Methods **48**(2–3): 289-302.

Lombard, F., L. Labeyrie, E. Michel, H. J. Spero and D. W. Lea (2009). "Modelling the temperature dependent growth rates of planktic foraminifera." Marine Micropaleontology **70**(1–2): 1-7.

Markou, G. and D. Georgakakis (2011). "Cultivation of filamentous cyanobacteria (blue-green algae) in agro-industrial wastes and wastewaters: A review." Applied Energy **88**(10): 3389-3401.

Markov, S. A., E. R. Eivazova and J. Greenwood (2006). "Photostimulation of H_2 production in the green alga *Chlamydomonas reinhardtii* upon photoinhibition of its O_2-evolving system." International Journal of Hydrogen Energy **31**(10): 1314-1317.

Martínez, L., A. Morán and A. García (2012). "Effect of light on Synechocystis sp. and modelling of its growth rate as a response to average irradiance." Journal of Applied Phycology **24**(1): 125-134.

Masukawa, H., M. Kitashima, K. Inoue, H. Sakurai and R. Hausinger (2012). "Genetic engineering of cyanobacteria to enhance biohydrogen production from sunlight and water." AMBIO **41**(2): 169-173.

Mathews, J. and G. Wang (2009). "Metabolic pathway engineering for enhanced biohydrogen production." International Journal of Hydrogen Energy **34**(17): 7404-7416.

Melis, A. (2002). "Green alga hydrogen production: progress, challenges and prospects." International Journal of Hydrogen Energy **27**(11-12): 1217-1228.

Melis, A. (2007). "Photosynthetic H_2 metabolism in *Chlamydomonas reinhardtii* (unicellular green algae)." Planta **226**(5): 1075-1086.

Melis, A. (2009). "Solar energy conversion efficiencies in photosynthesis: Minimizing the chlorophyll antennae to maximize efficiency." Plant Science **177**(4): 272-280.

Melis, A. (2012). "Photosynthesis-to-fuels: from sunlight to hydrogen, isoprene, and botryococcene production." Energy & Environmental Science **5**(2): 5531-5539.

Melis, A. and T. Happe (2001). "Hydrogen production. Green algae as a source of energy." Plant Physiology **127**(3): 740-748.

Melis, A. and T. Happe (2004). "Trails of green alga hydrogen research - from Hans Gaffron to new frontiers." Photosynthesis Research **80**(1-3): 401-409.

Melis, A. and M. R. Melnicki (2006). "Integrated biological hydrogen production." International Journal of Hydrogen Energy **31**(11): 1563-1573.

Melis, A., L. P. Zhang, M. Forestier, M. L. Ghirardi and M. Seibert (2000). "Sustained photobiological hydrogen gas production upon reversible inactivation of oxygen evolution in the green alga *Chlamydomonas reinhardtii*." Plant Physiology **122**(1): 127-135.

Melnicki, M. R., L. Bianchi, R. De Philippis and A. Melis (2008). "Hydrogen production during stationary phase in purple photosynthetic bacteria." International Journal of Hydrogen Energy **33**(22): 6525-6534.

Melnicki, M. R., G. E. Pinchuk, E. A. Hill, L. A. Kucek, J. K. Fredrickson, A. Konopka and A. S. Beliaev (2012). "Sustained H_2 production driven by photosynthetic water splitting in a unicellular cyanobacterium." Mbio **3**(4).

Meunier, P. C., M. S. Colón-López and L. A. Sherman (1998). "Photosystem II cyclic heterogeneity and photoactivation in the diazotrophic, unicellular cyanobacterium *Cyanothece* species ATCC 51142." Plant Physiology **116**(4): 1551-1562.

Min, H. and L. A. Sherman (2010). "Hydrogen production by the unicellular, diazotrophic cyanobacterium *Cyanothece* sp. strain ATCC 51142 under conditions of continuous light." Applied and Environmental Microbiology **76**(13): 4293-4301.

Molina, E., F. G. Acién Fernández, F. García Camacho, F. Camacho Rubio and Y. Chisti (2000). "Scale-up of tubular photobioreactors." Journal of Applied Phycology **12**(3-5): 355-368.

Molina Grima, E., F. G. A. Fernández, F. García Camacho and Y. Chisti (1999). "Photobioreactors: light regime, mass transfer, and scaleup." Journal of Biotechnology **70**(1–3): 231-247.

Momirlan, M. and T. Veziroğlu (1999). "Recent directions of world hydrogen production." Renewable and Sustainable Energy Reviews **3**(2–3): 219-231.

Morweiser, M., O. Kruse, B. Hankamer and C. Posten (2010). "Developments and perspectives of photobioreactors for biofuel production." Applied Microbiology and Biotechnology **87**(4): 1291-1301.

Mussgnug, J. H., V. Klassen, A. Schlüter and O. Kruse (2010). "Microalgae as substrates for fermentative biogas production in a combined biorefinery concept." Journal of Biotechnology **150**(1): 51-56.

Naik, S. N., V. V. Goud, P. K. Rout and A. K. Dalai (2010). "Production of first and second generation biofuels: A comprehensive review." Renewable and Sustainable Energy Reviews **14**(2): 578-597.

Nath, K., A. Kumar and D. Das (2005). "Hydrogen production by *Rhodobacter sphaeroides* strain O.U.001 using spent media of Enterobacter cloacae strain DM11." Applied Microbiology and Biotechnology **68**(4): 533-541.

Nigam, S., M.P. Rai and R. Sharma (2011). "Effect of nitrogen on growth and lipid content of *Chlorella pyrenoidosa*." American Journal of Biochemistry and Biotechnology **7**(3): 124-129.

Nixon, P. J., F. Michoux, J. Yu, M. Boehm and J. Komenda (2010). "Recent advances in understanding the assembly and repair of photosystem II." Annals of Botany **106**(1): 1-16.

Norsker, N.-H., M. J. Barbosa, M. H. Vermuë and R. H. Wijffels (2011). "Microalgal production — A close look at the economics." Biotechnology Advances **29**(1): 24-27.

Oncel, S. and F. Vardar-Sukan (2009). "Photo-bioproduction of hydrogen by *Chlamydomonas reinhardtii* using a semi-continuous process regime." International Journal of Hydrogen Energy **34**(18): 7592-7602.

Osmond, B., J. J. Cooper, S. Vigg and C. Buchen-Osmond (1985). "Photoinhibition of N_2 fixation, photosynthesis, and the collapse of blue-green algal blooms."

Park, W. and I. Moon (2007). "A discrete multi states model for the biological production of hydrogen by phototrophic microalga." Biochemical Engineering Journal **36**(1): 19-27.

Parmar, A., N. K. Singh, A. Pandey, E. Gnansounou and D. Madamwar (2011). "Cyanobacteria and microalgae: A positive prospect for biofuels." Bioresource Technology **102**(22): 10163-10172.

Patel, B., B. Tamburic, F. W. Zemichael, P. Dechatiwongse and K. Hellgardt (2012). "Algal biofuels: a credible prospective?" ISRN Renewable Energy **2012**: Article ID 631574.

Peharz, G., F. Dimroth and U. Wittstadt (2007). "Solar hydrogen production by water splitting with a conversion efficiency of 18%." International Journal of Hydrogen Energy **32**(15): 3248-3252.

Peschek, G. (1999). Photosynthesis and respiration of cyanobacteria. The Phototrophic Prokaryotes. G. Peschek, W. Löffelhardt and G. Schmetterer, Springer US**:** 201-209.

Pimentel, D., A. Marklein, M. Toth, M. Karpoff, G. Paul, R. McCormack, J. Kyriazis and T. Krueger (2009). "Food versus biofuels: environmental and economic costs." Human Ecology **37**(1): 1-12.

Pirt, S. J., Y. K. Lee, M. R. Walach, M. W. Pirt, H. H. M. Balyuzi and M. J. Bazin (1983). "A tubular bioreactor for photosynthetic production of biomass from carbon dioxide: Design and performance." Journal of Chemical Technology and Biotechnology. Biotechnology **33**(1): 35-58.

Polle, J. W., S. D. Kanakagiri and A. Melis (2003). "tla1, a DNA insertional transformant of the green alga *Chlamydomonas reinhardtii* with a truncated light-harvesting chlorophyll antenna size." Planta **217**(1): 49-59.

Posten, C. (2009). "Design principles of photobioreactors for cultivation of microalgae." Engineering in Life Sciences **9**(3): 165-177.

Posten, C. and G. Schaub (2009). "Microalgae and terrestrial biomass as source for fuels - A process view." Journal of Biotechnology **142**(1): 64-69.

Postgate, J. (1998). Nitrogen Fixation. Cambridge, UK, Cambridge University Press.

Powles, S. B. (1984). "Photoinhibition of photosynthesis induced by visible light." Annual Review of Plant Physiology **35**(1): 15-44.

Prevost, D., H. Antoun and L. M. Bordeleau (1987). "Effects of low temperatures on nitrogenase activity in sainfoin (*Onobrychis viciifolia*) nodulated by arctic rhizobia." Fems Microbiology Ecology **45**(4): 205-210.

Prince, R. C. and H. S. Kheshgi (2005). "The photobiological production of hydrogen: potential efficiency and effectiveness as a renewable fuel." Critical Reviews in Microbiology **31**(1): 19-31.

Provasoli, L., J.J.A. McLaughlin, and M.R. Droop (1957). "The development of artificial media for marine algae." Archiv für Mikrobiologie **25**(4): 392-428.

Przybyla, A. E., J. Robbins, N. Menon and H. D. Peck Jr (1992). "Structure-function relationships among the nickel-containing hydrogenases." FEMS Microbiology Letters **88**(2): 109-135.

Pulz, O. (2001). "Photobioreactors: production systems for phototrophic microorganisms." Applied Microbiology and Biotechnology **57**(3): 287-293.

Putt, R. (2007). "Algae as a biodiesel feedstock: A feasibility assessment." Center for Microfibrous Materials Manufacturing (CM3).

Ramsing, N. and J. Gundersen (Unisense). "Seawater and gases tabulated physical parameters of interest to people working with microsensors in marine systems". Data-table 8: Oxygen solubility at different temperatures and salinities of seawater. http://www.unisense.com/files/PDF/Diverse/Seawater%20&%20Gases%20table.pdf (accessed on 1st March 2015).

Rawson, D. M. (1985). "The effects of exogenous amino acids on growth and nitrogenase activity in the cyanobacterium *Anabaena cylindrica* PCC 7122." Journal of General Microbiology **131**(10): 2549-2554.

Reay, D. S., D. B. Nedwell, J. Priddle and J. C. Ellis-Evans (1999). "Temperature dependence of inorganic nitrogen uptake: Reduced affinity for nitrate at suboptimal temperatures in both algae and bacteria." Applied and Environmental Microbiology **65**(6): 2577-2584.

Redding, K., L. Cournac, I. R. Vassiliev, J. H. Golbeck, G. Peltier and J.-D. Rochaix (1999). "Photosystem I is indispensable for photoautotrophic growth, CO_2 fixation, and H_2 photoproduction in *Chlamydomonas reinhardtii*." Journal of Biological Chemistry **274**(15): 10466-10473.

Reddy, K. J., J. B. Haskell, D. M. Sherman and L. A. Sherman (1993). "Unicellular, aerobic nitrogen-fixing cyanobacteria of the genus *Cyanothece*." Journal of Bacteriology **175**(5): 1284-1292.

Ricci, M., P. Bellaby and R. Flynn (2008). "What do we know about public perceptions and acceptance of hydrogen? A critical review and new case study evidence." International Journal of Hydrogen Energy **33**(21): 5868-5880.

Richmond, A., E. Lichtenberg, B. Stahl and A. Vonshak (1990). "Quantitative assessment of the major limitations on productivity of *Spirulina platensis* in open raceways." Journal of Applied Phycology **2**(3): 195-206.

Rosello-Sastre, R. (2009). Kopplung physiologischer und verfahrenstechnischer Parameter beim Wachstum und bei der Produktbildung der Rotalge Porphyridium purpureum, Karlsruhe Institute of Technology.

Rosello Sastre, R., Z. Csögör, I. Perner-Nochta, P. Fleck-Schneider and C. Posten (2007). "Scale-down of microalgae cultivations in tubular photo-bioreactors - A conceptual approach." Journal of Biotechnology **132**(2): 127-133.

Royce, P. N. C. and N. F. Thornhill (1991). "Estimation of dissolved carbon dioxide concentrations in aerobic fermentations." AIChE Journal **37**(11): 1680-1686.

Rupprecht, J., B. Hankamer, J. H. Mussgnug, G. Ananyev, C. Dismukes and O. Kruse (2006). "Perspectives and advances of biological H_2 production in microorganisms." Applied Microbiology and Biotechnology **72**(3): 442-449.

Sánchez Mirón, A., M.-C. Cerón García, F. García Camacho, E. Molina Grima and Y. Chisti (2002). "Growth and biochemical characterization of microalgal biomass produced in bubble column and airlift photobioreactors: studies in fed-batch culture." Enzyme and Microbial Technology **31**(7): 1015-1023.

Sánchez Mirón, A., F. García Camacho, A. Contreras Gómez, E. M. Grima and Y. Chisti (2000). "Bubble-column and airlift photobioreactors for algal culture." AIChE Journal **46**(9): 1872-1887.

Schenk, P., S. Thomas-Hall, E. Stephens, U. Marx, J. Mussgnug, C. Posten, O. Kruse and B. Hankamer (2008). "Second generation biofuels: high-efficiency microalgae for biodiesel production." BioEnergy Research **1**(1): 20-43.

Schneegurt, M. A., B. Arieli, J. D. McKeehen, S. D. Stephens, S. S. Nielsen, P. R. Saha, P. R. Trumbo and L. A. Sherman (1995). "Compositional and toxicological evaluation of the diazotrophic cyanobacterium, *Cyanothece* sp. strain ATCC 51142." Aquaculture **134**(3-4): 339-349.

Schneegurt, M. A., D. M. Sherman, S. Nayar and L. A. Sherman (1994). "Oscillating behavior of carbohydrate granule formation and dinitrogen fixation in the cyanobacterium *Cyanothece* sp. strain ATCC 51142." Journal of Bacteriology **176**(6): 1586-1597.

Schneegurt, M. A., D. M. Sherman and L. A. Sherman (1997). "Composition of the carbohydrate granules of the cyanobacterium, *Cyanothece* sp strain ATCC 51142." Archives of Microbiology **167**(2-3): 89-98.

Schneegurt, M. A., D. M. Sherman and L. A. Sherman (1997). "Growth, physiology, and ultrastructure of a diazotrophic cyanobacterium, *Cyanothece* sp. strain ATCC 51142, in mixotrophic and chemoheterotrophic cultures." Journal of Phycology **33**(4): 632-642.

Schneegurt, M. A., Sherman, D. M., Nayar, S. and Sherman, L. A. (1994). "Oscillating behavior of carbohydrate granule formation and dinitrogen fixation in the cyanobacterium *Cyanothece* sp. strain ATCC 51142." J. Bacteriol **176**(6): 1586-1597.

Schneegurt, M. A., D. L. Tucker, J. K. Ondr, D. M. Sherman and L. A. Sherman (2000). "Metabolic rhythms of a diazotrophic cyanobacterium, Cyanothece sp strain ATCC 51142, heterotrophically grown in continuous dark." Journal of Phycology **36**(1): 107-117.

Searchinger, T. D., S. P. Hamburg, J. Melillo, W. Chameides, P. Havlik, D. M. Kammen, G. E. Likens, R. N. Lubowski, M. Obersteiner, M. Oppenheimer, G. Philip Robertson, W. H. Schlesinger and G. David Tilman (2009). "Fixing a critical climate accounting error." Science **326**(5952): 527-528.

Seefeldt, L. C., Z.-Y. Yang, S. Duval and D. R. Dean (2013). "Nitrogenase reduction of carbon-containing compounds." Biochimica et Biophysica Acta (BBA) - Bioenergetics **1827**(8–9): 1102-1111.

Sen, U., S. Manish and R. Banerjee (2008). "Status of biological hydrogen production." Journal of Scientific and Industrial Research **67**(11).

Sheehan, J., T. Dunahay, J. Benemann and P. Roessler (1998). Look back at the U.S. Department of Energy's Aquatic Species Program: biodiesel from algae; close-out report. Other Information: PBD: 1 Jul 1998**:** Medium: ED; Size: 325 pages.

Sherman, L., H. Min, J. Toepel and H. Pakrasi (2010). Better living through *Cyanothece* – unicellular diazotrophic cyanobacteria with highly versatile metabolic systems. Recent Advances in Phototrophic Prokaryotes. P. C. Hallenbeck, Springer New York. **675:** 275-290.

Sherman, L. A., P. Meunier and M. S. Colon-Lopez (1998). "Diurnal rhythms in metabolism: A day in the life of a unicellular, diazotrophic cyanobacterium." Photosynthesis Research **58**(1): 25-42.

Shevela, D., R. Pishchalnikov, L. A. Eichacker and G. Govindjee (2013). Oxygenic photosynthesis in cyanobacteria. Stress Biology of Cyanobacteria: Molecular Mechanisms to Cellular Responses. A. K. Srivastava, A. N. Rai and N. B. A., CRC Press/Taylor & Francis Group**:** 3 - 40.

Siaut, M., S. Cuine, C. Cagnon, B. Fessler, M. Nguyen, P. Carrier, A. Beyly, F. Beisson, C. Triantaphylides, Y. Li-Beisson and G. Peltier (2011). "Oil accumulation in the model green alga *Chlamydomonas reinhardtii*: characterization, variability between common laboratory strains and relationship with starch reserves." BMC Biotechnology **11**(1): 7.

Sierra, E., F. G. Acién, J. M. Fernández, J. L. García, C. González and E. Molina (2008). "Characterization of a flat plate photobioreactor for the production of microalgae." Chemical Engineering Journal **138**(1–3): 136-147.

Sinetova, M. A., J. Červený, T. Zavřel and L. Nedbal (2012). "On the dynamics and constraints of batch culture growth of the cyanobacterium *Cyanothece* sp. ATCC 51142." Journal of Biotechnology **162**(1): 148-155.

Spolaore, P., C. Joannis-Cassan, E. Duran and A. Isambert (2006). "Commercial applications of microalgae." Journal of Bioscience and Bioengineering **101**(2): 87-96.

Staal, M., S. T. L. Hekkert, P. Herman and L. J. Stal (2002). "Comparison of models describing light dependence of N_2 fixation in heterocystous cyanobacteria." Applied and Environmental Microbiology **68**(9): 4679-4683.

Staal, M., S. t. Lintel-Hekkert, F. Harren and L. Stal (2001). "Nitrogenase activity in cyanobacteria measured by the acetylene reduction assay: a comparison between batch incubation and on-line monitoring." Environmental Microbiology **3**(5): 343-351.

Staal, M., F. J. R. Meysman and L. J. Stal (2003). "Temperature excludes N_2-fixing heterocystous cyanobacteria in the tropical oceans." Nature **425**(6957): 504-507.

Stal, L. J. (2009). "Is the distribution of nitrogen-fixing cyanobacteria in the oceans related to temperature?" Environmental Microbiology **11**(7): 1632-1645.

Stephens, E., I. L. Ross, Z. King, J. H. Mussgnug, O. Kruse, C. Posten, M. A. Borowitzka and B. Hankamer (2010). "An economic and technical evaluation of microalgal biofuels." Nat Biotech **28**(2): 126-128.

Stephens, E., I. L. Ross, J. H. Mussgnug, L. D. Wagner, M. A. Borowitzka, C. Posten, O. Kruse and B. Hankamer (2010). "Future prospects of microalgal biofuel production systems." Trends in Plant Science **15**(10): 554-564.

Stern, D. (2006). "Stern review: the economics of climate change." UK Treasury.

Stöckel, J., J. M. Jacobs, T. R. Elvitigala, M. Liberton, E. A. Welsh, A. D. Polpitiya, M. A. Gritsenko, C. D. Nicora, D. W. Koppenaal, R. D. Smith and H. B. Pakrasi (2011). "Diurnal rhythms result in significant changes in the cellular protein complement in the cyanobacterium *Cyanothece* 51142." PLoS ONE **6**(2): e16680.

Subhadra, B. G. (2010). "Sustainability of algal biofuel production using integrated renewable energy park (IREP) and algal biorefinery approach." Energy Policy **38**(10): 5892-5901.

Tamagnini, P., R. Axelsson, P. Lindberg, F. Oxelfelt, R. Wunschiers and P. Lindblad (2002). "Hydrogenases and hydrogen metabolism of cyanobacteria." Microbiology and Molecular Biology Reviews **66**(1): 1-+.

Tamagnini, P., R. Axelsson, P. Lindberg, F. Oxelfelt, R. Wünschiers and P. Lindblad (2002). "Hydrogenases and hydrogen metabolism of cyanobacteria." Microbiology and Molecular Biology Reviews **66**(1): 1-20.

Tamburic, B., P. Dechatiwongse, F. W. Zemichael, G. C. Maitland and K. Hellgardt (2013). "Process and reactor design for biophotolytic hydrogen production." Physical Chemistry Chemical Physics **15**(26): 10783-10794.

Tamburic, B., F. W. Zemichael, P. Crudge, G. C. Maitland and K. Hellgardt (2011). "Design of a novel flat-plate photobioreactor system for green algal hydrogen production." International Journal of Hydrogen Energy **36**(11): 6578-6591.

Tamburic, B., F. W. Zemichael, G. C. Maitland and K. Hellgardt (2011). "Parameters affecting the growth and hydrogen production of the green alga *Chlamydomonas reinhardtii*." International Journal of Hydrogen Energy **36**(13): 7872-7876.

Tamburic, B., F. W. Zemichael, G. C. Maitland and K. Hellgardt (2012). "A novel nutrient control method to deprive green algae of sulphur and initiate spontaneous hydrogen production." International Journal of Hydrogen Energy **37**(11): 8988-9001.

Tao, Y., Y. He, Y. Wu, F. Liu, X. Li, W. Zong and Z. Zhou (2008). "Characteristics of a new photosynthetic bacterial strain for hydrogen production and its application in wastewater treatment." International Journal of Hydrogen Energy **33**(3): 963-973.

Taylor, G. (2008). "Biofuels and the biorefinery concept." Energy Policy **36**(12): 4406-4409.

Toepel, J., E. Welsh, T. C. Summerfield, H. B. Pakrasi and L. A. Sherman (2008). "Differential transcriptional analysis of the cyanobacterium *Cyanothece* sp strain ATCC 51142 during light-dark and continuous-light growth." Journal of Bacteriology **190**(11): 3904-3913.

Toepel, J. r., J. E. McDermott, T. C. Summerfield and L. A. Sherman (2009). "Transcriptional analysis *of the* unicellular, diazotrophic cyanobacterium *Cyanothece* sp. ATCC 51142 grown under short day / night cycles." Journal of Phycology **45**(3): 610-620.

Tomaselli, L. (2004). The Microalgal Cell. Handbook of Microalgal Culture: Biotechnology and Applied Phycology. A. Richmond. Oxford, UK, Blackwell Publishing.

Topic, M., K. Brecl and J. Sites (2006). "Performance assessment of PV modules - relationship between STC rating and field performance." Photovoltaic Energy Conversion, Conference Record of the 2006 IEEE 4th World Conference on.

Topiwala, H. and C. G. Sinclair (1971). "Temperature relationship in continuous culture." Biotechnology and Bioengineering **13**(6): 795-813.

Torzillo, G. and A. Vonshak (1994). "Effect of light and temperature on the photosynthetic activity of the cyanobacterium *Spirulina platensis*." Biomass & Bioenergy **6**(5): 399-403.

Tsygankov, A. A. (2007). "Nitrogen-fixing cyanobacteria: a review." Applied Biochemistry and Microbiology **43**(3): 250-259.

Tsygankov, A. A., A. S. Fedorov, S. N. Kosourov and K. K. Rao (2002). "Hydrogen production by cyanobacteria in an automated outdoor photobioreactor under aerobic conditions." Biotechnology and Bioengineering **80**(7): 777-783.

Tucker, D. L. and L. A. Sherman (2000). "Analysis of chlorophyll–protein complexes from the cyanobacterium Cyanothece sp. ATCC 51142 by non-denaturing gel electrophoresis." Biochimica et Biophysica Acta (BBA) - Biomembranes **1468**(1–2): 150-160.

Ugwu, C. U., H. Aoyagi and H. Uchiyama (2008). "Photobioreactors for mass cultivation of algae." Bioresource Technology **99**(10): 4021-4028.

US DoE (2005). "Basic research needs for solar energy utilization." US Department of Energy (US DoE) - Report of the Basic Energy Sciences Workshop on Solar Energy Utilization.

US DoE (2008). "Hydrogen & our energy future". US Department of Energy (US DoE) Hydrogen Program.

US DoE (2009). "Current state-of-the-art hydrogen production cost estimate using water electrolysis." US Department of Energy (US DoE) Hydrogen Program.

US DoE (2010). "Own your power! A consumer guide to solar electricity for the home." US Department of Energy (US DoE) Energy Efficiency & Renewable Energy.

Uyar, B., I. Eroglu, M. Yücel, U. Gündüz and L. Türker (2007). "Effect of light intensity, wavelength and illumination protocol on hydrogen production in photobioreactors." International Journal of Hydrogen Energy **32**(18): 4670-4677.

Vatcheva, I., H. de Jong, O. Bernard and N. J. I. Mars (2006). "Experiment selection for the discrimination of semi-quantitative models of dynamical systems." Artificial Intelligence **170**(4–5): 472-506.

Verhulst, P. F. (1838). "Notice sur la loi que la population poursuit dans son accroissement." Correspondance mathématique et physique **10**: 113 – 121.

Vignais, P. M., B. Billoud and J. Meyer (2001). "Classification and phylogeny of hydrogenases1." FEMS Microbiology Reviews **25**(4): 455-501.

Vonshak, A. and R. Guy (1992). "Photoadaptation, photoinhibition and productivity in the blue-green alga, Spirulina platensis grown outdoors." Plant, Cell & Environment **15**(5): 613-616.

Wang, B., Y. Li, N. Wu and C. Lan (2008). "CO_2 bio-mitigation using microalgae." Applied Microbiology and Biotechnology **79**(5): 707-718.

Wang, C. Y., C. C. Fu and Y. C. Liu (2007). "Effects of using light-emitting diodes on the cultivation of *Spirulina platensis*." Biochemical Engineering Journal **37**(1): 21-25.

Watanabe, Y. and H. Saiki (1997). "Development of a photobioreactor incorporating *Chlorella* sp. for removal of CO_2 in stack gas." Energy Conversion and Management **38, Supplement**(0): S499-S503.

Waughman, G. J. (1977). "The effect of temperature on nitrogenase activity." Journal of Experimental Botany **28**(4): 949-960.

WEC (2007). "Energy scenario development analysis: WEC policy to 2050." World Energy Council (WEC).

Weiss, M. A., J. B. Heywood, E. M. Drake, A. Schafer and F. F. AuYeung (2000). "On the road in 2020 - A life-cycle analysis of new automobile technologies." Massachusetts Institute of Technology (MIT) - Energy Laboratory Report.

Welsh, E. A., M. Liberton, J. Stoeckel, T. Loh, T. Elvitigala, C. Wang, A. Wollam, R. S. Fulton, S. W. Clifton, J. M. Jacobs, R. Aurora, B. K. Ghosh, L. A. Sherman, R. D. Smith, R. K. Wilson and H. B. Pakrasi (2008). "The genome of Cyanothece 51142, a unicellular diazotrophic cyanobacterium important in the marine nitrogen cycle." Proceedings of the National Academy of Sciences of the United States of America **105**(39): 15094-15099.

Wicks, R. J. and P. G. Thiel (1990). "Environmental factors affecting the production of peptide toxins in floating scums of the cyanobacterium *Microcystis aeruginosa* in a hypertrophic African reservoir." Environmental Science & Technology **24**(9): 1413-1418.

Wijffels, R. H. and M. J. Barbosa (2010). "An outlook on microalgal biofuels." Science **329**(5993): 796-799.

Withers, S. T. and J. D. Keasling (2007). "Biosynthesis and engineering of isoprenoid small molecules." Applied Microbiology and Biotechnology **73**(5): 980-990.

Xu, Z., L. Dapeng, Z. Yiping, Z. Xiaoyan, C. Zhaoling, C. Wei and O. Fan (2002). "Comparison of photobioreactors for cultivation of *Undaria pinnatifida* gametophytes." Biotechnology Letters **24**(18): 1499-1503.

Yamane, Y., Y. Kashino, H. Koike and K. Satoh (1998). "Effects of high temperatures on the photosynthetic systems in spinach: Oxygen-evolving activities,

fluorescence characteristics and the denaturation process." Photosynthesis Research **57**(1): 51-59.

Yang, F., M. Hanna, and R. Sun (2012). "Value-added uses for crude glycerol - a byproduct of biodiesel production." Biotechnology for Biofuels **5**(1): 13.

Yeager, C. M., C. E. Milliken, C. E. Bagwell, L. Staples, P. A. Berseth and H. T. Sessions (2011). "Evaluation of experimental conditions that influence hydrogen production among heterocystous cyanobacteria." International Journal of Hydrogen Energy **36**: 7487 - 7499.

Zhang, D., P. Dechatiwongse and K. Hellgardt (2015a). "Modelling light transmission, cyanobacterial growth kinetics and fluid dynamics in a laboratory scale multiphase photo-bioreactor for biological hydrogen production." Algal Research **8**(0): 99-107.

Zhang, D., P. Dechatiwongse, E. A. del Rio-Chanona, G. C. Maitland, K. Hellgardt and V. S. Vassiliadis (2015b). "Modelling of light and temperature influences on cyanobacterial growth and biohydrogen production." Algal Research **9**(0): 263-274.

9. Appendixes

9.1. Calculation of $[O_2^*]$

Henry's constant of O_2; $$H_{O_2} = \exp(12.74 - \frac{133.4}{(T-206.7)})$$ Equation 5.47

At temperature of 35 °C,

$$H_{O_2} = \exp\left(12.74 - \frac{133.4}{((35+273)-206.7)}\right) = 91{,}410 \text{ Pa m}^3 \text{ mol}^{-1}$$

Henry's law; $$P_{O_2} = [O_2^*] \cdot H_{O_2}$$ Equation 5.45

Rearrange, $$[O_2^*] = \frac{P_{O_2}}{H_{O_2}}$$

As O_2 is not present in the sparged gas mixture, it can only come from either photosynthesis or air. Therefore, it becomes reasonable to assume the partial pressure of O_2 as 0.21 bar = 21,000 Pa (same as that of ambient O_2)

$$[O_2^*] = \frac{P_{O_2}}{H_{O_2}} = \frac{21{,}000 \text{ Pa}}{91{,}410 \frac{\text{Pa m}^3}{\text{mol}}} = 0.23 \text{ mol } O_2 \text{ m}^{-3}$$

As molecular weight of O_2 = 32 g O_2 mol^{-1}, $[O_2^*] = 0.23 \frac{\text{mol } O_2}{\text{m}^3} \cdot 32 \frac{\text{g } O_2}{\text{mol } O_2} = 7.35 \text{ g } O_2 \text{ m}^{-3}$

9.2. Calculation of $[CO_2^*]$

Henry's constant of CO_2; $$H_{CO_2} = \exp\left(11.25 - \frac{395.9}{(T-175.9)}\right)$$ Equation 5.46

At temperature of 35 °C,

$$H_{CO_2} = \exp\left(11.25 - \frac{395.9}{((35+273)-175.9)}\right) = 3{,}840 \text{ Pa m}^3 \text{ mol}^{-1}$$

Henry's law; $$P_{CO_2} = [CO_2^*] \cdot H_{CO_2}$$ Equation 5.45

Rearrange, $$[CO_2{}^*] = \frac{P_{CO_2}}{H_{CO_2}}$$

As CO_2 directly comes from the sparged gas mixture, its partial pressure was assumed to be the same as that of the mixture (= 1.2 bar = 120,000 Pa, as the total pressure was fixed at 6 bar and the mole fraction of CO_2 = 0.2).

$$[CO_2{}^*] = \frac{P_{CO_2}}{H_{CO_2}} = \frac{120{,}000\ \text{Pa}}{3{,}840\ \frac{\text{Pa m}^3}{\text{mol}}} = 31.26\ \text{mol CO}_2\ \text{m}^{-3}$$

As molecular weight of CO_2 = 44 g CO_2 mol^{-1}, $[CO_2{}^*] = 31.26\ \frac{\text{mol CO}_2}{\text{m}^3} \cdot 44 \frac{\text{g CO}_2}{\text{mol CO}_2} = 1{,}375\ \text{g CO}_2\ \text{m}^{-3}$

9.3. Unit conversion of the steady-state carbon scarcity

Under steady-state conditions, the CO_2 scarcity was found to be -183 g CO_2 m^{-3}.

This value corresponds to the carbon scarcity of: $-183 \frac{\text{g CO}_2}{\text{m}^3} \cdot \frac{12\text{g C}}{44\ \text{g CO}_2} \sim$ -49.8 g C m^{-3} ~ -0.05 g C L^{-1}.

The steady-state biomass concentration = 2 g L^{-1}

So, this carbon shortage is equivalent to approximately $\frac{-0.05}{2} \cdot 100$ = -2.5% of dry *Cyanothece* 51142 biomass.

9.4. Quantification of chemostat cyanobacterial H_2 production

Using the perfect gas law; $$\rho = \frac{P \cdot M}{R \cdot T}$$ Equation 5.8

Under operating condition used in the secondary flat-plate PBR of a two-stage chemostat system: temperature of 35 ˚C and pressure of 1 bar

$$\rho = \frac{(1 \cdot 10^5) \cdot (2)}{(8.314) \cdot (308)} \sim 78\ \text{g m}^{-3} = 0.078\ \text{mg ml}^{-1}$$

By multiplying the volumetric H_2 productivity with the calculated density, the mass-based productivity can be subsequently estimated as ~ 0.26 mg H_2 L^{-1} hr^{-1}. Finally, the molar productivity of 0.13 mmol H_2 L^{-1} hr^{-1} can be deduced by dividing the obtained mass productivity by the molecular weight of H_2 – 2 g mol^{-1}.

The steady-state conversion from glycerol into H_2 can be simply calculated from the molar ratio of steady-state H_2 production rate over glycerol feed rate:

$$\%\ \text{Converison} = \frac{0.13\ \text{mmol}\ H_2\ L^{-1}\ hr^{-1}}{0.46\ \text{mmol glycerol}\ L^{-1}\ hr^{-1}} \cdot 100\ \sim\ 28.3\ \%$$

Under steady-state condition, the biomass concentration in the primary growth PBR is ~ 2 g L^{-1}. With the fixed liquid transfer rate of 12 ml hr^{-1}, the delivery rate of biomass into the secondary PBR is:

$$2\ \frac{\text{g}}{\text{L}} \cdot 12\ \frac{\text{ml}}{\text{hr}} \cdot \frac{\text{L}}{1000\ \text{ml}} = 24\ \text{mg}\ \text{hr}^{-1}$$

As the steady-state H_2 production rate is 2.6 ml hr^{-1} ~ 0.2 mg hr^{-1}, The ratio of H_2 produced to biomass transferred = $\frac{0.2\ \text{mg}\ H_2\ hr^{-1}}{24\ \text{mg biomass}\ hr^{-1}}$ ~ 0.0085 mg H_2 mg biomass^{-1} or 8.5 mg H_2 g biomass^{-1}.